

FROM BASALTS TO BADLANDS

Modelling long-term landscape response to lava
damming of an upland catchment in western Turkey

Wouter van Gorp

Thesis committee

Promotor

Prof. Dr A. Veldkamp
Professor of Land Dynamics
Wageningen University

Co-promotors

Dr J.M. Schoorl
Assistant professor, Soil Geography and Landscape Group
Wageningen University

Dr A.J.A.M. Temme
Assistant professor, Soil Geography and Landscape Group
Wageningen University

Other members

Prof. Dr C.J. Ritsema, Wageningen University
Prof. Dr V.G. Jetten, University of Twente, Enschede
Prof. Dr J. Wainwright, University of Durham, United Kingdom
Dr A. Mather, University of Plymouth, United Kingdom

This research was conducted under the auspices of the C.T. De Wit Graduate School for Production Ecology and Resource Conservation (PE&RC)

FROM BASALTS TO BADLANDS

Modelling long-term landscape response to lava
damming of an upland catchment in western Turkey

Wouter van Gorp

Thesis

submitted in fulfilment of the requirements for the degree of doctor
at Wageningen University
by the authority of the Rector Magnificus
Prof. Dr M.J. Kropff,
in the presence of the
Thesis Committee appointed by the Academic Board
to be defended in public
on Friday 12 September 2014
at 11 a.m. in the Aula.

Wouter van Gorp

From basalts to badlands. Modelling long-term landscape response to lava damming of an upland catchment in western Turkey,
184 pages.

PhD thesis, Wageningen University, Wageningen, NL (2014)

With references, with summaries in Turkish, Dutch and English

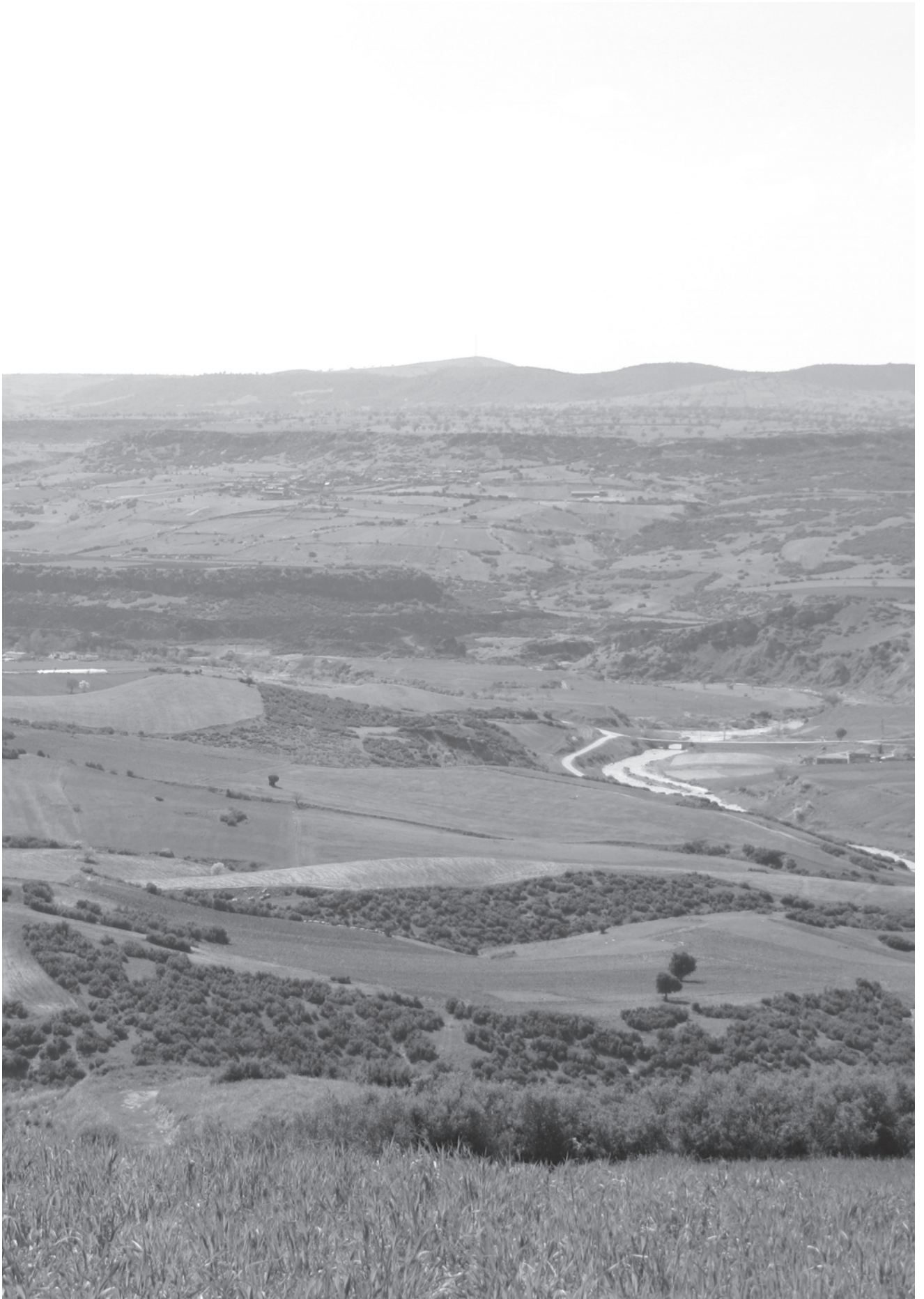
ISBN: 978-94-6257-048-1

Voor mijn ouders:
Hans van Gorp
Hankie van Gorp - Nieuwenhuis

Table of contents

Chapter 1 General introduction	9
1.1 Introduction	9
1.2 Field and dating based landscape reconstruction	10
1.3 Quaternary landscape reconstruction of Mediterranean catchments	11
1.4 Landscape evolution modelling	13
1.5 Study area	15
1.6 Aim and research questions	16
1.7 Thesis outline	17
Chapter 2 Landscape evolution modelling of naturally dammed rivers	19
2.1 Introduction	20
2.2 Methods	21
2.3 Results	27
2.4 Discussion	36
2.5 Conclusion	42
Chapter 3 Fluvial response to Holocene volcanic damming and breaching in the Gediz and Geren rivers, western Turkey	45
3.1 Introduction	46
3.2 Setting	47
3.3 Methods	52
3.4 Results and discussion	57
3.5 Conclusion	73
Appendix A3.1. $^{40}\text{Ar}/^{39}\text{Ar}$ dating results	74
Appendix A3.2. Luminescence dating	78
Chapter 4 Modelling long-term (300 ka) upland catchment response to multiple lava damming events	85
4.1 Introduction	86
4.2 Study site	87
4.3 Methods	88
4.4 Results	95
4.5 Discussion	103
4.6 Conclusion	105
Chapter 5 Long-term response of the Geren Catchment (western Turkey) to lava dam influenced base level change	107
5.1 Introduction	108
5.2 Regional setting	109
5.3 Materials and methods	110
5.4 Fieldwork and dating results	113
5.5 Discussion	120
5.6 Conclusion	131
Appendix A5.1. Radiocarbon calibration	132
Appendix A5.2. $^{40}\text{Ar}/^{39}\text{Ar}$ Age estimates and geochemistry	133
Appendix A5.3. Feldspar luminescence dating	140

Chapter 6 Synthesis	147
6.1 Drivers of middle Pleistocene to Holocene evolution of the Geren Catchment ..	147
6.2 LAPSUS, an ever evolving reduced complexity landscape evolution model	154
6.3 Research implications.....	156
6.4 Final conclusions.....	158
References	161
Summary	169
Samenvatting.....	171
Özet	174
Dankwoord	177
List of Publications.....	179
PE&RC Training and Education Statement	181



Chapter 1

General introduction

1.1 Introduction

The face of a landscape is the legacy of its history. Its current shape reflects the formation history of the relief, rocks and soil it is composed of. It reflects the tectonic, climatic and, in recent geological time, the human impacts it underwent. For instance, upland and tectonically uplifted landscapes are mostly erosive, while subsiding or lowland areas, mostly reflect its burial by sediments delivered from upstream. However, deposition occurs in erosion-dominated landscapes as well, and vice versa. Specific landscapes within each of these regions still differ due to the rate and magnitude of tectonic, climatic and human history. Therefore, present and future landscape evolution is not only determined by climatic, tectonic and human driving mechanisms, it is also determined by its past state and properties, and by its specific historical pathway (Phillips, 2006).

Unfortunately for those who want to understand present or even predict future landscape evolution, many traces of a landscape's past evolution are erased during the process, making reconstruction of a past landscape like "solving a large puzzle of which only few pieces are left". Nevertheless, key pieces of this puzzle derived from field-based reconstructions can tell geomorphologists a lot about this old landscape and the processes that shaped it.

In geomorphology we study the shape and other properties of the landscape combined with the processes that shaped the landscape. This helps us answering questions about why the landscape looks like it does, how it was formed and how it will further evolve. For example, in fluvial geomorphology, the grade of a river stretch can conceptually be determined by the balance of water discharge and sediment load the water can carry (Gilbert, 1880). Thus, when the slope of the river declines, stream capacity lowers and leading to decreased erosion or increased sediment deposition. When the slope increases, stream capacity increases, leading to increased erosion or decreased deposition. This concept was supposedly applicable to all rivers regardless of their location or state, illustrating that specific river evolution could be described by, or deduced from, a general law irrespective of its specific location.

However, landforms are shaped not only as a function of their geological structure and processes, but also with respect to the time that these processes had to shape the land, as classically postulated by Davis (1899). In his geographical cycle, a landscape becomes uplifted and then evolves through several phases of maturity, before it may be uplifted again. Young landscapes show initially incised plateaus, mature landscapes show an incised river system with slopes adjusting to it, while old landscapes have all their relief removed to become relatively flat. These classic examples (of Gilbert and Davis) were for a long time the most influential geomorphological models, although there would be many to follow (e.g. Grant et al., 2013). They both bear some truth, but in the end are incomplete in their explanation of landscape evolution. However, they hypothesized how a landscape works from (field) observations, using inductive reasoning, a tool that remains valuable today when doing explorative fieldwork. The concept of the graded river was put forward by Mackin (1948).

This concept related the river profile to its base level, which acts as a downstream control on profile evolution.

With the increasing availability of information on past climate variability, from marine sediment records, ice cores and lacustrine records (e.g. Emiliani and Milliman, 1966; Lisiecki and Raymo, 2005; Tzedakis et al., 2006), the notion of climate change as an important driver in long-term landscape evolution became apparent. In addition, it became acknowledged that landscapes that are influenced by a constant driver (e.g. constant rainfall, constant uplift rate), display features like thresholds and complex response (Schumm, 1973). This non-linear response of landscapes to both constant and changing drivers has been the subject of many studies since. Another concept that relates to this is equifinality: similar landscapes can arise as a result of different processes and pathways. For instance, alternating aggradation-incision phases of a river system can be caused by climatic variation or base level change. To investigate which pathway led to the current landscape, field-based reconstruction can be used.

1.2 Field and dating based landscape reconstruction

1.2.1 Sedimentary archives: key pieces of the puzzle

In deposition-dominated environments such as marine basins, lakes, deltas, subsiding grabens and foreland basins, a stacked sedimentary record can reveal its depositional history. Texture (clay, silt, sand, gravel) can inform us on the available transport energy during which the sediment was deposited (low to high energy) or weathering conditions. The presence of fossils or pollen can inform us on palaeoclimatic conditions, while organic rich layers in deep water sediments can indicate climatic variation, and fine laminated lake varves show annual deposition phases. In erosion-dominated landscapes, such as uplifted plateaus, horsts, or mountain ranges, it is the preservation of certain landforms or depositional events in and along its valleys that inform us on its landscape history. For instance, under ongoing incision, remnants of an old river valley elevated above the current river level indicate its past valley floor or floodplain. Preserved sorted stratified sands and gravels indicate its former fluvial activity, while poorly sorted and structured sediments indicate debris flows or landslides. Calcium carbonate cementation or the presence of an organic rich topsoil within these deposits can show subsequent stable landscape and climatic conditions, while truncated soils or soils buried by slope or fluvial deposits indicate subsequent landscape instability. In time, erosion-dominated landscapes could have changed into deposition-dominated landscapes and vice-versa. For example, finding dissected lake sediments in an erosional landscape indicate major shift from depositional to erosional conditions, for example due to a dam breach event. Interpreting sedimentary records leads to a stratigraphy. Dating techniques can time these ancient deposits and landscape surfaces. This can link them to climatic periods and for instance allows calculation of incision rates.

1.2.2 Dating as a tool for landscape reconstruction

Dating possibilities of Quaternary materials and surfaces have increased rapidly. Methods used in this thesis are radiocarbon dating, feldspar luminescence dating and $^{40}\text{Ar}/^{39}\text{Ar}$ -dating. Radiocarbon dating of the time since death of organic material is at present possible until

~50 ka (Reimer et al., 2013). Luminescence dating is used to date the burial age of quartz or feldspars in sandy deposits, by measuring the amount of natural radiation the grains received from surrounding materials since they were last exposed to light. Feldspar luminescence dating can be applied to a range of ages, from young Holocene samples (Reimann and Tsukamoto, 2012) to ~400 ka (Buylaert et al., 2012), depending on dose rate (see Chapter 3 and 5 for further explanation). $^{40}\text{Ar}/^{39}\text{Ar}$ -dating can be used to date lava flows, ranging from young Holocene (Wijbrans et al., 2011) to no maximum, by measuring the amount of potassium-derived radiogenic argon built up since cooling time in a stepped-heating procedure (McDougall and Harrison, 1999). If lava flows filled river valleys, this estimates the time of potential damming of this valley and serves as a minimum age for underlying fluvial deposits (Maddy et al., submitted). Other commonly used dating techniques include cosmogenic nuclide dating, which can date the time since a surface has been exposed and its erosion rate (Gosse and Phillips, 2001) and ranges from 0.1 ka to > 1 Ma (Darvill, 2013). Ages of fluvial terrace abandonment using ^{10}Be have been determined up to ~700 ka (Rixhon et al., 2011; Viveen et al., 2012). U-series dating, which has a ~600 ka age range (Cheng et al., 2000) is used to date carbonate precipitation and can be used to date coral, travertines (e.g. Veldkamp and Kroonenberg, 1993) or calcretes (e.g. Candy and Black, 2009).

Age estimates have uncertainties at different levels. First, they have an analytical uncertainty. This can be quantified and is dependent on measurement precision and sample quality. Second, based on sample characteristics, an informed choice is made on which type of age model or statistic to use to calculate the age. For instance in luminescence dating one could look at either the Central Age Model or the Minimum Age Model, which is an informed decision based on the expectation that grains are either generally well-bleached, or partially well-bleached, given that no post-burial disturbance occurred (Galbraith et al., 1999). In $^{40}\text{Ar}/^{39}\text{Ar}$ -dating the total fusion age is the age derived from all measured radiogenic argon. However, the stepped heating procedure can reveal that part of the sample generates e.g. an older age, implying contamination by alteration or inheritance of radiogenic argon from not entirely molten crystals in the magma (McDougall and Harrison, 1999). If several consecutive steps which give statistically the same age are observed, an acceptable plateau age can be derived. These choices are usually driven by statistics of the data and can therefore be seen as well informed decisions. However, sample context and interpretation have to be well-conveyed, as uncertainties in interpretation add another uncertainty on top of these analytical uncertainties. Using multiple dating techniques in one study can be an advantage to cross-validate age results. Furthermore, they can complement each other in Quaternary landscape reconstruction studies and allow correlations to other areas.

1.3 Quaternary landscape reconstruction of Mediterranean catchments

The catchment under study in this thesis is located in the eastern Mediterranean. The catchments surrounding the Mediterranean have been formed as a result of the Cenozoic collision of the African plate and the Eurasian plate. The complex tectonic processes and structures resulting from this collision caused areas of uplift and subsidence. All Mediterranean basins have the legacy of the Messinian Salinity crisis, causing a huge drop in base level and triggering all systems to incise significantly during the Late Miocene. This was

followed by a large transgression during the Early Pliocene, burying the Messinian gorges and related landscapes (Schoorl and Veldkamp, 2003). Uplifted areas with fluvial terraces around the Mediterranean have been the subject of many studies, because their sedimentary record and palaeo reconstruction can provide insight in fluvial development since their initiation (Maddy et al., 2007), leading to increased understanding of how these systems respond to climatic and tectonic constraints.

1.3.1 Climate and tectonic drivers

Reconstruction of Mediterranean catchments has been focussed on correlation of Quaternary river terrace staircases of large and regional rivers. These staircases occur in many uplifting areas in the world and they record a climatically controlled incision history, suggesting a global uplift – incision activity (Bridgland and Westaway, 2008; Gibbard and Lewin, 2009). Additionally, Mediterranean-wide aggradation sequences of catchments of different size and tectonic setting are suggested to be correlated to Pleistocene climatic fluctuations (Macklin et al., 2002). These studies thus focus on global similarities of regionally uplifted areas, all showing a similar climatically driven fluvial incision response.

1.3.2 Local drivers

Besides research on terrace staircase correlation, studies have focussed on specific catchment response of uplifting river reaches or basins. These studies illustrated how the specific base level history and boundary conditions of catchments influenced their Quaternary evolution. For instance in tectonically active southeast Spain, catchment response occurred through river capture-driven accelerated incision waves which still migrate through the catchment at present (Mather et al., 2002). In another catchment in southeast Spain, tectonic tilting invoked headward erosion and drainage expansion (Stokes and Mather, 2003). Examples of specific catchment response to uplift include northwest Spain, where local tectonics influence local terrace formation and preservation (Viveen et al., 2013). A study in northwest Europe indicates diachronous terrace abandonment and knickpoint retreat of a Meuse tributary as a response to uplift (Demoulin et al., 2012).

Other studies indicate the response to damming events. For instance in the United States, where Quaternary evolution of the Owyhee River has been seriously influenced by multiple lava dams (Ely et al., 2012). A catchment in southeast Spain has been temporally dammed in the late Pleistocene causing disequilibrium conditions in the Holocene (Baartman et al., 2011). In the Upper Gediz River area in Turkey (the study area of this thesis, see section 1.5), a tributary catchment endured major drainage diversion due to Early Pleistocene lava damming, while the trunk river was only mildly disturbed. Thus, local drivers such as local tectonics, river capture and damming events can significantly influence long-term catchment evolution and these studies suggest that knowledge of local history of catchments is important before making any regional correlations to climatic or uplift curves. This does not only apply to smaller catchments, but to regional rivers such as the Gediz River as well.

1.3.3 Natural dams

Natural damming of rivers occurs worldwide and its impact on river evolution can be

significant (Costa and Schuster, 1988). Natural dams obstruct or divert water and sediment routing and create local base levels within river reaches (Burchsted et al., 2014). They can be formed due to biological activity, such as beaver dams (Levine and Meyer, 2014) or log jams (Wohl and Beckman, 2014), biochemical and hydrochemical systems such as travertine and tufa dams (Florsheim et al., 2013; Ordóñez et al., 2005; Özkul et al., 2014), ice, moraine and landslide dams (Korup and Tweed, 2007), volcanic edifices (Macaire et al., 1992), volcanic debris flows (Capra, 2007) and lava dams (Ely et al., 2012; Hamblin, 1990). Landslide dams are often short-lived (Ermini and Casagli, 2003) due to their composition of often unconsolidated materials. Dam longevity however, depends on their composition. Nevertheless, landslide and lava dams which have been stable for a longer duration occur and can impact river channel evolution at a 10^4 timescale (Ely et al., 2012; Korup et al., 2010). Natural dams often breach catastrophically, creating outburst floods which can exceed those of peak meteoric floods, resulting in significant geomorphic impact on the landscape (O'Connor et al., 2013). However, long-lived lava dams are reported to have been gradually removed (Ely et al., 2012) and long-term knickpoint persistence due to landslide damming and breaching occurs (e.g. Korup, 2013).

1.4 Landscape evolution modelling

In the second half of the past century, many researchers started quantifying “geomorphic transport laws”, which are mathematical expressions of physical principles that describe erosion or movement of material due to certain processes (e.g. Dietrich et al., 2003), and which can be used to deduce landscape change at a specific area. It was the start of the digital era that brought application and testing hypotheses and equifinality issues within reach. In the last three decennia, increased computer power resulted in the development of spatial simulation models, such as braided river models (Murray and Paola, 1994) or models of Aeolian dunes (Werner, 1995). In addition, the increased availability of high-quality Digital Elevation Models (DEMs, a digital representation of the landscape’s surface elevation) led to the development of Landscape Evolution Models (LEMs) (Tucker and Hancock, 2010). LEMs are computer models that simulate landscape change over time. Almost without exception, these models use simplified process-descriptions that do not do full justice to Newtonian physics. However, their outcomes often show sometimes unexpected complex features which can help conceptualizing an actual field situation. Examples are lagged response to an external driver (Temme and Veldkamp, 2009), dampening of external signals (Veldkamp and Tebbens, 2001), self-organised criticality of catchments (Van De Wiel and Coulthard, 2010) and spatially and topography driven complex erosion-sedimentation dynamics (Schoorl et al., 2014). Many LEMs use rectangular-gridded DEMs as an input, such as LEMs SIBERIA (Hancock et al., 2010) and CEASAR (Coulthard et al., 2005) and the LEM used in this thesis, LAPSUS (Schoorl et al., 2000; Schoorl et al., 2002). More elaborate reviews of LEMs can be found in Chapter 2 and 4.

1.4.1 LAPSUS landscape evolution model

The LAPSUS LEM was originally designed as a spatially explicit water runoff and erosion-deposition model (Schoorl et al., 2000; Schoorl et al., 2002). It is able to route water down using a multiple flow routine (Freeman, 1991; Quinn et al., 1991), in which water can be

divided over multiple downstream cells. To calculate a cell's capacity to erode, it uses the continuity equation, based on principles of Kirkby (1971), where potential sediment transport, or transport capacity, is depending on the product of waterflow to a power and slope to a power. This principle, and elaborations of this principle still underlie many long-term landscape evolution studies (e.g. Lague, 2014). Calculation of actual sediment in transport in LAPSUS is based on principles of (Foster and Meyer, 1972; Foster and Meyer, 1975), in which actual runoff erosion or deposition of a location depends on the amount of sediment already in transport compared with transport capacity. The resulting sediment available for erosion or deposition will then be partly eroded or deposited, depending on an erodibility or sedimentation factor. In LAPSUS, the use of this relation was extended to landscapes, demonstrating the importance of spatial erosion deposition patterns (Schoorl et al., 2002). It has since then been extended to be able to deal with processes such as tillage erosion (Schoorl et al., 2004), shallow landsliding (Claessens et al., 2005), creep, solifluction and biological and frost weathering (Temme and Veldkamp, 2009) and fluvial behaviour (Baartman et al., 2012a). Furthermore, an algorithm to deal with natural depressions has been added (Temme et al., 2006) and event-based modelling with an improved infiltration description has been pursued (Buis and Veldkamp, 2008). Detailed descriptions of LAPSUS can be found in Chapter 2, 4 and 5. For this thesis, LAPSUS has been enhanced to incorporate separate erodibility values for a 3D lava dam body (Chapter 2) and redistributed sediments (Chapter 4 and 5). Furthermore, the routine that deals with deposition in depressions has been enhanced to be able to deal with multiple outlets (Chapter 2).

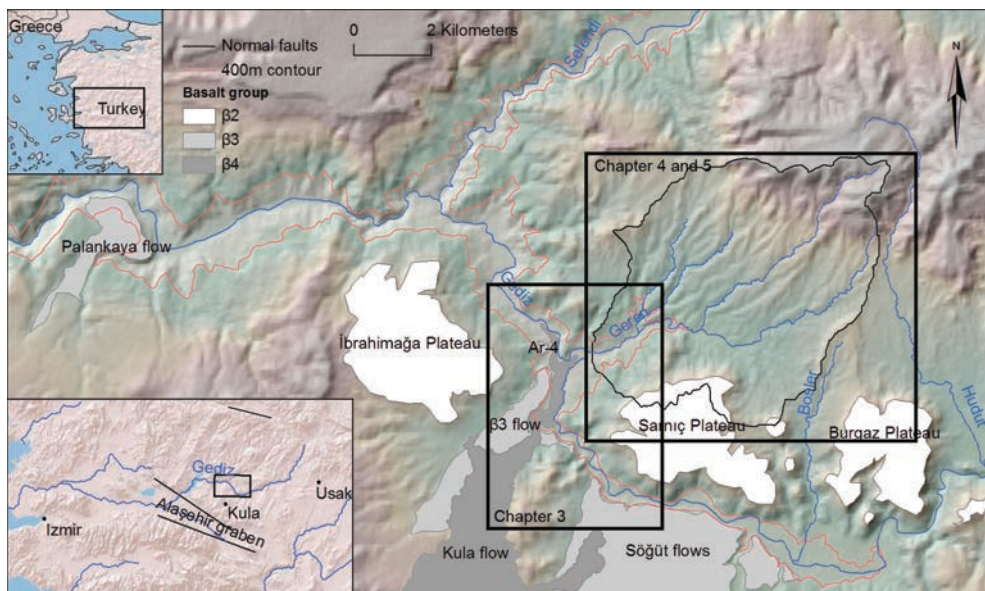


Fig. 1.1. Regional study area map. Rectangles depict extent of study sites of indicated Chapters.

1.5 Study area

Research was done in the Upper Gediz River stretch, located north of Kula (Manisa Province, western Turkey, Fig. 1.1). The Gediz River has formed a gorge in an uplifting footwall block of the Alaşehir graben and has cross-cut and incised into Miocene alluvial and lacustrine interior basin deposits, and it has locally exhumed meta-sedimentary basement rocks (Maddy et al., 2007). The area comprises a part of the Kula alkali volcanic field. In the first century, the Greek geographer Strabo visited the area, travelling upstream the Hermus River (the current Gediz) and described it as “Catacecaumene”, which means “burnt land”. In his translated description the area is described as follows: “The surface of the plains is covered with ashes, but the hilly and rocky part is black, as if it were the effect of combustion” (Falconer, 1903). However no historical account of active volcanism in the Kula area is known. Previous work showed that volcanism repeatedly produced lava flows which entered, filled and sometimes dammed the Gediz River in the early Pleistocene (Maddy et al., 2007; Maddy et al., 2012a), middle Pleistocene and Holocene (Bunbury et al., 2001) at consecutively lower levels due to river incision (Fig. 1.2). These levels were named β_2 , β_3 and β_4 , respectively (Richardson-Bunbury, 1996). This caused the formerly valley-filling basalt to remain as plateaus and ridges, creating a stepped relief-inverted landscape. Incision by the Gediz since 1 Ma has been around 140 m, and tributaries had to respond to this incision. The confluence of a small tributary, the Geren, with the Gediz River is located in the area where multiple lava flows are observed along the present river bed, suggesting that this tributary has been dammed by these lava flows. The Gediz stretch upstream of this confluence and the Geren Catchment were the main study sites in this research. The current landscape of the Geren consists of a ridge-gully landscape, where gently sloping palaeo surfaces are steeply dissected by gullies, sometimes leading to a badland morphology. The altitude of the study area ranges from around 300 to 850 m. Current average annual precipitation is around 600 mm with dry summers and wet winters. Average annual temperature is 15 °C, with hot summers and cold winters with a possibility of snowfall.

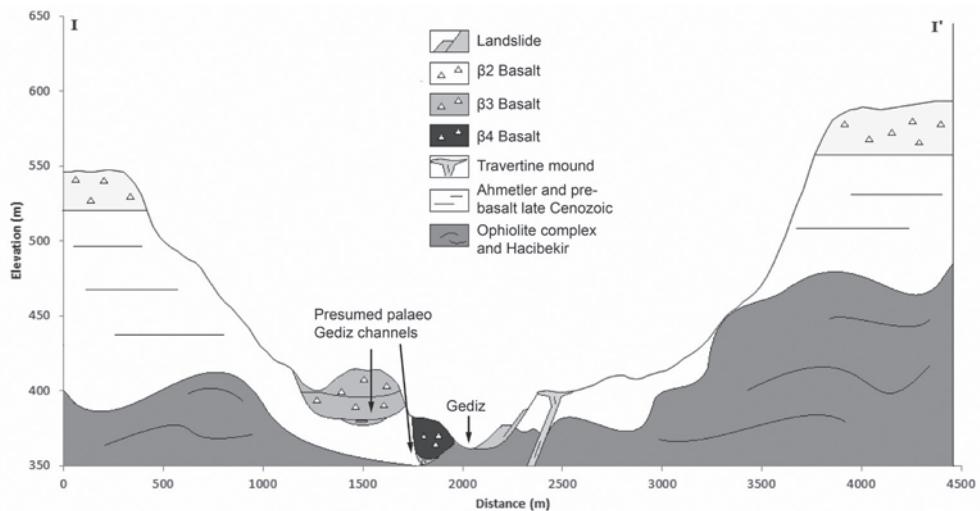


Fig. 1.2. Schematic cross-section through the Gediz valley. See Fig. 3.3 for its location.

1.6 Aim and research questions

Several studies thus emphasize the importance of local history of a catchment on Quaternary timescales, and the influence past events can have on current catchment evolution (Mather et al., 2002). Past lava damming events are a good example of such a past event as they can be long-lived and can exert a long-term influence on catchment evolution (Ely et al., 2012; Maddy et al., 2012a). The Quaternary evolution of the Geren Catchment has been influenced by lava damming events which influenced its base level. However, catchment response is unknown. Field-based landscape reconstruction and landscape evolution modelling are two methodologies to approach this problem (*cf.* Temme, 2008). These two approaches are combined to unravel landscape evolution on a 10^5 ka timescale.

In this thesis, both inductive, explorative fieldwork-based landscape reconstruction and deductive, geomorphic-transport-law-based landscape evolution modelling are conducted and combined to understand landscape evolution since the middle Pleistocene of a Mediterranean upland catchment (the Geren Catchment) that has endured multiple lava damming events. The following sub-objectives and research questions were formulated:

1. Simulate the impact of natural damming on upland catchment evolution.
 - What is the impact of damming on net erosion?
 - How are planform stream routing and longitudinal stream profiles affected through time?
 - Is this response influenced by dam and landscape substrate, and if so, how?
 - Do these results relate to field situations and how?
2. Investigate the impact of Holocene lava damming and breaching on adjacent Gediz and Geren reaches.
 - What was the age and duration of the Holocene damming event?
 - What was Gediz River and Geren Catchment response to damming?
 - How did breaching occur and what was the Gediz River and Geren Catchment response?
3. Simulate the long-term response of a small tributary catchment on multiple damming events in relation to 300 ka of gradual base level lowering.
 - What is the effect on net erosion?
 - What is the effect on longitudinal profile evolution?
 - What is the effect on spatial patterns of net erosion and sediment storage?
4. Reveal lava dam-influenced base level evolution of the Geren Catchment since the middle Pleistocene and unravel Geren Catchment response to this evolution.
 - Can palaeo-Gediz levels and lava damming events be identified and age-constrained?
 - Can palaeo-Geren levels be identified and age-constrained?
 - How did base level at the Geren Catchment outlet evolve since the identified damming events?
 - What was the Geren Catchment evolution, based on fieldwork evidence?
 - What is the Geren Catchment evolution, based on its base level evolution and landscape evolution modelling?

1.7 Thesis outline

The scope of this thesis spans an array of fieldwork and modelling approaches (Fig. 1.3). Chapter 2 is a model study based on an artificial catchment and presents results which demonstrate different responses to differences in dam and substrate erodibility. Chapter 3 contains fieldwork results only, leading to a conceptual diagram of dam response. Chapter 4 is a modelling study, already closer to our field situation and where response of a catchment is modelled by changing uplift and damming as external drivers. Chapter 5 shows an integrated approach, where fieldwork yields chronostratigraphical control and some initial conclusions. Modelling subsequently uses these results and gives insight in potential mechanisms of chronostratigraphy. Another way to subdivide Chapters is their applicability. Chapter 2 is the least related to a specific field situation, and its conclusions can be taken to be the most conceptual, followed by Chapter 4. Chapter 3 and 5 are the most specific to the fieldwork area.

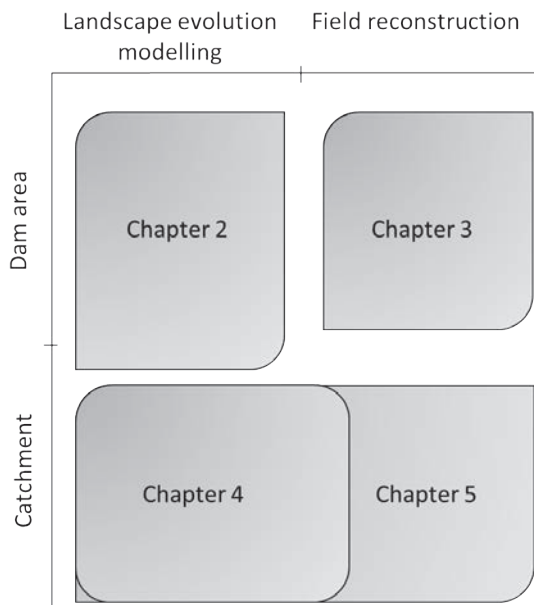


Fig. 1.3. Thesis outline.



Chapter 2

Landscape evolution modelling of naturally dammed rivers

Natural damming of upland river systems, such as landslide or lava damming, occurs worldwide. Many dams fail shortly after their creation, while other dams are long-lived and therefore have a long-term impact on fluvial and landscape evolution. This long-term impact is still poorly understood and landscape evolution modelling can increase our understanding of different aspects of this response. Our objective was to simulate fluvial response to damming, by monitoring sediment redistribution and river profile evolution for a range of geomorphic settings. We used landscape evolution model LAPSUS, which calculates runoff erosion and deposition and can deal with non-spurious sinks, such as dam-impounded areas. Because fluvial dynamics under detachment-limited and transport-limited conditions are different, we mimicked these conditions using low and high erodibility settings, respectively. To compare the relative impact of different dam types, we evaluated five scenarios for each landscape condition: one scenario without a dam and four scenarios with dams of increasing erodibility. Results showed that dam-related sediment storage persisted at least until 15000 yr for all dam scenarios. Incision and knickpoint retreat occurred faster in the detachment-limited landscape than in the transport-limited landscape. Furthermore, in the transport-limited landscape, knickpoint persistence decreased with increasing dam erodibility. Stream capture occurred only in the transport-limited landscape due to a persisting floodplain behind the dam and headward erosion of adjacent channels. Changes in sediment yield variation due to stream captures did occur but cannot be distinguished from other changes in variation of sediment yield. Comparison of the model results with field examples indicates that the model reproduces several key phenomena of damming response in both transport-limited and detachment-limited landscapes. We conclude that a damming event which occurred 15000 yr ago can influence present-day sediment yield, profile evolution and stream patterns.

Published as: Van Gorp, W., Temme, A.J., Baartman, J.E., Schoorl, J.M., 2014. Landscape Evolution Modelling of naturally dammed rivers. *Earth Surface Processes and Landforms*.

2.1 Introduction

Natural damming of upland river systems occurs worldwide (Costa and Schuster, 1988; Korup, 2002). Dams can be formed by landslides, volcanic edifices and lava flows, ice and glacial landforms such as moraines (Costa and Schuster, 1988; Korup and Tweed, 2007; O'Connor et al., 2013), fluvial activity such as levees or alluvial fans and bio- and hydrochemical systems such as travertine (Florsheim et al., 2013). Landslide dams are the most common dam type, occurring worldwide in high relief areas (Costa and Schuster, 1988). Landslides mostly are triggered by tectonic activity, intense rainfall or snowmelt events, as well as volcanic activity (Capra, 2007). Landslide dams are often short-lived and fail catastrophically within weeks (Costa and Schuster, 1988; Walder and O'Connor, 1997; Ermini and Casagli, 2003). However, longer-lived dams do occur and these can have a prolonged effect on fluvial evolution (Korup et al., 2006, 2013). Landslide dam stability largely depends on dam height, volume, material properties and the water influx into the dammed area (Costa and Schuster, 1988; Ermini and Casagli, 2003). Small dams made of loose matrix-supported debris flow material blocking a large catchment will be short lived, while large dams consisting of large blocks have longer lifespans (e.g. Capra, 2007). Other dams that generally have higher longevity are lava dams. These are not as widespread as landslide dams, but they can have significant impact on local or regional catchment evolution due to their relatively high longevity. Examples of lava dams and their effects are found along the Allier River in France (Macaire et al., 1992), the Tana River in Kenya (Veldkamp et al., 2007; 2012), the Gediz River in Turkey (Maddy et al., 2012a; Van Gorp et al., 2013) and the Colorado River (e.g. Hamblin, 1990; Dalrymple and Hamblin, 1998; Fenton et al., 2004, 2006; Crow et al., 2008) and Owyhee River in the U.S.A (Ely et al., 2012). A conceptual model of lava dam types presented in Crow et al. (2008) indicates the relatively long-lived nature of massive lava dams against the short-lived nature of more permeable dams. It must be noted however that if dam seepage equals inflow in the impoundment, lake filling does not occur, hampering dam destruction. The result of damming can be either partial or complete blocking of a river valley. For landslide dams, several types of blocking have been defined (Costa and Schuster, 1988), which can be extended to other dam types such as glacial or lava dams. For instance, a dam can fill a valley along its axis and block tributary valleys as well, block the same river at multiple locations or occur as a combination of these examples.

The response of the fluvial system to damming can include rapid dam removal, lake formation, drainage rearrangement, backwater aggradation and lake siltation. The dam can become a temporary local base level for a river expressed as a knickpoint in the river profile. These knickpoints can persist due to bed armouring by large blocks (Korup et al., 2006) and in mountainous areas, they are known to last up to 10^4 a (Korup et al., 2006, 2010). Persistence of sediment wedges could create hillslope-channel decoupling due to more complex landscape morphology (e.g. Baartman et al., 2013a), while erosion of these sediments after dam removal can create downstream aggradation, unpredictable sediment yields and river profile evolution. So far, analysis of catchment response to dams of various size and origin has mainly been done by field-based reconstruction studies (e.g. Korup et al., 2006; García-García et al., 2011). These studies are valuable, but often restricted to specific cases, limiting wider applicability. Damming also emerged as a controlling factor in some Quaternary catchment reconstruction studies (e.g. Baartman et al., 2011; Maddy et al., 2012a; Veldkamp et al., 2012; Van Gorp et al., 2013), even though the exact dams or dam locations have not always been found.

Despite these advances, there is insufficient understanding of which response follows which type of damming. Landscape evolution models (LEMs) can perform structured experiments that may provide such understanding. LEMs are nowadays widely used to understand and quantify landscape response to driving factors or to simulate internal complexity and process interactions. Several studies demonstrated complex landforms emerging from relatively simple drivers or process interactions. Examples are model studies on river-vegetation interaction (Murray and Paola, 2003), hillslope-river coupling for experimental catchments (Baartman et al., 2012a) and interaction of several mass movement processes and water flow interaction for an actual landscape (Temme and Veldkamp, 2009). At the same time, landscape evolution modelling still faces challenges to improve functionality and areas of application (Tucker and Hancock, 2010; Temme et al., 2011a). Landscape evolution modelling has not yet been applied to simulate response to damming. To simulate this response, two important aspects need to be incorporated in a LEM: adequate depression filling routines to deal with creating and filling depressions and incorporation of lithological boundaries between dams and the underlying substrate.

Since dammed landscapes involve natural depressions (e.g. lake formation), modelling these landscapes should include a routine to naturally deal with depressions. Water flow has to be routed to the depression outlet and sediments entering the depression should be deposited below water level. Several LEMs have a routine to deal with depressions dynamically (e.g. CHILD (Tucker et al., 2001), CEASAR (Coulthard et al., 1998) and LAPSUS (Temme et al., 2006)). The routine in LAPSUS is arguably most advanced because it allows for the formation of simplified deltas in depressions and for the fragmentation of depressions. With these routines, researchers have used LEMs to study the impact of depressions on catchment evolution (Hancock, 2008; Temme et al., 2011a).

It is our objective to provide structural understanding of catchment response to long-lived dams with a LEM that has been adapted for this purpose. Our main research questions are:

- What is the impact of long-lived dams on sediment redistribution?
- What is the impact of long-lived-dams on river profile evolution?
- How do different dam and substrate erodibilities influence these results?

To achieve our objective, idealised dams in a small, idealised catchment are used in simulations of catchment response.

2.2 Methods

2.2.1 Model

We selected LEM LAPSUS for this study, due to its advanced sink-filling routines, which will be discussed below. For further discussion on different LEMs the reader is referred to recent reviews by Tucker and Hancock, (2010) and Temme et al., (2013). LAPSUS is a cellular automaton model that simulates runoff erosion and deposition (Schoorl et al., 2000, 2002), landsliding (Claessens et al., 2005, 2007), weathering, creep and solifluction (Temme and Veldkamp, 2009) and which can mimic fluvial behaviour (Baartman et al., 2012a). To limit

the added effect of process interaction and complexity, we only used the runoff erosion and deposition process. LAPSUS deals with non-spurious sinks, which either could be small sinks in river channels or large lake-sized sinks (Temme et al., 2006). This last capability is particularly interesting for this study and is generally lacking in other LEMs. Below, the different model routines that are important for this study are discussed.

2.2.2 Water erosion and deposition

Water and sediment are routed down from each cell to its downstream neighbours using the multiple flow algorithm (Freeman, 1991; Quinn et al., 1991). Sediment transport capacity C (m) over time t (yr) and space s (m) between two cells is then calculated from the fractional discharge Q (m) and tangent of slope Λ (-) (Kirkby, 1971):

$$C_{s,t} = Q_{s,t}^m \cdot \Lambda_{s,t}^n \quad (2.1)$$

Parameters m and n are the discharge and slope exponent, respectively (Kirkby, 1987). The amount of sediment that will be transported is then calculated using (Foster and Meyer, 1972, 1975):

$$S_{s,t} = C_{s,t} + (S_{0,s,t} - C_{s,t}) \cdot e^{-cellsize/h} \quad (2.2)$$

where sediment in transport S (m) over one *cellsize* length is a function of transport capacity C and erodibility or sedimentation factor h (m), compared with the amount of sediment already in transport S_0 (m). If there is more sediment in transport than the transport capacity, deposition will occur and sedimentation factor h is calculated as follows:

$$h_{s,t} = \frac{C_{s,t}}{P_{s,t} \cdot Q_{s,t} \cdot \Lambda_{s,t}} \quad (2.3)$$

where P (m^{-1}) is a sedimentation factor. If sediment already in transport is smaller than transport capacity, erosion will occur and h is calculated as follows:

$$h_{s,t} = \frac{C_{s,t}}{K_{s,t} \cdot Q_{s,t} \cdot \Lambda_{s,t}} \quad (2.4)$$

where K (m^{-1}) is an erodibility factor. Both K and P are lumped factors, representing surface characteristics of a gridcell. This parameter is not an empirical value such as USLE based K -factors. However, it determines the detachment capacity of a cell (Schoorl and Veldkamp, 2001) and has been used as a calibration factor in many previous studies with LAPSUS, both in studies of actual landscapes (Schoorl et al., 2002, 2004; Temme et al., 2009; Temme and Veldkamp, 2009; Baartman et al., 2012b) as well as in experimental studies (Baartman et al., 2012a). Factors K and P can have different values (Temme and Veldkamp, 2009), however, they are kept equal in this study for simplicity. A combination of a low K and P implies that the substrate is hard to erode, but as soon as sediment is in transport, it is hard to deposit again. This mimics detachment limited conditions. On the other hand, a combination of a high K and P implies that sediment is easy to erode but also easy to deposit, mimicking transport-limited conditions. Furthermore, since sedimentation depends on the amount of sediment in transport, if the erodibility is low, a high sedimentation factor does not necessarily mean high

sedimentation. In this study, K and P of the dam body can be set at a different value than the surrounding and underlying substrate.

2.2.3 Sedimentation routine

An important algorithm in LAPSUS is the sedimentation routine. The sediment in transport that can be deposited according to equation (2.2) is not actually deposited in all cases. To avoid the creation of unrealistic spikes, the amount of sediment that is deposited depends on the lowest higher neighbour of the cell considered. If this amount exceeds the elevation difference between the current cell and its lowest higher neighbouring cell, excess sediment in transport will be “smeared” down using a steepest descent smearing routine, until all the sediment in transport has been deposited. If there is still sediment left after the smearing routine has reached the furthest downstream cell (usually the outlet of the catchment), the remaining sediment will be added to the sediment in transport of the original receiving cell, where it can be transported in the conventional way in the next timestep. This routine mimics annual sediment transport distance and is an effective way to avoid spikes, however, it is acknowledged that sediment can be transported unrealistically far within one timestep, especially in flat areas, such as backwaters or deltas. This routine is explained into more detail in Schoorl et al. (submitted).

2.2.4 Depression fill routine

The depression fill routine in LAPSUS is presented and discussed in Temme et al. (2006). In summary, LAPSUS deals with depressions by first defining the extent of all depressions and their outlet(s). Then it collects all the water and sediment flowing into a depression from its contributing area. In this study, it is assumed that a depression is filled with water at the start of the simulation, thus, that the lake is filled up to the outlet elevation. Therefore all water and sediment is routed to and equally divided over the depression’s outlet(s). This capability to deal with multiple outlets was developed for this study and was not yet described in Temme et al. (2006). As long as the depression has not been filled up with sediments, the depression outlets cannot be eroded and catastrophic failure at the outlet of an impounded area also does not occur. The model therefore only removes dam outlets by gradual incision after infilling. In this way, the role of sediment as an abrading tool at the depression outlet is taken into account (Cowie et al., 2008; Ely et al., 2012).

If a depression has a volume smaller than the total incoming sediment, it is completely filled with sediment, to an almost-flat surface, draining to each of the depression’s outlets. The steepness of this surface is user-specified and corresponds to Planchon and Darboux’s (2002) epsilon variable. The water volume that is displaced by sediment in the depression is added to the water flow draining from that depression.

If a depression has a volume larger than the total incoming sediment, sediment is deposited in deltas growing from every side-cell of the depression, with user-specified underwater steepness.

2.2.5 Boundary condition at outlet

The boundary condition used in this study is that the catchment outlet cell, thus the lowest cell at the edge of the DEM, is not considered for erosion or deposition. It therefore will never erode or deposit according to equations (2.1 – 2.4) and thus forms a base level of the catchment. However, sediment can be deposited on this lowest cell due to the sedimentation smearing routine. This potential base level rise can have implications on landscape evolution of the upstream area. We have minimized these implications by extending the experimental catchment significantly downstream of the dam edge.

2.2.6 Experimental design

Because the distinction between landscapes and rivers having detachment-limited and transport-limited conditions is often made (e.g. Tucker, 2009), we chose to study response to damming under these two landscape conditions. Additionally, the erodibility of the dam has been varied in four steps in each landscape to represent weakly and strongly erodible dams. Two additional simulations were done on low-erodibility and high erodibility landscapes without a dam. This resulted in a total of ten scenarios (Table 2.1).

In LAPSUS, the scenarios were translated into changes of the erodibility (K) and sediment potential (P) values (Table 2.1). The values used are within the range of calibrated K and P values used in literature (Schoorl et al., 2002, 2004; Temme and Veldkamp, 2009; Baartman et al., 2012a). For all simulations, annual rainfall was 700 mm, with an infiltration loss of 150 mm and a total evaporation loss of 350 mm. This conforms to a Mediterranean climatic setting. All 10 scenarios were run for 15000 yr to be able to record response to damming on a relevant timescale (Korup et al., 2010). Furthermore, landscapes were in a transient (i.e. non-equilibrium) state. The reason for this is that transient conditions may be the norm rather than the exception in landscape evolution (Tucker, 2009). Especially smaller tributary catchments, such as our experimental catchment, are often observed to be in transient condition in reaction to a base level perturbation (e.g. Snyder et al., 2003). Although we acknowledge that differential basin scale transient response might obscure dam perturbations, our starting landscape for both the detachment-limited and transport-limited landscape will be the same, which would not be the case if we first brought both these landscapes into equilibrium conditions.

Table 2.1. Simulated scenarios.

Scenario	K and P substrate	K and P dam
<i>A: transport limited</i>		
A0: no dam	0.0003	-
A1: K and P dam << K and P substrate	0.0003	0.000003
A2: K and P dam < K and P substrate	0.0003	0.00003
A3: K and P dam = K and P substrate	0.0003	0.0003
A4: K and P dam > K and P substrate	0.0003	0.003
<i>B: detachment limited</i>		
B0: no dam	0.00003	-
B1: K and P dam < K and P substrate	0.00003	0.000003
B2: K and P dam = K and P substrate	0.00003	0.00003
B3: K and P dam > K and P substrate	0.00003	0.0003
B4: K and P dam >> K and P substrate	0.00003	0.003

2.2.7 Experimental input DEM

The artificial input DEM (Fig. 2.1) is based on the DEM designed for the study of Baartman et al. (2012a). It measures 2100 x 6000 m with a resolution of 20 m (31500 cells). Compared to the DEM of Baartman et al. (2012a), slopes and profile gradients were steepened to create a simple, confined valley which is more suitable to model response to damming. It has a profile gradient around 12.5% in the upper part and 1.5% in the lower part and resembles a small upland catchment. The elevation range is 470 m. The dam was designed with two equally high outlets, 14.5 m above the deepest point of the valley at the dam location. One outlet routes over the dam body and the other outlet routes around the dam, where the dam and substrate touch. These locations were chosen to create the opportunity for incision to occur through the substrate or the dam, as both are observed in the field (Ouimet et al., 2008; Korup et al., 2010). The route over the dam drops down once it passes the dam, whereas the route along the dam has a longer pathway and a more gentle slope back towards the valley floor. The equal elevation of both outlets was designed in this way to test the effect of different erodibilities on the development of flow routing.

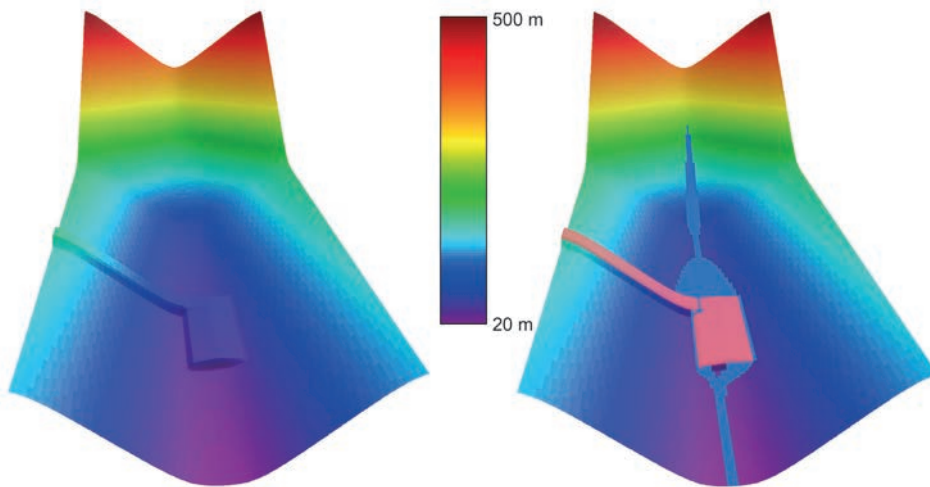


Fig. 2.1. Left: visualisation of DEM used for model simulations with LAPSUS. Right: Same DEM, dam body is highlighted in pink, areas with highest flow accumulation at $t = 1$ are added. Two spillways are visible, one over the dam (left) and one around the dam (right).

2.2.8 Evaluation characteristics

The following catchment characteristics were recorded from model simulations for evaluation of results.

1. Lake fill speed
2. Net erosion from the catchment
3. Drainage rearrangement
4. River profile development
5. Occurrence of phenomena derived from different field based and conceptual studies on fluvial response to natural damming.
6. Sediment storage on a cell

To be able to record sediment storage on a cell, a new capacity was added to the model. For each cell the minimum elevation since the start of the simulation is stored and subtracted from the current DEM. Unlike a map of cumulative net change in altitude, this records sedimentation locations and thicknesses even if the cell has experienced net erosion since the start of the simulation.

2.3 Results

2.3.1 Annual net erosion

Total annual net erosion varies between 40 and 100 Mg ha⁻¹ for the A-scenarios (high erodibility, transport-limited) and between 4.0 and 13.0 Mg ha⁻¹ for the B-scenarios (low erodibility, detachment-limited). For all scenarios, net erosion decreases over time (Fig. 2.2), which is because average slope is declining over time. Annual net erosion values of the A-scenarios are highly variable due to complex behaviour of sediments in transport which are repeatedly eroded and deposited within the catchment. Annual net erosion of the B-scenarios shows less variation, although variation increases for scenarios B3 and B4, which have more erodible dams. Introducing a more erodible surface, in other words introducing transport limited conditions, thus increases the variation of net erosion values. The duration of lake filling by sediments is around 50 yr for the transport-limited A-scenarios and around 400 yr for the detachment-limited B-scenarios (Table 2.2). This is due to the difference in sediment supply to the lake. The cumulative net erosion after 10000 and 15000 yr is always lower for the dam scenarios than for the non-dam scenarios, indicating a consistent long-term sediment storage effect.

This sediment storage effect is different for each dam scenario. Cumulative net erosion values and the amount of sediment stored in the originally inundated dam area are shown in Table 2.2. Total net erosion values of scenarios A3 and B2 (K, P dam = K, P substrate) differ least from their non-dam scenarios, respectively. For the transport-limited A-scenario, net erosion of A2 (K, P dam < K, P substrate) differs the most with A0 (no dam), whereas for the detachment-limited B-scenario, B3 at 10000 yr (K, P dam > K, P substrate) and B4 at 15000 yr (K, P dam \gg K, P substrate) differ the most with B0 (no dam). These differences reflect the summed effect of differential evolution of water and sediment routing as a complex response to initial erodibility.

2.3.2 Water and sediment routing evolution

Maps of flow accumulation, cumulative erosion and locations and thickness of sediments are shown for 1000, 5000 and 10000 yr for all dam scenarios and 15000 yr for the A-scenarios only because the B-scenarios at 15000 yr do not provide more information except for additional incision (Fig. 2.3 and Fig. 2.4). Green colours on the map indicate the thickness of redeposited sediment at a certain location. Note that these green colours can also occur on cells with net erosion. Yellow to red colours indicate low to high net erosion in the case that no sediment is present on that cell. In all dam scenarios, most of the catchment surface is only eroding. However, sedimentation is clearly visible upstream of the dammed area. In some cases, water routing over this filled area shows bifurcations and the course of the trunk stream changes over time. Sedimentation is also visible in some of the main channels and sediment storage locations vary over time. All scenarios still have notable dam remains at 15000 yr. In scenario A4 (K, P dam > K, P substrate), the dam is highly erodible and more erodible than the landscape, leaving only a very small part of the dam crest not entirely removed. In all scenarios, a large portion of the sediment initially deposited in the lake remains stored in the landscape at the end of the simulation (See Table 2.2). Scenario A1 even has more sediment

storage in the filled lake at 15000 yr compared with sediment storage at the time of lake filling, indicating net sedimentation since lake filling.

Scenario A1 ($K, P_{\text{dam}} \ll K, P_{\text{substrate}}$) shows the initial establishment of the trunk stream around the dam where it will remain until 15000 yr. Scenario A2 ($K, P_{\text{dam}} < K, P_{\text{substrate}}$) shows initial establishment of the trunk stream over the dam. Rerouting of the stream from over the more resistant dam to around the dam over the less resistant substrate occurs just after 10000 yr.

Scenario A3 ($K, P_{\text{dam}} = K, P_{\text{substrate}}$) shows initial establishment of the stream around the dam followed by stream rerouting 15 yr later. At $t = 15000$ yr, the trunk stream is routed around the dam. However, three stream reroutings have taken place between 7700 and 12250 yr (see Table 2.2). After the last rerouting, two periods of active headward erosion take place (Table 2.2), which coincide with two periods of increased variation of net erosion (Fig. 2.2). Scenario A4 ($K, P_{\text{dam}} > K, P_{\text{substrate}}$) also shows initial stream routing over the dam, followed by 4 reroutings in the period from 4000 to 8000 yr. These events do not coincide exactly with periods of increased and decreased variation of net erosion. Detachment-limited scenarios B1 ($K, P_{\text{dam}} < K, P_{\text{substrate}}$), B2 ($K, P_{\text{dam}} = K, P_{\text{substrate}}$) and B3 ($K, P_{\text{dam}} > K, P_{\text{substrate}}$) establish their initial channel around the dam (Fig. 2.4). They subsequently incise to form a gorge and remain in their initial location until the end of the simulation. Scenario B4 ($K, P_{\text{dam}} \gg K, P_{\text{substrate}}$) establishes its initial channel through the dam and creates a gorge where the channel remains until the end of the simulation.

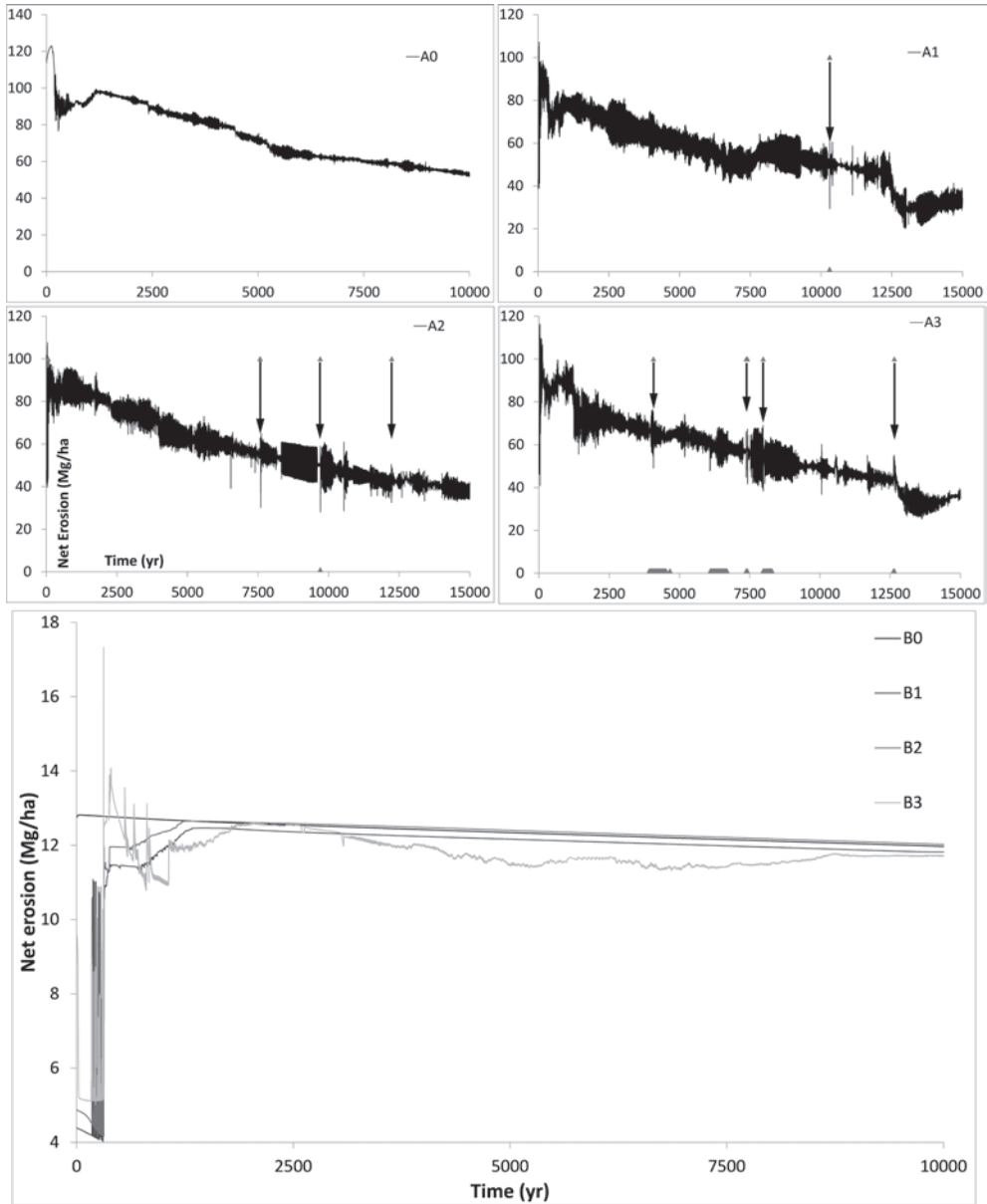


Fig.2.2. Annual net erosion. Left: A-scenarios, high erodibility and sedimentation factor, representing transport-limited conditions. Arrows indicate the moments of stream captures. Red traces below timeseries line indicate periods of diverging water flow on top of lake fills. Right: B-scenarios, low erodibility and sedimentation factor, representing detachment-limited conditions.

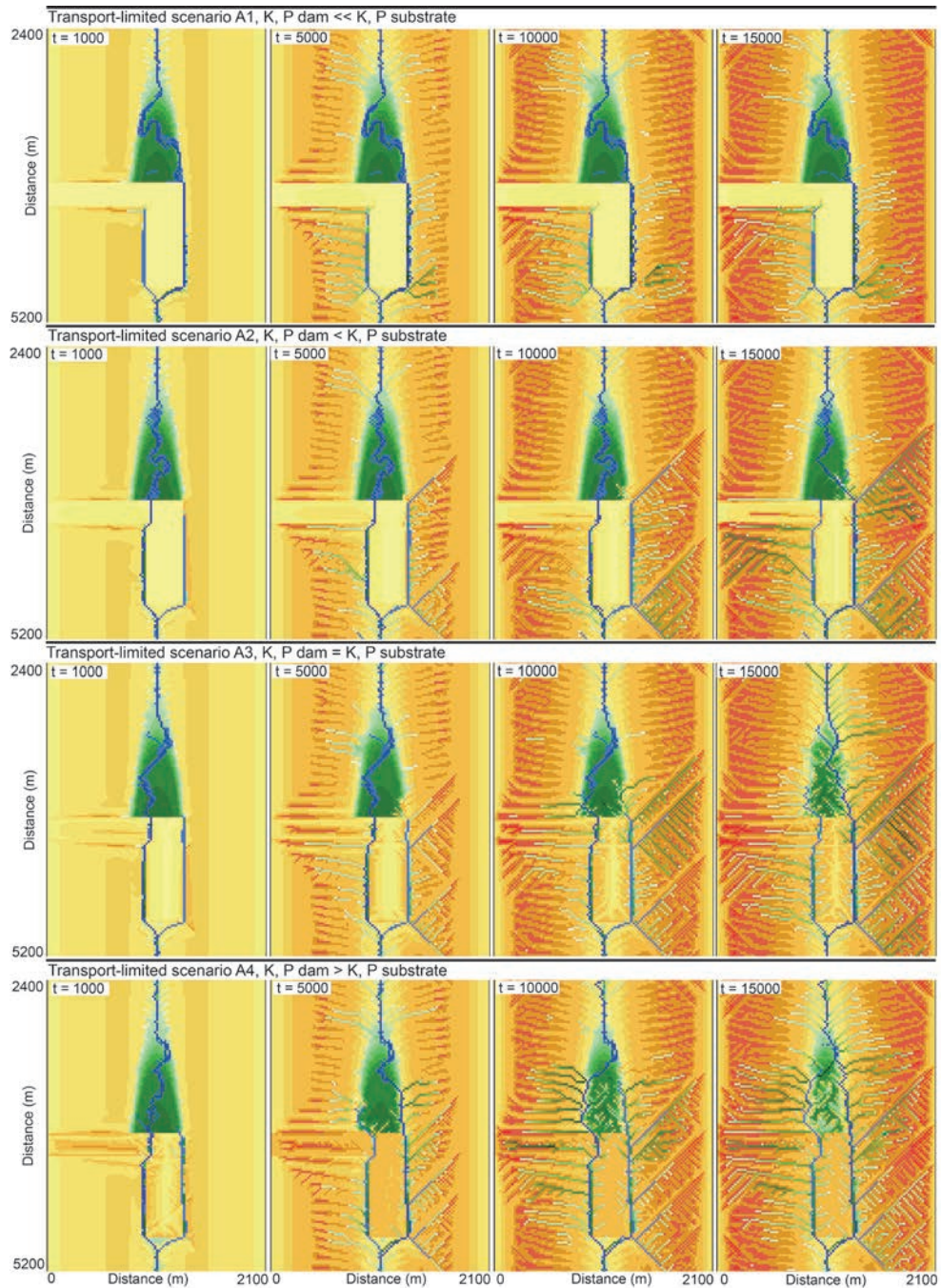


Fig. 2.3. Output maps of transport-limited scenarios A1 – A4 for the reach between 2400 m and 5200 m at different timesteps showing spatial evolution of the catchment reach around the dam. Cumulative erosion (yellow to red), sediment storage (green) and main water routing channels (blue) are depicted. Note distance labels attached to the top-left figure.

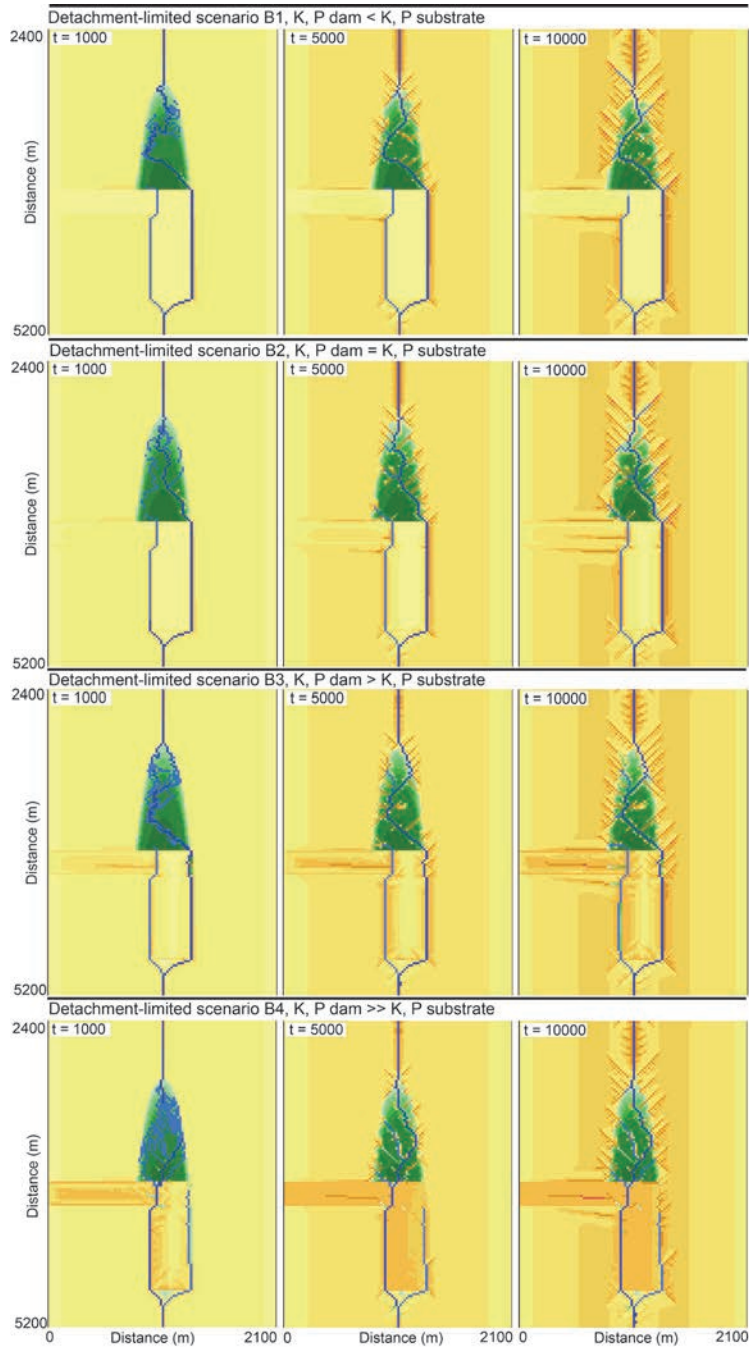


Fig. 2.4. Maps of detachment-limited scenarios B1 – B4 for the reach between 2400 m and 5200 m at different timesteps, showing spatial evolution of the catchment reach around the dam. Cumulative erosion (yellow to red: low to high), sediment storage (green) and main water routing channels (blue) at different timesteps are depicted. Note the distance labels attached to the top-center figure.

Table 2.2. Total net erosion and sequence of events.

Scenario	Outlet elevation (m)	Total net erosion (Mg/ha)		Lake sediment storage (m ³)		Event	Time (yr)	Channel through or around dam?
		t=10000	t=15000	t lake filled	t = 15000			
A: transport-limited								
<i>Scenario A0: No dam</i>								
	22.7	743190	975152		-			
<i>Scenario A1: K and P of dam 100 times smaller than K and P of substrate</i>								
	22.8	631859	833043	2.06E+06	2.10E+06	Lake filled	t = 44	Around
<i>Scenario A2: K and P of dam 10 times smaller than K and P of substrate</i>								
	24.2	623764	822341	2.08E+06	1.90E+06	Lake filled	t = 64	Through
						Capture	t = 10305	Around
<i>Scenario A3: K and P of dam equal to K and P of substrate</i>								
	24.2	662220	875873	2.08E+06	1.18E+06	Lake filled	t = 57	Around
						Capture	t = 67	Through
						Capture	t = 7700	Around
						Capture	t = 9705	Through
						Capture	t = 12239	Around
						headward erosion	t≈12800	Around
						headward erosion	t≈14200	Around
<i>Scenario A4: K and P of dam 10 times larger than K and P of substrate</i>								
	21.2	648822	852381	2.08E+06	1.05E+06	Lake filled	t = 44	Through
						Capture	t = 4082	Around
						Capture	t = 7381	Through
						Capture	t = 7421	Around
						Capture	t = 7984	Through

Table 2.2. (continued)

Scenario	Outlet elevation (m)	Total net erosion (Mg/ha)		Lake sediment storage (m ³)		Event	Time (yr)	Channel through or around dam?
		t=10000	t=15000	t lake filled	t = 15000			
B: detachment-limited								
<i>Scenario B0: No dam</i>								
	17.9	123543	182492		-			
<i>Scenario B1: K and P of dam 10 times smaller than K and P of substrate</i>								
	17.9	118430	176684	2.05E+06	1.30E+06	Lake filled	t = 383	Around
<i>Scenario B2: K and P of dam equal to K and P of substrate</i>								
	17.9	121000	180218	2.07E+06	1.16E+06	Lake filled	t = 385	Around
<i>Scenario B3: K and P of dam 10 times larger than K and P of substrate</i>								
	20.0	116292	175270	2.05E+06	1.21E+06	Lake filled	t = 347	Around
<i>Scenario B4: K and P of dam 100 times larger than K and P of substrate</i>								
	20.0	120565	172618	1.78E+06	1.14E+06	Lake filled	t = 252	Through

2.3.3 Profile evolution

For all scenarios, the longitudinal profile mostly shows net incision over time (Fig. 2.5). Aggradation occurs upstream of the dam and knickpoints are generated at the dam outlet, generally migrating backwards.

The longitudinal profiles of the A-scenarios show less deep incision than the B-scenarios. The zoomed-in section of longitudinal profiles between 2000 m and 5000 m distance along the valley axis (Fig. 2.5), shows profile evolution around the dam location. The A0 scenario (no dam) shows that this part of the profile remains at a constant level after 1000 yr. For the other A-scenarios, trunk stream incision upstream of the dam is more than 20 m less than in the A0 scenario. Scenario A1 (K, P dam $\ll K, P$ substrate) shows the profile of the route around the dam. At the dam location, a set of stepped knickpoints is created which remain quite stable throughout the 15000 yr. Scenario A2 and A3 show 1.5 to 2 m higher elevation at the outlet than A0 (Table 2.2), which is due to higher aggradation. Scenario A2 (K, P dam $< K, P$ substrate) shows a steep drop near the resistant dam spillway until 10000 yr. At 15000 yr, which is 5000 yr after stream capture occurred, the knickpoint has become less steep and has migrated backwards. Scenario A3 (K, P dam = K, P substrate) shows modest backwards incision from 1000 to 5000 yr. Between 5000 and 10000 yr, two captures occur. Despite this capture, hardly any backward knickpoint migration occurred. At 15000 yr a deeper incised profile with several smaller knickpoints is visible. Scenario A4 (K, P dam $> K, P$ substrate)

shows a backwards migrating knickpoint that becomes less pronounced. Captures take place between the profiles of 1000 and 5000 yr, and 5000 and 10000 yr, thus the profiles do not show straightforward backwards incision. Between 5000 yr and 10000 yr, backwards knickpoint migration is nearly zero, despite the fact that the trunk stream position has changed.

For detachment-limited scenarios B1, B2, B3 and B4 a knickpoint is visible at 1000 yr. Profiles of B1 ($K, P_{\text{dam}} < K, P_{\text{substrate}}$) and B2 ($K, P_{\text{dam}} = K, P_{\text{substrate}}$) at 5000 and 10000 yr are similar to those from scenario B0 (no dam), indicating that the effect of the dam on profile evolution has diminished over time due to fast headward knickpoint migration. Scenario B3 ($K, P_{\text{dam}} > K, P_{\text{substrate}}$) shows moderate backfilling in the trunk stream after incision. Scenario B4 ($K, P_{\text{dam}} \gg K, P_{\text{substrate}}$) shows enhanced backfilling at 10000 yr and 15000 yr, after initial incision. This can be attributed to higher dam erodibility and higher sediment supply to the trunk stream from dam slopes and indicates a long-term effect of locally high sediment supply to profile evolution.

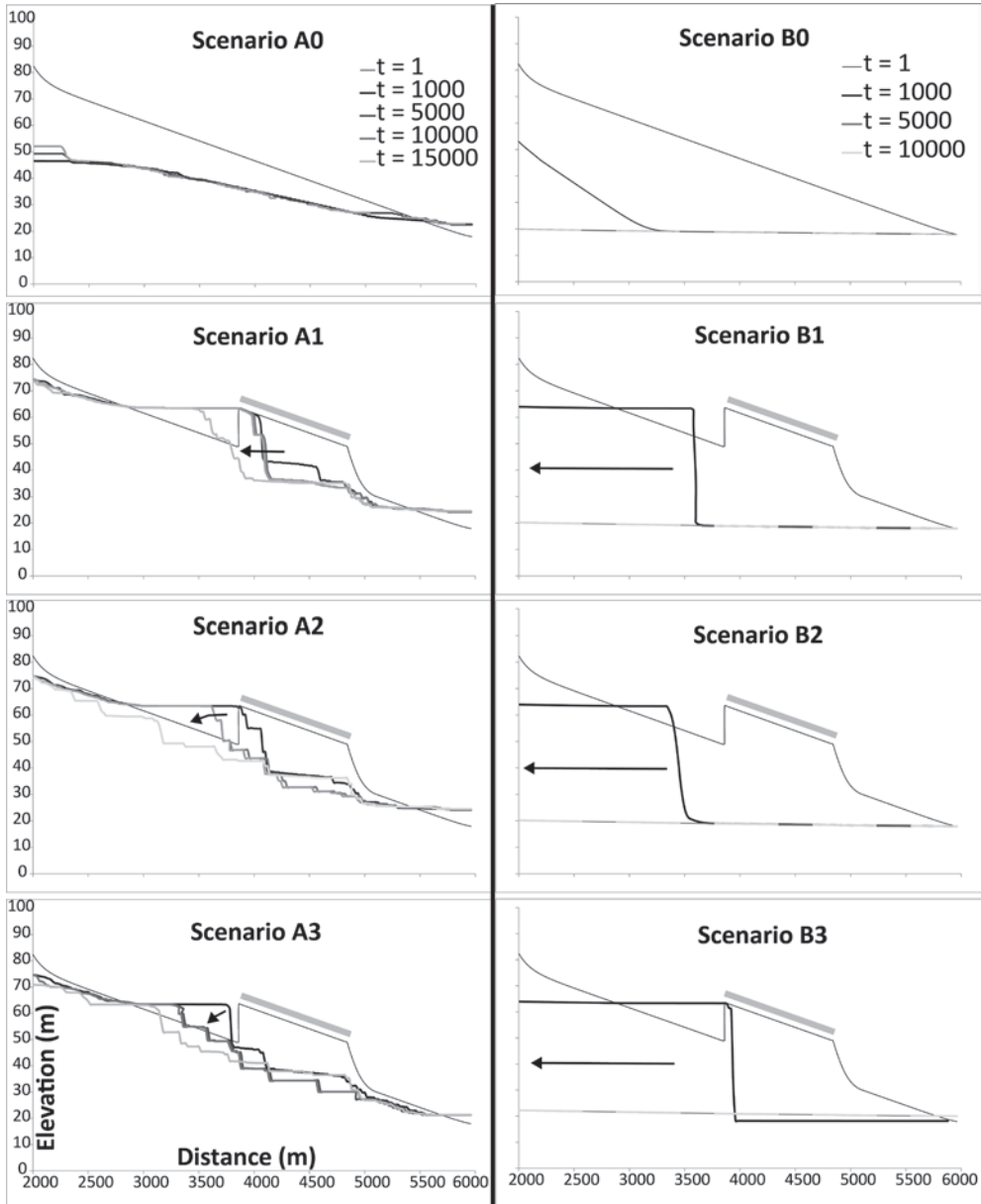


Fig. 2.5. Longitudinal profile evolution for all scenarios for the downstream reach of the catchment for different timesteps. X-axis shows the distance along the valley-axis (from 2400 to 6000 m). The profile of $t = 1$ yr shows the location and altitude of the dam. Arrows indicate direction and rate of knickpoint retreat. For scenarios B0 – B3, the longitudinal profile of $t = 15000$ yr is not shown because this profile does not differ significantly from that on $t = 10000$ yr.

2.4 Discussion

2.4.1 Scenario characteristics

Some differences were observed between the A- and B-scenarios irrespective of dam presence or absence. The transport-limited setting of the A-scenarios generates higher erosion on the slopes resulting in high sediment loads in the trunk stream. This can correspond to landscapes on highly erodible bedrock such as marls with low-vegetation cover, such as Mediterranean landscapes or degraded or abandoned agricultural landscapes. The transport-limitation is expressed in higher net erosion, higher sedimentation, lower incision and a convex shape of the trunk stream (Tucker, 2009). The transport-limited setting is also expressed in the complex variation of the net erosion timeseries. This variation has been observed in other landscape evolution modelling studies, and are similar to the nonlinear temporal dynamics illustrated by Van De Wiel and Coulthard (2010). The spatial expression of this variation is reflected in variations of sediment storage within streams over time (Fig. 2.3). Within the A-scenarios, the presence of a dam increases variation of net erosion, irrespective of dam erodibility. This points to a more complex transfer of sediment from behind the dam to the catchment outlet, which can be attributed to the more complex sediment transfer over the nearly flat surface space behind the dam. Total net erosion of the A-scenarios does not increase linearly with increasing dam erodibility (Table 2.2). For instance, despite the fact that scenario A1 has the least erodible dam and thus the most potential to store sediments, scenario A2 has the lowest total net erosion at 10000 yr and 15000 yr. This is determined by the specific history of the scenario. Scenario A1 establishes a route around the dam on top of more erodible substrate and remains there, while scenario A2 establishes a route over the less erodible dam, leading to more storage behind the dam. In both scenarios, incision in the first 10000 yr is limited. However, the trunk stream of scenario A2 is captured by a headward eroding stream at 10305 yr. Nevertheless, total net erosion remains higher in scenario A1, illustrating how this signal reflects the summed effect of different internal evolution events.

The detachment limited setting of the B-scenarios generates less erosion on the slopes resulting in low sediment loads in the trunk stream. This is expressed in lower net erosion, low variation of erosion over time, low sedimentation and deep incision of the trunk stream. This deep incision is due to sufficiently high water flow with low amounts of sediment in transport and thus high unfulfilled transport capacity. This also explains the low variation of net erosion: the bulk of the material is directly eroded from the stream bed of the trunk streams and immediately removed. A large part of the landscape as a sediment source is disconnected from the trunk stream, and the effective catchment area is small. This limits the influence of landscape complexity on net erosion to the trunk gullies only. Geomorphologically, this corresponds to landscapes found either on resistant bedrock, or under dense vegetation.

Although response to damming in both the A- and B-scenarios occurs through lake filling and subsequent re-incision, the high sediment load of the trunk stream in the transport-limited A-scenarios causes lake filling to occur faster. Low sediment load of the trunk stream causes backwards knickpoint migration to occur faster in the detachment-limited B-scenarios. Stream rerouting does occur in the A-scenarios and does not occur in the B-scenarios. The reason for this is that in all of the B-scenarios, incision into the substrate

and headward erosion is occurring at such a high rate that incision of smaller streams cannot keep up. In the A-scenarios, incision by the trunk stream is less severe. A probable reason for this slow migration is the low slope of the trunk stream on top of the lake sediments, combined with a high sediment load of the trunk stream, reducing eroding capacity. At the knickpoint, erosion is hampered due to the high sediment load, despite the steep slope. The gradual diminishing of the knickpoint suggests that the fluvial profile of the transport-limited stream is gradually changing into its linear to convex shape, similar to the profiles of A0 (and also see Tucker, 2009). The knickpoint remains the most pronounced for scenario A1 and A2 ($K, P_{\text{dam}} < K, P_{\text{substrate}}$) and least pronounced for A4 ($K, P_{\text{dam}} > K, P_{\text{substrate}}$). The lack of gorge formation makes potential capture by a smaller stream more likely. This suggests that in landscapes with more easily eroded lithology, stream capture is more likely to accompany damming than in landscapes with less erodible lithology.

2.4.2 Drainage rearrangements

Drainage rearrangement can be caused by aggradation processes, leading to avulsions, or by headward erosion driven stream capture. The frequent bifurcations of the trunk stream on top of the filled lake (Fig. 2.3 and Fig. 2.4) suggest that sediment redistribution on this floodplain plays a role, causing avulsions and potential switch of drainage from one outlet to the other. However, in all scenarios experiencing rearrangements (Table 2.2), the trunk stream at the dam location is flanked by a smaller stream discharging into the other outlet. The smaller stream manages to erode headwards faster than the trunk stream, despite that catchment area and thus water flow of the trunk stream is significantly larger than water flow of the smaller stream. For scenario A2 ($K, P_{\text{dam}} < K, P_{\text{substrate}}$), this stream capture can be explained by a higher erodibility of the substrate below the smaller stream around the dam (Fig. 2.6). For scenario A3 ($K, P_{\text{dam}} = K, P_{\text{substrate}}$) and A4 ($K, P_{\text{dam}} > K, P_{\text{substrate}}$), a possible cause for this behaviour is the high sediment load of the trunk stream in comparison with the smaller stream. Thus, the trunk stream is locally behaving like a transport limited stream, while the smaller stream is locally behaving like a detachment limited stream. This is visible by backwards knickpoint migration in the small stream after every capture and resembles the behaviour of the conceptual diagram depicted in Schumm (1979, Figure 15), where transport-limitation and detachment-limitation drive ongoing stream capture. The observed drainage rearrangements in our simulation generally start with a stream branching off the trunk stream into the smaller stream, with lower runoff than the trunk stream. Subsequently, rerouting of the trunk stream takes place and the main discharge switches either immediately or after a variable amount of time (up to more than 100 yr). After rearrangement, several years of continuing divergence in the streamflow of the two main streams can occur. The exact time and location of connection from the trunk stream to the smaller stream is not directly driven by the stream committing the piracy. Rather, local sediment redistribution and its influence on local small-scale topography determines this exact time and location. A change in net erosion variation after a capture is usually observed (Fig. 2.2), although comparable changes in variation can be observed when there is no preceding drainage rearrangement. This is an indication of unpredictable catchment behaviour, which has been investigated more systematically by Van de Wiel and Coulthard (2010). Thus, although capturing does affect the nature of sediment yield, captures cannot be distinguished from the catchment wide net erosion signal.

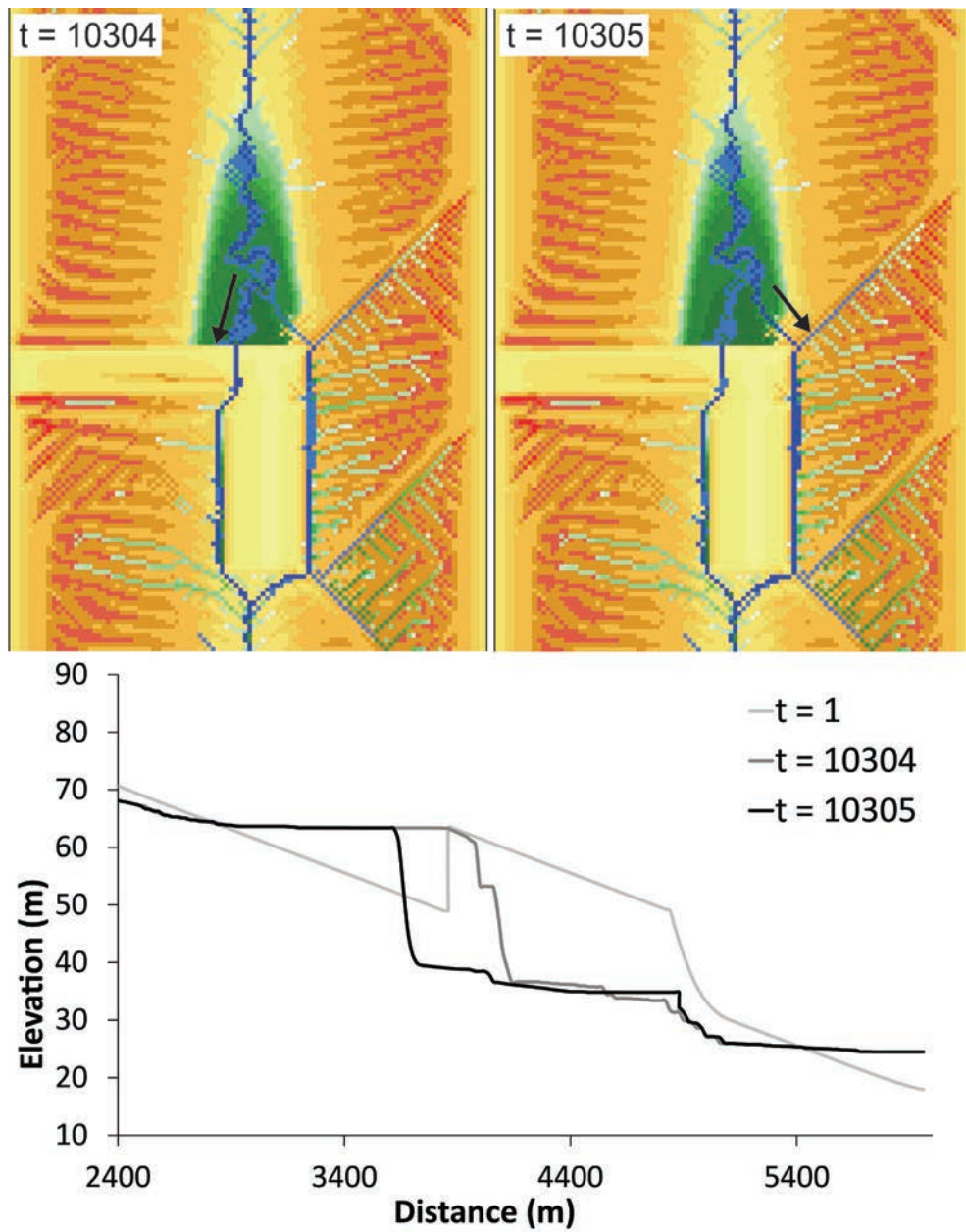


Fig. 2.6. Water routing (top) and profiles (bottom) before and after a river capture event of scenario A2. Profile at $t = 1$ is also displayed. Arrows added to maps indicate main drainage direction.

2.4.3 Comparison with actual dammings

The simulated damming and post-damming phenomena are compared with conceptual models and field observations from literature of fluvial response to long-lived dams (Table 2.3). All phenomena directly associated with damming listed in Table 2.3 occur in all modelled scenarios and are described in studies of long-lived dams. For instance lake siltation or the creation of a sediment wedge occurs both in the model and in all fieldwork studies considered in Table 2.3. Although LAPSUS does not distinguish between fine and coarse material and sediment distribution occurs by bedload transport, it does reproduce the sediment wedge of a filled lake. In reality, long-lived dams do not always lead to lakes and sediment wedges, for instance dams that did not create filled lakes (Van Gorp et al., 2013) due to low sediment supply, or where lakes were absent due to dam leakage (Crow et al., 2008). On the other hand, situations such as modelled in scenario A4, where lake sediments remain in the landscape but a dam body has been removed, have been reported in literature (e.g. Baartman et al., 2011).

Post-damming phenomena are variable both within the modelled scenarios and between model and field studies. Detailed comparison remains difficult as different dam studies involve different catchment sizes and settings and different dam elevations, sizes and removal mechanisms. For instance, our study deals with long-lived dams that do not breach and create outburst floods, as opposed to many natural dams, which are short-lived (Costa and Schuster, 1988). These outburst floods can create peak flows with shear stresses orders of magnitude larger than meteoric floods and therefore do important geomorphic work (O'Connor and Beebe, 2009). Outburst floods of lava dam breaches occurred in the Grand Canyon (Fenton et al., 2004) and the lava dam study of Van Gorp et al. (2013) shows evidence of dam breaching, although here local factors such as downstream dam removal or geothermal activity could have caused this. However, the more conceptual models based on many observations of landslide dams of Korup et al. (2010) and Hewitt (1998) demonstrate examples of both breached and incised landslide and rockslide dams. Furthermore, the lava dam studies of Ely et al. (2012) and Knudsen and Marren (2002), which are situated in detachment-limited landscapes, explicitly mention gradual removal or headward erosion as the dam removal process, where bedload is considered important as a tool for river incision (Ely et al., 2012). Ouimet et al. (2008) also describe epigenetic gorge formation after damming as a process of gradual incision. It is thus clear that various long-lived dam types can be removed by gradual dam incision. This incision does not necessarily start directly after the lake has been filled. García-García et al. (2011) describe a phase with fluvial aggradation and the establishment of a meandering river and a floodplain on top of the lake deposits, receiving sediments from tributaries. This corresponds well to the modelled transport-limited A-scenarios in which a floodplain is established on top of the filled lake (Fig. 2.3). Scenario A1 even showed a net increase in sediment storage behind the dam since the lake was filled (Table 2.3), due to lack of incision and absence capture of the trunk stream and the consequent large flat area which persisted until the end of the run. Ultimately, the landslide dam of García-García et al. (2011) has been gradually removed by headward erosion and a gorge was formed. Knudsen and Marren (2002) also describe a fluvial aggradation phase before dam incision took place. This is not reproduced by the modelled detachment-limited scenarios, although the specific nature of Knudsen and Marren's (2002) proglacial lake environment, in which loose sediments are derived from glacial processes, could account for this.

Table 2.3. Phenomena produced by different scenarios compared with field based natural dam studies interpreted from literature (Hewitt, 1998; Knudsen and Marren, 2002; Ouitmet et al., 2008; Korup et al., 2010; Garcia-Garcia et al., 2011; Ely et al., 2012; Van Gorp et al., 2013). ‘++’ and ‘+’ mean that the phenomena occurs strongly or moderately, ‘+-’ means that it occurs sometimes or very weakly, ‘-’ means that it does not occur. NA means that the phenomena is not applicable or considered in that study.

Phenomena	Scenario										Literature					
	A1	A2	A3	A4	B1	B2	B3	B4	Ely (2012)	Garcia-Garcia(2011)	Hewitt (1998)	Korup (2010)	Knudsen and Marren (2002)	Ouitmet (2008)	Van Gorp (2013)	
Damming																
Sediment wedge	++	++	++	++	+	+	+	+	++	++	++	++	++	++	+	+
Lake	++	++	++	++	++	++	++	++	++	++	+	++	++	++	+	+
Dam overtopping	++	++	++	++	++	++	++	++	++	++	++	++	+	++	++	++
Upstream gradient decrease	++	++	++	++	++	++	++	++	++	++	++	++	+	++	++	++
Dam gradient increase	+	+	+	+	+	+	+	+	++	++	++	++	+	++	++	++
Post - damming																
dam breach	NA	NA	NA	NA	NA	NA	NA	NA	--	--	+	++	--	--	--	++
Downstream breach deposition	NA	NA	NA	NA	NA	NA	NA	NA	--	+	++	++	--	--	--	++
Downstream fluvial deposition	+	+	+	+	--	--	+	+	NA	+	++	++	--	NA	+	+
Dam erosion by overtopping	-	+	++	++	+	+	++	++	++	++	++	++	++	++	++	++
Abandoned spillways	++	++	++	++	++	++	++	++	++	NA	++	+	NA	NA	--	++
Delayed upstream incision	++	++	++	++	+	+	+	+	+-	++	++	++	+	+	+	+
Dam knickpoint persistence*	++	++	+	+-	--	--	--	--	+	+	NA	++	-	++	++	+
Backwards knickpoint migration	-	+	+	+	++	++	++	++	NA	++	+	--	++	NA	++	++
Sediment wedge remnants	++	++	++	+	++	++	++	++	++	++	++	+	++	++	++	+
Stream rerouting/River capture	--	+	++	++	--	--	--	--	+	+-	NA	NA	NA	NA	+	+-
Epigenetic gorge formation	+-	+	+	+	++	++	++	++	+	NA	++	++	++	++	++	++
Post dam landsliding	NA	NA	NA	NA	NA	NA	NA	NA	++	+	NA	+	NA	NA	NA	++

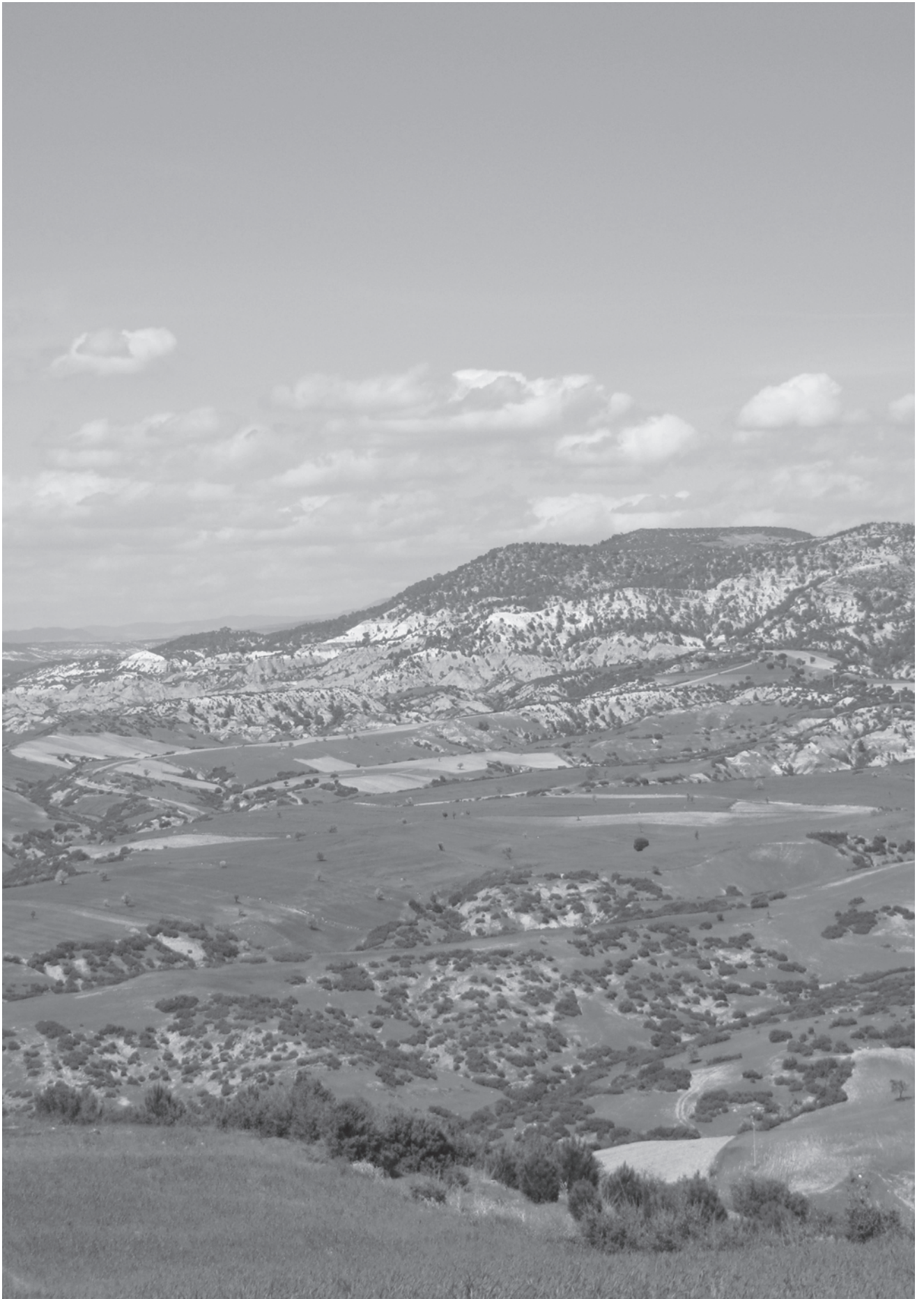
*on a timescale of 10^4 yr

Profile evolution of transport-limited scenarios with a less erodible dam (A1 and A2) and an equally erodible dam (A3) is similar to considered actual situations (Hewitt, 1998; Korup et al., 2010; García-García et al., 2011; Van Gorp et al., 2013), in which examples of knickpoint persistence and delayed upstream incision are described (Table 2.3). Furthermore, scenarios A2 and A3 show increased downstream aggradation compared to scenario A0 (no dam). This effect is also visible when outlet elevations of detachment-limited scenarios B3 (K, P dam $> K, P$ substrate) and B4 (K, P dam $\gg K, P$ substrate) are compared with scenario B0 (no dam). Detachment-limited scenarios are more similar to the lava dam studies of Knudsen and Marren (2002) and to a lesser extent Ely et al. (2012). This is expressed in faster backwards knickpoint migration and lower knickpoint persistence, respectively. Most of the simulated sediment wedge deposits are still present after 15000 yr and all field studies report sediment wedges or backwater aggradation persisting in the landscape. The occurrence of river capture on a 10^3 - 10^4 timescale as response to damming is hardly explicitly mentioned as a factor in literature, although abandoned spillovers, fluvial re-establishments and epigenetic gorges have been observed in several studies (Hewitt, 1998; Ouimet et al., 2008; Korup et al., 2010; Ely et al., 2012; Van Gorp et al., 2013). However these stream captures occur right after lake filling and overtopping, while in the modelled A-scenarios, captures still occur after 10000 yr. It seems conceivable that stream captures as a long-term result of damming, such as the ones simulated in this study, could take place in dammed catchments, under certain conditions of sediment supply and base level. The role of sediment transport in the trunk stream appears important for the response of streams to damming. This has been suggested from other studies on fluvial response to base level change (e.g. Snyder et al., 2003) and further modelling studies could focus on this subject.

Our relatively simple single-process model setup of an artificial small upland catchment with spatially uniform substrate reproduces several phenomena observed in the field. Results additionally suggest some processes and mechanisms which may be important in field situations where long-lived natural damming occurs. Nevertheless, differences between the model results and field observations remain. We therefore recommend to model response to damming of an actual catchment of which dam and substrate information constrained, using an improved model. The LAPSUS model could be improved by including different substrate layers (including newly deposited sediments) and possibly by investigating how dam breaching could be incorporated in an annual model such as LAPSUS.

2.5 Conclusion

Simulation of fluvial response to damming resulted in systematically lower cumulative sediment yields in the dam scenarios than in the non-dam scenarios until at least 15000 yr after the start of the simulation. This is due to partial preservation of the sediment wedge that originally forms behind the dam. Scenarios with low erodibility (detachment-limited) demonstrated gorge formation around the dam. Scenarios with high erodibilities (transport-limited) showed less incision by the trunk stream due to high sediment loads. In these scenarios river capture occurred, in many cases unrelated to differences in substrate erodibilities. River capture occurred multiple times through headward erosion, driven by base level and sediment load of trunk and side stream. These capture events are reflected in temporarily increased variation of annual catchment net erosion, which however cannot be distinguished from increased variation in erosion occurring at other points in time that are unrelated to capture. Longitudinal profiles show that incision of detachment limited streams is impacted for a shorter time than transport limited streams. However, effects on a landscape scale of all modelled damming events, such as sediment wedge remnants, drainage rearrangement and epigenetic gorge formation, are visible in high and low erodible landscapes at least until 15000 yr after damming. A qualitative comparison of modelled phenomena with field studies revealed that the modelled sediment wedge preservation corresponded well with all scenarios. Delayed upstream incision, knickpoint persistence but also knickpoint migration occurred in the transport-limited scenarios and correspond to findings in various field studies. Rapid incision such as observed in the detachment-limited scenarios has also been reported from field situations. Therefore, it is concluded that the model has correctly reproduced a set of key phenomena associated with damming and fluvial response to damming, although we recommend to apply an improved version of the model to a specific field situation. Fluvial response to damming occurs at least on timescales of 10^3 yr and catchment and dam-specific properties such as erodibility determine whether response is simple or complex. Apparently, a damming event that occurred 15000 yr ago can have effects on present-day sediment yield, profile evolution, and stream patterns.



Chapter 3

Fluvial response to Holocene volcanic damming and breaching in the Gediz and Geren rivers, western Turkey

This Chapter discusses the complex late Holocene evolution of the Gediz River north of Kula, western Turkey, when a basaltic lava flow dammed and filled this river valley. Age control was obtained using established and novel feldspar luminescence techniques on fluvial sands below and on top of the flow. This dating constrained the age of the lava flow to 3.0-2.6 ka. Two damming locations caused by the lava flow have been investigated. The upstream dam caused lake formation and siltation of the upstream Gediz. The downstream dam blocked both the Gediz and a tributary river, the Geren. The associated lake was not silted up because the upstream dam already trapped all the Gediz sediments. Backfillings of the downstream lake are found 1.5 km upstream into the Geren valley. The downstream dam breached first, after which the upstream dam breached creating an outburst flood that imbricated boulders of 10 m³ size and created an epigenetic gorge. The Gediz has lowered its floodplain level at least 15 m since the time of damming, triggering landslides, some of which are active until present. The lower reach of the Geren has experienced fast base level lowering and changed regime from meandering to a straight channel. Complex response to base level change is still ongoing in the Geren and Gediz catchments. These findings are summarized in a diagram conceptualizing lava damming and breaching events. This study demonstrates that one lava flow filling a valley floor can block a river at several locations, leading to different but interrelated fluvial responses of the same river system to the same lava flow.

Published as: Van Gorp, W., Veldkamp, A., Temme, A.J.A.M., Maddy, D., Demir, T., Van der Schriek, T., Reimann, T., Wallinga, J., Wijbrans, J., Schoorl, J.M., 2013. Fluvial response to Holocene volcanic damming and breaching in the Gediz and Geren rivers, western Turkey. *Geomorphology* 201, 430-448.

3.1 Introduction

Volcanic dams occur worldwide and their role in fluvial landscape evolution can be significant. A volcanic dam can block a valley floor and its tributaries partly, entirely, or at several locations. These different volcanic dam settings are analogous to the classification of landslide dams by Costa and Schuster (1988), who gave the first worldwide overview of natural dams, particularly discussing landslide and moraine dams but also mentioning different types of volcanic dams. Volcanic damming of river systems can occur because of blocking by volcanic cones (Macaire et al., 1992), pyroclastic flows, debris flows and lahars (Capra, 2007), or lava flows (Hamblin, 1990). Examples of existing lava dams are found worldwide; for instance in Iceland (Olafsson, 1979), New Zealand (Manville et al., 2007), and Canada (Stasiuk et al., 2003) where they usually created minor lakes in upstream confined valleys or control major lake levels in tectonic basins or calderas. Large lava flows of regional importance can invoke river cutoff and rerouting of main rivers (Veldkamp et al., 2012); and smaller lava flows can cause temporary base level rise, temporary damming of major river systems (Hamblin, 1990; Dalrymple and Hamblin, 1998; Knudsen and Marren, 2002; Duffield et al., 2006; Maddy et al., 2007; Crow et al., 2008; Demir et al., 2009; Ely et al., 2012), and can reroute or obliterate smaller river systems (Roach et al., 2008; Maddy et al., 2012a). Lake formation caused by a lava dam, or by any dam, can have a significant effect on local upstream and downstream catchment evolution. When describing landscape evolution associated with damming, fluvial profile evolution can give valuable insights. Korup et al. (2006) analysed fluvial response of bedrock rivers to large landslide dams in uplifting mountainous areas using profile characteristics. Natural dams can force the relocation of rivers and can delay incision on a scale of 10^1 - 10^4 a. Knickpoints may be formed caused by the river eventually flowing over the dam without incising it or because of incision downstream of the dam. Damming a valley with a landslide is known to lead to lake formation, delta formation, lake siltation, and fluvial regime change (Baartman et al., 2011; García-García et al., 2011). A lake may also trigger landslides by saturating and destabilizing slopes. These landslides may then form subsequent dams.

Lava dams can be removed in several ways. Firstly, when the dam overflows, erosion by overtopping may gradually decrease dam height or undercut the dam. Secondly, the river may bypass the dam; and thirdly, the dam may breach partly or completely, as a result of water pressure from the lake it formed, generating an outburst flood. Partial collapse of the dam may occur because of headward erosion, while seepage may weaken the dam causing collapse of the dam. Often dams are removed by a combination of the above mentioned ways. The response to dam breach may be in the form of locally increased incision rates. If the river bypasses the dam, it creates an epigenetic gorge (Ouimet et al., 2008). Increased incision rates and gorge formation can trigger slope failures and terrace formation up- and downstream of the dam. These terraces are not equilibrium terraces but represent local variations in erosion-aggradation pulses. This complex response to local base level change could be mistakenly interpreted as response to climate or tectonics (Ouimet et al., 2008). Knowledge of this complex response and its associated landscape dynamics is currently limited but would aid in understanding how rivers and catchments of different sizes respond to such a base level control. In the western Grand Canyon, USA, many examples of breached or eroded lava dams are found. Lucchitta et al. (2000) mapped and described incision-aggradation cycles associated with middle to late Pleistocene lava damming and breaching. Individual outburst

deposits of several lava dam breaches have also been distinguished in this region (Fenton et al., 2004), although there is discussion about the exact origin of these deposits (Crow et al., 2008). Cenozoic examples of lava dams causing rerouting and stream piracy are found in Kenya (Veldkamp et al., 2012) and Turkey (Maddy et al., 2007, 2012a). In these cases it was concluded that at longer timescales ($> 10^5$ ka), larger rivers such as the (palaeo) Gediz reattain grade quickly and long-lasting impact on fluvial evolution is limited (Maddy et al., 2012a; Veldkamp et al., 2012). However, for small catchments (< 500 m²) and shorter timescales, the impact of lava damming can be significant.

Middle to late Pleistocene-Holocene lava damming of the Gediz River and its tributaries in the Kula volcanic field, Western Turkey is mentioned in literature on the Kula volcanic field and its general geology and geomorphology (Bunbury et al., 2001; Westaway et al., 2004). However, its impact on fluvial and landscape evolution has so far not been investigated systematically. Specifically, the most recent lava flow entering the Gediz valley is investigated, as evidence of fluvial response has not been removed yet. This Chapter explores response to the most recent damming and breaching events. The aim of this Chapter is to identify damming and breaching events and fluvial response to these events. To achieve this aim:

- The lower part of the Geren Catchment and the adjacent reach of the Gediz River are characterized geologically, geomorphologically, and stratigraphically.
- Field evidence for the fluvial response to damming is interpreted.
- ⁴⁰Ar/³⁹Ar and luminescence dating are used to determine timing of lava dams and response rates.

This study aims at delivering insight into fluvial response to lava damming and aims at providing a framework for analysis of fluvial response to damming at other sites.

3.2 Setting

3.2.1 Regional setting

The Kula area is located in the upstream part of the Gediz basin, western Turkey. The region is marked by an east-west trending horst-graben structure of which the main grabens are the Büyük Menderes graben and the Alaşehir graben (Fig. 3.1). The Gediz River has its origin in the highlands north of Uşak. It drains toward the west along the northern shoulder of the Alaşehir graben, which it ultimately enters. The river then continues west and discharges into the Mediterranean Sea north of İzmir. The Gediz River drains an area of about 17,000 km² (IWMI and GDRS, 2000). In the upstream part, altitude ranges from 200 to 1100 m above sea level. It has a Mediterranean climate with hot, dry summers and cool winters.

In its upper reach, the Gediz River crosses several SSW-NNE oriented Miocene extensional basins (e.g., Purvis and Robertson, 2004). One of them is the Selendi basin, which comprises the area for this study. The Selendi basin is underlain and bordered by mainly metamorphic basement rocks, such as schists and marbles, and an ophiolitic melange overlying these basement rocks (Purvis and Robertson, 2004). The basins have been filled by a Miocene fining-upward sequence (Seyitoglu, 1997). At the base of this sequence lie the now deformed conglomerates and sands of the Hacibekir group, which were deposited in the early Miocene.

After a deformation phase, the fluvio-lacustrine sequence of the Inay group was deposited. The lower part of the Inay group is mainly formed by fluvial gravels, sands, and silts from the Ahmetler Formation. The upper part consists of mainly lacustrine limestones of the Ulubey Formation. These formations are separated by tephra deposits that originate from Miocene stratovolcanoes north of the study area. After deposition, north-south extensional tectonics in the Plio-Pleistocene created the east-west oriented Alaşehir graben. Uplift along normal faults combined with regional uplift caused headward erosion by externally draining river systems. This unlocked the Miocene basins and created the current Gediz river system (Maddy et al., 2007). In the early Pleistocene, a climate-controlled, uplift-driven terrace staircase was formed. The readily erodible Miocene basinfill provided an appropriate substrate for the Gediz River to incise and to form a terrace level for each climate cycle (Maddy et al., 2005, 2012b). Associated with the north-south extension, crustal thinning, and activity of the Alaşehir graben, basaltic volcanism initiated in the early Pleistocene on the northern shoulder of the graben (Richardson-Bunbury, 1996; Westaway et al., 2004; Ersoy et al., 2010). Since then, periodic volcanic activity has constructed several cones and lava flows that filled and dammed the palaeo-Gediz River (Maddy et al., 2007, 2012a). A reassessment of earlier work on the stratigraphic age of the lavas done by Richardson-Bunbury et al. (1996) resulted in three lava groups, β_2 , β_3 , and β_4 . This nomenclature will also be used in this Chapter. The early Pleistocene staircase got capped by the earliest phase of Quaternary volcanism (group β_2 ; Richardson-Bunbury, 1996). Volcanic cones and lava flows of this phase are now left as the Burgaz, Sarnıç, and İbrahimpaşa plateaus and the Delihasan ridge. The climate-controlled, uplift-driven terrace staircase formation was interrupted (Maddy et al., 2007) and evidence of the location of the Gediz River during the middle Pleistocene is sparse. What is known is that the Gediz valley came to be located south of the early Pleistocene plateaus after about 150 m of incision. At this time, volcanic activity had shifted southward, creating cones in the southern tributaries of the Gediz from which lava flows moved north, down into the Gediz valley. This created the β_3 lava fields, which by surface are the largest group (Richardson-Bunbury, 1996). After an additional 20-40 m of incision, the Gediz reached its present level. The present river is gravel-bed and often is located directly on top of basement lithologies. It has a straight to braided channel. The most recent lava flows of group β_4 (Richardson-Bunbury, 1996) also originate from the south, and some of them have reached the present river floor as, e.g., is the case in the area around Kula bridge and the Gediz-Geren confluence (Figs. 3.2 and 3.3), which is the focus area of this research.

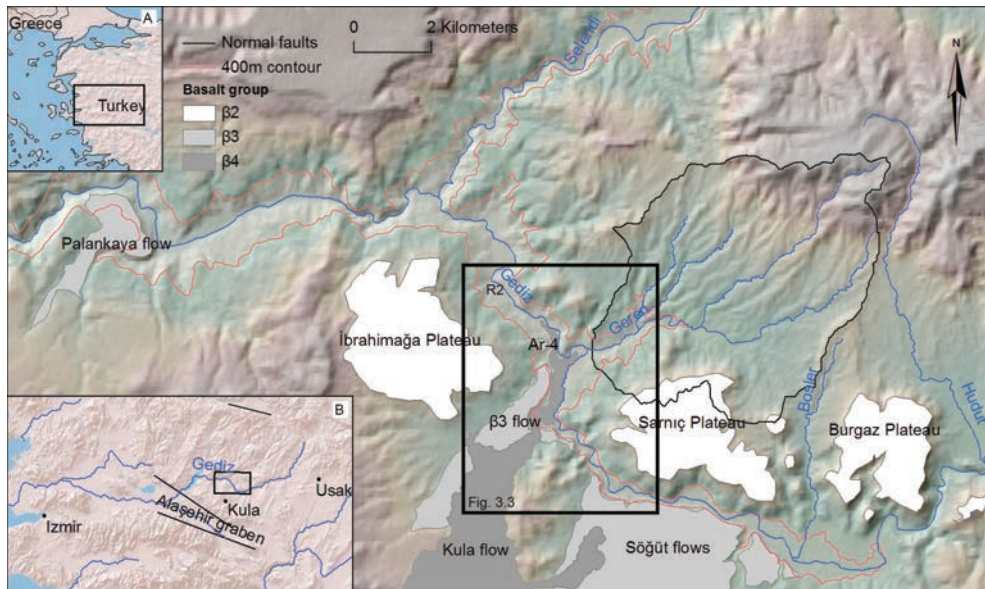


Fig. 3.1. Hill-shaded SRTM-DEM of the fieldwork area near Kula, western Turkey. Main basalt flows are shown and categorized into three groups (Richardson-Bunbury, 1996) by greyscale. From light (old) to dark (young): β_2 , β_3 , β_4 . R1 = basalt remnant 1, R2 = basalt remnant 2. Extent of Fig. 3.3 is depicted by boxed area. Inset A: the eastern Mediterranean with the bounding box of the lower left inset. Inset B: western Turkey with relevant horst-graben normal faults and the bounding box of the fieldwork area.

3.2.2 Local setting

Recent geomorphological studies of the area around Kula bridge and the Gediz-Geren confluence have been mainly carried out by Richardson-Bunbury et al. (1996), Bunbury et al. (2001), and Westaway et al. (2004, 2006). Here, the Gediz River has incised between two β_2 basalt plateaus, the İbrahimağa and Sarnıç plateaus. Younger β_3 and β_4 lava flows coming from the south have filled the contemporary valley floor and now stand out as ridges. This stepped, inverted relief (e.g. Pain and Oilier, 1995) makes this area one of the most striking to observe past interaction of fluvial incision with volcanic activity since the onset of the Kula volcanism (Figs. 3.4 and 3.5). A fluvial terrace has been recognised at the base of one of the β_3 flows (R1 in Fig. 3.1), around 25 m above the current river level (Westaway et al., 2004). Bunbury et al. (2001) reported on β_3 remnants several kilometres downstream of the Gediz-Geren confluence (R2 in Fig. 3.1). The 'Kula flow' complex (Fig. 3.1) is a β_4 flow and originates from the Kara Divlit cone near the town of Kula. It has a fresh, unweathered, barely vegetated rubbly surface that is impassible by foot. It has flowed northward down into the former valley of the Kula River. It crosses β_3 flows near Kula bridge and stretches along the current Gediz River to its endpoint. Near Kula bridge, the contact of the eastern side of the flow with underlying Hacibekir conglomerates is elevated about 10 m above the current river level. Here, the Gediz River flows through a 20-m-deep gorge that has been cut into these basal conglomerates. Fine silts and sands located 15 m above river level, next to Kula Bridge, have been interpreted as lake sediments associated with damming of the Gediz River by the Kula flow (Richardson-Bunbury, 1996; Bunbury et al., 2001; Westaway et al., 2004).

This flow has filled the present river valley, and its base reaches current river level at several locations (Westaway et al., 2006). At the Gediz-Geren confluence, it splits into two branches. One branch has flowed several hundred meters up into the Geren Catchment, while the other followed the Gediz valley for 1 km downstream. The current Gediz River has bypassed the lava flow. From these observations we can deduce that there are two main damming locations (see Fig. 3.2). However, it has not been investigated yet how exactly the process of damming and breaching took place and how the rivers and landscape responded.

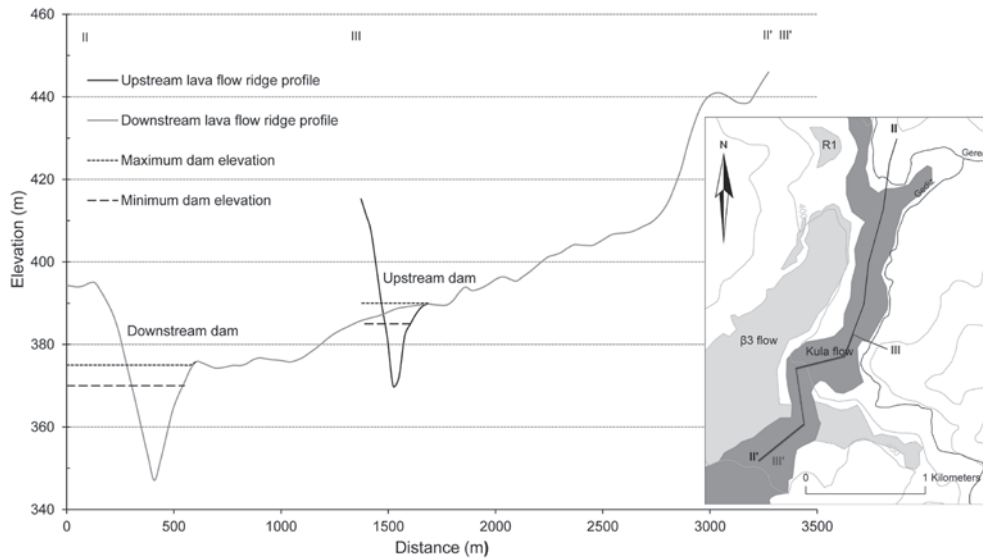


Fig. 3.2. Altitude profiles of the Kula flow and potential minimum and maximum dam altitudes at the upstream and downstream location. Profile II shows the downstream dam location, with a dam altitude range between 370 and 375 m. Profile III shows the upstream dam location, with a dam altitude range between 385 and 390 m.

Fluvial response to Holocene volcanic damming and breaching in the Gediz and Geren rivers, western Turkey

Table 3.1. Field observations (coordinates are in UTM-35N, datum WGS-84).

Name	Elevation (m)	Thickness (m)	UTM - X (m)	UTM - Y (m)	Material	Remarks
Upstream Gediz						
<i>Key Observations (Fig.3.3)</i>						
Kula Bridge	375		649234	4276846		
A	362		649488	4277338	Cobbles, boulders	Imbrication
B	397		649778	4277585	Travertine	Collapsed
IR-4	380	>4	649215	4276969	Silts against basalt flow	Massive
IR-5	390	6	649371	4277022	Sand, fine sand, tephra, gravel,	Parallel and cross-bedding, fining-upward, top debris
F	390	0	649912	4278792	Basalt	Smoothed basalt surface
G	382	7-13	649411	4276743	Sand, tephra, ophiolite gravels	Sands alternated with local gravel and tephra layers
H	387		649694	4276463	Rounded basalt and limestone gravels	Many rounded basalts and limestones in field
I			649699	4276376	Fine sands, gravels	Debris material on top of fine, parallel sands
J	381	> 3	650335	4275515	Coarse, layered sand overlying fine sands	Cross-bedding, calcium carbonate cemented
<i>Other observations</i>						
15	379		650541	4275108	Silt, sand	
20	376		649558	4276579		Alluvial fan from Sarnic
21	386		649926	4276362		Palaeosurface level
24	383		650317	4275934	Fine sand, rounded basalts	Sand body with fluvial gravels
25	382		650850	4275063		Palaeosurface level, inside meander bend
26	379		650740	4274995		Palaeosurface level, inside meander bend
28	383		651244	4275089		Palaeosurface level
700			649400	4276658	Cemented gravels w/ basalt, sand, local debris	Cemented fluvial terrace, base on hardrock. Buried by a body of alternating fine sand and local angular gravel layers.
722			649490	4276515	Cemented gravels, with rounded basalts	Cemented gravels, base on hardrock ridge now serving as a knckpoint for current Gediz
723			649494	4276564	Cemented gravels, with rounded basalts	
724			649525	4276571	Cemented gravels, with rounded basalts	Cemented gravels buried by fine sands
733			649974	4276307	Cemented gravels, with rounded basalts	Cemented gravels, base on hardrock
734			649992	4276170	Cemented gravels, with rounded basalts	
735			649984	4276168	Cemented gravels, with rounded basalts	Cemented gravels, base on hardrock
742			650096	4275665	Cemented gravels, with rounded basalts	Cemented gravels, base on hardrock
753			649792	4276292	Cemented gravels, with rounded basalts	

Table 3.1 (continued)

Name	Elevation (m)	Thickness (m)	UTM - X (m)	UTM - Y (m)	Material	Remarks
Upstream - Lower Geren						
<i>Key Observations (Fig. 3.3)</i>						
E	372	8	651303	4279265	Silt, sand, gravel, limestone gravels	Parallel and cross strat., fining upwards
C-1	383	10	651416	4279062	Calcium-rich muds, organic-rich layers	Parallel strat. (0.5-3 cm thick)
IR-2	378	4	651243	4278958	Sand, gravel, limestone, basalt, ahmetler	Parallel strat., fining upwards
IR-3	374	1.5-3.5	651224	4278973	Sand, gravel, limestone, basalt, ahmetler	Parallel, cross strat., asymm. chann., fining upw.
<i>Other observations</i>						
105	374		650582	4278786	Ahmetler gravel	Small surface level, saddle,
106	372		650611	4278722	Basalt, limestone gravel	Surface level
107	360		650663	4278683	Debris	Surface level, underlain by debris
129	375		651355	4279031	Polygenetic gravels, sand, silt, clay,	Horizontal strat., imbrication, terrestrial snails
183	373		650300	4278503	Rounded basalt gravels	Surface level
184	363		650613	4278593		Sinuuous palaeofloodpl., young collapses
303	377		651003	4278690	Silt, sand, Tephra	Tributary deposits
311	376		651030	4278852	Hardrock outcrop, ophiolite	Small hardrock knickpoint in Geren river
314	372		651578	4279290	Silt, sand	Aggradation
330	367		649193	4278582	Basalt, top	Sample AR-2
547	376		651327	4279263	Silt, sand, gravel, Limestone gravels	Parallel and cross strat., fining upward
566	376		651377	4279369	Sand, gravel, limestone	Fining upward
Gediz-Geren confluence						
<i>Key Observations (Fig. 3.3)</i>						
C	375		649191	4278440	Basalt	Smoothed basalt surface
D	359		649412	4278465	Basalt boulders, cobbles, pebbles	Landslide with basalt boulder
IR-1, Ar-1	349	> 0.60	649551	4278345	Basalt, base, sand, horizontally layered	Iron, manganese oxidation
Ar-2	367		651356	4279031	Basalt	
IR-6	360		649320	4278391	Fine sand, silt	structureless, on top of basalt
<i>Other observations</i>						
169	373		649267	4278554	Top of basalt	
177	366	0.5	650098	4278474	Gravels, basalt, ahmetler	Rounded, fluvial
315	374		649892	4278769	Sands, basalt gravels	
316	365		649850	4278740	Basalt gravels, sand	Slumped deposits in outer meander curve
317	357		649572	4278456	Basalt-rich gravels	Palaeo river level

3.3 Methods

3.3.1 Fieldwork

During fieldwork campaigns in the period 2009-2012, basalt flows, landslides, basalt- and limestone-bearing gravels, fluvial terraces, and other significant geomorphological features were mapped. Their locations and altitudes were taken using handheld EGNOS-enabled GPS devices. A limited amount of differential GPS (dGPS) altitudes were taken as well,

using Sokkia Radian IS equipment. Table 3.1 summarizes field observations such as relevant landforms and sediments. The top and the base of the youngest lava flow were sampled for $^{40}\text{Ar}/^{39}\text{Ar}$ dating. The Miocene basin-fills and the Pleistocene-Holocene fluvial sediments can have similar texture, therefore young sediments and terraces were mapped and classified based on presence of basalt or limestone gravels, as these indicate deposition after uplift and erosion of the Ulubey Limestones and/or after initiation of Pleistocene volcanism. Altitudes of sediments were mapped and (where observed) thickness, structure, and composition were logged and suitable sites for luminescence and radiocarbon dating were selected and sampled. Using a combination of GPS and a laser rangefinder (TruPulse 360), locations and elevations of current river level, terrace levels, locations, and thicknesses of sediment bodies and other points of interest were recorded. Their location and altitude are related to each other and connected to a reference elevation at the Gediz-Geren confluence obtained from a dGPS. Then they were plotted along the gradient of the current Gediz River. The river gradient is obtained from an ALOS-PRISM derived DEM with a 15-m horizontal resolution.

3.3.2 Dating

Dating of basaltic lava is generally done using $^{40}\text{K}/^{40}\text{Ar}$ or $^{40}\text{Ar}/^{39}\text{Ar}$ dating techniques (e.g. Westaway et al., 2004, 2006; Duffield et al., 2006; Crow et al., 2008; Wijbrans et al., 2011; Del Carlo et al., 2012). These techniques have often proven to be useful, but when used with relatively young basalts (e.g. < 0.5 Ma) uncertainties increase because of the long half-life of ^{40}K and the low potassium content of basalts (Duffield et al., 2006). However, under favourable conditions, it is possible to date Late Pleistocene to Holocene basalts (Wijbrans et al., 2011). Results can be cross-checked by using other dating techniques. In this study, luminescence dating of fluvial sediments underlying and overlying a basalt flow was used for validation of results.

$^{40}\text{Ar}/^{39}\text{Ar}$ dating

Two unweathered samples of the Kula flow were dated using the $^{40}\text{Ar}/^{39}\text{Ar}$ technique. In this technique, a rock sample is irradiated in a nuclear reactor to produce ^{39}Ar from ^{39}K . The age of the sample is then calculated as follows:

$$t = \frac{1}{\lambda} \ln \left(1 + J \frac{{}^{40}\text{Ar}^*}{{}^{39}\text{Ar}} \right) \quad (3.1)$$

where t is the age (a), λ is the decay constant (a^{-1}), J is a dimensionless irradiation parameter, $^{40}\text{Ar}^*$ is the amount of radiogenic argon, and ^{39}Ar is the amount of ^{39}Ar produced from irradiation. The $^{40}\text{Ar}^*/^{39}\text{Ar}$ ratio gives a relative age only, which has to be converted to an absolute age using the irradiation parameter J . This parameter is determined by irradiating a sample of known age together with the samples to be measured (McDougall and Harrison, 1999).

In this study, groundmass separates have been measured. Sample preparation and measurement was done in the Geochronology Laboratory, VU University, Amsterdam, The Netherlands. After crushing and sieving, the 250-500 μm fraction was density separated using heavy liquids (2.70-2.90 g/cm^3) to remove phenocrysts. Samples were hand-picked to further remove phenocrysts and anomalous grains. Experiments were done on groundmass separates using a laser heating system, a semiautomatic gas cleanup system, and a quadrupole mass

spectrometer (QMS) (Schneider et al., 2009). Samples were loaded into 65-mm Cu-heating trays, each containing five positions of 17 mm diameter each. Samples were preheated to bake out organic material after which a laser incremental heating technique was applied using a 25 W CW carbon dioxide laser with custom beam delivery based on an industrial scanhead set up for sample rastering and for beam diffusion into a bar form with a length of 2 mm and a width of 0.3 mm. This technique allows us to distinguish inherited ^{40}Ar from radiogenic ^{40}Ar formed since basalt formation. The Drachenfels sanidine standard of 25.4 Ma was used. We used the ArArCalc 2.4 software for data reduction, analysis, and presentation (see Appendix A3.1) (Koppers, 2002).

Luminescence dating

In the Gediz and lower Geren reach, seven sediment samples of fluvial origin were taken for OSL (optically stimulated luminescence) dating (see e.g. Wallinga, 2002). The method estimates the time of deposition and burial of sand or silt deposits.

For luminescence dating the amount of ionizing radiation received by the mineral grains since deposition (palaeodose, Gy) is determined using a tiny light signal (luminescence) that can be emitted by quartz or feldspar minerals. The annual ionizing radiation dose to the mineral grains in the natural environment is also determined (dose rate, Gy/ka). The luminescence age is then obtained by dividing these two quantities:

$$\text{Age (ka)} = \text{palaeodose (Gy)} / \text{dose rate (Gy/ka)} \quad (3.2)$$

Measurements were done at the Netherlands Centre for Luminescence Dating, Delft University of Technology, The Netherlands. Luminescence sensitivity of quartz grains proved to be too low for accurate dating. We therefore shifted our attention to feldspars, even though the feldspar luminescence signals may be affected by anomalous fading that causes age underestimation (e.g. Wallinga et al., 2007). To avoid or reduce this, we used the post Infra-Red-Infra-Red stimulated luminescence signal (pIRIR) (Thomsen et al., 2008; Buylaert et al., 2012; Kars et al., 2012). Two different pIRIR luminescence measurement procedures were applied, reflecting the rapid development of pIRIR dating methods, and advances in available instrumentation at the NCL.

A first set of three samples (NCL-2209135, -36, and -37; see Table 3.2) was measured on small aliquots (multiple-grain subsamples containing about 100 grains each). The measurement protocol for this multiple-grain analysis was identical to that described by Kars et al. (2012). For the second set of three samples (NCL-2111095, -099, -103) single-grain feldspar measurements were carried out. The single-grain measurement procedure and single-grain infra-red laser equipment was similar to that described by Reimann et al. (2012). Single-grain pIRIR measurement parameters were optimized to avoid age overestimation caused by incomplete resetting and thermal transfer. Details on measurement procedures for both single-aliquot and single-grain analysis are given in Appendix A3.2.

Equivalent dose (D_e) measurements for the conventional multiple-grain procedure were repeated on at least 32 aliquots to obtain meaningful D_e distributions. All samples showed large overdispersion values (48 to 138%), indicating that the spread in the multiple-grain equivalent dose distribution cannot be explained from measurement uncertainties alone. The

pIRIR single-grain D_e measurements were repeated on 200 to 400 individual feldspar grains. Approximately 30-40% of the grains fulfilled the quality criteria proposed by Reimann et al. (2012). The single-grain D_e distributions of all samples show very large over-dispersion values (85 to 120%). These values are much greater than the small aliquot values, which is likely caused by averaging effects within multiple-grain aliquots (Cunningham et al., 2011).

The most likely cause for the high overdispersion in both single-grain and single-aliquot D_e distributions is that the pIRIR signal was not completely reset for all grains at the time of deposition. Notably, the pIRIR signal is known to be less readily reset than the quartz OSL signal and the conventional feldspar IRSL signal (Reimann et al., 2011; Alexanderson and Murray, 2012). To avoid age overestimation caused by incomplete resetting of the pIRIR signal in part of the grains, we employed the Minimum Age Model (MAM; Galbraith et al., 1999) to determine the burial dose from the equivalent dose distribution. The expected overdispersion for well-bleached samples was estimated to be 20% and 27%, for single-aliquot and single-grain D_e distributions, respectively (see Appendix A3.2). The MAM was combined with a simplified bootstrapping approach to obtain meaningful uncertainty estimates (Cunningham and Wallinga, 2012)

Laboratory fading measurements (see Wallinga et al., 2007 for details) for the single-aliquot samples show that anomalous fading in these is negligible and a fading correction is not needed. In contrast, a laboratory fading rate of $2.1 \pm 0.4\%$ /decade was measured for the single grains (likely related to lower preheat and pIRIR measurement temperature); this rate was used to correct the single-grain pIRIR burial ages for fading following the correction model of Huntley and Lamothe (2001).

Dose rates were determined for each sample separately. Samples were ground, mixed with molten wax and cast into a puck of fixed geometry. After a delay of at least 2 weeks to allow Radon buildup, the samples were measured for at least 24 hours in a Canberra broad-energy gamma spectrometer. Activity concentrations were subsequently converted into dose rate, which was attenuated for water content, organic content, and grain size. Furthermore, a minor contribution of cosmic radiation (attenuated for depth) and internal alpha radiation was added. A contribution from internal dose rate within the K-feldspar samples as a result of K and Rb decay was also taken into account (Kars et al., 2012).

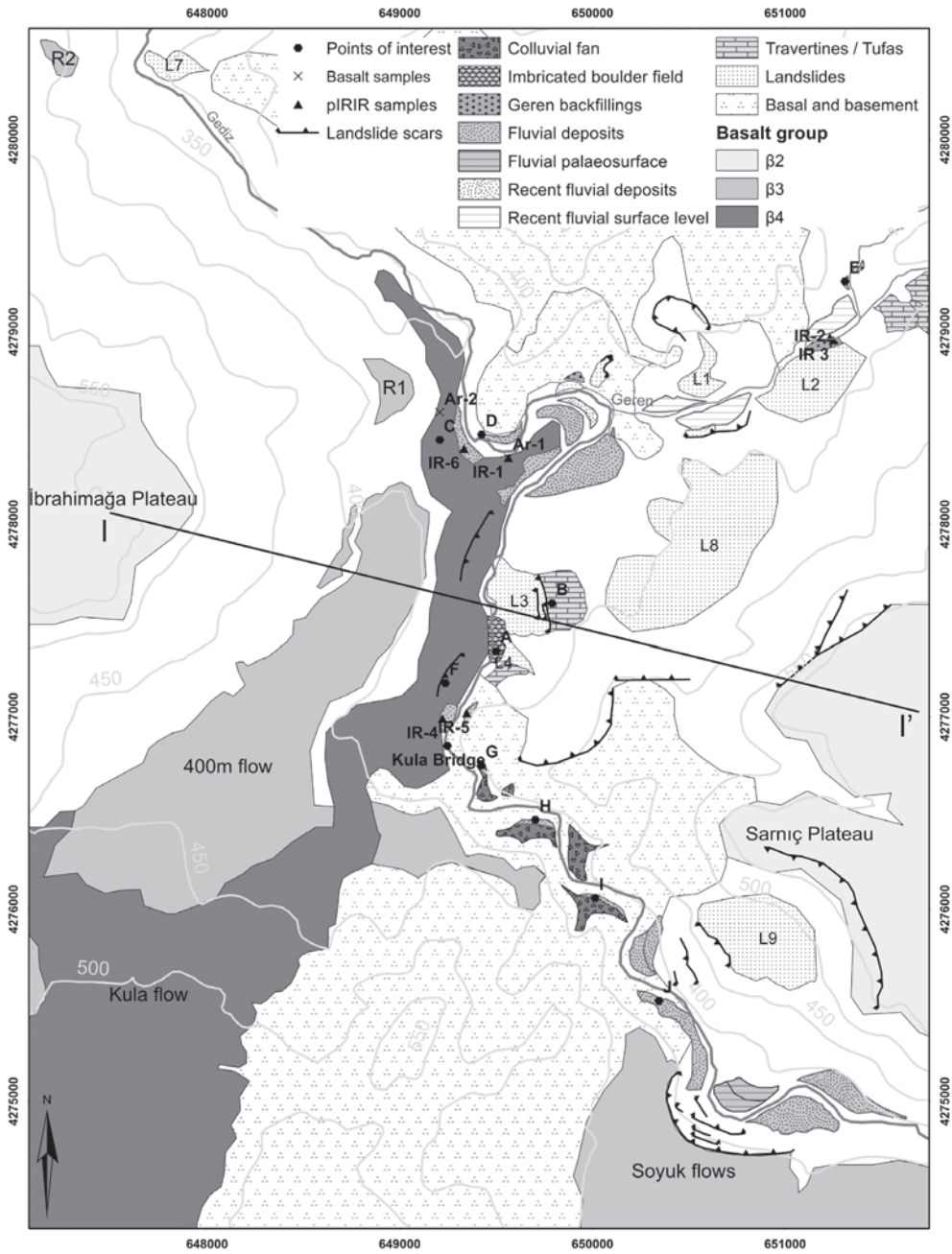


Fig. 3.3. Geology and geomorphology of the Gediz-Geren research area. Fluvial landforms at different levels are shown with or without observed deposits. See Fig. 3.5 for cross section I-I'.

3.4 Results and discussion

3.4.1 Fieldwork results

The upstream Gediz River around Kula bridge

Upstream of Kula bridge, the Gediz River flows through a gorge cut into a NNE-SSW oriented basement ridge. The current river cuts through several hardrock knickpoints, visible as small rapids. The structural control on the river can also be seen from the right angles it makes in planview. Observations of sediment bodies along the current Gediz reveal a complex mix of different sediment types. Along the Gediz, several subhorizontal surface levels can be observed both on the left and right bank, which have an altitude around 380-385 m and can be traced to at least 3 km upstream, where the current river level has this altitude. At several locations, the surface levels consist of fine-layered, fine sands that sometimes contain fluvial gravels or sands on top (e.g. locations H, J in Fig. 3.3, Table 3.1). At other locations, the fine sands are overlain by debris or colluvium coming from the slopes and small tributaries of both basalt plateaus. These deposits truncated the sand bodies (e.g. location I, Fig. 3.3, Table 3.1). In addition, sediment bodies consisting of intercalations of local colluvial gravel layers and fine sands are found (near location G, Fig. 3.3, Table 3.1). At location G itself, tephra layers are found in the top part of the sands. The vertical difference between the surface levels and the current Gediz River level generally increases when going downstream toward Kula bridge; but because surface levels consist of truncated fans, erosive surfaces, and fluvial surfaces, local variations in elevation occur. At some locations the edge of the basalt of the Soyuk flows has collapsed or slumped down. Throughout the gorge upstream of Kula bridge, heavily calcium-carbonate-cemented terrace remnants are found. They consist of clast-supported, rounded gravels and sands. The gravels are derived from basement, Miocene basinfill, Ulubey limestones, and Pleistocene basalts. Although actual proportions of these lithologies are not counted because of their cemented nature, they resemble an earlier recognized Gediz signature (Maddy et al., 2008) but with a higher proportion of basalt. The terraces occur at different altitudes above river level and almost all of them have basal contact with pre-Miocene basement rocks. Some of them are buried by the fine sand bodies mentioned above. Results of a gradient analysis on surface levels, terraces, and the current Gediz River will be presented in section 3.4.3.

Downstream of Kula bridge, the current Gediz turns to the North and forms a more or less straight channel adjacent to the Kula flow. At the left bank of the Gediz, just downstream of Kula bridge, fine silts are plastered in pores, cracks, and holes in the now collapsed basalt. They show wavy lamination (see Fig. 3.4C). The top of the basalt just downstream of Kula bridge contains pillow structures (near IR-4, Figs. 3.3 and 3.4A). Adjacent, the basalt has a smoothed surface, part of which has collapsed toward the Gediz River. On top of and against the basalt, a bed of structureless fine sand and silt is present (location IR-4 in Figs. 3.3 and 3.7). At the right bank of the Gediz, a sandy sequence is present with a top altitude of approximately 385-390 m, corresponding to the top of the basalt flow at this point (location IR-5, see Figs. 3.3, 3.4D and 3.7; as mentioned in Bunbury et al., 2001). This sequence contains several tephra layers and cross-bedded fine sands and silts with some tephra (Fig. 3.4C). Locally, the beds form wavy laminations (see Fig. 3.4E). It is topped by debris and slope deposits. The area downstream of Kula bridge (Fig. 3.7A) consists of a 500m long gorge, partly incised into the youngest lava

flow ('Kula flow' Fig. 3.1) but mostly into Hacibekir conglomerates. The observed contact of the flow with Hacibekir conglomerates is 15 m above current river level near Kula bridge; but following the contact downstream, it descends to current river level and below. The former Gediz River bed is still buried below the centre of the flow and may have been lower than the present river level (see Fig. 3.5). A sediment outcrop below the basalt at about 15 m above current river level, which is presented in Bunbury et al. (2001) and Westaway et al. (2004), is interpreted here as coming from a local stream that discharged towards the now buried Gediz channel. The material is unsorted, matrix supported, and angular and is thus interpreted as locally derived debris material. The outcrop thus does not represent the true base of the Kula flow at the palaeo-river level as proposed by Bunbury et al. (2001).

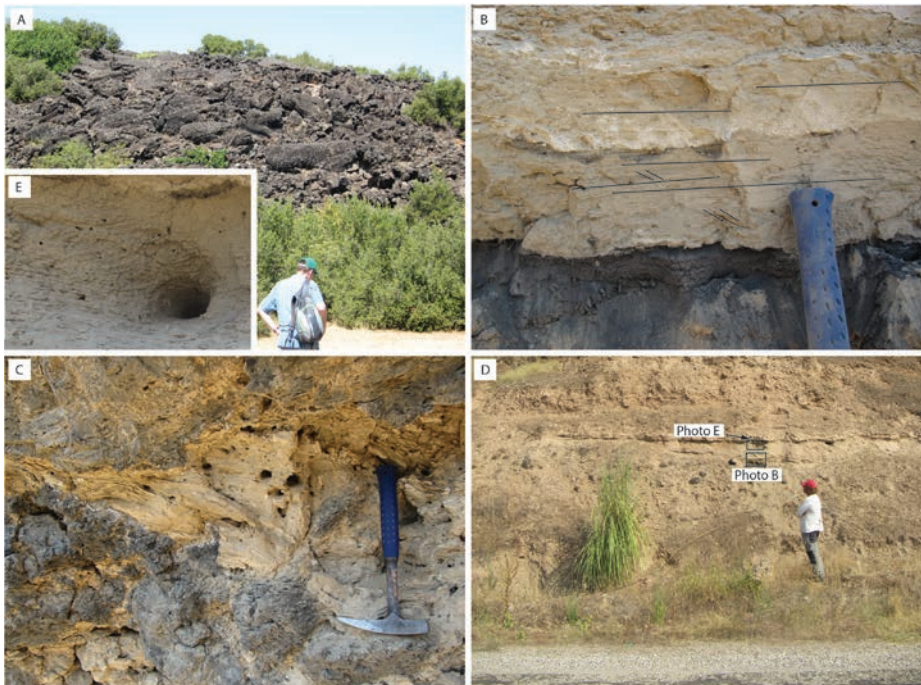


Fig. 3.4. (A) Pillow structures in Kula flow near IR-4 (see Fig. 3.3). (B) Layered tephra overlain by cross-bedded sands (emphasized by drawn lines). (C) Laminated silts deposited in cavities of the lava flow. (D) Tephra bearing cross-bedded sands at sample location IR-5. Person measures 1.75 m. (E) Sample hole of IR-5. Wavy laminations of fine sands and silts are visible.

Where the gorge widens, conglomerates and basaltic boulders are found in and along the river, as also described in Westaway et al. (2006). These boulders of up to 10 m³ in size have been imbricated to the north and are found along and downstream of landslide L3 (location A in Fig. 3.3, Fig. 3.7). Boulder size decreases going downstream. Adjacent to this boulder field, the basalt flow has partly collapsed into the Gediz River. At the right slope of the Gediz, a travertine mound was formed (Fig. 3.3, location B). The current altitude of the top of this mound is around 395-400 m. Part of the mound has collapsed and slumped down into the current Gediz River (Figs. 3.5, 3.6 and 3.7C). More to the east and upslope of the travertine mound, a large landslide is present (L8, Fig. 3.3). Its base has not been observed lower than

390 m, but it serves as source material for younger landslides and is eroded by younger gully systems draining toward the Geren and Gediz, and which are partly ploughed over for agricultural purposes. At the right bank of the Gediz, a subhorizontal surface level with agricultural fields containing rounded basalt and limestone pebbles is present that has the appearance of a river terrace. Just downstream, a basalt-rich gravel outcrop can be observed. At the left bank, a surface level with finer deposits is present on top of the lava flow, which is now used for agriculture (Fig. 3.6, location U).

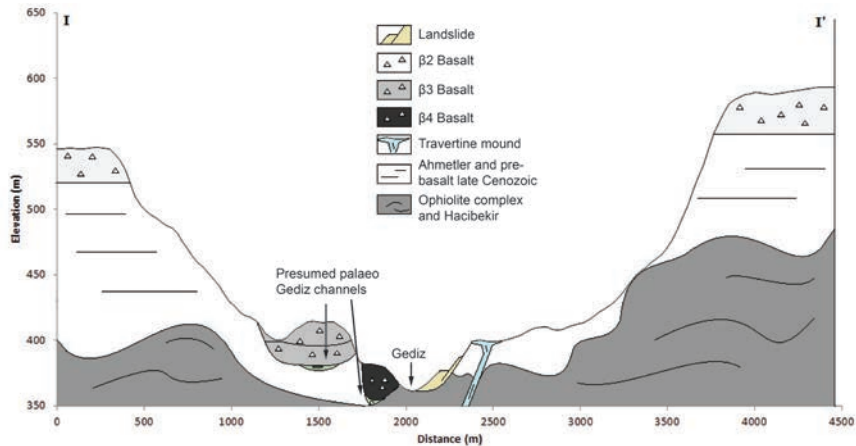


Fig. 3.5. Cross section I through Gediz valley in between Kula bridge and the Geren-Gediz confluence, demonstrating different lava flows infilling the palaeo valleys of the Gediz. See Fig. 3.3 for location.



Fig. 3.6. View to the north west from the travertine mound at location (B) in Fig 3.3. The different basalt flows that filled the Gediz valley are visible. P = Top of the İbrahimğa plateau. Q= The tip of the '400-m flow'. R = Basalt remnant R1. S= top surface of the youngest 'Kula flow'. T = Edge of Gediz gorge, conglomerate hill. U = sediments plastered against Kula flow. V = Debris at current river level of landslide L3. The green field in the bottom left is part of the landslide. The buildings on the right belong to the Kula bottle plant.



Fig. 3.7. (A) View downstream in the Gediz gorge near Kula bridge. On the left, the Kula flow is visible, on the right, basement lithologies and Miocene basal conglomerates are present. IR-4 = sandy/silty deposit on top of Kula flow. IR-5 = layered sandy fluvial deposits with tephra layers (see Fig. 3.3 for location). (B) Imbricated conglomerate boulders (Location A in Fig. 3.3). (C) View to the South West from the travertine mound at location (B), toward location (A) (Fig. 3.3). The Gediz River contains basalt and conglomerate boulders, some of which are imbricated. F = smoothed and collapsed area on top of the otherwise rubbly lava flow surface.

The Gediz-Geren confluence area and downstream

At the location of Ar-1 and IR-1 (Fig. 3.3; Table 3.1), a well exposed section of the basalt reveals its internal structure. Here, the basalt has a rubbly base, overlain by a 1-2 m thick platy section. Then the centre part of the flow (5-10 m) shows a columnar structure. The top of the flow is rubbly again (1-2 m). This internal structure roughly coincides with descriptions of a single Kula basalt flow from literature (Bunbury et al., 2001). At location Ar-1, the basalt flow splits into two branches, one continuing northwest down the Gediz valley and the other flowing northeast, upstream into the former Geren valley (Westaway et al., 2004). North of the tip of the eastern branch, across the Gediz River, sediments aggraded from a small northern tributary at around 370 m. These sediments and underlying Miocene strata are being undermined because of undercutting by a meander curve of the Gediz River. They form an active slumping, rockfall, and shallow landsliding area. Right where the basalt flow splits, the current Gediz forms a gorge once again. Here, the lava is underlain by well-sorted, fine fluvial sands of at least 60 cm thickness (IR-1; see Fig. 3.9).

At the south bank of the Gediz, structureless fine sands are draped over the basalt flow, similar to those near Kula bridge (Fig. 3.3, location IR-6, Fig. 3.8A, location S). Downstream, these sands are flanked by a narrow saddle with a smoothed, streamlined, basalt surface resembling channel forms that follow a steepest-descent route. This surface crosses the width of the basalt flow. Down to 2 km from the downstream dam location, large (up to 10 m³), solitary basalt boulders are observed in the current river channel. At location D (Fig. 3.3), a debris flow deposit is present on the northern, right bank of the Gediz. It mainly consists of angular basaltic debris and its downstream tip is formed by an oversized basalt boulder with a long axis of at least 6 m (Fig. 3.8). In the 1.5-km-long river stretch from the farthest downstream tip of the Kula flow toward L4 (Fig. 3.3), several basalt boulders are scattered along and in the current Gediz floodplain.

The southern and outlet section of the lower Geren Catchment

The southern section of the Geren Catchment comprises the outlet, the trunk gully, and southern slopes draining the Sarnıç plateau. At location E (Fig. 3.3), about 1.75 km upstream of the Geren-Gediz confluence, where a main tributary of the Geren joins the trunk stream, a limestone-rich fining-upward sequence of at least 6 m thickness is present. Its base is 2 m above the current gully level and overlies Miocene gravelly strata. The deposits contain horizontal stratification, cross-bedding and imbrication to the South. In the lower part, the fining-upward sequences show fluvial gravels, horizontal layering, channel-fills, and cross bedding. The higher part consists of fine-layered sands and silts, sometimes intercalated with gravel bands.



Fig. 3.8. (A) View towards the downstream dam-breach area. Gediz River flows to the left. P = Gediz gorge, Q = smoothed area on basalt, spillway. R = location of photo (B). S = fine sands against and on top of lava flow. (B) Debris flow remnant containing a very large basalt block on the right bank of the Gediz, at location (D) in Fig. 3.3.

At locations IR-2 and IR-3 (Fig. 3.3) ± 1.5 km upstream into the Geren from the outlet, an aggradation sequence with an altitude between 370 and 378 m can be traced along the current gully over 100 m (Figs. 3.9C, 3.9D). It consists of two stacked fluvial fining-upward sequences, which range from gravels (Gr) via sands (S) to silts (St; Fig. 3.9). The gravels contain a high proportion of limestone and basement derived lithologies and basalts. Gravels are subrounded, suggesting short transport distance; but sedimentary properties such as imbrication to the west, cross-bedding, and the presence of asymmetric channel fills show its fluvial origin. Its base is about 1-1.5 m above the current gully floor (which is at 369 m altitude). The base is a coarse gravelly lag deposit overlain by a fining-upward sequence rising up to 4-5 m above the current floodplain. The uppermost 1.5-2 m of the lower fining-upward sequence consists of sands and fines and the upper meter shows soil development, indicated by the subangular blocky structure of the sediments. This lower sequence is truncated by the upper sequence having a gravelly lag deposit. The upper sequence fines up to 7 m above the base of the total sediment body and 8 m above the current gully floor. This altitude decreases when following the sequence downstream. The fines in the top part also show soil development, but the transition to the modern soil is obscured.

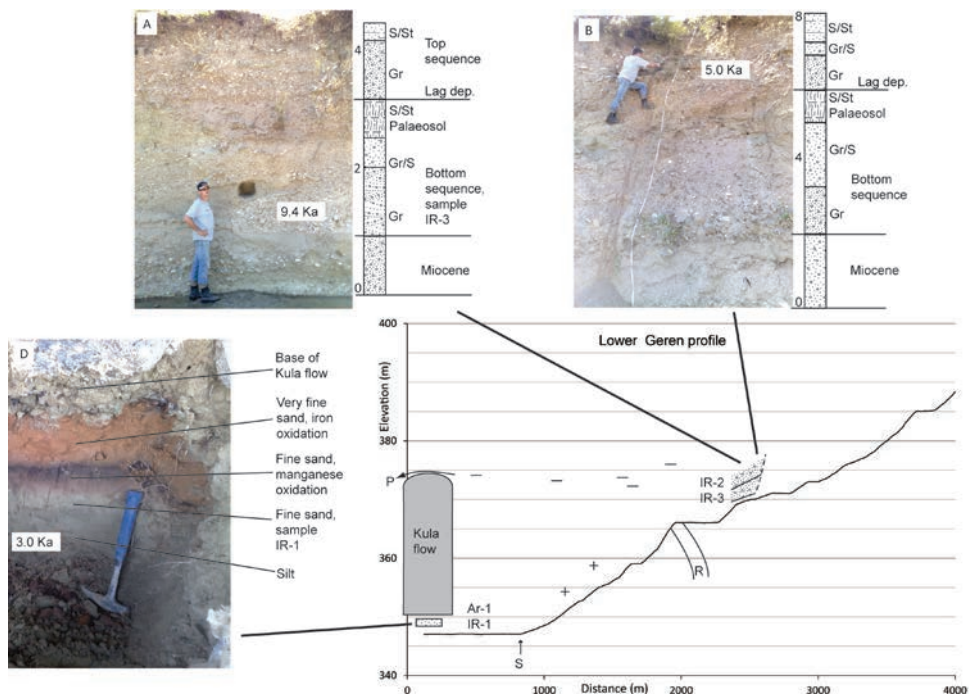


Fig. 3.9. Lower right: schematic profile drawing of the lower Geren area. P = spillway, R = knickpoint in the current Geren River where basement hardrock crops out, S = Gediz-Geren confluence. Young terrace levels are indicated with '+', the '-' indicate observed bench-like surface levels. These indicate levels of the young meandering palaeo-Geren. Photos present sediment sequences and sample locations for dating. (A) Two stacked fining upward sequences. Gr = gravel, S = sand, St = silt. (B) Same two fining upward sequences as photo (A), but 50 m downstream. (C) Deposits 200m upstream of photo A and B, consisting of a lower fluvial gravelly sandy unit and an upper unit of lime-rich sands at the upstream part and lime-rich fine-layered mud at the downstream part. (D) Sandy deposit below the Kula flow.

Downstream of this sediment body, the Geren cuts through an ophiolitic basement ridge. Fluvial terrace-like features are present, predominantly at the southern side of the gully. The Geren passes at least two young landslides (L1 and L2; Fig. 3.3). The surface of landslide L1 shows some steps of which one contains basalt gravels at an altitude of 372 m; and near the river, an outcrop with debris material is visible. Along the Geren, more bench-like flat surfaces are observed around 370-375 m elevation. Opposite of L1 a clear palaeosurface is present resembling a meander curve and another one is visible downstream, on the right bank, close to the Gediz-Geren confluence. These palaeosurfaces are present at an altitude of 360 m going down to 355 m moving downstream. They are flat and currently contain agricultural fields and are interpreted as a former floodplain level.

3.4.2 Age control

Results of $^{40}\text{Ar}/^{39}\text{Ar}$ and pIRIR dating are presented in Table 3.2. Figure 3.3 shows sample locations.

Table 3.2. Dating results.

pIRIR									
Lab code	Sample	Location	Altitude (m)	Relative altitude (m)	Measurement procedure	Equivalent dose (Gy)	Dose rate (Gy/ka)	Age $\pm 1\sigma$ (ka)	Validity
NCL-2209135	IR-1	Below kula flow	348	1	Multiple-grain pIRIR ₂₃₀	9.2 \pm 0.4	3.0 \pm 0.1	3.0 \pm 0.2	Likely OK
NCL-2209136	IR-2	Lower geren top	378	8	Multiple-grain pIRIR ₂₃₀	12.6 \pm 5.3	2.5 \pm 0.1	5.0 \pm 2.1	Questionable
NCL-2209137	IR-3	Lower Geren bottom	372	2	Multiple-grain pIRIR ₂₃₀	22.1 \pm 6.2	2.4 \pm 0.1	9.4 \pm 2.7	Likely OK
NCL-2111098	IR-4	Top lavaflow KB	385	15	Single-grain pIRIR ₁₅₀	7.3 \pm 1.1	3.3 \pm 0.1	2.6 \pm 0.4 ^a	Likely OK
NCL-2111099	IR-5	Accross lavaflow KB	385	15	Single-grain pIRIR ₁₅₀	7.5 \pm 0.6	3.6 \pm 0.1	2.5 \pm 0.3 ^a	Likely OK
NCL-2111103	IR-6	Top lavaflow downstream	360	10	Single-grain pIRIR ₁₅₀	5.8 \pm 1.6	3.3 \pm 0.1	2.1 \pm 0.5 ^a	Likely OK

$^{40}\text{Ar}/^{39}\text{Ar}$									
Lab code	Sample	Location	Altitude (m)	Relative altitude (m)	K/Ca $\pm 1\sigma$	Normal Isochron age $\pm 1\sigma$ (ka)	Inverse Isochron Age $\pm 1\sigma$ (ka)	Plateau age $\pm 1\sigma$ (ka)	
11WG1_A2-W333	Ar-1	Bottom Kula flow	348	1	0.124 \pm 0.031	34.5 \pm 70.3	33.4 \pm 24.7	69.8 \pm 20.4	
11WG1_B3-W330	Ar-2	Top Kula flow	366	19	0.421 \pm 0.018	7.7 \pm 47.7	8.0 \pm 6.2	60.5 \pm 13.9	

^a These burial ages were corrected for anomalous fading using a laboratory fading rate of 2.1 \pm 0.4%/decade.

Age control of the Kula flow

The Kula flow belongs to the youngest $\beta 4$ basalt group, which overlies fluvial sandy and silty deposits at location Ar-1 (Fig. 3.9B). Two basalt samples of this flow were taken to attempt

$^{40}\text{Ar}/^{39}\text{Ar}$ dating (Table 3.2). One was taken from the top of the flow at location Ar-2, which yielded an age of 69.8 ± 20.4 ka, and one was taken at the platy base of the flow at location Ar-1, giving an age of 60.5 ± 13.9 ka (see Fig. 3.3 for locations). However, another sample taken from the sediments below sample Ar-1 has been pIRIR dated to 3.0 ± 0.2 ka (sample IR-1; Table 3.2), giving an upper limit to the Kula flow age. This discrepancy follows a tradition of difficulties with dating this young basalt flow. Westaway et al. (2004) reviewed older attempts to date this flow and present K-Ar ages of the Kula flow. One is 60 ± 9 ka and is taken at the base of the flow just north of Kula bridge. Another was taken below Kula bridge from basalt that was believed to stratigraphically underlie the youngest flow. However, it yielded an age of 16 ± 4 ka and was considered unreliable owing to chemical weathering caused by interaction with river water. Westaway et al. (2006) presented K-Ar ages of several samples of the Kula flow and concluded that the youngest flow is Holocene based on sample splits ranging from 7 ± 2 ka to zero age. Improved laboratory techniques would explain the difference and favour the young K-Ar ages over the 60 ka age. Furthermore, the appearance of the fresh, unweathered lava flow surface makes an age of 60 ka unlikely, especially as climatic conditions during the last glacial maximum and the Pleistocene-Holocene transition would have enhanced weathering of the top surface. A possible explanation for the age discrepancy may be the existence of two different β_4 flows, the lower being 60 ka and the one now at the surface 3 ka. However, from the three 60 ka dates known, one is from the top of the flow and two are from the base. This, together with no clear evidence of different flow units or a re-establishment of the Gediz River between these two flows, makes this possibility highly unlikely. Although it has been shown that $^{40}\text{Ar}/^{39}\text{Ar}$ dating is suitable for young samples under favourable conditions (Wijbrans et al., 2011), there are clear indications that conditions for the samples of this study were not favourable, resulting in a systematic overestimation of the age. One indication is that isochron statistics are poor because of extremely low enrichment in radiogenic argon in all steps, placing the age anywhere between zero and 100 ka. The minimum criteria for acceptance of a $^{40}\text{Ar}/^{39}\text{Ar}$ age, as listed by McDougall and Harrison (1999), have not been met. Isochrons are not well defined, and isochron ages are discordant with plateau ages (see Appendix A3.1). These poor statistics may be explained by the potentially young age in combination with low potassium content of the sample. Because enrichment in ^{40}Ar is very low, one needs a fair amount of potassium to obtain a reliable signal. If not, a small influence from other sources, such as inherited argon, or variability in atmospheric argon may influence the result. Thus, the obtained age of around 60 ka is doubtful. If the Kula flow would be 3.0 ka or younger, as the IR-1 age indicates, it has experienced a relatively short time with a dry climate, explaining the unweathered state of the lava flow surface. From the multiple-grain pIRIR dating results (Table 3.2), IR-1 is the most robust sample, showing a clear minimum equivalent dose (D_e). Therefore, we conclude that for such young samples the pIRIR date is the most reliable date. This date will be used as an upper age for further landscape reconstruction.

The single-grain pIRIR ages are expected to be more robust than the multiple-grain estimates because the observed scatter in D_e is not affected by averaging effects, the measured grain populations are larger, and the parameters used for the MAM are better justified (see Appendix A3.2). All single grain samples show a clear minimum D_e population. Within the single-grain pIRIR data set, the dating result on sample IR-6 is least reliable as it is based on a population of only $\sim 10\%$ of the measured feldspar grains, whereas the age estimates of samples IR-4 and IR-5 are based on 35% and 65% of the feldspar grains, respectively.

Two samples of fine sandy sediments on top of the Kula flow have been dated by single-grain pIRIR. Sample IR-4, near Kula bridge yielded an age of 2.6 ± 0.4 ka and sample IR-6 generated an age of 2.1 ± 0.5 ka (Table 3.2; Fig. 3.3). This constrains the age range of the emplacement of the Kula flow to 3.0-2.6 ka, based on average ages. The tephra-bearing sands of sample IR-5 yielded a single-grain pIRIR age of 2.5 ± 0.3 ka.

Dated sediments in the lower Geren

The lower fining-upward sequence at location IR-3 has been pIRIR dated to 9.4 ± 2.7 ka. Sample IR-3 shows a less robust minimum D_e , but its validity is considered as 'likely OK' (Table 3.2). The upper fining upward sequence at location IR-2 yielded a pIRIR-age of 5.0 ± 2.1 ka, but its validity is questionable as the minimum age is based on only a few aliquots. The sequences are separated by a soil and a lag deposit.

3.4.3 Chronostratigraphical analysis, evidence of damming, breaching and response

The obtained age range for the Kula flow of 3.0-2.6 ka also constrains the timing of the formation of the two dam locations of Fig. 3.2. These dams were formed by the same flow and thus more or less at the same time. This information forms the starting point for discussing their formation, breaching, and fluvial response.

Downstream damming

The downstream dam was created just downstream of the Geren-Gediz confluence near locations AR-1 and D (Fig. 3.3). Here, the Kula flow has collided with a promontory consisting of Hacibekir conglomerates, located right at the contemporary Gediz-Geren confluence. The flow split here and flowed into both valleys making it an evident south-to north-oriented damming location for both the Gediz and Geren at an approximate dam altitude of 370-375 m (Fig. 3.2). The length of the dam may have been at least 300 m, spanning westward from location Ar-1 to location C (Fig. 3.3). At location C, the basalt shows a smoothed surface at ± 370 m altitude. Its anomalous smoothness and its shape and orientation suggest that it was a spillway, formed by water coming from the east. This would imply that the backwater or lake level has at least temporarily reached this altitude (Figs. 3.8A and 3.11B).

Downstream dam: fluvial response

There are some indications that the Gediz-Geren endured limited siltation from the downstream dam, although true laminated lake sediments have not been found. The lower surface levels found on top of the eastern side (Figs. 3.3 and 3.6, location U) and the northern side (Fig. 3.3, location IR-6) of the downstream part of the lava flow consist of fine sands. Their current extent is limited to the area around the basalt. The deposition of the fine sands of IR-6 may be representing the gradual siltation of the downstream lake, but post-dam deposition (e.g. overbank deposits during floods) cannot be ruled out. Similar fine deposits within the potential downstream lake extent have not been found upstream into the Geren and Gediz. However, flat benches are present along the Geren at an approximate altitude of the lake level (around 370-375 m altitude; see Fig. 3.9). Some of them have some rounded gravels at the surface.

The low siltation is plausible if the upstream lake existed at the same time, trapping all the Gediz sediments. In this case, the downstream lake only received water with some suspended clays from the upstream Gediz and only minor sediment input from the Geren. The Gediz therefore did not build a delta in this downstream lake.

The 100-m-long fluvial fining upward sequence of location IR-2 indicates that the Geren was affected by the downstream lake (Fig. 3.3). The base of the lower IR-3 fining-upward sequence dated to 9.4 ka cannot be correlated to the Kula basalt flow. The upper IR-2 sequence is dated to 5.0 ka but has a large (2.1 ka) standard error derived from a 1σ standard deviation and a questionable reliability (see Table 3.2). Given this standard error, two options are possible: (i) the upper sequence is older than the damming and thus reflects fluvial evolution of the Geren Catchment unrelated to damming; or (ii) it is an aggradation associated with this downstream lake. The fining-upward trend of this aggradation then indicates a shift to a less active regime. The buried palaeosol that separates the IR-2 and IR-3 sequences also indicates a locally raised base level that may be easily explained by the damming event. Additionally, location E also consists of a fining-upward sequence at a similar elevation. These observations all point to a deltaic regime.

Upstream damming

The upstream dam was located near Kula bridge (Fig. 3.3), where now a gorge is present. The roughly north-south oriented length of the dam could have been up to 500 m. Dam presence is indicated by different observations. First, the presence of pillow structures in the top section of the basalt just downstream of Kula bridge imply contact of the basalt flow with water at the time of cooling. Furthermore, the former river bed of the Gediz is still filled by the Kula flow. Observations of laminated curved silts within cracks and pores of the now exposed basalt near Kula bridge indicate that seepage through the basalt occurred (Fig. 3.4C). Throughflow and also subsurface flow associated with lava dams are mechanisms that already have been proposed (Crow et al., 2008), and this may explain why there are no clay deposits found upstream of the dam.

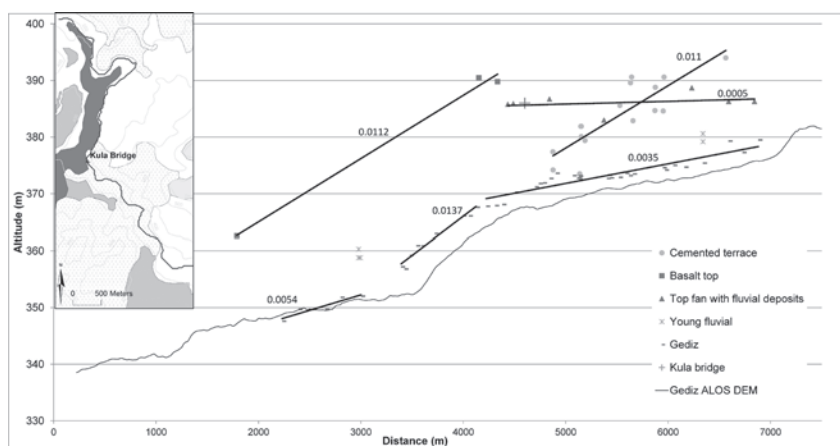


Fig. 3.10. Profile analysis of the Gediz River. Points represent laser ranged observations. For each group, trend lines are shown together with their slope (m/m). Map shows location of Gediz profile (based on ALOS-PRISM derived DEM with 15-m resolution).

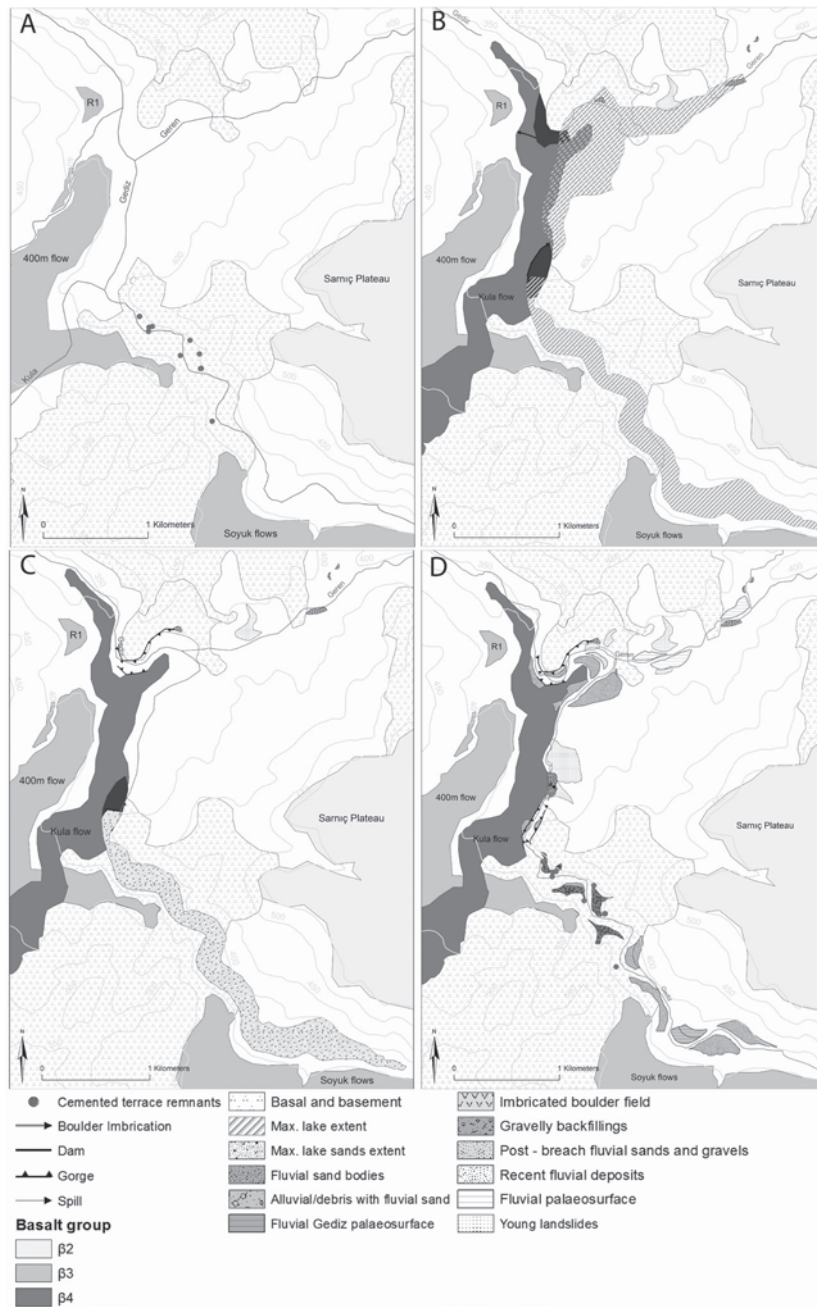


Fig. 3.11. Evolution of Holocene damming and breaching events in the Gediz-Geren area. (A) Pre-dam situation. With the now non-existent Kula River draining into the Gediz from the south. (B) Kula flow emplacement and dam, spillway, maximum lake extent and Geren delta formation. (C) Breach of downstream dam, gorge formation. Siltation and east overspill of upstream dam. (D) Breaching of upstream dam, resulting in landsliding, Imbrication and terrace formation.

Upstream dam response

To understand whether and how the Gediz responded to the upstream dam, the fluvial behaviour of the current Gediz and the Gediz before the dam has been determined and analysed. Figure 3.10 shows results of a gradient analysis of the Gediz and adjacent palaeosurfaces and terraces based on relative elevation measured with a laser rangefinder. There is a difference in elevation between the ALOS-PRISM derived river profile and the measured profile, but their general gradients and knickpoints compare reasonably well. According to this analysis, the current Gediz gradient can be divided into three different parts. The upper gradient is 0.0035 m/m, followed by a distinct steeper part downstream with a gradient of 0.0137 m/m, followed by a flatter part with a gradient of 0.0054 m/m. The average larger scale gradient of the Gediz is around 0.004 m/m (e.g. Maddy et al., 2012b), but local variation clearly occurs in the study area.

The gorge upstream of Kula bridge contains different, heavily cemented gravel units. Their strong cementation indicates that the terraces are not recent. They are considered to belong to a Gediz river prior to the damming. The average gradient of these terrace relicts is 0.011 m/m. This is steeper than the current Gediz right below, but comparable to the current Gediz gradient and the pre-basalt gradient downstream of Kula bridge. However, the age of these terraces is unknown so it is unclear if they represent the Gediz gradient during the blocking by the Kula flow. Nevertheless, a pre-Kula flow Gediz gradient between the current gradient of 0.0035 and reconstructed 0.011 is probable.

The palaeo surface levels, alluvial fans, layered or laminated sand bodies, and fields containing high concentrations of fluvial gravels upstream of Kula bridge are difficult to correlate because they are eroded and truncated by the current Gediz River. Nevertheless, a general trend that was observed shows a Gediz valley filled in by laminated sandy deposits and colluvial fans. The sandy fluvial deposits can be observed to at least 2.5 km upstream from Kula bridge. Their thicknesses are difficult to reconstruct as a clear base could usually not be observed, and their tops are eroded; but thickness roughly varies between 5 and 10 m. In some locations, their tops contain high concentrations of rounded gravels including basalts and limestones and occasionally a cemented sandy channel fill. If we extract a gradient from the highest observations of fluvial sandy tops and connect them to the sandy sediments located at IR-4 and IR-5, a low gradient is reconstructed (Fig 3.10, triangle points). Chronologically, an image emerges of a relatively steep, gravel-bearing river that suddenly gains accommodation space and transforms into an aggrading, low energy river. A sandy sediment wedge is created in this low energy environment. Finally, reactivation of the system reintroduces gravel-bearing channels that sometimes flow on top of the sands. Together with the age control of the sands of IR-4 and IR-5 these are clear indications for a response of the river to damming by the Kula flow. The dating results create a time window of max 1000 a (3.2-2.2 ka) in which the sediment wedge may have been formed. This time window is more than sufficient to fill in the dammed area. How and at what rate this infilling can occur depends on climate and vegetation cover conditions. The tephra-bearing sands around Kula bridge indicate aggradation occurring during volcanic activity, but it is unclear whether the tephra originated from volcanic activity associated with the Kula flow or from other Holocene eruptions in the Kula volcanic area that are known to have occurred (Westaway et al., 2006). The sandy tephra could also be washout from the adjacent lava flow.

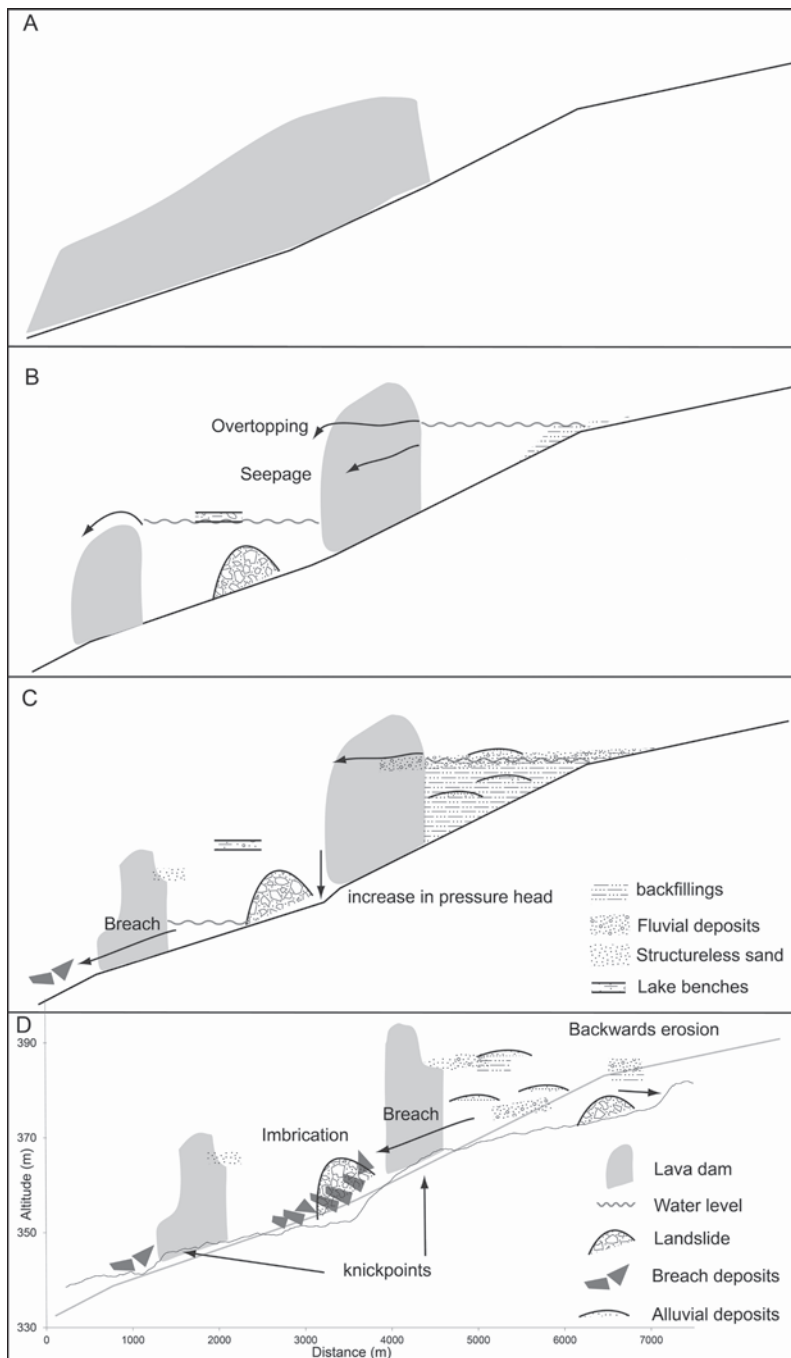


Fig. 3.12. Diagram of river profiles showing potential evolution pathway after lava damming of a river. Stages A-C show an assumed profile, stage D shows the actual profile based on an ALOS-PRISM-derived DEM.

Evidence of breach and response

The damming of the Geren and the Gediz rivers created around 20 m of base level rise at both the upstream and downstream location. Since then, 15 to 20 m of base level lowering has taken place in maximum 2.8 ka. This leads to a temporary local incision rate between 5 and 7 mm a⁻¹. This is high compared to the reported average incision rate of the Gediz in the last 1 Ma of 0.14 mm a⁻¹ (Maddy et al., 2012b). This temporary high incision rate invoked upstream response in both the Gediz and Geren Rivers. For both locations, a cause for this rapid incision may be the fast removal of the lava dam, and in both cases there are indeed indications that such a rapid breach took place.

The downstream dam location contains landslide debris (Fig. 3.5) immediately downstream of the dam at location D in Fig. 3.3. This debris mainly consists of basalt and is most likely part of the collapsed dam. The basalt blocks in the straight river reach downstream of the lava flow appear fresh and not disintegrated and therefore belong to the young Kula flow. They have been transported by the Gediz, implying a very powerful flood such as an outburst flood. In this case, the boulders may originate from the lava dam itself.

At the upstream dam location, the Gediz reincised along the edge of the lava flow through the contact with the Hacibekir conglomerates. It bypassed the resistant basalt and incised into the conglomerates on its former eastern slope and created an epigenetic gorge (Ouimet et al., 2008). Gorge formation may have been initiated by headward erosion, eventually leading to dam breaching. The dam breach resulted in an outburst flood, evidenced by a field of large northward-imbricated and sculpted boulders of up to 10 m³ in size originating from the Kula flow and local basal conglomerates (Fig. 3.7B). Most of these boulders originated from the actual dam, while part of the basal conglomerate boulders could originate from landslide L4 and became imbricated during flooding. Boulder size decreases in a downstream direction, indicating attenuation of the flood peak. This may well have been the case and could have been reinforced by widening of the valley downstream (Carrivick et al., 2013). This imbrication and the lack of fine sediments right downstream of the upstream breach indicate that the extent of the downstream lake at the time of breaching was more downstream than location A or that the downstream lake did not exist anymore. Therefore, the upstream breach may have been caused by the downstream breach and subsequent increase in pressure head (Fig. 3.12) thus making it a cascading event. It must be noted, however, that this area at present contains geothermal springs at the current river level. Thus destabilisation of the dam by geothermal waters could have played a role as well. Landslide L3, the collapsed travertine mound, is a likely direct effect of undercutting by the outburst flood.

After breaching, the Gediz and Geren incised down to their present location, but different types of deposits at different locations indicate that the pathway shows signs of autogenic behaviour (Fig. 3.11D). A lower, basalt gravel-rich level emerges near the Gediz-Geren outlet and upstream of location D, Fig. 3.3. This may reflect the temporary reestablishment of the river after such a breach. Its local occurrence suggests that it is not an equilibrium terrace but a redistribution of sediments after rapid incision upstream. The fine sands at IR-6 could represent a sandier phase in this reestablishment. The source for these sands may be the sand originally deposited behind the upstream dam. Upstream of the Kula bridge, the Gediz has incised into the sand bodies and alluvial fans, whose toes are truncated and do not connect

anymore to the landscape that they were formed on. The current Gediz flows on bedrock throughout the studied reach. Its gradient shows a steeper section where the upstream dam was located. This probably points to dam-related knickpoint creation that is discussed in the literature (Korup et al., 2006; Maddy et al., 2007), but it could in this case also be caused by variation in bedrock erodibility or structural preferences within the basement lithologies. Unfortunately, pinpointing the exact cause is difficult, and a combination of both is possible.

The downstream dam breach and the upstream dam outburst flood potentially triggered increased erosion and base level lowering of the Geren Catchment, which is active until the present day. Since the post-3.0 ka breaching, the base level of the Geren not only was lowered, but the location of the Geren outlet shifted to the east, toward the Geren Catchment caused by the Gediz River creating its meander loop around the eastern lava flow tip. This river reach shortening enhanced the potential for incision of the lower Geren. A knickpoint is present in the current Geren profile, near the location of a hardrock outcrop (Fig. 3.9). The steeper gradient of the Geren downstream of this knickpoint may represent the erosion pulse moving backward into the Geren. This apparently occurred by stepwise incision, as paleosurfaces of an intermediate meandering Geren stream are observed (Fig. 3.11D). Landslide L1 along the northern slopes of the lower Geren may have been triggered by the lake and subsequently seems to have pushed the Geren River southward, which is suggested by an undercut abandoned meander curve at the opposite southern bank. The present Geren removed part of the landslide material. It has to be noted that the landslide also could have dammed the Geren. Afterward, the Geren reincised because of ongoing base level lowering and the shift of the confluence, causing the regime of the lower Geren to change from meandering to its present, more straight and braided channel.

3.4.4 Conceptual framework

Maddy et al. (2007) sketched a diagram of longitudinal profile response of the Gediz to lava damming that described damming, lake formation, delta formation, upstream gradient lowering, and downstream gradient increase because of clear water erosion. This diagram serves as a base for a conceptual framework (Fig. 3.12) of dam formation and fluvial response as presented in this Chapter and is enhanced with global observations of natural dams and their effects (Costa and Schuster, 1988; Korup et al., 2006; Crow et al., 2008; Baartman et al., 2011; García-García et al., 2011).

Stage 1:

- Simplified pre-dam river course and profile with emplacement of lava flow in Fig. 3.12. The outlet of the Geren River was more westward than at present. The profile represents the contact of the river with bedrock.

Stage 2:

- Formation of dam locations and possibly lakes. The upstream lake shows seepage and initial backfilling, while the lower lake shows overspilling and delta formation in the Geren and possibly landsliding caused by water saturation at the lakeshore.

Stage 3:

- Siltation of the upstream impounded area by fluvial sands and alluvial deposits. The rate of siltation is not discussed here but depends on the climatic and vegetation conditions.
- The fluvial sand bodies are locally topped by coarser fluvial material as the system reactivates.
- Breach of the downstream lake causes deposition of breach debris downstream of the downstream lake and leads to incision downstream of the upstream dam. This triggers landslides from basalts and from the surrounding substrate and increase of pressure head of the upper lake.

Stage 4:

- Breach of the upstream dam, triggering landslides owing to (sudden) oversteepening, imbrication of large boulders.
- Backward erosion in sediments upstream of the upstream dam. The river becomes a bedrock river again.
- Gradient reveals knickpoints that may be caused by damming and breaching.

Although the framework is not exhaustive, it emphasizes that fluvial response to damming events is not necessarily straightforward. Local configuration of the dam controls how the river responds. The Gediz River is still responding to a damming event that was initiated between 3.0 and 2.6 ka. Over longer timescales (10^4 to 10^5 a), the influence of this dam will diminish. However, volcanism occurred frequently throughout the late Quaternary and there is no reason to believe that the fluvial system will be not disturbed by lava flows again.

3.5 Conclusion

The age of a young lava flow that filled the Gediz valley near Kula bridge has been constrained to 3.0-2.6 ka using luminescence dating on buried feldspar grains below and on top of the flow. The reconstruction of fluvial response to damming by this lava flow illustrates two important features. Firstly, multiple damming by the same lava flow caused different fluvial responses to the different damming events. The reason for this difference is that the sandy and coarser sediments were captured behind the upstream dam. The downstream impounded area only received a limited amount of sediments but did have a sufficient water supply. This led to erosion by overtopping of the downstream dam and its subsequent breach. Secondly, breaching of these multiple dams may have occurred as a cascading event. The downstream breach may have triggered the breach of the upstream dam. This interrelation between the two dams is quite important and similar situations are expected to occur in valleys that experienced multiple or serial dammings, even when dam remnants are not that obvious. The Gediz River is still responding to these local base level changes. This study serves as an example of Gediz fluvial dynamics during the late Quaternary when disturbance by lava flows was the rule rather than the exception.

Appendix A3.1. $^{40}\text{Ar}/^{39}\text{Ar}$ dating results

Incremental Heating	36Ar(a)	37Ar(ca)	38Ar(cl)	39Ar(k)	40Ar(r)	Age $\pm 1\sigma$ (Ka)	40Ar(r) (%)	39Ar(k) (%)	K/Ca $\pm 1\sigma$
11WG1_10W_A 10.00 W	237	81	1	201	1202	2559.1 \pm 1854.4	1.69	0.27	1.066 \pm 0.297
11WG1_15W_A 15.00 W	87	643	0	1273	1003	337.9 \pm 227.0	3.75	1.74	0.851 \pm 0.053
11WG1_20W_A 20.00 W	78	3291	0	6263	347	23.8 \pm 44.5	1.48	8.55	0.818 \pm 0.029
11WG1_25W_A 25.00 W	542	5517	0	10447	4047	166.1 \pm 40.2	2.46	14.26	0.814 \pm 0.029
11WG1_35W_A 35.00 W	184	15352	0	20250	1125	23.8 \pm 12.5	2.03	27.63	0.567 \pm 0.017
11WG1_50W_A 50.00 W 4	226	27021	0	18416	3048	71.0 \pm 26.8	4.36	25.13	0.293 \pm 0.008
11WG1_70W_A 70.00 W 4	198	27517	0	10428	1490	61.3 \pm 34.6	2.48	14.23	0.163 \pm 0.005
11WG1_95W_A 95.00 W 4	31	4343	0	1600	0	-89.6 \pm 165.8	0.00	2.18	0.158 \pm 0.005
11WG1_120W_ 120.00 W 4	86	13603	0	2773	982	151.8 \pm 85.1	3.72	3.78	0.088 \pm 0.003
11WG1_135W_ 135.00 W	57	8329	0	1630	1125	295.8 \pm 88.4	6.27	2.22	0.084 \pm 0.003
Σ	1726	105697	0	73282	14034				

Information on Analysis	Results	40(r)/39(k) $\pm 1\sigma$	Age $\pm 1\sigma$ (Ka)	MSWD	39Ar(k) (%),n	K/Ca $\pm 1\sigma$
WG1:1 groundmass Kula wij	Weighted Plateau	0.1628 \pm 0.0476 \pm 29.24%	69.8 \pm 20.4 \pm 29.24%	0.64	45.33 4	0.124 \pm 0.031
			External Error \pm 20.4	1.10	Statistical T Ratio	
			Analytical Error \pm 20.4	1.0000	Error Magnification	
Project = VU87-WG Irradiation = VU87 J = 0.0002377 \pm 0.0000002 DRA 1 = 25.260 \pm 0.076 Ma	Total Fusion Age	0.1915 \pm 0.0328 \pm 17.13%	82.1 \pm 14.1 \pm 17.13%		10	0.015 \pm 0.000
			External Error \pm 14.1			
			Analytical Error \pm 14.1			

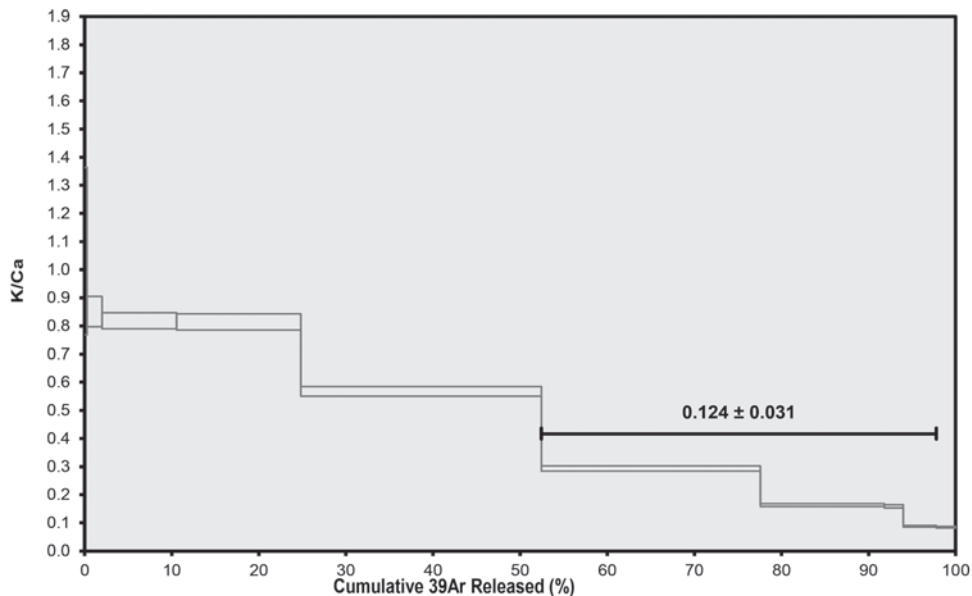


Fig. A3.1.1. Sample Ar-1 plateau age data (top) and K/Ca plateau (bottom).

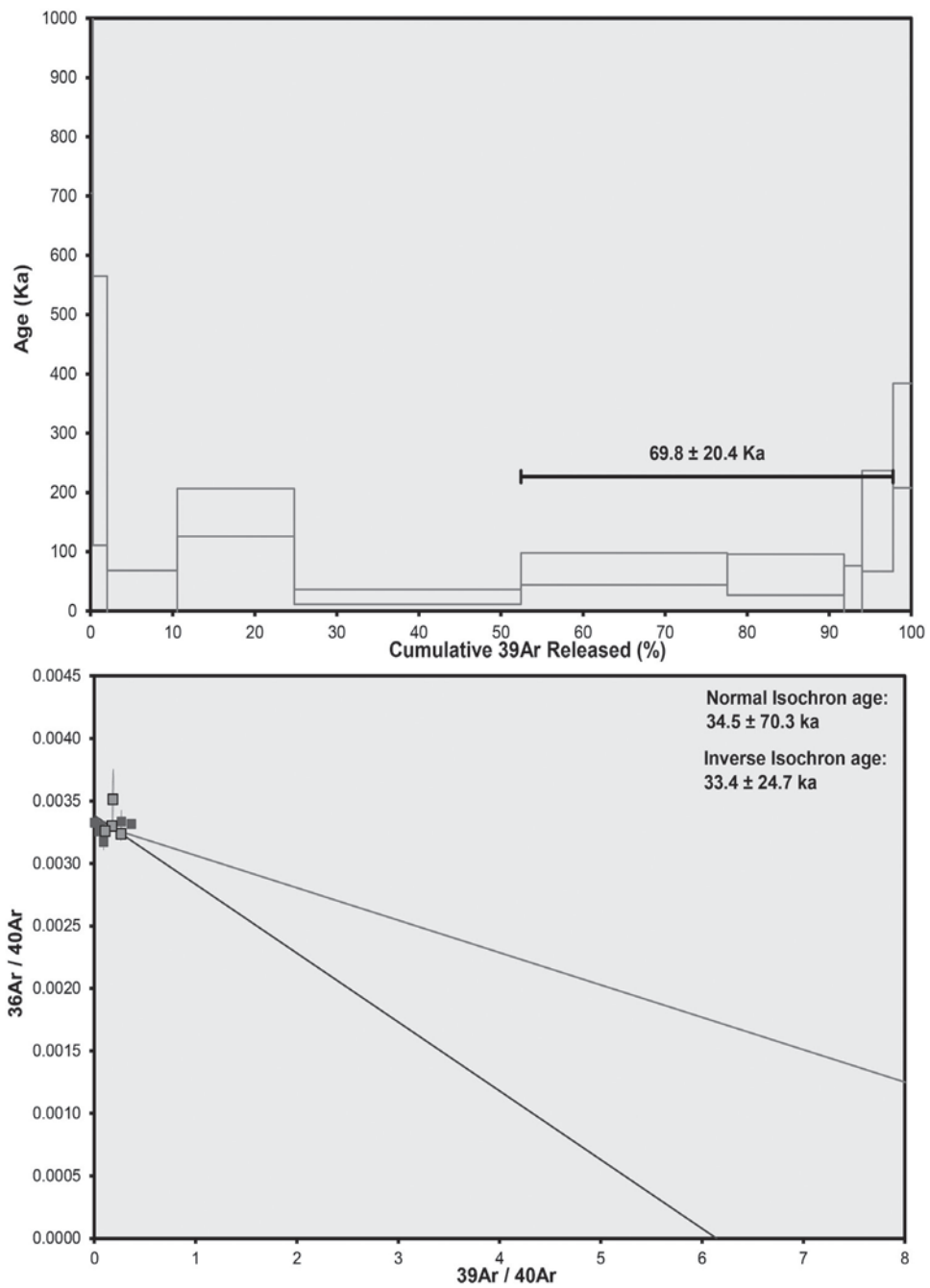


Fig. A3.1.2. Sample Ar-1 Age plateau (top) and inverse isochron (bottom).

Incremental Heating	36Ar(a)	37Ar(ca)	38Ar(cl)	39Ar(k)	40Ar(r)	Age $\pm 1\sigma$ (Ka)	40Ar(r) (%)	39Ar(k) (%)	K/Ca $\pm 1\sigma$
11WG1_10W_B 10.00 W	323	7	6	11	3092	118820.4 \pm 31231.3	3.14	0.02	0.657 \pm 1.343
11WG1_15W_B 15.00 W	83	294	7	272	305	485.5 \pm 1056.0	1.23	0.38	0.398 \pm 0.045
11WG1_20W_B 20.00 W	48	947	10	1382	786	245.7 \pm 221.9	5.22	1.93	0.627 \pm 0.038
11WG1_25W_B 25.00 W	62	1436	9	2214	1993	389.0 \pm 118.4	9.85	3.08	0.663 \pm 0.027
11WG1_35W_B 35.00 W 4	236	3861	14	4961	1708	148.7 \pm 52.0	2.39	6.91	0.553 \pm 0.021
11WG1_50W_B 50.00 W 4	707	12266	43	11308	2494	95.3 \pm 83.6	1.18	15.76	0.396 \pm 0.013
11WG1_70W_B 70.00 W 4	524	16287	82	15112	2069	59.2 \pm 32.0	1.32	21.06	0.399 \pm 0.013
11WG1_95W_B 95.00 W 4	201	8640	40	8571	562	28.3 \pm 37.0	0.94	11.94	0.427 \pm 0.013
11WG1_120W_1 120.00 W 4	415	18198	82	16936	2388	60.9 \pm 22.2	1.91	23.60	0.400 \pm 0.012
11WG1_135W_1 135.00 W 4	256	10714	58	10993	1145	45.0 \pm 33.6	1.49	15.32	0.441 \pm 0.014
Σ	2854	72649	351	71759	16543				

Information on Analysis	Results	40(r)/39(k) $\pm 1\sigma$	Age $\pm 1\sigma$ (Ka)	MSWD	39Ar(k) (%),n	K/Ca $\pm 1\sigma$
WG1:1 groundmass Kula wij	Weighted Plateau	0.1400 \pm 0.0323 \pm 23.05%	60.5 \pm 13.9 \pm 23.05%	0.80	94.60 6	0.421 \pm 0.018
			External Error \pm 13.9 Analytical Error \pm 13.9	1.03 1.0000	Statistical T Ratio Error Magnification	
Project = VU87-WG Irradiation = VU87 J = 0.0002395 \pm 0.0000002 DRA 1 = 25.260 \pm 0.076 Ma	Total Fusion Age	0.2305 \pm 0.0448 \pm 19.42%	99.6 \pm 19.3 \pm 19.42%		10	0.022 \pm 0.000
			External Error \pm 19.3 Analytical Error \pm 19.3			

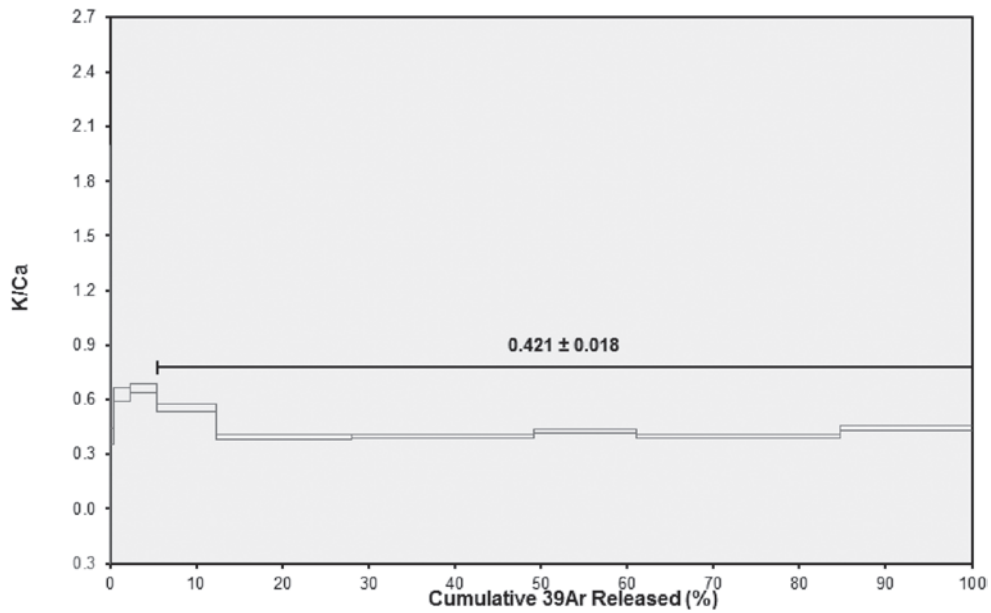


Fig. A3.1.3. Sample Ar-2 plateau age data (top) and K/Ca plateau (bottom).

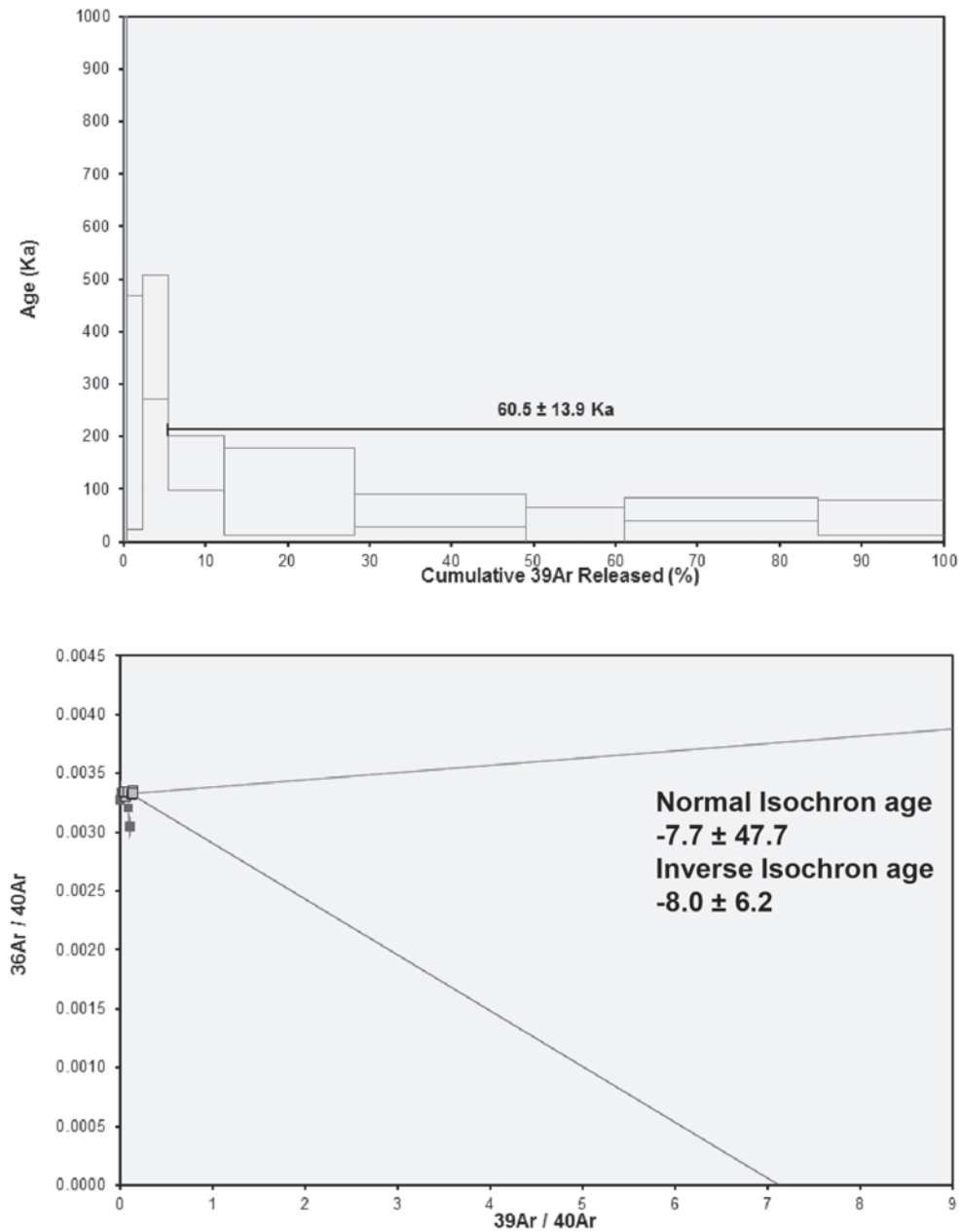


Fig. A3.1.4. Sample Ar-2 age plateau (top) and inverse isochron (bottom).

Appendix A3.2. Luminescence dating

Multiple-grain post-Infrared-Infrared (pIRIR) luminescence analysis

First, optically stimulated luminescence tests were conducted on quartz extracts, but luminescence sensitivity of the quartz grains turned out to be too low to allow accurate dating. Attention was therefore shifted to feldspar minerals. The feldspar grain-size fraction of 180-212 μm was purified by sieving and chemical treatment (HCl, H₂O₂, 15 min HF 10%, 20 min HF 40%). Density separation was performed to obtain a K-rich feldspar extract ($\rho < 2.58 \text{ g/cm}^3$). The K-rich feldspar extracts were stimulated using an array of infrared LEDs (870 \pm 40 nm, \sim 140 mW/cm²) for 100 s stimulation. Infrared-stimulated luminescence (IRSL) measurements were performed on automated Risø TL/OSL readers (DA 15, DA 20) (Bøtter-Jensen et al., 2003). To avoid underestimation of dose due to anomalous fading, the post-IR IRSL (pIRIR) signal was used for palaeodose estimation (Thomsen et al., 2008). A modified Single Aliquot Regenerative (SAR) dose procedure (Murray and Wintle, 2003) was employed. Details of the SAR pIRIR measurement protocol for K-rich feldspars including the thermal treatment are reported in Kars et al. (2012). A dose recovery test result confirms the suitability of the measurement procedure for our samples.

To obtain a good estimate of the burial dose, measurements are repeated on at least 32 aliquots per sample. Each of these aliquots consists of a sample disc containing 20-30 grains (1-mm diameter mask). Single-aliquot palaeodose (also equivalent dose, D_e) distributions were over-dispersed, i.e. they were more scattered than expected based on the measurement uncertainties. This suggests an additional source of scatter, e.g. mixing of grains of different ages or incomplete resetting of the pIRIR signal in some grains prior to deposition (heterogeneous bleaching). Given the D_e distributions obtained (Fig. A3.2.1) and the depositional environment of these samples we interpret the spread to be caused by heterogeneous bleaching which is a common phenomenon for fluvial deposited sediments (Wallinga, 2002). To obtain a reliable burial dose estimate from the D_e distribution, we employed the Minimum Age Model (MAM; Galbraith et al., 1999) which selects the youngest part (i.e. the lowest D_e population) of the distribution. The model was run with an over-dispersion input parameter (σ_b) of 20%. To obtain a fair estimate of the error on the burial dose, the MAM model was repeatedly run in a bootstrapping procedure (Cunningham and Wallinga, 2012). The resulting burial dose estimate and associated uncertainty are used for the age calculation and are shown by the dark grey bar in the radial plots (Galbraith, 1990) and histograms of Fig. A3.2.1. For comparison, the Central Age Model (CAM, Galbraith et al., 1999) D_e estimate which represents a weighted mean of the respective D_e distribution is shown by a light grey bar (Fig. A3.2.1).

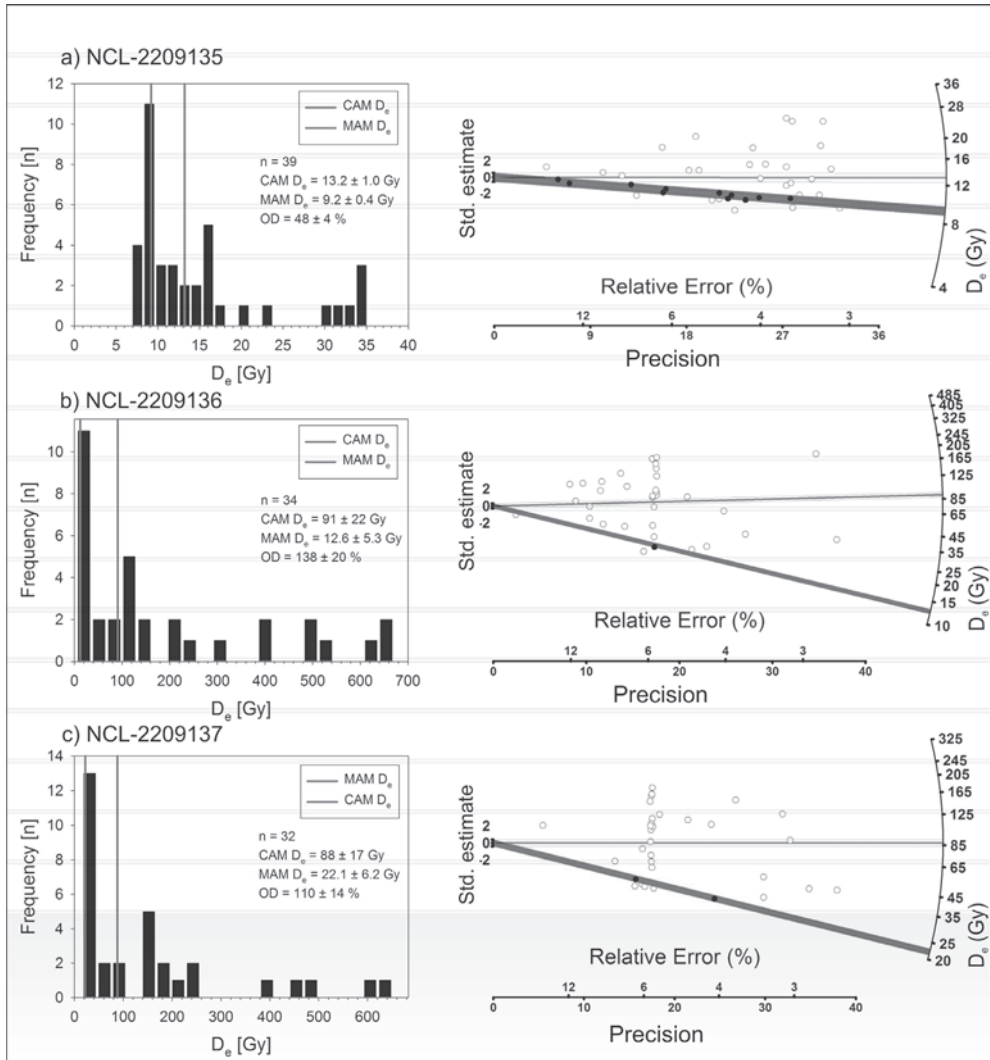


Fig. A3.2.1. The D_e distributions of a) NCL-2209135, b) NCL-2209136 and c) NCL-220913 are shown as histograms (left column) and radial plots (right column). The dark grey and light grey bands shown are centered on the doses determined using the Minimum Age Model (MAM) and Central Age Model (CAM) of Galbraith et al. (1999), respectively. The MAM was combined with a bootstrapping procedure (Cunningham and Wallinga, 2012). The over-dispersion (OD) of the distributions was calculated using the CAM.

Single-grain post-Infrared-Infrared (pIRIR) luminescence analysis

For the pIRIR feldspar single-grain measurements an automated Risø TL/OSL reader (DA 15) fitted with a dual (red and green) laser single-grain attachment (Bøtter-Jensen et al., 2003; Duller et al., 2003) was used. The grains were loaded into aluminium single-grain discs with a 10 x 10 grid of 300 μm grain holes. To confirm that only one grain was loaded into each hole the discs were visual inspected using a microscope. The feldspar grains were each optically stimulated for 1.68 s with a 150 mW 830 nm IR laser. The IRSL at 50 °C was released prior to the pIRIR single-grain measurement using an array of infrared LEDs (870 \pm 40 nm, \sim 140 mW/cm²) for 100 s stimulation. All feldspar signals were detected through a LOT/Oriel 410/30 interference filter to select the K-rich feldspar emission around 410 nm (Krbetschek et al., 1997). In situ irradiations were made using a ⁹⁰Sr/⁹⁰Y beta source.

A pIRIR protocol (Thomsen et al., 2008) was employed using a relatively low preheat of 175°C for 60 s and pIRIR stimulation temperature of 150°C in order to reduce the unwanted effect of thermal transfer in our young samples (Reimann et al., 2011; Reimann and Tsukamoto, 2012). The signal of the first 0.07 s after the IR laser was switched on was used as the initial signal and the signal observed in the last 0.48 s (1.20 – 1.68 s) was subtracted as background. All dose estimates were derived by fitting the regenerated dose points by an exponential function. For dose estimation each dose response curve was forced through the origin. For all experiments only single-grains with a test dose error of less than 20% and a recycling consistent with unity within 2 σ were accepted. Furthermore, all grains displaying non-monotonically growing dose response curves or other “abnormal” luminescence behaviour were rejected from further analysis.

To test the performance of the applied single-grain procedure a few hundred K-rich feldspar grains of sample NCL-2111099 were bleached for 5 hours using a solar simulator cabinet (Hönle SOL2). The grains were subsequently loaded into four single-grain disc (\sim 400 grains). Two single-grain disc were directly measured and analysed (details above) to determining the residual dose level (Fig. A3.2.2). The vast majority of grains show D_e values well below 1 Gy and close to zero indicating (i) good bleachability of the pIRIR signal and (ii) a low thermal transfer. The remaining 2 single-grain discs (\sim 200 grains) were given a beta dose of 9.9 Gy prior to the pIRIR single-grain measurement. The measured D_e distribution is symmetric and centred around 10 Gy (Fig. A3.2.2). The weighted mean of the single-grain pIRIR distribution was calculated using the Central Age Model (CAM, Galbraith et al., 1999). The measured CAM D_e is 10.3 \pm 0.3 Gy. The dose recovery ratio (measured/given dose) derived from this distribution is 1.04 demonstrating the suitability of the pIRIR single-grain procedure for these samples. The slight overestimation of the given dose is likely caused by a small residual dose in the grains (see Fig. A3.2.2). Furthermore, the over-dispersion value of the dose recovery pIRIR single-grain D_e distribution was calculated (Galbraith et al., 1999). An over-dispersion of \sim 18% indicates that the spread in the dose recovery distribution cannot be explained by the associated uncertainties on individual D_e values which are only made up of contributions from counting statistics and curve fitting errors calculated using “Analyst 3.24” (Duller, 2007). Thus, from now on, the dose recovery over-dispersion of 18% was added in quadrature to the uncertainties on the individual D_e s to account for other intrinsic sources of uncertainty (e.g. instrumental reproducibility, luminescence characteristics of the grains).

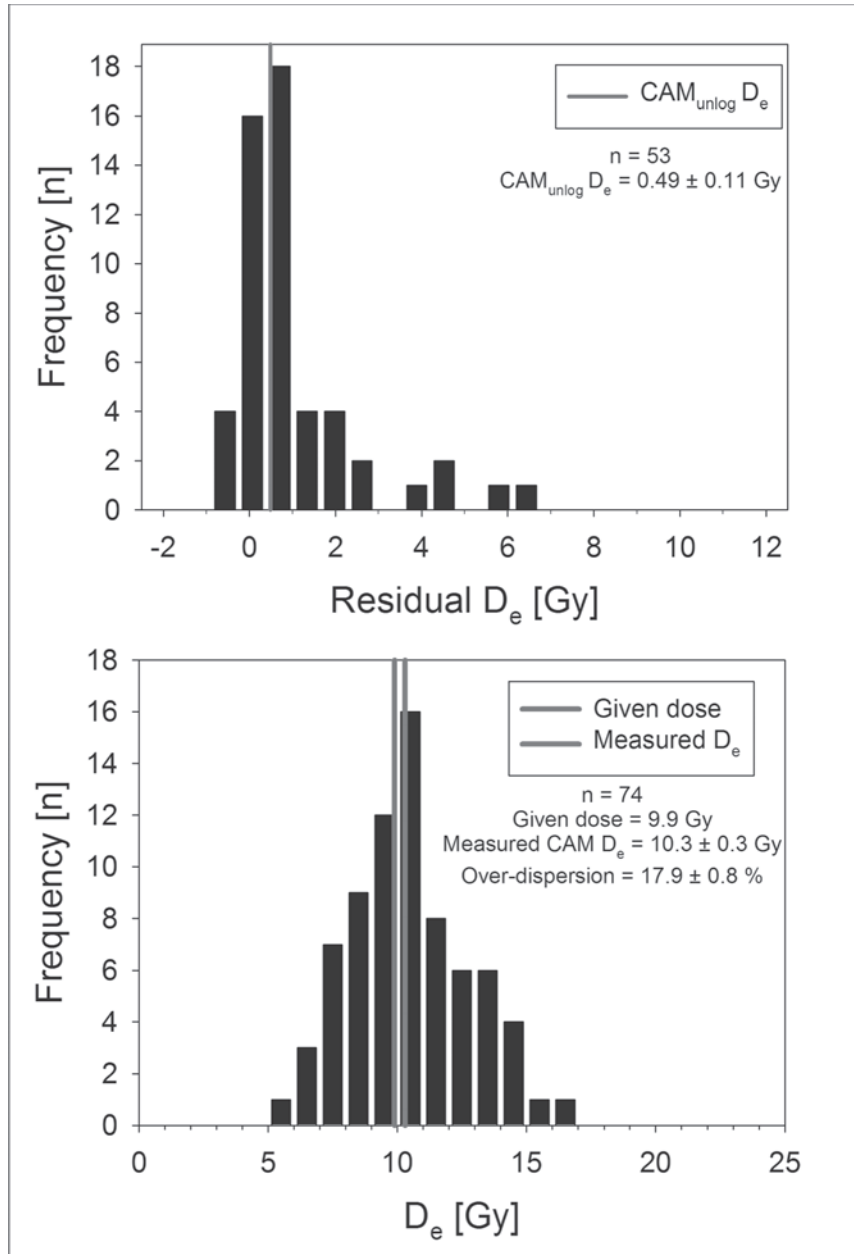


Fig. A3.2.2. Top: residual dose distribution from K-rich feldspar grains which were bleached in a solar simulator for 5h. The weighted mean (red line) was calculated with the unlogged version of the Central Age Model (CAM_{unlog}, Arnold et al., 2009). Bottom: K-rich feldspar single-grain dose recovery distribution. After the grains were bleached a laboratory beta dose of 9.9 Gy was given. The weighted mean and the over-dispersion of this distribution was calculated using the Central Age Model of Galbraith et al. (1999).

The three natural single-grain pIRIR D_e distributions (Fig. A3.2.3) of sample NCL-211095, -099, and 103 show very large over-dispersion values (85-120%) indicating that the assigned intrinsic uncertainties (see above) are too small to explain the spread in the natural distributions. All three distributions are furthermore clearly positively skewed with a well-defined leading edge D_e population around 5-10 Gy. The most likely reason for the large spread and shape of the natural single-grain D_e distributions is that the pIRIR signal of not all feldspar grains was completely reset prior to the deposition which is a common phenomenon for fluvial transported sediments (Wallinga, 2002). However, the amount of scattering in the pIRIR single-grain distributions is very prominent especially when compared with more common quartz single-grain analysis from other fluvial systems. This was previously reported by Reimann et al. (2012) for coastal over-wash sediments and can be explained by the lower rate of pIRIR signal resetting compared to the quartz OSL and the feldspar IRSL signal (Reimann et al., 2011; Reimann and Tsukamoto, 2012).

The Minimum Age Model (MAM, Galbraith et al., 1999) was applied to the natural single-grain D_e distributions to avoid overestimation of the burial dose by the feldspar grains that were not fully reset at the time of deposition. We defined the extra spread in a well-bleached D_e population that remains unexplained by the intrinsic sources of D_e scatter (i.e. the extrinsic over-dispersion) to be 20%. Adding in quadrature the intrinsic over-dispersion of 18% from the dose recovery distribution (see above) the overall unexplained scatter in a well-bleached D_e population was anticipated to be 27%. This value was used as input parameter for running the MAM. The MAM was combined with a bootstrapping approach to obtain meaningful uncertainty estimates (Cunningham and Wallinga, 2012).

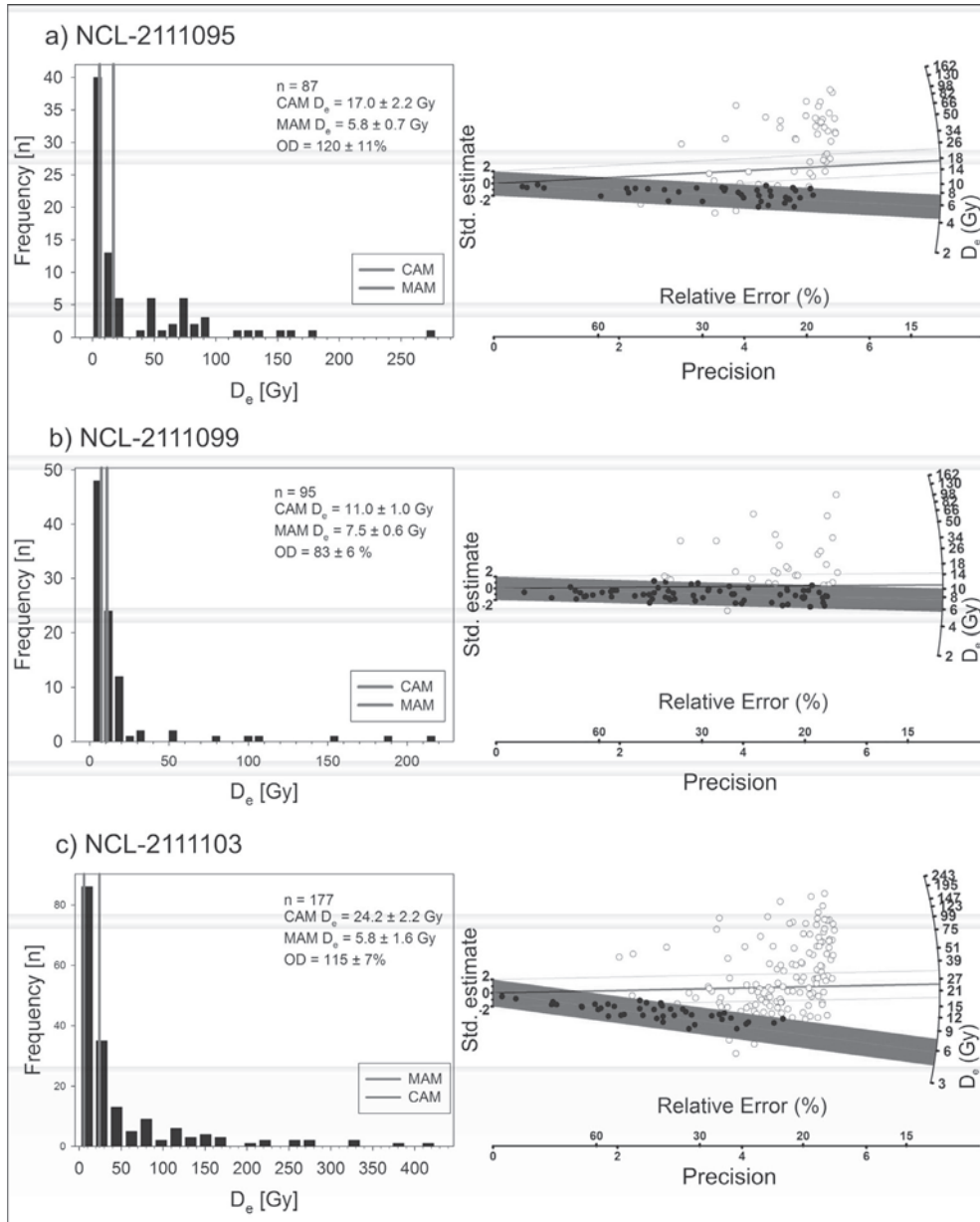


Fig. A3.2.3. D_e distributions of a) NCL-2111095, b) NCL-2111099 and c) 2111103 are shown as histograms (left column) and radial plots (right column). The dark grey and light grey bands shown are centred on the doses determined using the Central Age Model (CAM) and the Minimum Age Model (MAM) of Galbraith et al. (1999), respectively. The MAM was combined with a bootstrapping approach according to Cunningham and Wallinga (2012). The over-dispersion (OD) of the distributions was calculated using the CAM.



Chapter 4

Modelling long-term (300 ka) upland catchment response to multiple lava damming events

Landscapes respond in complex ways to external drivers such as base level change due to damming events. In this study, landscape evolution modelling was used to understand and analyse long-term catchment response to lava damming events. PalaeoDEM reconstruction of a small Turkish catchment (45 km²) which endured multiple lava damming events in the past 300 ka, was used to derive long-term net erosion rates. These erosion rates were used for parameter calibration and led to a best fit parameter set. This optimal parameter set was used to compare net erosion landscape time series of four scenarios: i) no uplift and no damming events, ii) no uplift and 3 damming events, iii) uplift and no damming events and iv) uplift and 3 damming events. Spatial evolution of net erosion and sediment storage of scenario iii) and iv) were compared. Simulation results demonstrate net erosion differences after 250 ka between scenarios with and without dams. Initially, trunk gullies show less net erosion in the scenario with damming events compared to the scenario without damming events. This effect of dampened erosion migrates upstream to smaller gullies and local slopes. Finally, an intrinsic incision pulse in the dam scenario results in a higher net erosion of trunk gullies while decoupled local slopes are still responding to the pre-incision landscape conditions. Sediment storage differences also occur on a 100 ka scale. These differences behaved in a complex manner due to different timings of the migration of erosion and sediment waves along the gullies for each scenario. Although the specific spatial and temporal sequence of erosion and deposition events is sensitive to local parameters, this model study shows the manner in which past short-lived events like lava dams have long lasting effects on catchment evolution.

Based on: Van Gorp, W., Veldkamp, A., Temme, A.J., Schoorl, J.M. Modelling long-term (300 ka) upland catchment response to multiple lava damming events. Under revision for *Earth Surface Processes & Landforms*.

4.1 Introduction

It has been recognized that geomorphic systems usually respond in complex nonlinear ways to external drivers such as climate or base level and that internal system dynamics exist even in absence of external forcing (Schumm, 1979; Phillips, 2006). Landscape evolution models (LEMs) allow simulation of this complexity and nonlinearity. However, model results have to be analysed with caution due to uncertainties in input data, spatial and temporal scale issues, simplifications in process descriptions and calibration and validation issues (Van De Wiel et al., 2011). Furthermore, outputs of LEMs demonstrate this complexity and the necessity to acknowledge the significance of initial conditions, topography and historical contingency (Wainwright, 2006; Coulthard et al., 2007). Although different modelling studies using reconstructed palaeo landscapes (palaeoDEMs) have yielded successful results in reconstructing sediment volumes or landform patterns (Peeters et al., 2008; Temme and Veldkamp, 2009; Baartman et al., 2012b), large uncertainties remain. In particular, the lack of information about palaeo landscapes and the associated lack of data to validate model inputs and outcomes remain challenging for this approach.

Despite these limitations, frameworks emerge that landscape evolution modellers can use to simulate landscape response. Temme et al. (2011a) argue among others that decisions on model setup and which processes to incorporate are case-specific and should be consciously made and tested. Tucker (2009) stresses that modelling landscape change of actual landscapes requires i) that only one variable, such as base level, changes significantly, while the rest remains fairly constant, ii) needs temporal control on palaeosurfaces or rates of change, iii) demands knowledge of the main processes active and iv) requires elevation data of sufficient quality. Van De Wiel et al. (2011) similarly emphasize the value of numerical models to test different external forcing scenarios of which results can be compared. All these workers stress that the introduction of too many parameters or too detailed process descriptions in landscape evolution studies is not desirable because it increases uncertainty of model outputs. Due to such limitations the aim of such studies should not be an exact reconstruction of elevations or sediment thicknesses at specific locations. Better, general patterns of landscape change such as catchment sediment yields, river profile development and general sediment redistribution patterns through time and space should be used to constrain model parameters and to inform choices between model versions (Tucker and Hancock, 2010; Temme et al., 2011a). This line of reasoning can be extended by arguing that model simulations that aim to clarify the effect of external drivers, such as lava dams, on landscape evolution are more robust when based on actual landscapes with known geomorphic setting and validation data than on entirely fictitious landscapes.

Many landscape evolution modelling studies have investigated landscape response to external drivers (e.g., Tucker et al., 2001; Coulthard et al., 2005; Temme et al., 2009; Hancock and Coulthard, 2012). The main advantage of using LEMs for this purpose is the possibility to analyse landscape evolution on spatial and temporal scales beyond the limitations of fieldwork or laboratory based experiments. One of the specific cases where LEMs can be useful is the modelling of long-term landscape response to temporary damming, blocking and dam removal. These damming events are interesting from a geomorphological viewpoint because they have significant influence on river profile evolution, for instance in the case of landslide

dams (Korup et al., 2006; Korup et al., 2010) and could divert drainage of channels and entire river catchments, exemplified by different lava dam studies (Roach et al., 2008; Maddy et al., 2012a; Veldkamp et al., 2012). Furthermore, LEMs potentially valuable to increase knowledge on long-term response to human induced dammings and dam removals (Sawaske and Freyberg, 2012). Dams can either breach suddenly, leading to extreme flooding events (Fenton et al., 2006), or can be incised gradually, temporarily hampering fluvial incision (Ely et al., 2012). Response to damming is not necessarily straightforward. Besides the known effects of sediment deposition and knickpoint creation, damming can lead to complex responses such as stream rerouting and complex river profile evolution (Ely et al., 2012; Maddy et al., 2012a; Van Gorp et al., 2013).

Our interest in this Chapter is the effect of lava dams on landscape evolution. We therefore base our study on an actual upland catchment that is known to be affected by multiple lava dams at its outlet, the Geren Catchment in western Turkey (Van Gorp et al., 2013). Our aim in this study is to elucidate the long-term response to damming events and uplift on the landscape evolution of a small upland catchment such as the Geren Catchment.

Specific objectives are:

1. To calibrate model parameters using reconstructed average net erosion over 300 ka and
2. To compare the effect of different scenarios of driving factors on landscape evolution.

4.2 Study site

The Geren Catchment drains into the upper Gediz River, Western Turkey. Both rivers have mainly incised into Miocene fining-upward basinfills, containing gravels at the base, sands and silts of the Ahmetler formation in the middle part and lacustrine limestone deposits of the Ulubey formation on top (Seyitoglu, 1997). Fault-driven Plio-Pleistocene drainage diversion created the current Gediz River which incised into the readily erodible Ahmetler in the early Pleistocene (Maddy et al., 2007). Since then, the upper Gediz River is responding to uplift with a time-averaged incision rate of 0.14 mm a^{-1} , while differential tectonics are not known to have occurred (Maddy et al., 2012b). Initiation of volcanism in the early Pleistocene led to damming of the upper Gediz River system by lava flows in the early and middle Pleistocene and the Holocene at subsequently lower levels due to ongoing fluvial incision by the Gediz River (Richardson-Bunbury, 1996; Westaway et al., 2004; Maddy et al., 2012a; Van Gorp et al., 2013). The incision of the Gediz River in combination with repeated damming events just downstream of the Gediz-Geren confluence controls the base level of the Geren Catchment. At this location, middle Pleistocene lava flows are present with their top elevation around 40 m above current river level and which are capped by fluvial deposits, indicating that the upstream Gediz reach and the Geren Catchment have been dammed (see Chapter 5). While generally dam duration of the middle Pleistocene dams is unknown, dam duration of the youngest recognized dam is in the order of magnitude of 1 ka, where dam elevation in this case is approximately 20 m (Chapter 1).

The Ulubey limestones now border the northern part of the Geren Catchment in the form of a limestone escarpment. The larger part of the southern border of the Geren Catchment

consists of an early Pleistocene Lava plateau, capping unconsolidated Miocene Ahmetler sands, silts and gravels. The Geren Catchment is dominantly incising into these Miocene basinfills, although at present, it hits underlying basement rocks near its outlet. In these reaches it mostly has a ridge-gully landscape, where ridges are often, but not always, capped by fluvial deposits derived from the upstream northern limestone plateau. These deposits either consist of coarse fluvial gravels, or of fine layered to laminated semi-horizontal sands and silts which can reach thicknesses of up to 20 m, indicating regime changes from more high energy fluvial conditions to low-energy conditions. Confined in the gullies, fluvial fill sequences are found at various levels. These aggradation - incision cycles are formed by at least 300 ka of catchment response to base level lowering of the Gediz River and we expect that repeated damming events have co-shaped the landscape evolution of the Geren Catchment.

4.3 Methods

4.3.1 DEM extraction

Because the accuracy of the freely available SRTM and ASTER-GDEM was limited for the area, it was chosen to construct a Digital Elevation Model (DEM) from stereo-satellite imagery. An ALOS-PRISM panchromatic imagery triplet with a pixel resolution of 2.5 - 3 m was obtained (Takaku and Tadono, 2009). The cloud-free forward, backward and nadir images date from April 2007 and have an image scene centre latitude-longitude of 38.696 N and 28.714 E. Ground control points were measured using a Sokkia dGPS and 15 of them were used for dem extraction with the DEM extraction tool in ENVI 4.7. A systematic shift in the resulting DEM was corrected and spatial resolution was upscaled to 30 m for the purpose of the simulation in this Chapter.

4.3.2 PalaeoDEM creation

As a start landscape for modelling, a palaeoDEM was created based on the 30 m ALOS-PRISM-derived current topography of the Geren Catchment. Gradient and elevation of gently sloping ridge surface levels and crests suggest their correlation to a catchment outlet around 40 m above current outlet level. A simple reproducible method was used to extract the DEM. Current channel elevations were derived from the channel network of the DEM (Fig. 4.1). Subsequently, All DEM gridcells which were more than 40 m above the elevation of the nearest channel were extracted (Fig. 4.2). A palaeosurface base level was imposed 40 m above current outlet level, leading to a palaeo-outlet of 390 m. Surfaces were then interpolated between palaeosurface cells using Topo to Raster in ArcGIS, leading to a simplified 30 m resolution PalaeoDEM. Finally, sinks were filled using Planchon and Darboux (2002) sink fill method in SAGA-GIS, with a tangent of 0.01 degrees.

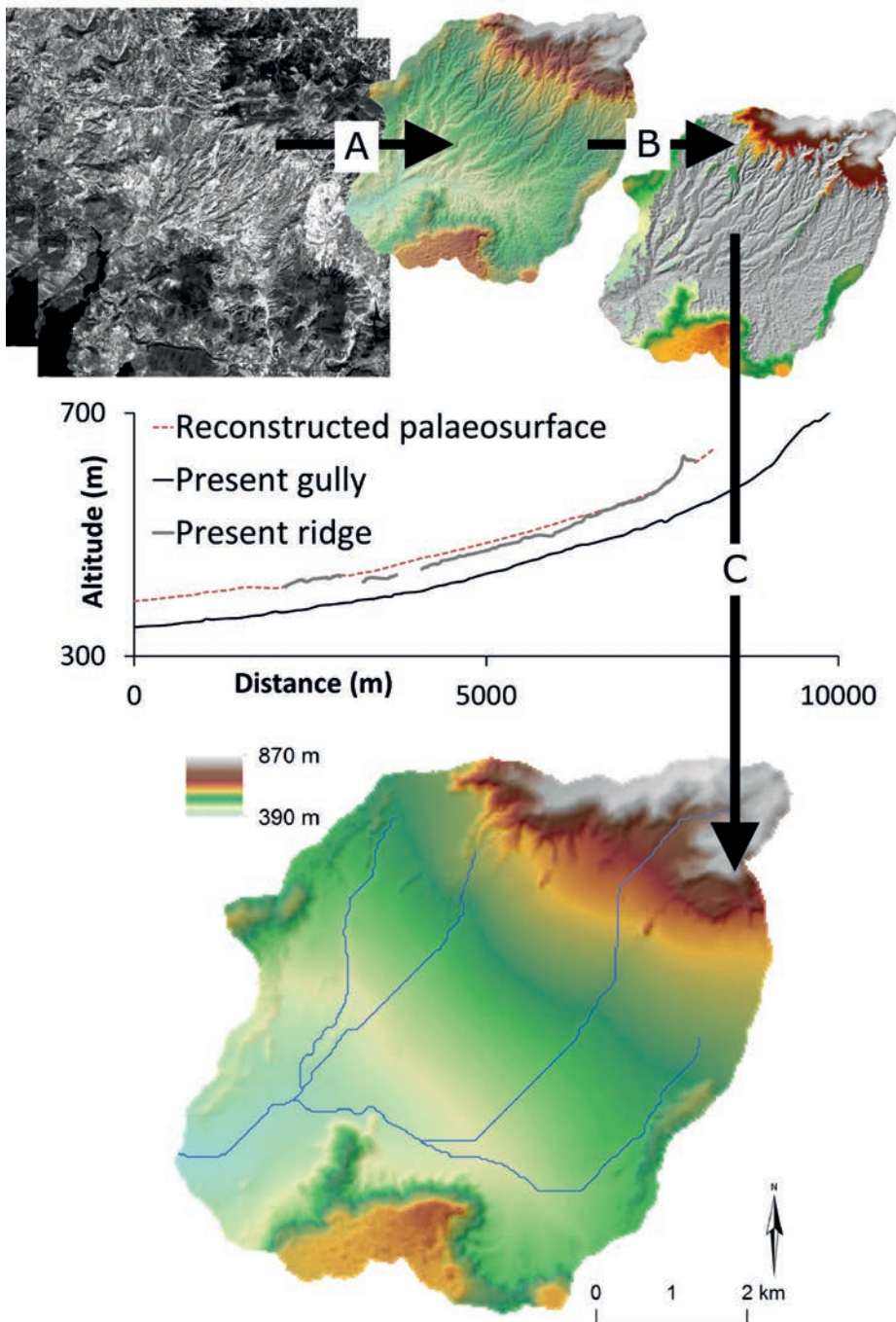


Fig. 4.1. A: DEM-extraction from a forward and backward image pair of ALOS-PRISM panchromatic satellite imagery. B: extraction of those locations 40 meter above current river level. C: palaeoDEM creation, using locations of B and a 390 m elevation outlet area.

The actual DEM was subtracted from the constructed palaeoDEM. This led to a volume of $784 \cdot 10^6 \text{ m}^3$ that was assumedly removed in 300 ka. Using average bulk density of 1500 kg/m^3 , this corresponds to an approximate net erosion of $0.97 \text{ Mg ha}^{-1} \text{ a}^{-1}$. This rate is low but within the lower range of erosion rates reported of some other uplifting areas (Safran et al., 2005). The calculated erosion rate was used to calibrate model parameters as discussed below and in Fig. 4.2.

4.3.3 Model framework

Reduced complexity LEM LAPSUS was used for simulations (Schoorl et al., 2000; Schoorl et al., 2002; Temme et al., 2009). LAPSUS is a cellular automaton that models a suite of geomorphic processes including water erosion and deposition and that can dynamically deal with non-spurious depressions (Temme et al., 2006) and lakes (Van Gorp et al., accepted). This makes it a suitable model for this study.

In LAPSUS, the multiple flow algorithm (Freeman, 1991; Quinn et al., 1991) is used to route water down from a cell to each of its downstream neighbours. Water arriving in depressions is routed to the outlet of those depressions. Sediment transport capacity C (m) between two cells over distance s and timestep t (usually yr) is then calculated from the fractional discharge Q (m) and tangent of slope Λ (-) (Kirkby, 1971):

$$C_{s,t} = Q_{s,t}^m \cdot \Lambda_{s,t}^n \quad (4.1)$$

Where parameters m and n are the discharge and slope exponent, respectively (Kirkby, 1987). The values of m and n reflect the type of runoff that is modelled. The sediment transport is then calculated based on (Foster and Meyer, 1972, 1975).

$$S_{s,t} = C_{s,t} + (S_{0s,t} - C_{s,t}) \cdot e^{-\text{cellsize} / h} \quad (4.2)$$

Where sediment in transport S (m) is a function of cellsize (m), transport capacity C and erosion or sedimentation component h (m), compared with the amount of sediment already in transport S_0 . If there is more sediment in transport than the transport capacity, deposition will occur and sedimentation component h is calculated as follows:

$$h_{s,t} = \frac{C_{s,t}}{P_{s,t} \cdot Q_{s,t} \cdot \Lambda_{s,t}} \quad (4.3)$$

Where P (m^{-1}) is a sedimentation factor. If sediment already in transport is smaller than transport capacity, erosion will occur and h is calculated as follows:

$$h_{s,t} = \frac{C_{s,t}}{K_{s,t} \cdot Q_{s,t} \cdot \Lambda_{s,t}} \quad (4.4)$$

Where K (m^{-1}) is an erodibility factor. Both K and P are lumped factors, representing surface characteristics for each cell of the catchment and are thus not empirically determined.

4.3.4 Parameter settings

In this study, erodibility factor K and sedimentation factor P are varied spatially according

to geological substrate (Schoorl et al., 2002). Initial K and P values were assigned to those areas underlain by Miocene alternating sands, silts and gravels. For the limestone plateau at the northern border, and the high basalt plateau at the southern border, K and P values were multiplied by 0.5 to mimic the more resistant bedrock (Table 4.1, Fig. 4.2). These resistant plateaus are both underlain by the Miocene sands, silts and gravel. The base of the northern plateau is estimated to be at 700 m, while the base height of the southern plateau is estimated to be at 580 m. Of course actual base heights are more variable, but a constant elevation is chosen for simplification reasons. This base height made it possible to change to the initial K and P values as soon as the bedrock was incised to its base height. Additionally, cells with a redistributed sediment layer of at least 0.1 m thick were given a ten times higher K and P than the underlying substrate to mimic transport limited conditions of coarse bedload sediment. Furthermore, sedimentation factor P is 4 magnitudes higher than erodibility factor K (Table 4.1). The reason for this large difference between P and K is that, for the long simulation timescale of this study, P is found to influence profile gradient of trunk streams, where higher P values generated more realistic profile gradients. Parameters m and n were set at 1.65, which is in between typical values for hillslope processes and fluvial processes (Baartman et al., 2012a), while the runoff convergence factor P_{conv} , which controls if water follows a steepest descent path or a more multiple flow path (Quinn et al., 1991), was set to 2, (Baartman et al., 2012b, our Table 4.1).

Table 4.1. LAPSUS model and parameter settings.

Model settings			
Model duration	300	[ka]	
Effective Rainfall	50	[mm/a]	
Uplift rate	0.00014	[m/a]	
Damming events	50, 150, 250	[ka]	
Dam duration	1	[ka]	
Dam elevation:	20	[m]	
LAPSUS parameter			
LAPSUS parameter	Value		Step
m	1.65		
n	1.65		
P_{conv}	2		
K	$1.3 \cdot 10^{-5} - 1.8 \cdot 10^{-5}$	[m^{-1}]	$1 \cdot 10^{-6}$
P	0.13 - 0.18	[m^{-1}]	0.01
$KP_{plateau}$	$K \cdot 0.5, P \cdot 0.5$	[m^{-1}]	
KP_{newsed}	$K \cdot 10, P \cdot 10$	[m^{-1}]	
Grid size	30*30	[m]	
Time step	1	[yr]	

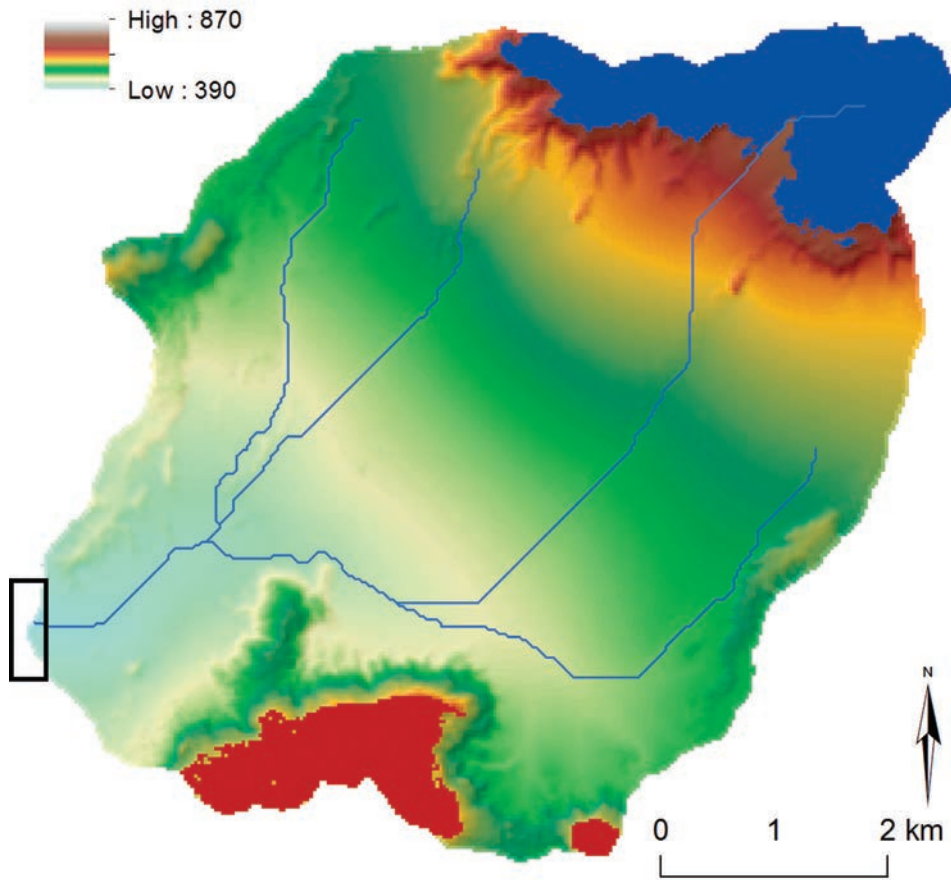


Fig. 4.2. Simulation boundary conditions on top of the hillshaded palaeoDEM. The black rectangle shows the area where base level change occurs (both gradual and damming). Regions where K and P are multiplied by 0.5 are coloured. In the blue region (a plateau consisting of Miocene/Pliocene limestones), this multiplying occurs if cell elevation is higher than 700 m. In the light grey-coloured region (a basalt plateau of early-Pleistocene age), this multiplying occurs if cell elevation is higher than 580 m.

4.3.5 Model calibration

The erodibility factor K and sedimentation factor P , which reflect parent material properties, were calibrated (Fig. 4.3). Erodibility factor K was varied in a calibration exercise which had as its objective to minimize the difference between simulated net erosion and calculated net erosion. This was done by comparing net erosion from runs where uplift and 3 damming events were imposed, with net erosion calculated from the difference between the palaeoDEM and the current DEM. The value of K was varied from $1.3 \times 10^{-5} \text{ m}^{-1}$ to $1.8 \times 10^{-5} \text{ m}^{-1}$, with steps of $1 \times 10^{-6} \text{ m}^{-1}$. Synchronously, P was varied from 0.13 to 0.18 with steps of 0.01 (Table 4.1). The best fit K (and hence, P) values derived from the stepped calibration were selected for further analysis of spatial-temporal impacts. The base level lowering rate of 0.14 mm a^{-1} was imposed on the outlet cells in the calibration phase.

4.3.6 Model scenarios

The model with the calibrated parameter set was run for different scenarios (Fig. 4.3): 1) no change in external drivers, 2) impose 3 damming events at 50 ka, 150 ka and 250 ka, 3) a constant base level lowering of the outlet cells by 0.14 mm a^{-1} , mimicking uplift-driven incision of the trunk river, and 4) scenario 2 and 3 combined, thus constant base level lowering with 3 damming events. The constant base level lowering and the lava dams were imposed at the catchment outlet. Base level lowering was imposed by lowering the outlet cells with 0.14 mm a^{-1} . Lava damming was imposed by adding 20m to the westernmost part of the Geren outlet area (Fig. 4.2) and dam duration was 1 ka, both based on field observations of the most recent damming event (Van Gorp et al., 2013). Each damming event was ended by lowering the westernmost part of the outlet area by 20 m, 1 ka after the start of damming.

4.3.7 Evaluation values

To assess differences in spatial and temporal response between scenarios, four catchment properties were compared; i) the time series of net erosion, ii) profile evolution of the main gully, iii) the difference in net erosion between scenarios and iv) the difference in storage of newly deposited sediments between scenarios. The latter two are shown separately because net erosion and sediment thickness on a cell can differ (Fig. 4.4), resulting in different spatial patterns. Thus a cell can experience net erosion, but still contain a certain sediment thickness. The use of sediment thickness has the advantage that it gives information about sediment redistribution within the catchment.

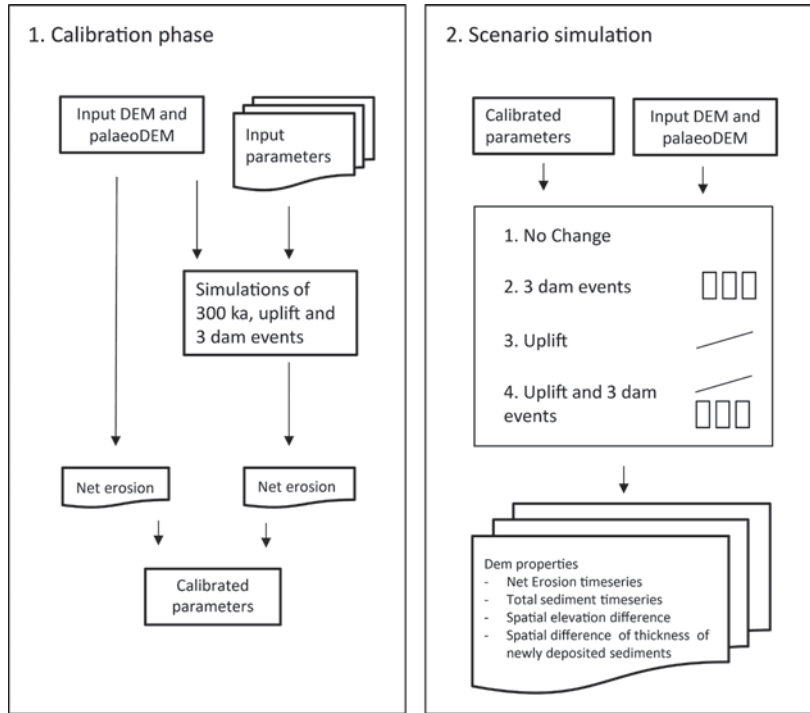


Fig. 4.3. Experimental setup of model simulations.

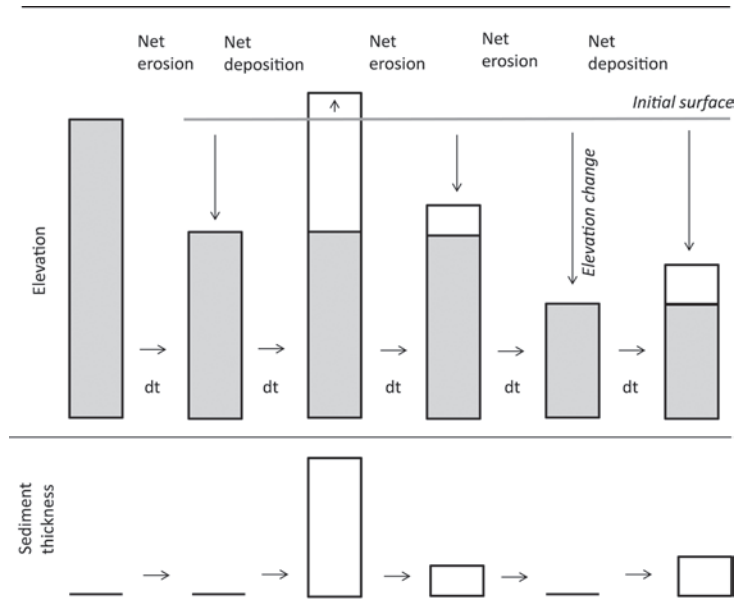


Fig. 4.4. Schematic diagram of elevation change versus thickness of newly deposited sediments of a cell over time.

4.4 Results

4.4.1 Step 1: Calibration

Average net erosion values for the calibration runs (Table 4.2) show a gradual increase of net erosion with increasing K and P. The optimal parameter set has a net erosion of about 0.986 Mg ha⁻¹ yr⁻¹, which is closest to the erosion rate from the palaeoDEM reconstruction. This optimal set is used for further scenario modelling.

Table 4.2. Total net erosion of scenario 4 (uplift and 3 damming events) for different calibration settings of K and P.

Parameter		
Erodibility K	Sediment factor P	Net erosion (Mg/ha/yr)
0.000013	0.13	0.851
0.000014	0.14	0.907
0.000015	0.15	0.921
0.000016	0.16	0.986
0.000017	0.17	1.023
0.000018	0.18	1.036

4.4.2 Step 2: Scenario modelling

For all four scenarios, a complex 1000 yr averaged net erosion timeseries is simulated, in which erosion is not a linear or other simple function of driving factors (see Fig. 4.5). Net erosion of the scenario 1 “No change” shows variable but generally declining annual net erosion. Further analysis of differences and similarities between different scenarios shows that: i) average net erosion and its standard deviation are consistently higher for the scenarios with uplift than for scenarios without uplift, ii) damming significantly changes annual net erosion and standard deviation of annual net erosion both with and without uplift, and iii) temporal variability of scenarios 3 (uplift) and 4 (uplift with dams) differ significantly. On the contrary, temporal variability is not significantly different between scenario 1 and scenario 2. The presence of uplift apparently enhances the variability of net erosion. The net erosion signal often shows alternating periods of higher and lower variability, which indicates phases of enhanced activity.

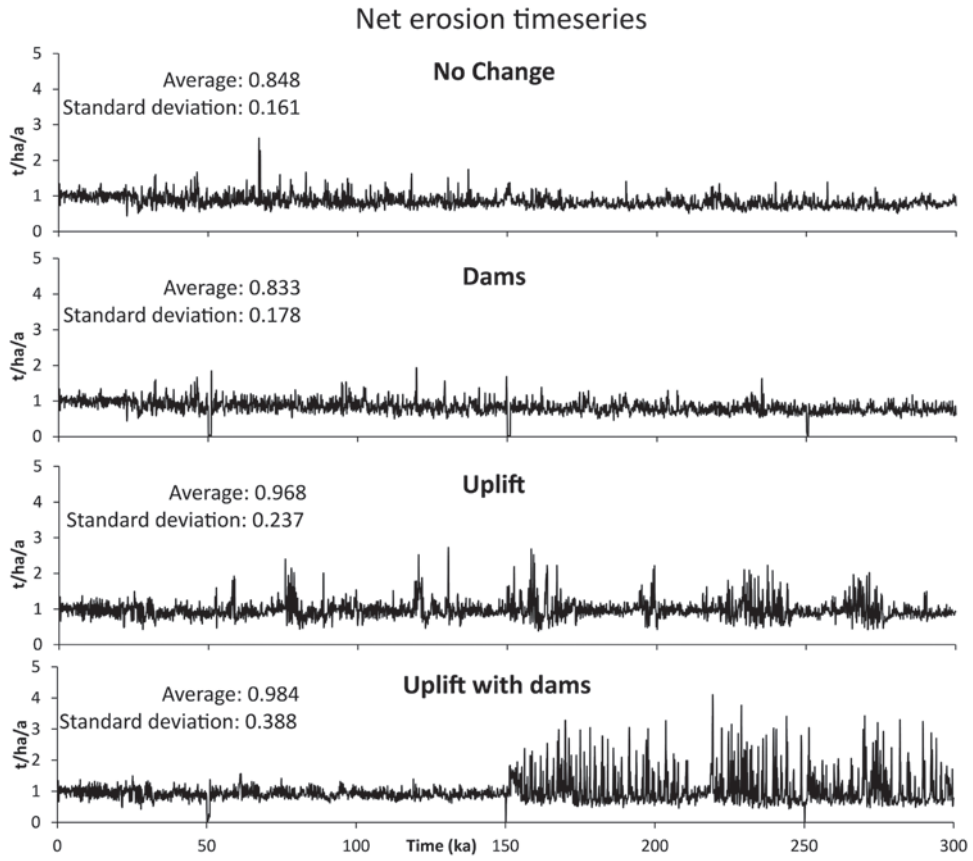


Fig. 4.5. Timeseries of net erosion for scenario 1-4 for the optimal parameter set.

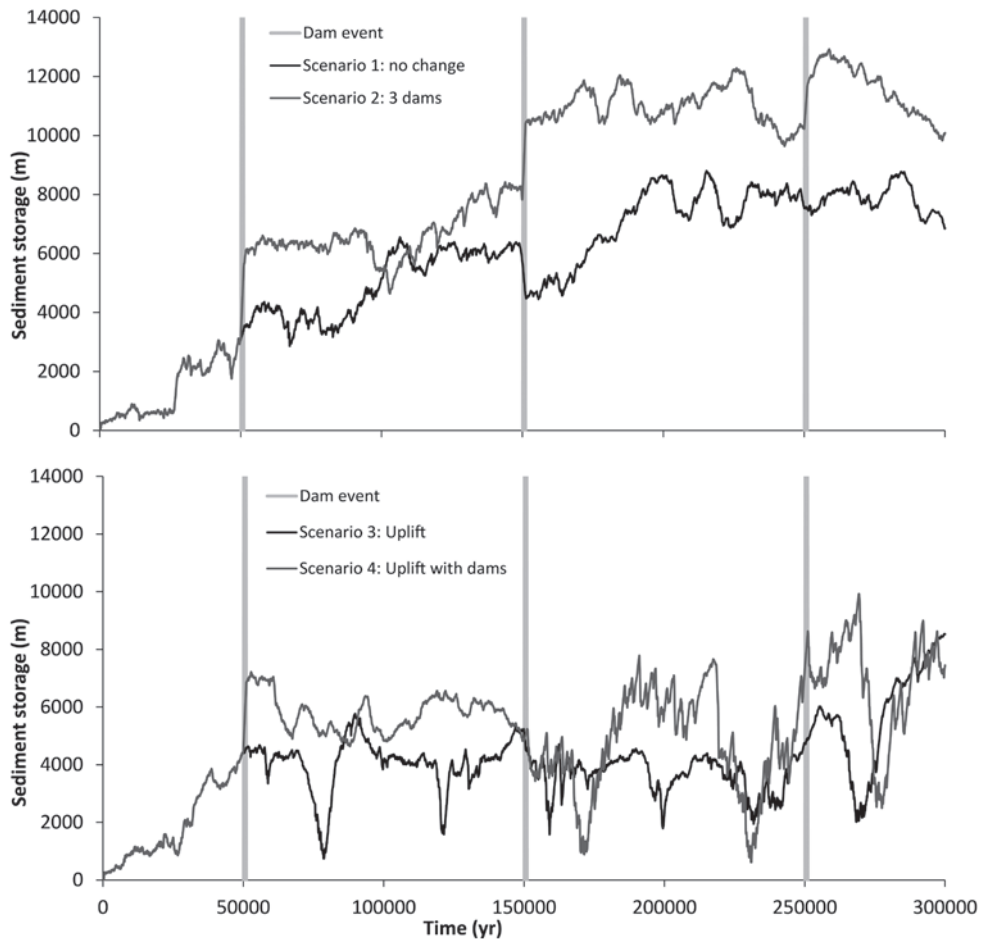


Fig. 4.6. Timeseries of sediment storage. Top: Scenario 1 and 2. Bottom: scenario 3 and 4.

Timeseries of sediment storage also show a difference in sediment dynamics between scenarios (Fig. 4.6). Scenarios 1 and 2, without uplift, show a progressive although not a gradual increase in sediment storage, whereas scenario 3 and 4, with uplift, do not. In scenario 3, uplift only, quasi-periodic periods of sharp decrease occur which coincide with the high variability periods of net erosion. Damming has a positive effect on sediment storage both with and without uplift. Periods of sharp increase in sediment storage during damming events of scenario 2 at 50 ka, 150 ka, and 250 ka are directly related to lake formation and siltation behind the dam body. Scenario 4 shows a similar sharp increase of sediment storage after the dam at 50 ka, but at 150 ka and 250 ka this increase is absent. Differences between scenarios at other points in time are related to complex response caused by the initial differences in elevation and sediment distribution right after damming. To relate model results to the existing field setting, profile and spatial analysis of simulations will be done on scenarios 3 and 4, which include uplift.

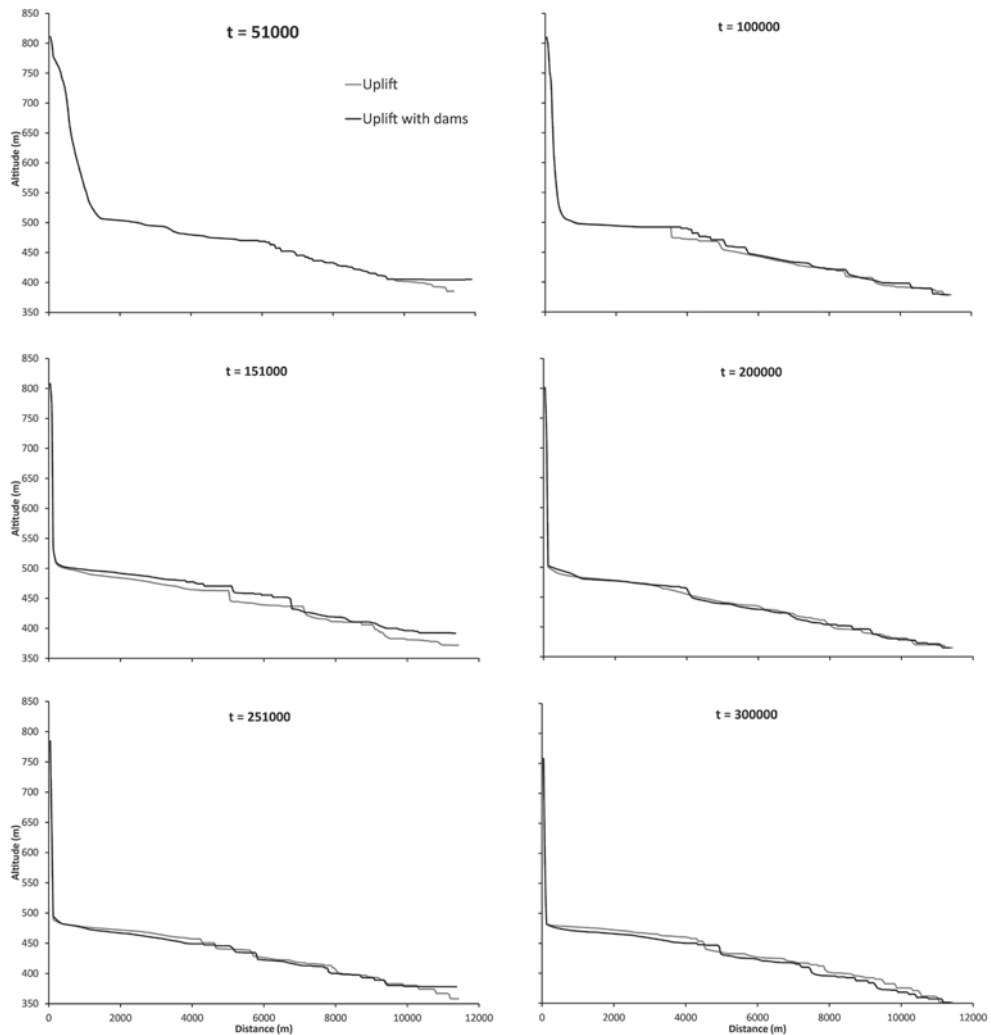


Fig. 4.7. Longitudinal profiles of uplift and uplift with dams of the principal trunk gully at several timesteps.

River profile evolution generally shows a profile that is adapting to the constant uplift rate (Fig. 4.7). A detachment limited profile is visible in the upper part of the catchment, where the low erodible plateau is incised. Below around 500 m altitude, sediment loads become higher and the profile forms a more linear to convex shape. Different knickpoints are visible which migrate upstream, or profile sections aggrade in the downstream direction. For instance, top-down driven aggradation is visible when comparing the profiles of 51 ka and 100 ka at an elevation around 500 m. Comparison of profile evolution between scenarios 3 and 4 reveals differences in elevation of up to 15 meters within the trunk gully. Infilling right after damming is visible at 51, 151 and 251 ka.

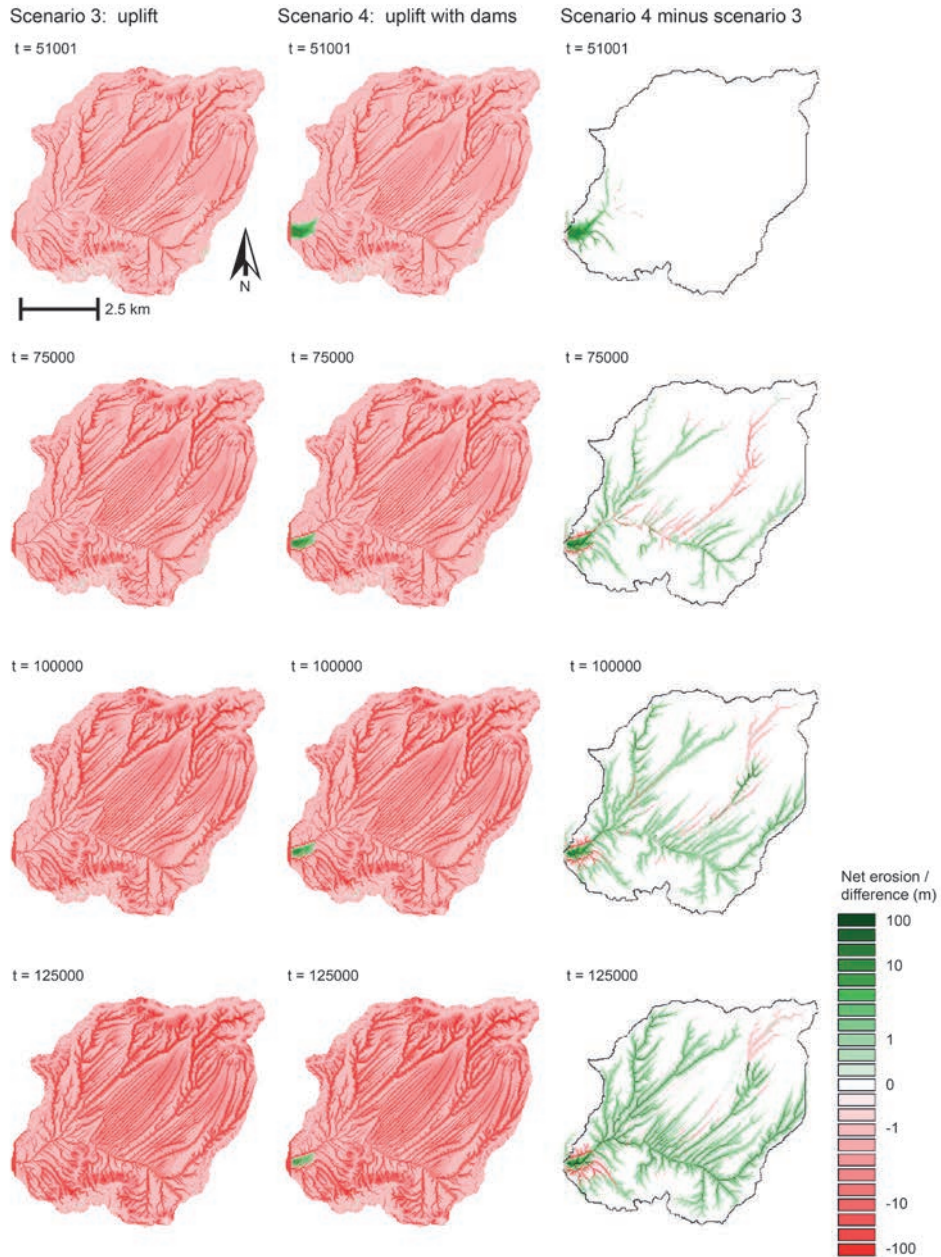


Fig. 4.8. Maps of elevation change since the start of the run (Column A and B) and difference in elevation change between scenario 4 “Uplift with 3 damming events” and scenario 3 “Uplift” (Column C) for $t = 51001$ to $t = 125000$.

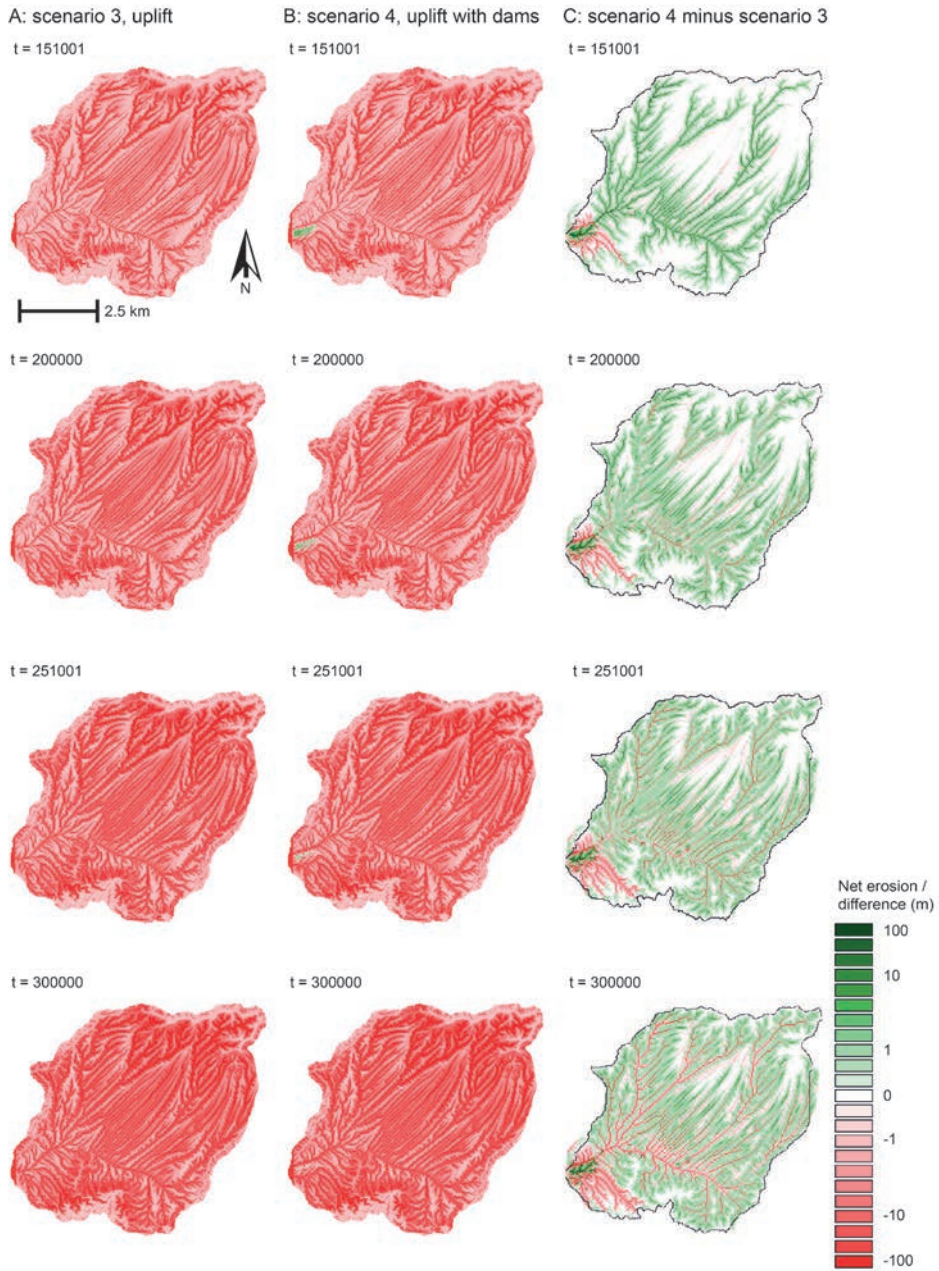


Fig. 4.9. Maps of elevation change since the start of the run (Column A and B) and difference in elevation change between scenario 4 “Uplift with 3 damming events” and scenario 3 “Uplift” (Column C) for $t = 151001$ to $t = 300000$.

Spatial patterns through time are assessed by looking at differences between elevation maps (thus, differences in net erosion) and differences between sediment storage maps. Difference between elevation maps are shown in Fig. 4.8 and 4.9. At $t = 51001$, one yr after removal of the first dam, the sediment storage behind the dam is clearly visible as a positive difference. This difference extends to upstream regions via the main gully systems when looking at $t = 75000$ and onwards until $t = 151001$. This visual difference is mostly positive, thus, net erosion is less for scenario 4 “uplift with 3 damming events” than for scenario 3 “uplift”. However, negative differences occur in different gully systems at different points in time. For instance, negative differences occur near the catchment outlet. This is due to stream rerouting on top of the lake sediments and post-dam incision in scenario 4. Over time, this incision shortcuts local streams, creating more incision and thus a negative elevation difference. At the time of removal of the third dam at $t = 251001$ and onwards, positive differences extend to slopes adjacent to gullies while the gullies themselves switch to a negative difference.

Snapshots through time of sediment storage difference maps between scenario 4 and 3 again show the direct effect of damming due to lake sediment storage behind the first dam, right after its removal at $t = 51001$ (Fig. 4.10). Storage difference rapidly extends to upstream gullies and sometimes switches from a positive to a negative difference. The difference due to the sediment body directly behind the dam gradually diminishes over time. After the second and third damming event at $t = 151001$ and $t = 251001$, the difference due to sediment storage being confined to the trunk gully. The changes from positive to negative differences through space and time indicate sediment waves which are active at different moments for the different scenarios.

In summary, results show a clear difference in net erosion and sediment storage between uplift and no uplift scenarios, while the difference between dam and no dam scenarios is especially expressed when looking at timeseries and spatial patterns of net erosion and sediment storage. More sediment is stored when damming occurs. This is due to remnants of storage directly behind the dam body, and to upstream storage in the trunk and other gullies.

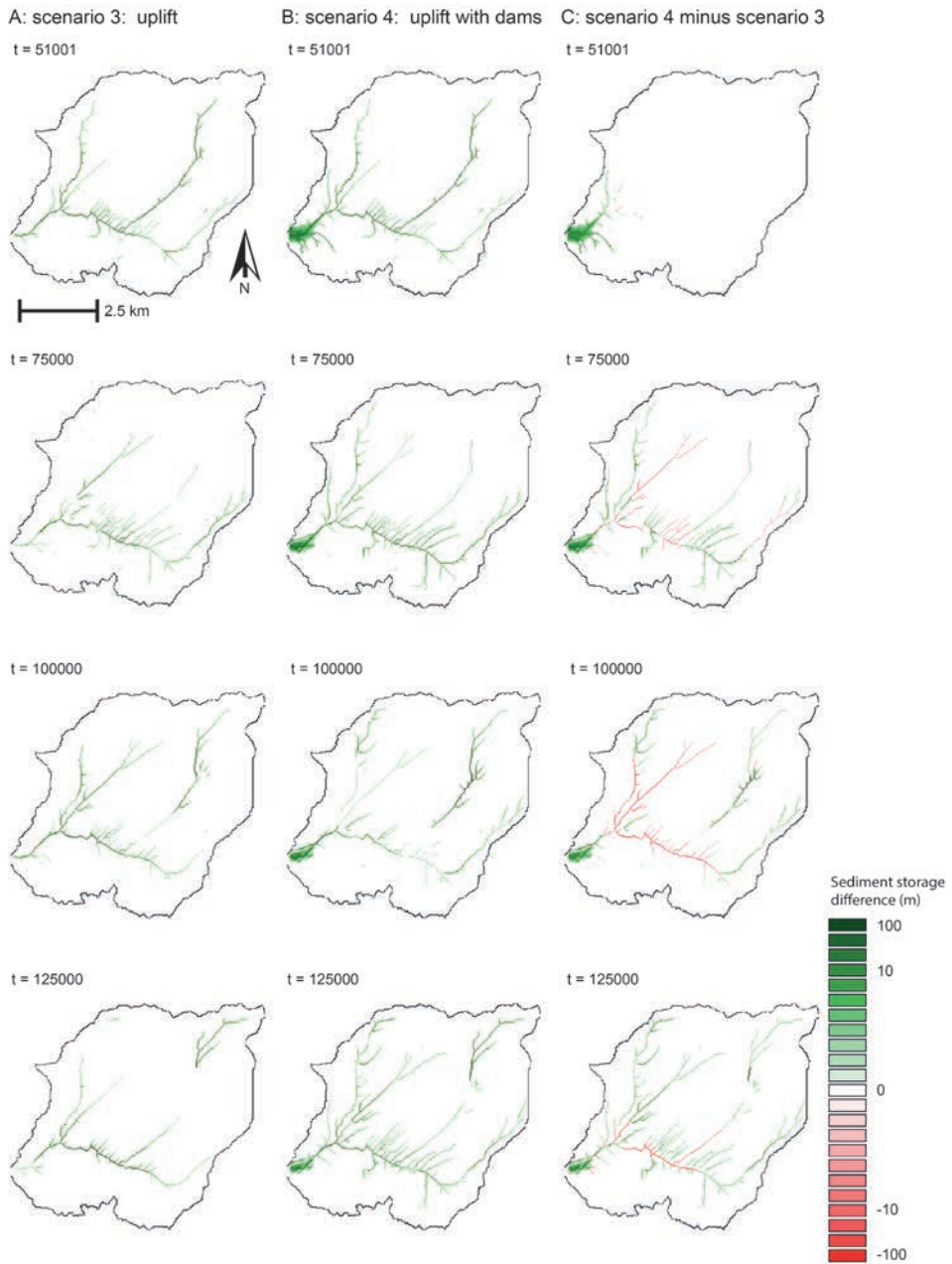


Fig. 4.10. Sediment storage of scenario 3 “uplift” (column A) and scenario 4 “Uplift with 3 damming events” (column B) and their difference (column C) for t = 51001, 75000, 100000 and 151001 ka.

4.5 Discussion

The simulated timeseries of net erosion and sediment storage show autogenic behaviour and non-linearity (cf. Coulthard and Van De Wiel, 2007) in all four scenarios. However the type of behaviour differs. The difference in pattern between the variability in timeseries of net erosion between scenario 1 and 3 (no uplift and uplift) suggests that uplift shifts complex response into another state. Gradual base level lowering causes high variability and low variability net erosion phases to alternate quasi-periodic. Which suggests that autogenic behaviour can generate non-climatically driven cyclic patterns in e.g. sediment archives. Rather, it is the episodic buildup and release of sediments by the catchment. Which is controlled by catchment topography, but apparently unlocked by gradual base level lowering.

Most of the times, response to damming is not visible in the net erosion signal, suggesting shredding of the dam signal due to sediment redistribution (a mechanism suggested a.o. by Jerolmack and Paola, 2010). However, after the second damming in scenario 4, the net erosion signal shifts from a weakly variable to a highly variable signal. This is visible in the sediment storage signal as an increase in variation. Increased sedimentation during damming is the most direct effect of lava dams on spatial catchment evolution (Fig 4.8 – 4.10), as further documented by numerous reconstruction studies (e.g. Ely et al., 2012; Van Gorp et al., 2013).

The more interesting effect in the simulations is upstream migration of elevation differences between dam and non-dam scenarios (Fig. 4.8 and 4.9). This migration starts at the start of the first damming at 50 ka and extends over an ever increasing area of the catchment until the end of the 300 ka simulation. Differences first arise in the main gullies after which they extend to smaller gullies and slopes along gullies. The generally lower net erosion in the dam scenario extends to upstream regions until $t = 150000$. However, from $t = 200000$ and onwards (Fig. 4.8), a negative difference extends into all main gullies. This results in channel-hillslope decoupling with a positive difference in smaller gullies and slopes and a negative difference in the main gullies. This indicates an increase in local relief in scenario 4 “uplift with dams” compared with scenario 3 “uplift”. This suggests that the damming effect amplifies the decoupling between main gullies and their tributaries and slopes. Furthermore, it demonstrates a legacy effect in the landscape over timescales of 300 ka. The more complex signal of spatial sediment storage difference (Fig. 4.10) is due to the fact that the location of gully stretches containing sediments differs through time, which can lead to zero difference between scenario 3 and 4 at one timestep, while a large difference was present at an earlier timestep. Nevertheless, differences of sediment storage migrate upstream at least until $t = 125000$ ka. Drainage rearrangement after the first damming (50 ka) affects local stream paths and stream lengths and over time affects the stream length of the trunk gullies as well. The main gully is rerouted to the north of the dam body, shortening the trunk stream length. This difference in drainage path of local and trunk streams can play a role in increasing long-term incision in scenario 4 “uplift with 3 damming events”, 150 ka after occurrence of rearrangement, around 200 ka. The damming therefore does not only cause a delay and decoupling of different river reaches, it also can lead to an amplified incision rate.

4.5.1 Model sensitivity

The sensitivity of simulation outputs to small changes in parameters was assessed by an analysis of the outputs for the parameter sets that were not selected after calibration. The average and variation of net erosion for the parameter settings that were not selected after calibration show similar trends as those of the optimal parameter set depicted in Fig. 4.5. However, the exact shape of the time series is sensitive to parameter settings in a complex way. Likewise, upstream migration of net erosion differences (Fig. 4.8 and 4.9) occurs in all parameter settings, but the exact pattern is dependent on parameter settings. So, exact locations of positive and negative differences vary between parameter settings. Nevertheless, for all parameter sets, damming events in an uplift driven landscape have a similar long-term effect on landscape evolution as discussed above for the calibrated parameter set.

4.5.2 Model setup limitations

Several external climate related controls which are known to have varied within the modelled temporal extent have been held constant in our simulations. Effective rainfall is held constant over the 300 ka simulation period, although over this temporal extent, climate change is thought to play a significant role (e.g. Tzedakis et al., 2006 for the Eastern Mediterranean). The reasons to keep rainfall constant are firstly to keep the simulation results as generic as possible, and secondly the large uncertainty that reconstructions of rainfall records could have. Rainfall reconstructions on these timescales often rely on reconstructions of sea surface temperature curves and evaporation reconstruction rely on $\delta^{18}\text{O}$ curves. Successful rainfall reconstructions have been done for systems where a direct link with a certain oceanic system is established (e.g. the Atlantic ocean, Stemerink et al., 2010; Viveen et al., 2013). However, such a reconstruction is more problematic for more continental systems. Another external control which is not varied is vegetation cover, which influences the erodibility of the landscape. This was done as well to keep outputs as widely applicable as possible.

Within this experiment, the initial PalaeoDEM surface is kept constant. Although it is based on interpolation of palaeosurfaces, its smoothed surfaces is unlikely to be the actual palaeosurface. However we chose to use this surface to keep model inputs as clean and simple as possible. We do acknowledge that a better uncertainty analysis of initial surface conditions would be advisable.

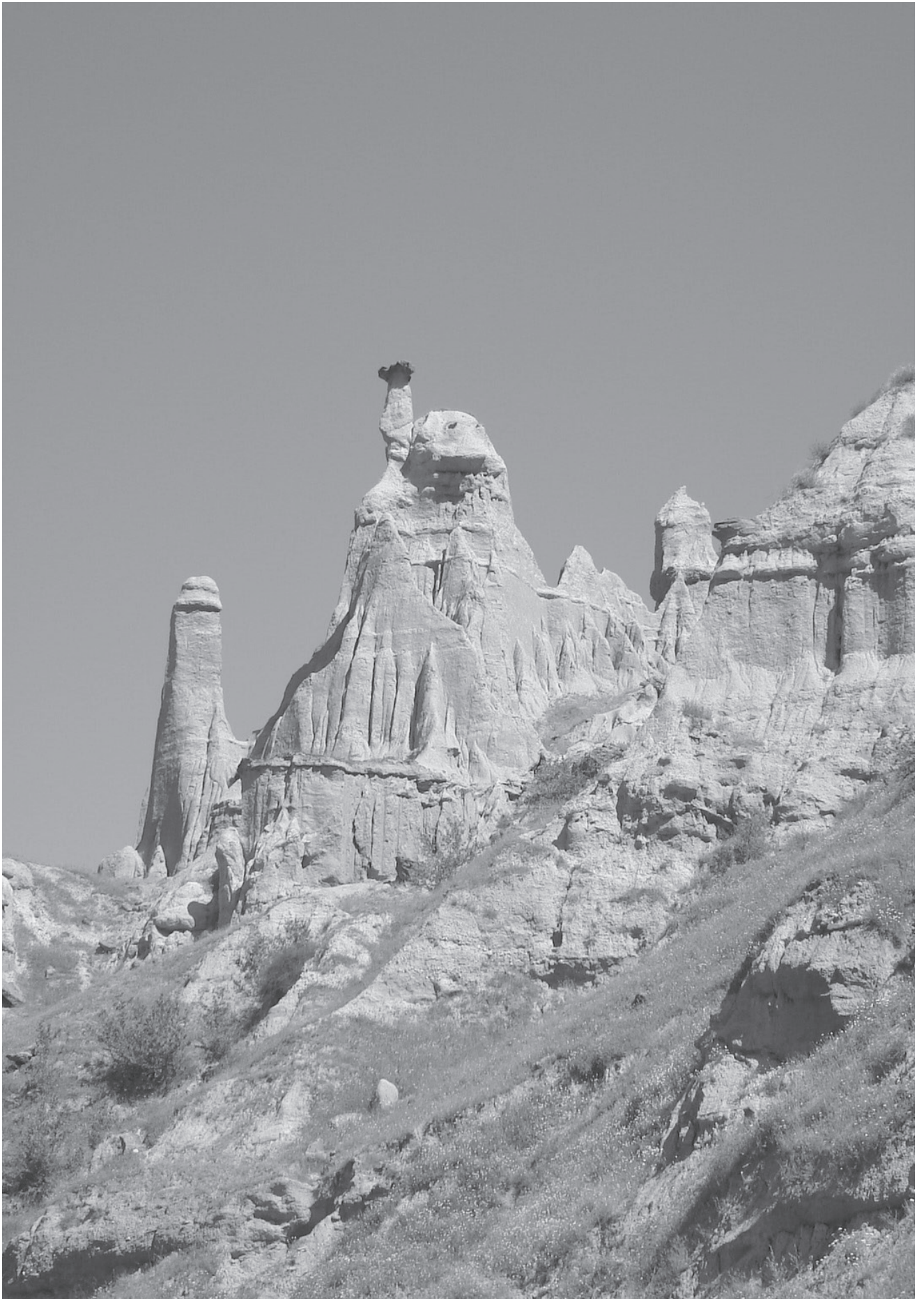
Although keeping these parameters constant implies a significant simplification compared to actual landscape evolution, it allows a clean assessment of the impact of changing base level scenarios on an upland catchment. This approach is widely taken in landscape evolution modelling literature (Coulthard and Van De Wiel, 2007; Tucker, 2009; Temme et al., 2011a).

One other step towards a clean assessment that is often taken in literature, is imposing equilibrium conditions on the study area before the start of comparative simulations (such as suggested by Tucker, 2009). This was not done in the present study because the imposition of equilibrium conditions, where erosion equals uplift averaged over the study area, would result in two different starting landscapes for the non-uplift and uplift scenarios. This would have meant that results could not be compared between these scenarios. Since such comparison was our objective, no equilibrium was imposed.

Conceptually, it is currently debated whether equilibrium conditions exist in actual field conditions (Phillips, 2013a). Both field and modelling studies suggest that the establishment of equilibrium in a wide variety of geological and climatic settings takes millions of years of constant forcing (Goren et al., 2013). Such constancy is rare. In the upper Gediz basin where this study is based on, equilibrium conditions did not exist 300 ka ago nor do they in the actual landscape.

4.6 Conclusion

Landscape evolution modelling revealed that lava damming events of 1 ka duration can have demonstrable net effects on catchment evolution on a 100 ka scale. Furthermore, it demonstrated that adding gradual base lowering as a boundary condition unlocks a different, more variable autogenic catchment behaviour compared to absence of base level lowering. Model parameters were calibrated to net erosion rates over 300 ka that were derived from palaeoDEM reconstruction of the small (45 km²) Geren Catchment which is known to have endured several damming events. Results showed that upstream migration of net erosion difference between scenarios with and without damming events is still on-going 250 ka after the first damming event. At first, trunk gullies show less net erosion in the scenario with damming events compared to the scenario without damming events. Then this effect migrates to smaller gullies and local slopes. Finally, an intrinsic incision pulse in the dam scenario results in a higher net erosion of trunk gullies while decoupled local slopes are still responding the pre-incision landscape. Sediment storage differences occurred on a 100 ka scale as well. However, they behaved in a complex manner due to different timings of the migration of sediment waves through gullies for each scenario. Although the exact spatial and temporal sequence of erosion and deposition events is sensitive to parameters and the initial palaeoDEM is uncertain, this model study demonstrates how short-lived events such as a lava dam can have long lived effects on catchment evolution. These events can even amplify the erosion rates due to prolonged decoupling of channels and slopes.



Chapter 5

Long-term response of the Geren Catchment (western Turkey) to lava dam influenced base level change

Combining field reconstruction and landscape evolution modelling can be useful to investigate the relative role of different drivers on catchment response. The Geren Catchment, a small (~45 km²) upland catchment in western Turkey is a suitable catchment for such a study. Field reconstruction and luminescence dating suggest that ridges in the catchment are capped by middle Pleistocene aggradational fills. Four middle Pleistocene lavaflows (310 – 175 ka, ⁴⁰Ar/³⁹Ar) repeatedly filled and dammed the Gediz River at the Gediz - Geren outlet resulting in infrequent base level rise and fall. Incision of the Geren trunk gully has been delayed until at least the end of MIS 5, after which an incision phase lowered the Gediz by around 30 m. Subsequent erosion and aggradation sequences demonstrate how the Geren Catchment has responded to base level lowering at least since MIS 4 by stepped net incision. Field reconstruction left us with uncertainty about what the main drivers of terrace formation were, therefore, possible scenarios were simulated using landscape evolution modelling. Three scenarios of landscape evolution in the Geren Catchment were investigated: i) uplift with climate (rainfall and vegetation based on arboreal pollen), ii) uplift, climate and short damming events and iii) climate, uplift and long damming events. Output was evaluated for erosion-aggradation evolution in trunk gullies at two different distances from the catchment outlet. Climate influences erosion – aggradation activity in the upstream reach, although internal feedbacks influence timing and magnitude. Lava damming events leave an aggradation signal in the downstream reach, while complex and lagged response to these dams obscure correlations with climate and leave a legacy on current landscape evolution. Catchment response to long damming events correspond best with field reconstruction and dating. The combination of climate and base level explains a significant part of the landscape evolution history of the Geren Catchment. By combining model results with fieldwork, additional conclusions on landscape evolution could be drawn.

Based on: Van Gorp, W., Schoorl, J.M., Temme, A.J.A.M., Reimann, T., Wijbrans, J.R., Maddy, D., Demir, T., Veldkamp, A. Catchment response to lava dam influenced base level change: an integrated field and landscape evolution modelling approach. In preparation for submission to *Geomorphology*.

5.1 Introduction

The impact of natural damming on catchment evolution can be significant, especially on 10^3 - 10^4 timescales (Korup et al., 2006; Maddy et al., 2012a; Van Gorp et al., 2013). River incision can cause landslides which consequently can dam the river. This internal feedback mechanism in river incision is important as it both causes external base level controls to not reach upstream areas, while the landslide induced sediment supply to the river either modulates or increases sediment discharge from the catchment (Korup et al., 2010). While landslide dams are usually short-lived, in the order of weeks (Ermini and Casagli, 2003), long-lived dams which can have a longer duration and higher impact do occur. This depends on size, shape and dam composition (Capra, 2007). Landslide dams can occur in any upland river system but quantifying timing and upstream spatial catchment response is often difficult due to lack of dam remnants or associated sediments (*cf.* Baartman et al., 2011). A natural dam where dam remnants often do remain and where direct age constraining is possible is lava damming. Recent studies from Kenya (Veldkamp et al., 2012), the United States (Crow et al., 2008; Ely et al., 2012), Australia (Roach et al., 2008) and Turkey (Maddy et al., 2012a; Van Gorp et al., 2013) indicate their significance for fluvial evolution on Quaternary timescales. Field reconstruction and dating of both basalts and fluvial deposits often reveals direct impacts such as stream rerouting, lake formation, infilling and dam removal. However the long-term response of upstream catchment evolution is hard to illustrate from fieldwork alone. In this case, a landscape evolution model (LEM) can be a useful tool to investigate the relative role of different drivers on catchment response, using field information on timing of damming events as an input, and known catchment characteristics. The Geren Catchment, a small (45 km²) upland catchment in western Turkey is a suitable catchment for such a study, because its base level has been influenced by volcanic damming at least in the Holocene (Van Gorp et al., 2013). The presence of older valley-filling lava flow remnants near the Geren outlet (Westaway et al., 2004) suggests that the Geren has been influenced by damming during the Pleistocene as well.

Upland catchment response to lava damming has been modelled using an artificial catchment, revealing response at and around the dam location at 10^4 ka timescale in the form of knickpoint persistence, delayed incision, sediment storage and stream reroutings on top of lake deposits (Van Gorp et al., accepted). Subsequent model work on catchment response to damming calibrated for the Geren Catchment already revealed how it responds at a 300 ka scale to lava dams under an uplifting regime (Van Gorp et al., in revision). Modelling results showed dampened incision and denudation of gullies and slopes, which migrates upstream. This dampening can subsequently be overtaken by renewed incision pulses through gullies, leading to decoupled landscape response. These results are valuable because they demonstrate that long-term response to dammings can be observed and modelled in a catchment such as the Geren. However, in that study, the goal was more conceptual and rainfall was held constant, while damming events were short (1 ka) and occurred once each 100 ka. Thus, some field-site specific information such as timing and duration of observed lava dams as well as climate data was not used.

The combination of field-derived landscape reconstruction with landscape evolution modelling is a promising methodology to understand landscape evolution, not only of specific

field areas but also by disclosing feedbacks or responses that can have a wider impact (Temme and Veldkamp, 2009). Fieldwork will herein always be indispensable because stratigraphic and landscape context can only be derived from it, next to aspects such as obtaining samples for dating or other types of analyses. Many landscape reconstruction studies are done by conducting fieldwork alone, while modelling studies are often only conceptual.

5.1.1 Aim

The aim of this Chapter is twofold: i) to reconstruct the actual response of the Geren Catchment to gradual base level lowering and actual lava damming events, and ii) to use a LEM to explore possible drivers for the observed behaviour. It is hoped that this demonstrates how field-based reconstruction and landscape evolution modelling can complement each other. To achieve this aim, first, new field and dating results are presented which constrain lava damming events and catchment evolution, leading to a base level reconstruction and determination of incision and aggradation phases within the Geren. Second, a 300 ka LEM simulation was done using this base level reconstruction and climate input to unravel long-term spatial response mechanisms to these dammings. Finally, model results and field results were combined to obtain new insights on Geren Catchment evolution.

5.2 Regional setting

The Geren Catchment is a small tributary catchment of the Upper Gediz River and is located in the Kula volcanic area, western Turkey. Here, the Gediz River is currently cross-cutting and incising into Miocene interior basin fills (Maddy et al., 2007) which are enclosed and underlain by metamorphic and metasedimentary basement rocks (e.g. Purvis and Robertson, 2004). These basin fills consist of a fining upward sequence (e.g. Seyitoglu, 1997), with deformed conglomerates and sands of the Hacibekir group at the base, which are unconformably overlain by fluviolacustrine deposits of the Inay group. The lower part of the Inay group consists of fluvial gravels and sands, fining up to silts forming the Ahmetler formation. This formation is overlain by lake-accumulated tephra which originated from Miocene stratovolcanoes, and which are topped by lacustrine limestones of the Ulubey formation. The onset of graben formation caused basin inversion and the Ulubey limestones now form plateaus in the study reach. Fluvial incision of the basin fills by the Gediz has mainly been driven by regional uplift and climate variability in the early Pleistocene (Maddy et al., 2012b). However, the Kula volcanic area is increasingly recognized as an area where lava damming has influenced fluvial evolution of the Gediz River and its tributaries since the onset of volcanism in the early Pleistocene until the present (Maddy et al., 2007; Maddy et al., 2012a; Van Gorp et al., 2013), in which three volcanism groups have been categorized, early Pleistocene β_2 , middle Pleistocene β_3 , and most recent β_4 lavas (Richardson-Bunbury, 1996). Early Pleistocene landscape reconstruction has benefited from clear preservation of Gediz terraces capped by β_2 basalts (Maddy et al., 2012a, 2012b). However, evolution of the Gediz in the period between 1 Ma and 250 ka remains poorly documented due to lack of known preserved records along both the Gediz and its tributaries such as the Geren. However, since 250 ka, fluvial terrace remnants were preserved again, when volcanic activity restarted (β_3 group). Radiometric basalt ages between 250 to 100 ka have been reported (Richardson-Bunbury, 1996; Westaway et al., 2006; Westaway et al., 2004). Most of these dates cluster between 100 and 200 ka. Some

of these dated basalts overlie fluvial Gediz terraces (Westaway et al., 2004), such as below the Söğüt flow unit upstream of the Geren outlet and the Palankaya flow downstream of the Geren Catchment outlet (Fig. 5.1) which have been $^{40}\text{K}/^{40}\text{Ar}$ dated to 236 ± 6 ka and 175 ± 3 ka, respectively (Westaway et al., 2006). However, near the Gediz-Geren confluence, there is no relation between dated basalts and fluvial terraces and thus a clear link between lavaflows and middle Pleistocene fluvial landscape evolution could not be made. The youngest basalts are Holocene of age and are sometimes located adjacent to current river level, such as near the Gediz-Geren confluence, where a 3-2.6 ka dated lava flow (Kula flow (Fig. 5.1) dammed the Gediz and Geren (Van Gorp et al., 2013).

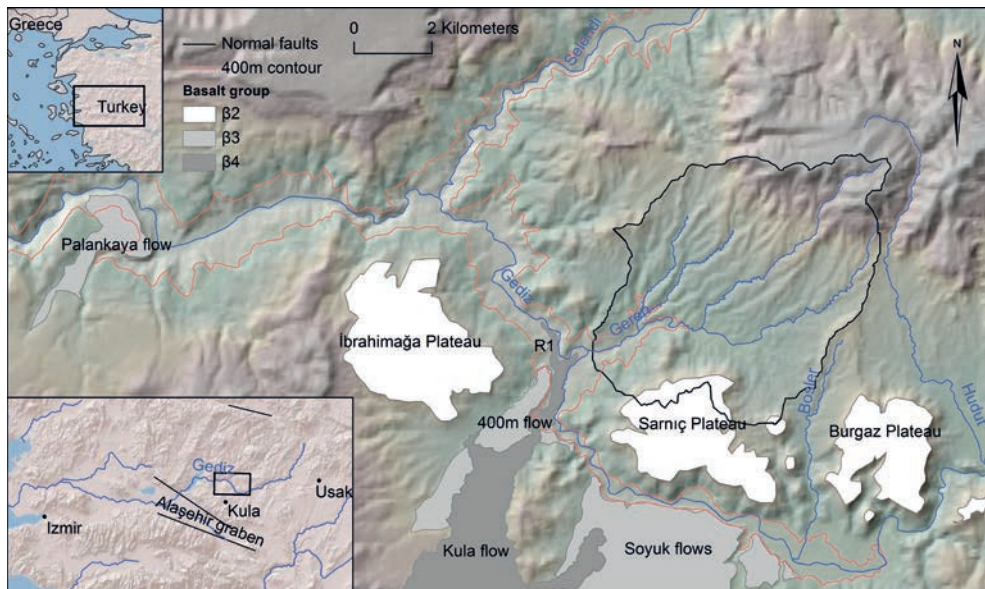


Fig. 5.1. Location and overview of the upper Gediz-Geren area. with some of the main volcanic units. Black line depicts Geren Catchment border.

5.3 Materials and methods

5.3.1 Approach

In this Chapter, landscape evolution modelling and field reconstruction are combined. First, fieldwork and dating results are presented. Second, the sequence of middle Pleistocene to Holocene lava damming events which influenced the Geren Catchment outlet is reconstructed. This reconstruction of damming events is translated into an input base level curve for a 300 ka landscape evolution modelling simulation, and model scenario setup is presented. Third, fieldwork and modelling results of Geren Catchment evolution are presented and discussed together.

5.3.2 Fieldwork

During fieldwork campaigns in 2009 – 2012, the Geren Catchment and the Geren-Gediz confluence area were geomorphologically mapped. Palaeosurfaces and fluvial terraces were recorded as well as areas with limestone-derived fluvial gravels and fines. Individual lavaflores and their relation with palaeo-Gediz valleys were determined. Samples for dating of basalts and sediments were taken.

5.3.3 Elevation model

Using ALOS-PRISM stereo-satellite imagery, a DEM was reconstructed with the DEM-extraction tool of ENVI 4.7. Ground control points were taken using a Sokkia dGPS. A palaeoDEM was created from a reconstruction and interpolation of palaeosurfaces (see Fig. 4.1).

5.3.4 Radiocarbon dating

Radiocarbon dating was done on an organic rich sample from fine layered mud-deposits using the Accelerator Mass Spectrometer (AMS) at the Centre for Isotope Research, University of Groningen, the Netherlands (Gott dang et al., 1995). Conversion of ^{14}C years BP to calibrated years BP was done using the IntCal04 calibration curve (Reimer et al., 2004) and the WinCal25 calibration program (See Appendix A5.1).

5.3.5 $^{40}\text{Ar}/^{39}\text{Ar}$ dating

Basaltic samples were taken for $^{40}\text{Ar}/^{39}\text{Ar}$ radio-isotopic dating from locations with a good correlation to the fluvial valley they filled. Age estimates were obtained by incremental heating experiments carried out at the VU University, Amsterdam, the Netherlands. Groundmass separates were prepared by obtaining homogenous fragments of microcrystalline groundmass to minimize the chance of inherited argon from phenocryst phases (Wijbrans et al., 2011). Data reduction and age calculations were made using ArArCalc v2.5 (Koppers, 2002). The detailed procedure is described in Van Gorp et al. (2013), Maddy et al. (submitted) and Schoorl et al. (submitted). Detailed age data are presented in Appendix A5.2.

5.3.6 Luminescence dating

Luminescence dating was done on fluvial sands of six samples. In this method the burial time of sand or silt deposits is estimated. The amount of ionizing radiation received by quartz or feldspar grains (palaeodose, Gy) since the time of burial is determined by measuring a light signal emitted by the minerals. The annual ionizing radiation dose received from surrounding materials is also determined (dose rate, Gy/ka). Luminescence age is then determined by:

$$\text{Age (ka)} = \text{palaeodose (Gy)} / \text{dose rate (Gy/ka)} \quad (5.1)$$

Measurements were carried out at the Netherlands Centre for Luminescence Dating, Delft University of Technology and Wageningen University, The Netherlands. Earlier experience with fluvial sediments from the study area showed that luminescence sensitivity of the quartz fraction is too low (Van Gorp et al., 2013) for accurate OSL dating. Therefore, the

sand-sized (180-212 μm) K-rich feldspar fraction was used for luminescence dating although the feldspar luminescence signals may be affected by anomalous fading, which causes age underestimation (Wallinga et al., 2007). To avoid or reduce this malign effect the post-IR IRSL luminescence signal (pIRIR) was used (Buylaert et al., 2012; Kars et al., 2012; Thomsen et al., 2008). For four samples we used conventional multiple-grain subsamples where a bulk pIRIR feldspar signal from 50 to 100 grains is measured. To reduce the unwanted effect of thermal transfer and residual dose, which is especially important for young Holocene samples (Reimann et al., 2011), we applied a low-temperature pIRIR signal (Reimann and Tsukamoto, 2012), and measured K-feldspar single grains (Reimann et al., 2012) for three samples which turned out to be Holocene. For details on measurement procedures, the reader is referred to Appendix A5.3.

5.3.7 Model

Landscape evolution model (LEM) LAPSUS (Schoorl et al., 2002; Temme and Veldkamp, 2009) was used to simulate a 300000 yr period of landscape evolution of the Geren Catchment. In the remainder of the text, the notation “ka” is used for field reconstructed ages in ka, while “yr” is used for simulation runtime, where yr 0 is equivalent to 300 ka ago and 300000 yr to present. LAPSUS is a grid-based model which models water runoff erosion and deposition. It routes water and sediment using multiple flow (Freeman, 1991; Quinn et al., 1991) and calculates sediment transport capacity C over time t (yr) and space s (m) between a cell and each of its downslope neighbours following Kirkby (1971).

$$C_{s,t} = Q_{s,t}^m \cdot \Lambda_{s,t}^n \quad (5.2)$$

Where $Q_{s,t}$ is fractional discharge (m) and Λ tangent of slope (-). Parameter m is the discharge, and n the slope exponent (Kirkby, 1971). The amount of sediment S (m) that will actually be transported over one *cellsize* length depends on transport capacity C and sediment in already in transport S_0 (m) and is calculated according to Foster and Meyer (1972, 1975):

$$S_{s,t} = C_{s,t} + (S_{0s,t} - C_{s,t}) \cdot e^{-\text{cellsize} / h} \quad (5.3)$$

Where h is an erodibility or sedimentation factor. When sediment already in transport is smaller than transport capacity, erosion occurs and h is calculated as follows:

$$h_{s,t} = \frac{C_{s,t}}{P_{s,t} \cdot Q_{s,t} \cdot \Lambda_{s,t}} \quad (5.4)$$

where K (m^{-1}) is an erodibility factor. If the amount of sediment already in transport is larger than transport capacity C , deposition will occur and h is calculated as follows:

$$h_{s,t} = \frac{C_{s,t}}{K_{s,t} \cdot Q_{s,t} \cdot \Lambda_{s,t}} \quad (5.5)$$

Where P (m^{-1}) is a sedimentation factor. K and P represent surface characteristics of a gridcell and have been used as calibration factors (Bartman et al., 2012b; Schoorl et al., 2002; Schoorl et al., 2004; Temme and Veldkamp, 2009; Van Gorp et al., in revision). Furthermore, LAPSUS can deal with non-spurious sinks dynamically (Temme et al., 2006). For recent further

explanations of model behaviour, the reader is referred to van Van Gorp et al. (in revision) and Schoorl et al. (2014) .

The model scenario setup will be discussed in paragraph 5.5.2, because its explanation requires fieldwork results, which will be presented in section 5.4.

5.4 Fieldwork and dating results

The current Geren Catchment can be roughly divided into four areas (Fig. 5.2). The first area is the outlet and trunk stream area (1), which is incising into Ahmetler silts, sands and gravels, but also into Palaeozoic basement, the Hacibekir group and basal conglomerates of the Ahmetler formation. Elongated ridges at about 2 km from the outlet are formed by a local limestone unit within the Miocene deposits. All these units are present in the downstream part of the western subcatchment as well (2). This second subcatchment is underlain by Ahmetler sands and silts and has some limestone gravels and sands in its upstream part. The central part of the catchment (3) is underlain by Ahmetler silts, sands and gravel only. Here, the highest volumes and thicknesses of limestone gravels are observed (limestone gravels 1, Fig. 5.2), which are capping many of the ridges. The eastern part of the catchment (4) is underlain by Ahmetler silts and sands. Limestone gravels are present but not so extensive as those in the central part. It has a generally lower ridge-gully relief, while the trunk stream has a lower gradient.

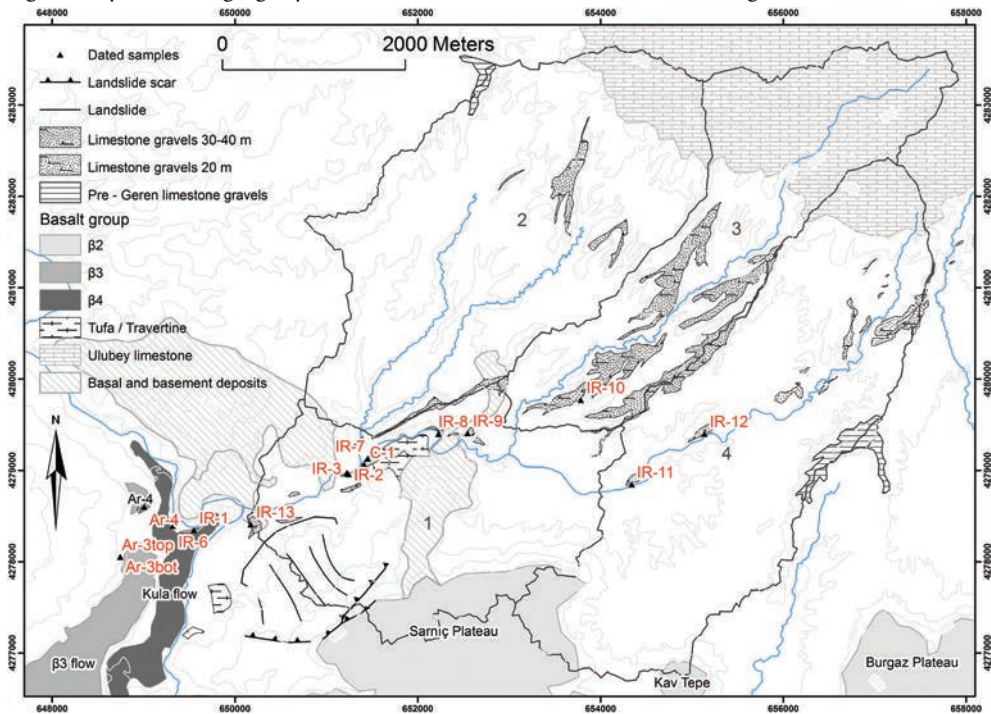


Fig. 5.2. Study area, showing i) main geological units, ii) geomorphology such as landslides and ridges capped with limestone deposits, approximate elevation above current stream level is indicated iii) locations and names of dated samples and iv) delineated areas 1 to 4 as the main subcatchments of the Geren.

5.4.1 Geren-Gediz confluence

Downstream of the Geren outlet, at the left bank of the Gediz River, lava remnants of β_3 flows are observed (Richardson-Bunbury, 1996). Here, a lava tongue which has filled the former Gediz valley, originates from the south. These basaltic lavas consist of at least two different flows stacked on top of each other, separated by a sandy layer containing fluviially transported tephra. Just downstream, an isolated lava remnant (Ar-4, Fig. 5.2, Fig. 5.3C) is not attached to one of these flows and from fieldwork their relation is unclear. This remnant is both underlain and overlain by fluvial gravels, evidencing base level rise of the Gediz since the establishment of this lava flow.

About 200 m southeast of the Gediz-Geren confluence, a calcium carbonate cemented fluvial terrace is present on top of Hacibekir conglomerates at around 375 m, approximately 20-25 m above present river level (Fig. 5.3A). It can be traced along the slope and resembles a meander. This terrace is buried by a gravel bearing sandy aggradational fill of up to 10m thick, reaching to 385 m elevation, 30 – 35 m above current river level. This fill shows fluvial sand layers and gravel bands which contain rounded basalts and limestones. Its exact thickness is unknown, as the top is not preserved and has a sloping agricultural field on it. However scattered in this field rounded basalts and limestones can be found. This whole sediment body resembles a fluvial terrace buried by a deltaic infill. Fluvial sand has been sampled for luminescence dating (IR-13). Upslope of this aggradation, a big landslide is present, containing big basalt blocks from the Sarnic scar. It has an observed base around 40 m above current river level. A direct contact has not been observed but their field relation suggests that this landslide entered the valley of the palaeo-Gediz around the time of IR-13. Further south, a now partly collapsed travertine mound is present (Van Gorp et al., 2013), with a current top around 400 m.

5.4.2 Geren trunk stream

Along the trunk stream of the lower Geren, several fluvial terraces and aggradational fills are observed at different elevations. The lowest fills usually have their base around 0.5 to 1 m above current river level. In addition to the Holocene aggradational fills IR-3 and IR-4, located 2 km upstream from the Geren outlet and which are described by Van Gorp et al. (2013), aggradational fills at similar heights above current river level are observed at different locations upstream. At location IR-8, an 8 m thick sandy fining upwards sequence is present, with its base around 0.5 to 1 m above current river level. The bottom part contains gravel bands, which diminish towards the top, a fine sandy layer around 2.5 m above current river level is sampled for dating. Location IR-11 contains 4 meters of fluvial sands and gravels, with its base around 1m above current river level. These gravels contain basalts, limestone and pottery at several locations. A sandy layer has been sampled for luminescence dating (IR-11). At locations C-1 and IR-7 (Fig. 5.2 and 5.4), a fluvial aggradational fill consisting of several sedimentary units is observed. The base of around 4 m thick fluvial deposits is observed around 5 m above current river level and consists of mainly gravels in a silty matrix, alternated with gravel bands. This fluvial body is overlain by a sedimentary body which is associated with tufa formation and which is tentatively classified as paludal (Pedley et al., 2003). At the downstream side the fluvial unit is overlain by fine layered muddy lime deposits, sometimes intercalated with dark coloured muds, probably due to enrichment of organic material. Other layers contain calcified organic macrorests, mainly reed stems and seeds, and

some layers are almost entirely calcified into tufa layers with a phytoherm structure. Such a layer at the base of the muddy deposit has been sampled for radiocarbon dating (C-1). At the upstream side, the fluvial deposits are overlain by light-coloured limestone rich fine sands, which are capped by tufas up to around 20m above current river level. The sands have been sampled for luminescence dating (IR-7) around 1 m below the top of the sequence. From the exposure it is unclear how these muds and sands are related. The genesis of this sediment body is reconstructed as follows: the base consists of sediments of a braided Geren river, which becomes abandoned at some stage (reflected by the presence of mollusk shells). The upper part is unique for the area and has a more local character, influenced by nearby springs and tufa formation [e.g. analogous to Kaufmann et al., (2002)]. It can be the infill of an abandoned Geren channel which has been cut off and choked with sediments, finally becoming a shallow water environment with fluctuating water table. The sediments of IR-7 are topped by a tufa and afterwards, or perhaps already partly during tufa formation, a channel incision of 20 meters has taken place. Just upstream of this tufa, another, more extensive tufa body is present (Fig. 5.2). Its base is not visibly overlying fluvial deposits, but its landscape position and lobate nature suggests that it is a perched springline deposit which entered a palaeoGeren valley. Its top is around 400 m. The tufas, sands and muds of IR-7 and C-1 appear to be inset and thus younger than this tufa body.

Location IR-9 is a 3m thick fluvial terrace consisting of gravel and sand bars. It contains imbricated gravels consisting of subrounded basalts and limestones as well as subangular limestones. Its base is located around 30 m above current river level (Fig. 5.3B). A sample for luminescence dating has been taken from a sandy layer.

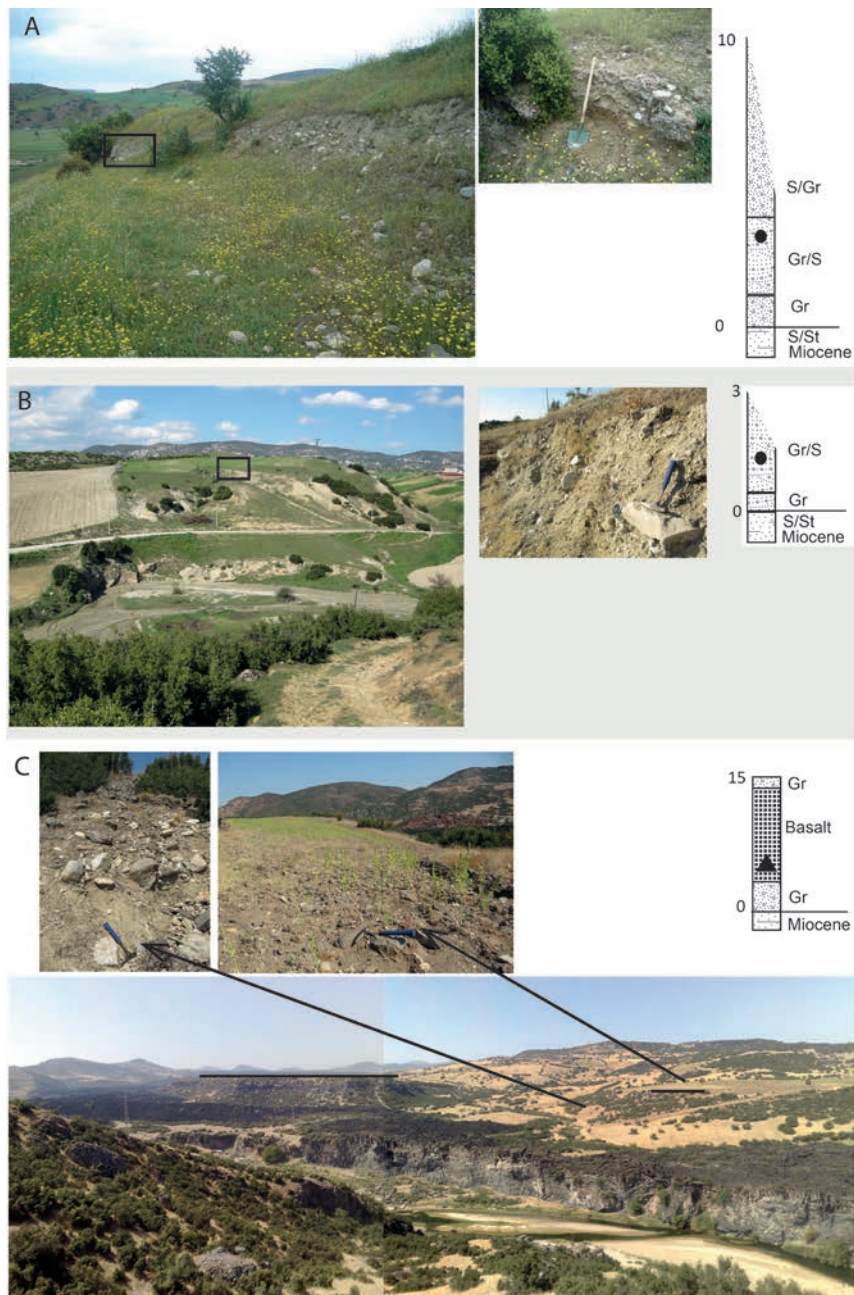


Fig. 5.3. A: Overviews and details including sediment logs of A: Gediz terrace IR-13. B: Location of Gerent terrace IR-9. C: Location of Gediz terrace below and on top of lava dam Ar-4. Tops of lavaflow are indicated by horizontal lines. Note that sediment logs are not scaled to the photos. Sample locations are indicated in the sediment logs. Circles indicate luminescence dated samples, triangles indicate radiocarbon dated samples.

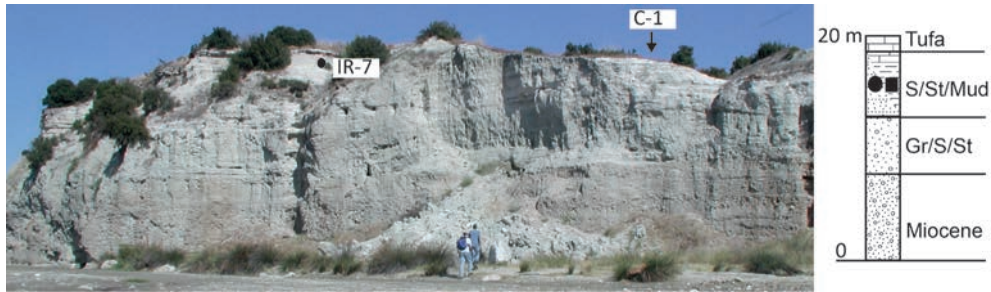


Fig. 5.4. Overview and sediment log including sample setting of IR-7 and C-1. Person in blue is 1.90 m. Sample locations are depicted in the sediment log. Circles indicate luminescence dated samples, squares indicate radiocarbon dated samples.

5.4.3 Upstream Geren gullies

Upstream of IR-9, a main tributary discharging the central part of the limestone plateau joins the trunk stream (Fig. 5.2). Comparison of this stream to the trunk stream shows they are quite different. The upper part of this tributary, which extends into the northern limestone plateau has a gradient which is comparable to other tributaries west of this tributary. This gully is located in a narrow gorge bordered by limestone-capped ridges which are on average 30-40 m higher than the current gully and extend from the Ulubey limestone scar in the north to the confluence with the Geren trunk stream. Limestone ridges are now present as either elongated or fork-shaped ridges in the landscape. However, similar fork-like ridges are observed at locations without limestone deposits. Location IR-10 is a fine layered sandy-silty sediment body of at least 15 m thickness, which is part of one of the elongated ridges. Its distal base contains often fluvial gravels and coarse sands with cross-bedding which are sometimes cemented. The sample is taken around 35 - 40 m above current river level, which could correlate it, by simple gradient extrapolation, to sample IR-9 and IR-13 (Fig. 5.5). The eastern trunk stream has a less steep gradient and is bordered by ridges which are around 20 m higher than current stream level and which are sometimes limestone-capped. Location IR-12 consists of fluvial sands and gravels, entirely consisting of limestone clasts. Its base was difficult to observe but the sample elevation is around 10m above current river level. A sample for luminescence dating was taken from a sandy layer. The distinction between the central and eastern trunk stream points to different evolution histories.

Table 5.1. Results of pIRIR luminescence, $^{40}\text{Ar}/^{39}\text{Ar}$ and radiocarbon dating. ^athese samples already have been described in Van Gorp et al. (2013).

pIRIR								
Lab code	Sample	Location	Altitude (m)	Measurement procedure	Equivalent dose (Gy)	Dose rate (Gy/ka)	Age $\pm 1\sigma$ (ka)	Validity
NCL-2209135	IR-1 ^a	Below kula flow	348	Multiple-grain pIRIR ₂₃₀	9.2 \pm 0.4	3.0 \pm 0.1	3.0 \pm 0.2	Likely OK
NCL-2209136	IR-2 ^a	Lower Geren top	378	Multiple-grain pIRIR ₂₃₀	12.6 \pm 5.3	2.5 \pm 0.1	5.0 \pm 2.1	Questionable
NCL-2209137	IR-3 ^a	Lower Geren bottom	372	Multiple-grain pIRIR ₂₃₀	22.1 \pm 6.2	2.4 \pm 0.1	9.4 \pm 2.7	Likely OK
NCL-2209138	IR-7	Lower Geren tufa	390	Multiple-grain pIRIR ₂₃₁	50.3 \pm 5.5	3.0 \pm 0.1	16.8 \pm 1.9	Likely OK
NCL-2111095	IR-8	Geren spa bridge	389	Single-grain pIRIR ₁₅₀	5.8 \pm 0.7	2.74 \pm 0.11	2.5 \pm 0.3*	Likely OK
NCL-2111096	IR-9	Geren village terrace	427	multiple grain pIRIR ₂₉₀	280 \pm 22	3.40 \pm 0.12	82 \pm 9	Questionable, poor dose rec.
NCL-2111097	IR-10	aggradation tephra	445	multiple grain pIRIR ₂₉₀	\geq 574 \pm 32	4.10 \pm 0.15	\geq 140 \pm 10	In saturation, minimum age
NCL-2111100	IR-11	young Geren pottery	429	Single-grain pIRIR ₁₅₀	6.7 \pm 0.6	3.18 \pm 0.12	2.5 \pm 0.3*	Likely OK
NCL-2111101	IR-12	Up Geren fluv terrace	451	Single-grain pIRIR ₁₅₀	6.1 \pm 0.8	2.78 \pm 0.11	2.7 \pm 0.3*	Likely OK
NCL-2111102	IR-13	Gediz paleomeander	377	multiple grain pIRIR ₂₉₀	\geq 572 \pm 53	3.30 \pm 0.12	\geq 173 \pm 15	In saturation, minimum age

$^{40}\text{Ar}/^{39}\text{Ar}$								
Lab code	Sample	Location	Altitude (m)	K/Ca $\pm 1\sigma$	Normal Isochron age $\pm 1\sigma$ (ka)	Inverse Isochron Age $\pm 1\sigma$ (ka)	Plateau Age $\pm 1\sigma$ (ka)	MSWD
11WG1_C2	Ar-3top		391	0.076 \pm 0.028	256.8 \pm 73.2	257.1 \pm 69.2	240.2 \pm 18.2	0.79
11WG1_B2	Ar-3bot		391	0.692 \pm 0.072	265.2 \pm 16.1	265.2 \pm 16.1	273.9 \pm 12.8	0.60
11WG1_B1	Ar-4	Above gravel	372	0.598 \pm 0.113	327.2 \pm 36.5	326.5 \pm 36.6	310.5 \pm 14.8	1.17

14C				
Sample	Location	Altitude (m)	14C Age BP (yr)	1 σ cal BP range (yr)
C-1	Lower Geren tufa	380	11400 \pm 45	13290 - 13230

5.4.4 $^{40}\text{Ar}/^{39}\text{Ar}$ dating results

Ages for $\beta 3$ basalt flows in the vicinity of Kula bridge have been discussed by Westaway et al. (2006). They presented an age of 180 ± 5 ka and linked it to the basalt remnant at location Ar-4 (Fig. 5.2) which overlies a fluvial terrace. However, their sample location is at least 5 km to the south from Ar-4. There are different possible cones that could have produced different flows which may or may not have reached the Gediz River. Steps in the surface of the basalt flows have been interpreted to be flow fronts (e.g. Fig. 4 in Westaway et al., (2004)), but there are also indications that the basalt flowed over terrace bluffs. Either way, making a link from

the 180 ± 5 ka date to the Ar-4 basalt is difficult. Therefore, in the present study a new attempt is done to date $\beta 3$ basalts near the Gediz-Geren outlet. Sample location Ar-4 has a lowest observed base at around 372 m and is on top of and overlain by a fluvial terrace at 390 m (Fig. 5.3C). The two stacked basalt flows at sample location Ar-3 (Ar-3bottom and Ar-3top) are at the tip of the lava tongue which entered the Gediz valley from the south.

Fieldwork evidence and dating shows that probably three $\beta 3$ basalt flows have filled the contemporary valleyfloor near the Geren-Gediz confluence. $^{40}\text{Ar}^{39}\text{Ar}$ dating evidence gives the basalt sample Ar-4 an age estimate of 311 ± 15 ka, sample Ar-3a is dated 274 ± 13 Ka and sample Ar-3b is dated 240 ± 18 ka, (Table 5.1). This last sample interestingly coincides with an age of 236 ± 6 ka (Westaway et al., 2006) of a $\beta 3$ basalt near the north-eastern edge of the Söğüt flows (Fig. 5.1). These new dates suggest that at least three different flows entered the Gediz River over a time span of 70 ka.

5.4.5 Luminescence dating results

The sandy aggradation at location IR-7 which is capped by a tufa at ± 20 m above current stream level is dated to 16.8 ± 1.9 ka (Fig. 5.4 and 5.5). The dating results show that this sediment body predates the Kula flow volcanic event (3 ka, Van Gorp et al., 2013) and suggests an aggradation phase at the end of the Pleistocene and into the Allerød interstadial (16 ka to 13 ka). The dates also suggest that the muddy deposit at C-1 is younger than IR-7 (13 ka), this would mean that the muddy deposit of C-1 is inset in the sands of IR-7, however one should be cautious given the possible presence of mobile fractions in the carbon of sample C-1. Since the dates come from the finer upper part of the sediment body, the age of the lower gravelly aggradation could be significantly older.

Sample IR-8, IR-11 and IR 12 have age estimates from 2.5 to 2.7 ka. This indicates an aggradation phase along a large stretch of the trunk gully. The 82 ± 9 ka of sample IR-9 places this terrace in MIS 5a/b. Its age estimate is questionable due to a poor dose recovery. Sample IR-10 and IR-13 exceed the saturation limits, thus we could only assign minimum age estimates of 140 ka and 173 ka, respectively. Due to unusually high dose rates, these minimum ages are relatively low compared to other other feldspar pIRIR-studies (Buylaert et al., 2012).

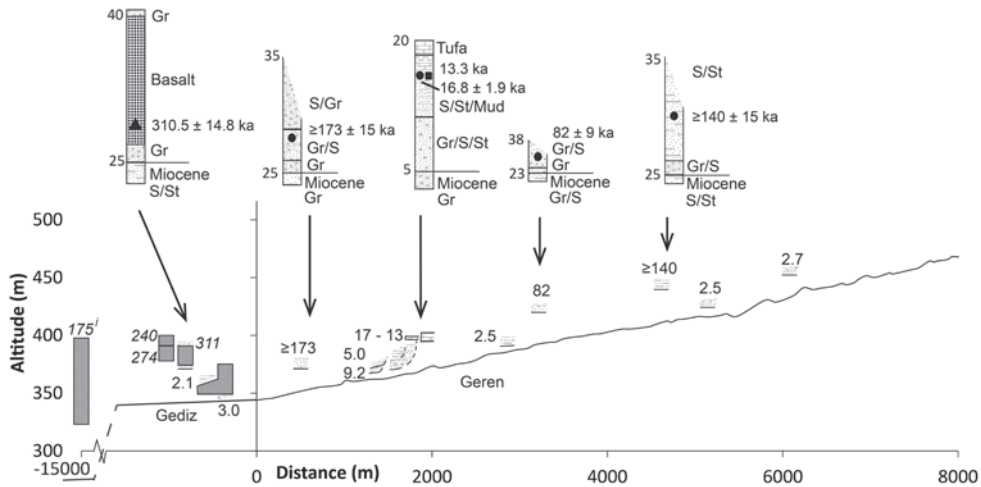


Fig. 5.5. Sample elevations and dates plotted along the western trunk stream of the Geren Catchment. For selected samples, sediment logs are displayed. Triangles indicate dated basalt, circles indicate luminescence dated samples, squares indicate radiocarbon dated samples (calibrated age displayed).

5.5 Discussion

5.5.1 Base level reconstruction

The Gediz River has a known long-term incision rate of 0.14 mm a^{-1} (Maddy et al., 2012b). Early Pleistocene dammings caused mild disturbance to this incision rate, while tributary streams were affected more severely in the form of channel infilling and stream reroutings (Maddy et al., 2012a). The middle Pleistocene damming situation near the Geren – Gediz confluence differs from the early Pleistocene in the sense that the Gediz valley was more confined than in the early Pleistocene and therefore, basalt flows have repeatedly entered the same valley. Furthermore, the tributary stream, the Geren, had not been filled by the lava flows, but only endured their influence on its base level. At least two of the newly dated middle Pleistocene basalt flows have filled the Gediz valley and dammed the Geren Catchment. The basalt flow at IR-4 is both underlain and overlain by a fluvial terrace. Its age estimate of 311 ka thus provides a minimum age for the location of the pre-basalt river valley at an elevation around 372 m, approximately 25 m above present river level. The river terrace on top of basalt Ar-4 is located at ± 390 m elevation. It is unclear whether the river flowed here directly after placement of the Ar-4 basalt or at a later stage, but it is evident that the river level has risen by ± 20 meters from 311 to 240 ka. The top of the “ $\beta 3$ flow”, at sample location Ar-3b is around 400-410 m elevation. This upper basalt flow is about 20m thick. At the end of the flow, rubbly material containing scoria and ashes has been observed. Although this would normally be expected near a volcanic cone, it could have been transported all the way from the cone as a solid patch floating on top of the lava. Another plausible alternative is interaction of the lava with water, which is known to create ashes and scoria and even pseudocraters. A pseudocrater has not been observed, but interaction with water probably took place as the “ $\beta 3$ flow” is assumed to have flowed over the contemporary Gediz valleyfloor or perhaps the edges of the

lake formed by lava flow Ar-4. The following chronology is reconstructed using all field and dating results.

Before the first known middle Pleistocene damming occurred, the Gediz formed a base level for the Geren at around 25 m altitude above current river level, suggested by the bottom Gediz terrace at Ar-4. The Geren Catchment outlet must have been upstream of this location because northern adjacent higher basement ridges confined the Geren outlet. It is not unlikely that the Geren outlet was south of its current location (Fig. 5.6A). A main channel within the Geren Catchment already was located in the centre of the current catchment, evidenced by the largest volume and thickness of limestone gravels and fluvial deposits in the catchment, with some tributaries from the north (Fig. 5.2). All these gullies were gravel bearing, either with limestone gravels only, or with limestone and Miocene-derived gravels. Damming started at 311 ka (Fig. 5.6B) with the emplacement of flow Ar-4 in the Gediz valley, causing base level rise to around 40 m above current river level and perhaps a lake. Flow Ar-3bottom (274 ka) subsequently entered the valley, but it is unclear if and how this flow dammed the Gediz and Geren. Subsequently, the “ β 3 flow” of sample location Ar-3top (240 ka) flowed on top of flow Ar-3bottom and possibly into the lake caused by flow Ar-4 (Fig. 5.6C). The duration of these lava dammings is uncertain. The fluvial terrace on top of Ar-4 suggests that the Gediz River established a stable course with the lava dam still partly in place, indicating elevated base level for a prolonged period. Other known lava dams often had fluvial reestablishment on top of the flow or on lake sediments behind the dams (Ely et al., 2012; Macaire et al., 1992), suggesting long dam stability. The Holocene damming by the Kula flow in our study area had a duration of 0.5 – 1.2 ka (Van Gorp et al., 2013). The size of this dam is comparable to those of Ar-3 and Ar-4. However reestablishment of a fluvial terrace has not been observed on the Kula flow. This suggests that dam duration of the Ar-4 flow has been significantly longer than 1 ka. After lake drainage, flow Ar-3top diverted the Gediz eastwards (Fig. 5.6D), similar to how it at present still is diverted due to the Kula flow (Van Gorp et al., 2013) and flowed at the location of terrace IR-13, where a gravelly strath terrace resembling a meander bend is preserved around 25 m above current river level. As opposed to the terraces underlying and overlying Ar-4, this terrace is Ca-cemented, which, assuming relatively arid conditions for such cementation to occur, could link this post-240 \pm 18 ka terrace to either the end of MIS 8, stadial MIS 7d or the start of interglacial MIS 6. The stratified sands and gravels overlying this terrace which resemble a deltaic infill are not cemented and from these sands the minimum burial age of 173 \pm 15 ka is obtained. Its present, already eroded top of 385 m, around 35 m above current river level, suggests that a damming event reaching at least that height can be responsible. The most likely dam candidate already known is the lava flow near Palankaya (Fig. 5.1), around 15 km downstream of the Gediz-Geren confluence. The flow overlies a Gediz terrace at 315 m, around 40 m above current river level (Westaway et al., 2004) which, using 0.004 for the average Gediz gradient (Maddy et al., 2012b), corresponds to the altitude of terrace IR-13. An average date of 175 \pm 3 ka calculated from three different samples both from the top and the base of the Palankaya flow, indicating it has been one flow blocking the Gediz (Westaway et al., 2006). The current top has an elevation of around 390 - 400 m where it has blocked the Gediz. The volume of the basalt that flowed into the river valley is significant (roughly estimated valleyfill of \sim 0.1 km³) and could have created a lake all the way up into the Geren Catchment. It is not proven that the lake was filled up all the way to the top of the lava dam, but a base level rise affecting the Geren-Gediz confluence area is

likely and corresponds both in elevation and timing with the deltaic sediments at IR-13 (Fig. 5.6E). The duration of the Palankaya dam could have been significant, up to several 10 ka, given its volume. However, in between the Gediz-Geren confluence and Palankaya, 15 km downstream, no clear evidence of lake sediments has been observed. A possible reason for this absence of lake sediments is that upstream, the Gediz may have been still been dammed by the Söğüt lava flow which has been dated to 236 ± 6 ka at its most upstream edge (Westaway et al., 2006, our Fig. 5.1), which formed another large lava dam and could have trapped all fine sediments. Damming by the Palankaya flow would furthermore also block the Selendi catchment to the north (Fig. 5.1). Currently the Selendi catchment is deeply and broadly incised, and it thus could potentially have stored a lot of water. However late Quaternary evolution of this basin is unknown and detailed research on lake sediments in this region has not been carried out. The southern slopes of the Gediz-Geren confluence and the gorge area between the Gediz-Geren confluence and the Gediz-Selendi confluence show signs of fossil and active landsliding and mass movements. Lake sediments may therefore either be removed or obscured. It is possible that lake formation and subsequent dam removal has destabilized slopes more than they would have been from an incising river only and that landslides were most active along the former lake shore area. The fluvial terrace dated to 82 ka (MIS 5a), at 30 m above current river level, suggests that the Geren trunk stream did not incise much until 90 ka after Palankaya dam formation, suggesting a long lasting impact of the Palankaya dam on base level. Associated with this 310 – 82 ka damming period are two travertines, one south of the Gediz-Geren confluence (Fig. 5.2 and 5.6) and one near sample IR-9 (Fig. 5.2). Although they are not dated, their landscape position and both their tops suggest that they are formed in the 310 - 82 ka damming period. Interestingly, the large landslide from the Sarnic plateau appears to be contemporary or post – IR-13 and its emplacement could have had major impact on the Geren base level as well and has at least migrated the Geren stream to its current position. While, the Gediz migrated back east and attained its pre-Kula flow position (Fig. 5.6F). For details on Gediz response to the Holocene damming, the reader is referred to Van Gorp et al. (2013).

In summary, up to three different lava flows have been recognized from 310.5 ka to 175 ka which have dammed the Geren Catchment. However, besides this base level control, climate is also an important driver for incision-aggradation cycles and their relative impact on the evolution of the Geren Catchment is not yet clear. LEM simulations were intended to help answer this question. Before discussing and interpreting the field results of the more upstream parts of the Geren Catchment, the base level reconstruction is translated into a model input and other LEM scenario inputs and results are presented.

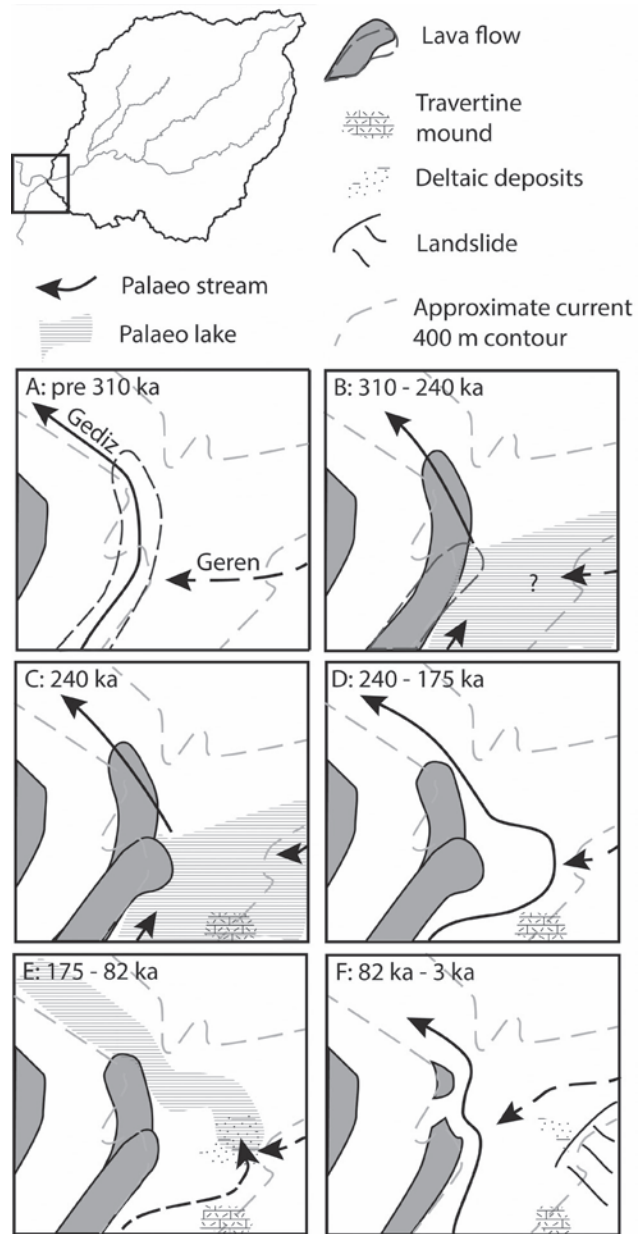


Fig. 5.6. Overview and reconstruction of middle Pleistocene to Holocene evolution of the Gediz -Geren confluence (from A 310 ka to F 3 ka).

5.5.2 Model inputs and scenarios

Three main inputs have been used for modelling: a palaeoDEM, a base level change record and a climate record influencing effective rainfall (Fig. 5.7). The palaeoDEM used is the same as used in Van Gorp et al. (in revision) and is derived by interpolating field recognized palaeosurfaces and creating a hydrologically correct DEM with an outlet at 390 m, which is based on the Gediz terrace capping the post-310.5 ka lavaflow of Ar-4. No drainage network was artificially incised into this DEM. Although substantially simplified, the overall drainage pattern of the current Geren Catchment, with three main northern branches draining into the southern trunk, emerges from the reconstructed palaeoDEM.

Effective rainfall was derived from the Tenaghi Phillipon arboreal pollen (%AP) record (Tzedakis et al., 2006; Tzedakis et al., 2003), which is the closest and most complete record spanning our 300 ka timescale. An annual record was created using linear interpolation. Subsequently, effective rainfall was linearly scaled from the arboreal pollen record, resulting in an average effective rainfall of 47 mm a^{-1} (Fig. 5.7B).

Vegetation feedbacks are important for landscape evolution (Macklin and Lewin, 2008; Veldkamp et al., 2014 Submitted). A climate driven vegetation effect is incorporated in the model by scaling erodibility factor K and sedimentation factor P. According to the %AP record, vegetation cover has been varying between tree dominated and shrub dominated. If effective rainfall is higher than 50 mm, K will be lowered by 25% due to vegetation stabilising the soil. P will be increased by 25% due to vegetation being able to capture more sediments. If effective rainfall is lower than 50 mm, erodibility factor K is increased by 25% due to less vegetation stabilizing the soil. Sedimentation factor P is increased by 25% due to the decrease in potential capture by vegetation. This is a simplified version of how the effect of vegetation on erosion is incorporated in Temme et al. (2009).

As mentioned, the initial base level of the catchment was set to 390 m. Base level change was imposed on the first 210 m (7 columns) of gridcells at the outlet (Fig. 5.7A). With 390 m as a start outlet cell elevation, three scenarios of base level change are imposed on the catchment. The first scenario is gradual base level lowering according to the known average incision of the Gediz River of 0.14 mm a^{-1} (Maddy et al., 2012b). In the second and third base level scenario, damming events are added, corresponding to the events at 310, 274, 240, 175 and 3 ka (Table 5.2). They are simplified from the field reconstruction. Their elevations are approximated from corresponding basalt tops. Their emplacement and removal occurs instantaneous and is imposed, thus not modelled. Given that the work to remove dams is done by the Gediz River rather than the Geren, while it is Geren Catchment evolution that is modelled, we consider this is an acceptable assumption. In the second scenario, damming durations were 1 ka, based on the maximum age constraint damming duration of around 1ka of the Kula flow (Van Gorp et al., 2013). The Palankaya dam (175 ka) was given a 5 times longer duration based on its approximate 5 wider dam. However, as discussed above, durations of the older lava dammings are not directly age constrained. Due to this uncertainty of dam duration, and given the field indications that the Gediz flowed over the Ar-4 dam for a longer period and that the Geren trunk stream did not incise much until around 82 ka, we used a third base level scenario with longer dam durations (Table 5.2).

In this scenario dams from 0 yr (300 ka) to 59800 yr (240.2 ka) form a stable and finally increased base level (Fig. 5.7B) and Palankaya dam has a duration of 50000 yr.

Table 5.2. Dates and durations of damming events for the long and short dam duration scenarios.

Age (ka)	Simulation time (yr)	Dam nr	Elevation	Dam duration (yr)		Based on
				Short	Long	
300	0	1	390	Gradual Incision	59800	This study
273.9	26100	2	390	1000	-	This study
240.2	59800	3	400	1000	10000	This study
175	125000	4	400	10000	50000	Westaway et al., (2006)
3	297000	5	375	900	2000	Van Gorp et al., (2013)

LAPSUS was simulated 300000 yr for all three scenarios. Results were assessed by monitoring the evolution of 1 ka-averaged gully elevations of a downstream gully location, closest to the location of sample IR-9 and an upstream gully location, closest to the location of sample IR-10 (Fig. 5.7A). We remind the reader that the notation “ka” is used for field reconstructed ages in ka, while yr is used for simulation runtime, where 0 yr is equivalent to 300 ka and 300000 yr to present.

5.5.3 Model results

The results of 300 ka evolution of upstream and downstream gully elevation show different pathways (Fig. 5.8). Upstream evolution shows a clearer top-down signal, where incision generally occurs in low rainfall periods due to low sediment load but sufficient incision power in the trunk gullies, and aggradation or hampered incision in high rainfall periods due to high sediment supply when transport capacity is often exceeded. This image roughly coincides with sediment accumulation rates derived from the Tenaghi Phillipon record, which are higher during interglacials (Tzedakis et al., 2003).

For all three scenarios, the upstream gully location first incises and then becomes relatively stable around 20000 yr (Fig 5.8, 5.9). From then onwards, alternating incision and aggradation phases can be observed, varying in length from 1000 yr to more than 50000 yr. In all three scenarios, the downstream gully elevation starts with a long relatively stable phase until 75000 simulation years, which is probably due to continuously high sediment load. The downstream reach of the long dam scenario has a sustained stable level until 10 ka after the Palankaya dam is removed. Correlating aggradation and incision phases (Fig. 5.9) with climate shows that correlation is weak, although the no dams scenario perhaps is bit more sensitive to 100 ka cycles, showing increased alternating activity. However the overprint of complexity is high. Correlation of these phases in both dam scenarios is even weaker, suggesting their dampening influence on climate signals (Veldkamp and Tebbens, 2001).

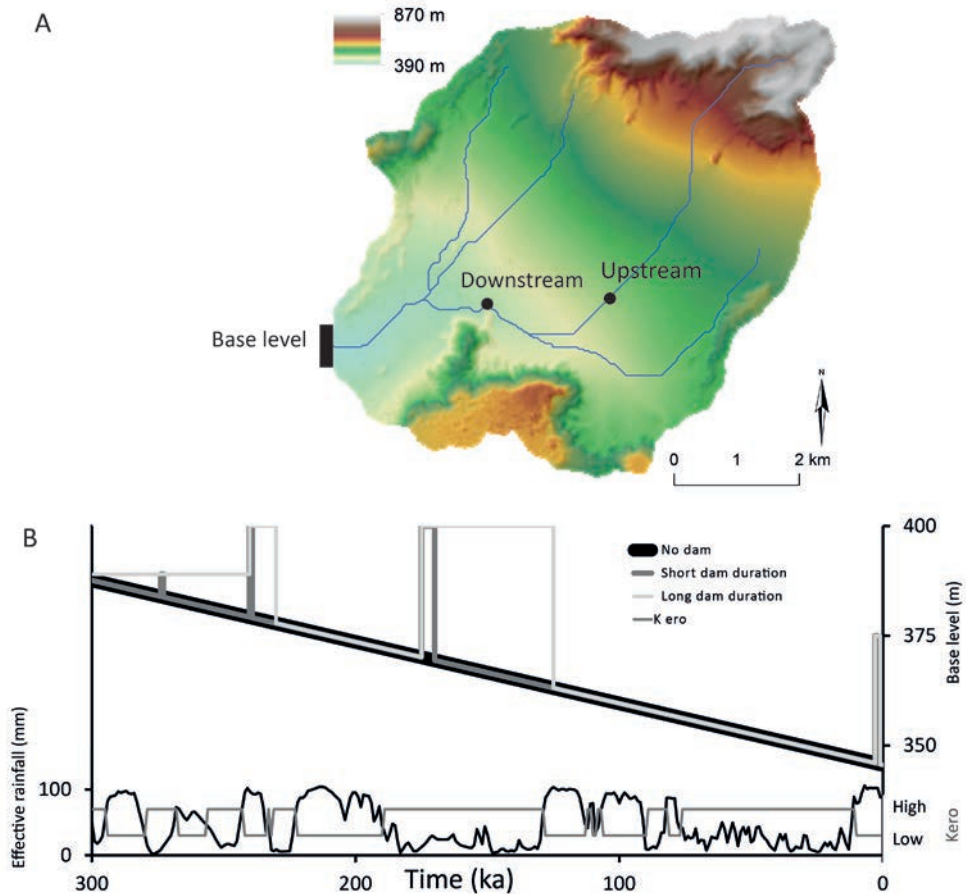


Fig. 5.7. Main model inputs with A: palaeoDEM with drainage network, the area of which base level was changed, and tracked gully locations are indicated. B: field-derived base level change without, with short and with long duration dammings, effective rainfall input and erodibility factor.

The no-dam scenario shows a wave of incision and aggradation in MIS 6, between 125000 yr and 175000 yr of simulation. Its magnitude is large and not observed in the field. Timing of these large scale incision-aggradation phase is similar for up- and downstream reaches, while on a smaller scale their pathways differ. In the short dam duration scenario, this incision wave is delayed. In the long dam scenario, it is absent. From 200000 to 300000 simulation years, alternating incision-aggradation occurs in the no dam and short dam scenario, while net incision is limited. In the long dam scenario, Post- Palankaya incision of the downstream gully occurs a bit more intense. Upstream incision is delayed until around 250000 yr, after which an continuous incision occurs. With the increase of rainfall at the end of the Pleistocene, the dam scenarios respond directly by gully aggradation. These differences suggests a long-term response due to middle Pleistocene dammings and demonstrates that these disturbed landscapes are less efficient in coping with increased sediment supply. The last dam shows a relatively minor impact on trunk stream evolution, which is already coping with increased sediment supply. However, future long-term response to this recent damming event is likely.

Modelling thus suggests the influence of gradual incision, climate and damming events on gully elevations. Interpreting them together with obtained fieldwork results could increase our understanding of both history of and mechanisms in the Geren Catchment.

5.5.4 Field – model integration: 300 – 82 ka landscape evolution of the Geren Catchment

The presence of limestone deposits in the western and especially central part of the Geren Catchment, which have a basal, Calcium carbonate cemented strath that grades to a base level around 20-30 m above the current level, suggests that here the main drainage took place when these limestone deposits at IR-10 were formed at or before 140 ka. Because we only obtained a lower age boundary, this aggradation cannot be specified more than that it could have been synchronous to the middle Pleistocene damming phase. The planform fork-like sediment units suggest divergent flow patterns at different locations, which could indicate different delta forks, while the fining-upward texture of the deposits suggests a shift from active fluvial to low energy flow conditions. Nevertheless, due to the elongated structure and the elevation range the limestone units cover, it is rather a backfilling than deltaic sediment. Like location IR-13, at IR-10 a cemented terrace is overlain by an uncemented aggradation of fines, while its elevation relative to the current river level is similar as well. Although none of these indications are definite, it is probable that the limestone IR-10 is contemporary with the 310 – 175 ka damming events and more specifically with the Gediz aggradation found at IR-13 at the Gediz-Geren confluence.

All three model results show aggradation phases pre-140000 yr. Climate – driven major aggradational phases in catchments of the Mediterranean basin have been recognised in the middle and late Pleistocene, although data coverage is still limited (Macklin et al., 2002). Nevertheless, an aggradation phase in MIS 6 is recognized in Macklin et al. (2002), while a Pre- MIS 5 aggradation is suggested from samples IR-10 and IR-13. Modelling suggests that this upstream >140 ka gully aggradation took place in MIS 6 or 7.

The >50 m incision and subsequent > 50m aggradation of the no dam and short dam duration scenarios around MIS 5 are not observed in the field. The long dam scenario demonstrates has aggradation – incision cycles from MIS 5 until the end of the Pleistocene which are from the same order of magnitude as the observed incision and aggradations in this period. The elevation of the downstream date of IR-9 of 82 ka is higher than gully elevation of the long dam duration scenario, which could both be caused by age uncertainty or model uncertainty.

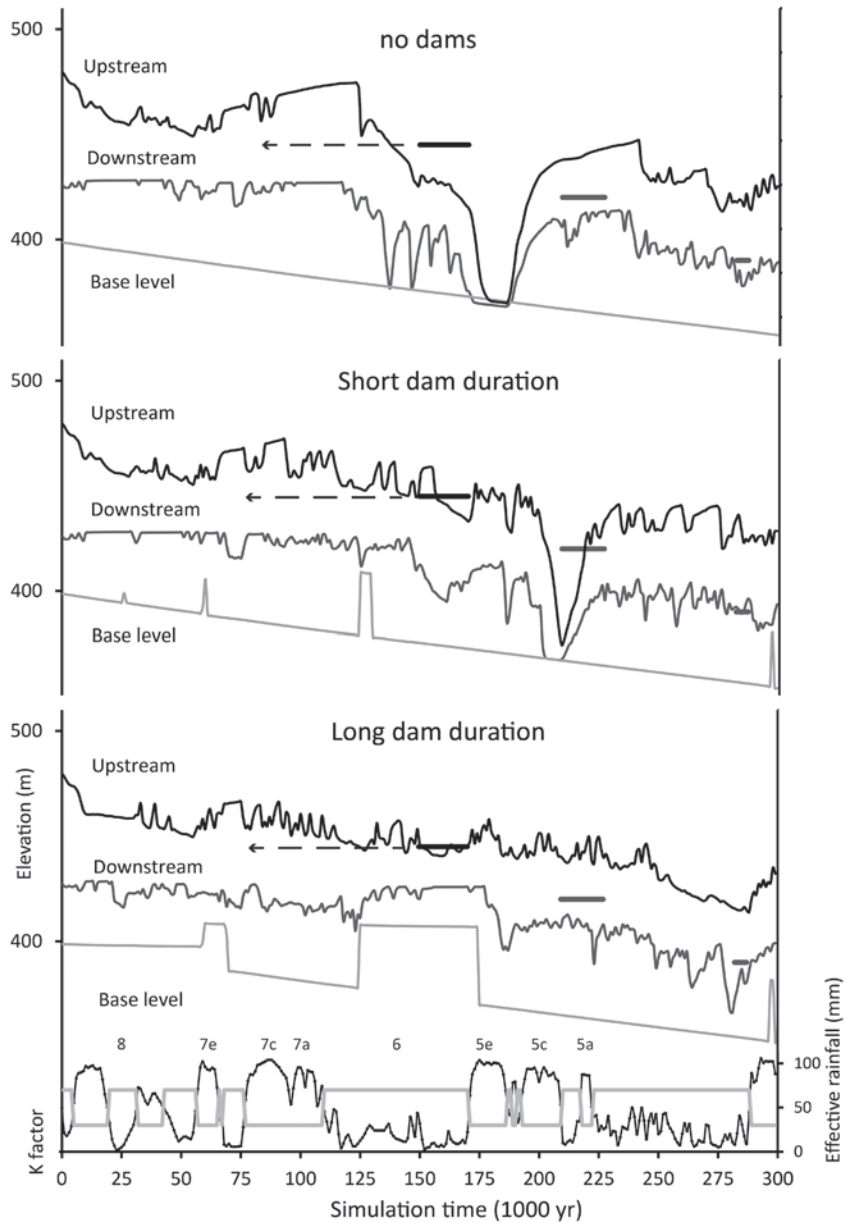


Fig. 5.8. Model output showing 1000 yr averaged gully elevation development at an upstream and downstream location within the trunk gully for the “no dams”, “short dam duration” and “long dam duration scenario”. Imposed base level change and age estimates of fluvial deposits of up and downstream stream locations are plotted as thick horizontal bars for comparison (Upstream: IR-10 with dotted arrows indicating minimum age, Downstream: IR-9 and IR-7). Bottom part shows for reference the % arboreal pollen of the last 300 ka of Tenaghi Phillipon which is used as a climate input, in grey, the alternation of high and low k-factors is shown, see text for explanation. Some marine isotope stages are indicated.

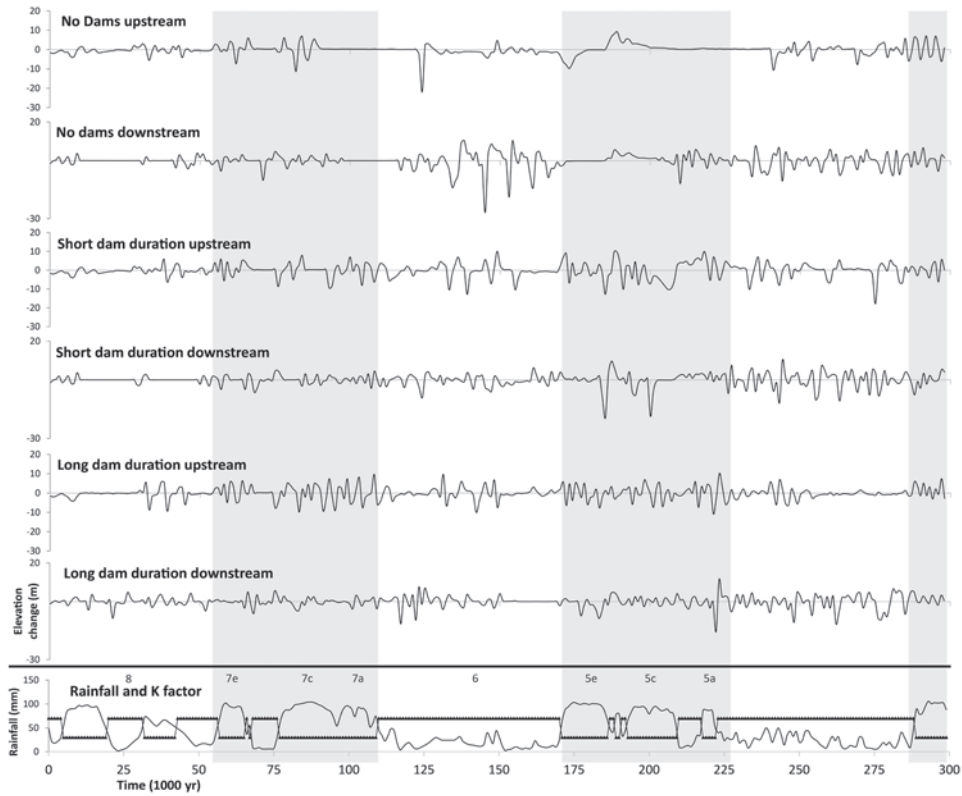


Fig. 5.9. Simulation output of 1000 yr averaged erosion and deposition amounts (m) of the three scenarios at upstream and downstream gully locations. Rainfall, K factor variation (no scale) and MIS stages are added for comparison.

5.5.5 Post-82 ka landscape evolution: stepped incision

From fieldwork it is unknown when the aggradation associated with sample IR-10 and IR-13 ended. The age and elevation of fill terrace IR-9 of 82 ka suggests that post 175ka incision of the Geren trunk river has been limited throughout MIS 6 and 5. Noting the questionable validity of the luminescence date, the burial age itself falls in MIS 5a/b, which already has been mentioned as a climate-driven fluvial deposition phase in the Mediterranean (Macklin et al., 2002). During subsequent incision of around 35 meter, no significant terraces have been found. However, confinement of gullies in this period could have caused a lack of preservation. The end of this incision phase is not specified, but maximum incision to around 3-5m above current stream level is reached at the base of the fluvial deposits at location IR-7. This incision phase is simulated well and its simulated end is around 382000 yr (18 ka) in the downstream gully and around 28800 yr (12 ka) in the upstream gully. Thus a downstream aggradation phase is already initiated but has not yet reached the elevations which follow from the dated sediments of IR-7 in the downstream reach. At this location the basal fluvial gravel aggradation phase is not dated, but its lower age is constrained by the fine sands covering it and which are dated to 16.8 ka. This simulated aggradation phase seems overestimated and

subsequent gully incision leading to the present gully form is not reproduced. This incision of approximately 20 m occurs between 16.8 and 9.2 ka, when deposition starts at location IR-3. A final deposition phase occurs along the whole length of the trunk stream around 2.5 ka, after which incision to the current stream level is established. This final aggradation occurs synchronous with the Holocene damming event, suggesting that it is a backfilling response to this damming event. The downstream deposits of IR-3 have already been correlated to the 3 ka damming event (Van Gorp et al., 2013) and location IR-8, which consists of an 8 m sandy fining upward sequence, can be a dam response. The more upstream samples of IR-11 and IR-12 are coarse sandy and gravelly aggradations where IR-11 resembles a fluvial strath which is probably driven by sediment supply, and IR-12 contains pottery, indicating a possible human induced land use change driven control.

In summary, fieldwork and dating clarified that the Gediz-Geren outlet area experienced multiple damming events, which are contemporary with aggradation-incision phases in the Geren. Landscape evolution modelling demonstrated that long duration damming events reproduce the general evolution of the gully locations best. It has to be noted that timing of damming events in relation to prevailing climate could also have been a factor determining dam duration. In the scenarios used in this Chapter, differences in damming duration are based field reconstruction and are predetermined instead of modelled, however for instance the Palankaya dam (175 ka) occurs in the dry conditions of MIS6, which could have delayed dam lake infilling, siltation and subsequent erosion by overtopping. Late Pleistocene incision is reproduced as well, while observed late Pleistocene-Holocene incision-aggradation cycles were not simulated.

5.5.6 Limitations and advantages

When modelling on timescales such as is done in this study, initial palaeoDEMs and rainfall records can only be reconstructed in a generalized form. Furthermore, we have only used water runoff erosion and deposition as a process, which limits potentially important process interactions. However, slow mass movement processes such as creep are likely to have played minor role in this catchment. Nevertheless, besides the recognized landslide at the Gediz-Geren confluence, landsliding in the rest of the catchment will have had a significant impact on catchment evolution and its incorporation in studies like this one is recommended, as their effect may have been felt throughout the Geren Catchment (*cf.* Temme et al., 2011a). A possible reason that the model is unable to reproduce the most recent aggradation-incision history could be the lack of these landslide effects, a divergence of the 300 ka simulated DEM from the actual Late Pleistocene topography, and, for the late Holocene, human impact of land use – land cover change.

Nevertheless, we think that by keeping input parameters relatively simple, we already demonstrate that model results indicate long duration dammings, and demonstrate the complexity of spatial catchment evolution under simple changing driving conditions. The suggested long damming durations provide testable hypotheses for further fieldwork research, in which for instance either the influence of the landslide at the Gediz-Geren confluence on Geren Catchment evolution can be further researched, or the Palankaya lava dam on the Gediz and the Selendi catchments can confirm whether this lava dam was long-lived. Although in our model output, preservation of terraces only occurred near the dam location and not in

confined gullies, major aggradation – incision cycles within the confined gullies are presumed to represent potential terraces that can be preserved within the actual gullies and which could now be better recognized in the field. Late Pleistocene-Holocene evolution until present could be further investigated using a more detailed late Pleistocene-Holocene PalaeoDEM, a more detailed climate-landcover input and a more detailed version of LEM LAPSUS (*cf.* Baartman et al., 2012b; Temme and Veldkamp, 2009).

5.6 Conclusion

A combined field-model study of middle Pleistocene to Holocene evolution of the Geren Catchment, western Turkey, demonstrated that persistent middle Pleistocene lava dams can explain 200 ka hampered incision and subsequent enhanced incision. Furthermore, catchment response differs between up and downstream locations and its evolution is complex. Lava damming events in the period 310.5 – 175 ka were dated and identified, leading to base level reconstruction from 300 ka until present. Identification and luminescence dating of fluvial deposits in the Geren Catchment demonstrated that trunk stream incision was limited in the middle Pleistocene, while major incision occurred after 82 ka. Landscape Evolution Modelling results suggest that major aggradation-incision in upstream parts are driven by climate, while in the downstream part, damming events obscure this effect. If dam durations are long, downstream and upstream incision is delayed, but subsequently occurs more rapidly. To better simulate Late Pleistocene evolution until present, it is suggested to perform a more detailed landscape evolution model simulation which takes the most recent human induced landcover changes into account. Combined field - landscape evolution model studies such as this one are useful in unravelling spatially explicit feedbacks and will enhance our understanding of landscapes compared to either fieldwork or modelling studies alone.

Appendix A5.1. Radiocarbon calibration

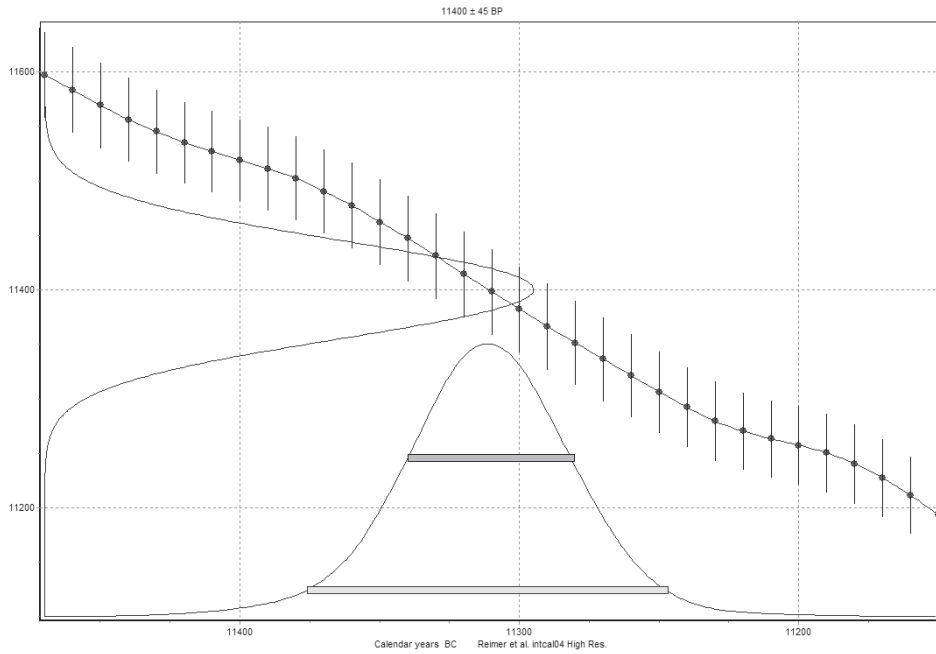


Fig. A5.1.1. Calibration of sample C-1 with the INTCAL04 calibration curve (Reimer et al., 2004) resulted in a 1 sigma range of 11340-11280 cal BC and a 2 sigma range of 11376-11247 cal BC.

Appendix A5.2. $^{40}\text{Ar}/^{39}\text{Ar}$ Age estimates and geochemistry

All measurements were done on groundmass separates. The recalculated DRA-1 standard of 25.45 Ma was used (Wijbrans et al., 1995; Kuiper et al., 2008), which incorporated the updated ^{40}K total decay constant (Min et al., 2000). The ArArCalc software, version 2.5 was used for data reduction and age calculation (Koppers et al., 2002).

Plateau ages (Table A5.2.1) were calculated and are tested for the following quality criteria: 1) a well-defined plateau exists at 1σ with MSWD values close to 1 calculated for the steps included in the plateau, 2) three or more steps are included in the plateau, which contain 50% or more of the ^{39}Ar released, 3) isochron ages should agree with plateau ages within analytical error, and 4) $^{40}\text{Ar}/^{36}\text{Ar}$ intercepts derived from regression analysis should not be significantly different from the atmospheric level of 298.56 (Lee et al., 2006; O'Connor et al., 2012). Despite that samples are relatively young, acceptable ages were obtained. Detailed age data and plots of each sample are depicted in Fig. A5.2.1 – A5.2.6.

Table A5.2.1. $^{40}\text{Ar}/^{39}\text{Ar}$ Ar age estimates.

Lab code	Sample	Location	Altitude (m)	K/Ca $\pm 1\sigma$	Normal			MSWD
					Isochron age $\pm 1\sigma$ (ka)	Inverse Isochron Age $\pm 1\sigma$ (ka)	Plateau Age $\pm 1\sigma$ (ka)	
11WG1_C2	Ar-3top		391	0.076 \pm 0.028	256.8 \pm 73.2	257.1 \pm 69.2	240.2 \pm 18.2	0.79
11WG1_B2	Ar-3bot		391	0.692 \pm 0.072	265.2 \pm 16.1	265.2 \pm 16.1	273.9 \pm 12.8	0.60
11WG1_B1	Ar-4	Above gravel	372	0.598 \pm 0.113	327.2 \pm 36.5	326.5 \pm 36.6	310.5 \pm 14.8	1.17

Geochemistry of the samples was carried out at Activation Laboratories, Lancaster, Canada. Rock classification was done based on a TAS diagram (Total alkalis, Table A5.2.2).

Table A5.2.2. Volcanic rock classification based on SiO_2 and $(\text{K}_2\text{O} + \text{Na}_2\text{O})$. Tephrite or Basanite depends on the percentage of the mineral olivine (ol) in the rock.

		Analyte Symbol-->	SiO ₂	Na ₂ O+K ₂ O	Na ₂ O	K ₂ O	Na ₂ O-2
		Unit Symbol-->	%		%	%	
		Detection Limit-->	0.01		0.01	0.01	
		Analysis Method-->	FUS-ICP		FUS-ICP	FUS-ICP	
Code	Sample code	Rock Type name					
Ar-2*	T-14-W330	Phonotephrite	48.08	9.65	5.98	3.67	3.98
Ar-4	T-8-W331	Tephrite or Basanite	45.41	7.75	4.96	2.79	2.96
Ar-1*	T-9-W333	Phonotephrite	47.9	9.34	5.74	3.6	3.74
Ar-3bottom	T-11-W360A	Tephrite or Basanite	45.15	8.13	4.96	3.17	2.96
Ar-3top	T-12-W360B	Tephrite or Basanite	43.28	7.41	5.09	2.32	3.09

*Samples described in Chapter 3.

Sample Ar3-top 11WG1_C2

Relative Abundance	36Ar	%1σ	37Ar	%1σ	38Ar	%1σ	39Ar	%1σ	40Ar	%1σ	Age ± 1σ (Ka)	40Ar(t) 39Ar(K) (%)	K/Ca ± 1σ
11WG1_10W_C2 10.00 W	1212.932	0.610	3.714	467.675	238.950	2.244	17.852	7.537	370418.532	0.043	186960.8 ± 50877.0	2.24	0.05
11WG1_15W_C2 15.00 W	356.775	0.560	264.381	12.516	79.815	3.188	337.879	1.040	109420.305	0.109	3721.8 ± 787.3	2.67	1.00
11WG1_20W_C2 20.00 W	90.497	2.919	1598.836	4.343	50.109	7.630	2085.286	0.327	29526.659	0.395	564.4 ± 184.7	9.22	6.18
11WG1_25W_C2 25.00 W	72.848	2.955	4842.342	3.549	86.254	6.638	4744.579	0.113	25377.900	0.198	384.1 ± 51.5	15.80	14.05
11WG1_35W_C2 35.00 W	111.174	1.664	13037.186	2.884	154.607	2.905	8965.217	0.116	37541.880	0.194	261.7 ± 27.2	14.34	26.25
11WG1_50W_C2 50.00 W	160.361	1.054	37785.275	2.628	192.908	2.277	8380.130	0.141	49030.346	0.119	215.6 ± 26.7	8.53	24.76
11WG1_70W_C2 70.00 W	141.251	1.424	30718.022	2.622	123.340	3.758	4312.239	0.258	42301.060	0.133	260.6 ± 61.0	6.14	12.72
11WG1_95W_C2 95.00 W	46.985	3.149	8881.955	3.244	45.489	7.389	1319.248	0.476	13491.237	0.321	58.0 ± 145.8	1.31	3.89
11WG1_120W_C 120.00 W	65.085	2.825	16741.318	2.979	63.150	7.085	1945.324	0.361	20300.054	0.438	493.0 ± 124.2	10.91	5.73
11WG1_135W_C 135.00 W	51.981	4.245	16959.504	3.056	59.372	5.451	1820.743	0.279	16105.422	0.300	464.0 ± 157.5	12.11	5.36
Σ	2309.888	0.411	130630.934	1.268	1094.004	1.237	33328.498	0.071	713613.526	0.040			

Results	40(e)/36(e) ± 1σ	40(t)/39(K) ± 1σ	Age ± 1σ (Ka)	MWD
Normal Isochron	296.1391 ± 9.7812 ± 3.30%	0.5584 ± 0.1700 ± 2.849%	256.8 ± 72.2 ± 28.50%	1.51
			Minimal External Error ± 75.3	
			Analytical Error ± 73.2	
Statistics	Statistical F ratio 0.87	Convergence 0.000000317		
	Error Magnification 1.2286	Number of Iterations 8		
	Number of Data Points 3	Calculated Line Weighted York-2		
Results	40(e)/36(e) ± 1σ	40(t)/39(K) ± 1σ	Age ± 1σ (Ka)	MWD
Inverse Isochron	296.1850 ± 9.7050 ± 3.27%	0.5972 ± 0.1607 ± 2.680%	257.1 ± 69.2 ± 26.81%	1.51
			Minimal External Error ± 69.9	
			Analytical Error ± 69.2	
Statistics	Statistical F ratio 0.87	Convergence 0.0000003168		
	Error Magnification 1.2287	Number of Iterations 4		
	Number of Data Points 3	Calculated Line Weighted York-2		

Fig. A5.2.1. Summarised statistics of sample Ar3-top, including plateau age, normal isochron age and inverse isochron age statistics.

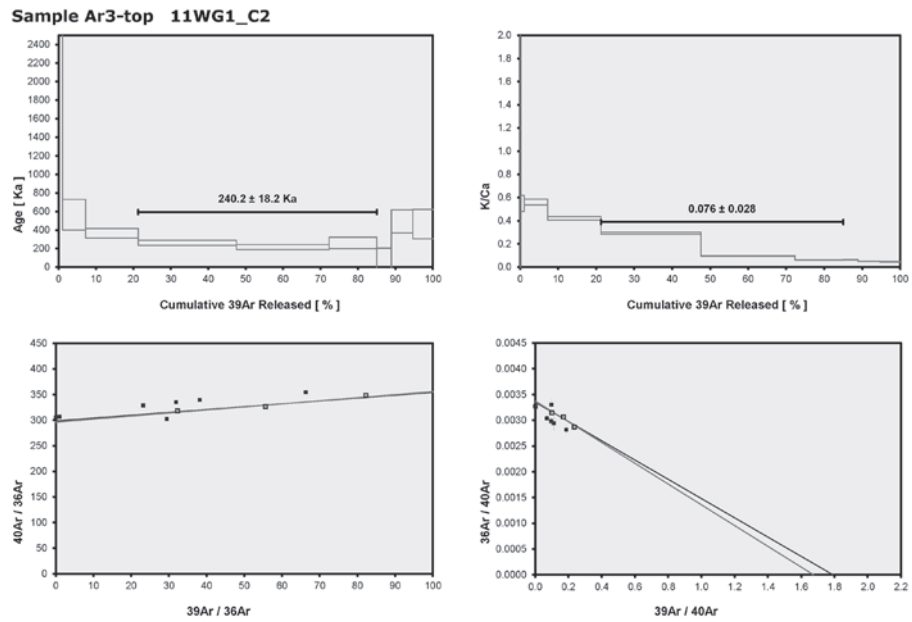


Fig. A5.2.2. Plots of sample Ar3-top, including plateau age, K/Ca plateau, normal isochron and inverse isochron.

Sample Ar3-bot 11WG1_B2

Relative Abundances	36Ar	%1σ	37Ar	%1σ	38Ar	%1σ	39Ar	%1σ	40Ar	%1σ	Age ± 1σ (Ka)	40Ar(t) 39Ar(k) (%) (%)	K/Ca ± 1σ
11WG1_10W_B2_10.00 W	965.256	0.473	37.479	47.446	183.284	2.967	71.452	2.594	29392.817	0.055	35252.0 ± 8565.8	1.84	0.10
11WG1_15W_B2_15.00 W	228.976	1.206	263.773	8.604	48.246	6.313	522.702	0.695	69194.445	0.111	700.8 ± 683.5	1.23	0.76
11WG1_20W_B2_20.00 W	77.765	2.886	2321.760	3.441	91.583	3.391	4850.975	0.264	26939.489	0.344	345.8 ± 62.0	14.48	7.07
11WG1_25W_B2_25.00 W	90.678	1.987	859.754	3.007	261.260	2.233	14683.316	0.082	3837.188	0.149	270.1 ± 15.6	26.27	21.84
11WG1_30W_B2_35.00 W	59.834	3.569	8518.656	3.131	206.178	2.590	11412.578	0.165	24402.210	0.286	271.5 ± 24.2	16.64	0.576 ± 0.018
11WG1_50W_B2_50.00 W	95.354	1.352	1759.163	3.000	257.166	2.596	13123.390	0.103	38954.875	0.190	320.7 ± 12.9	26.53	19.12
11WG1_70W_B2_70.00 W	243.121	1.064	63130.826	2.835	378.761	1.766	16815.072	0.147	86278.423	0.077	480.7 ± 20.3	21.73	24.46
11WG1_85W_B2_85.00 W	20.914	9.108	5544.561	3.454	44.389	7.551	1617.548	0.387	6311.277	0.907	88.3 ± 152.3	5.40	2.35
11WG1_120W_B_120.00 W	84.836	1.648	25409.733	2.994	97.494	4.167	3698.848	0.272	28114.000	0.245	563.7 ± 55.8	17.17	5.37
11WG1_138W_B_135.00 W	27.835	7.120	10433.649	3.156	46.976	6.073	1566.767	0.291	10189.453	0.548	749.1 ± 164.0	26.67	2.27
Σ	1895.568	0.409	141830.344	1.470	1615.348	0.949	68662.627	0.059	617824.156	0.042			

Results	40(e)/36(e) ± 1σ	40(f)/39(k) ± 1σ	Age ± 1σ (Ka)	MSTD	Results	40(f)/39(k) ± 1σ	Age ± 1σ (Ka)	MSTD	39Ar(k) (%/n)	K/Ca ± 1σ
Normal Isochron	301 7159 ± 3.5888 ± 1.19%	0.6168 ± 0.0374 ± 0.608%	265.2 ± 16.1 ± 6.08%	0.47	Age Plateau	0.6370 ± 0.0298 ± 4.67%	273.9 ± 12.8 ± 4.67%	0.60	46.32 ± 4	0.692 ± 0.072
Statistical F ratio	1.05	Convergence	0.000000372		Minimal External Error ± 16.7	Minimal External Error ± 16.7		1.10	Statistical T Ratio	
Error Magnification	1.0000	Number of Iterations	10		Analytical Error ± 12.8	Analytical Error ± 12.8		1.0000	Error Magnification	
Number of Data Points	4	Calculated Line	Weighted 70x.2							

Results	40(e)/36(e) ± 1σ	40(f)/39(k) ± 1σ	Age ± 1σ (Ka)	MSTD	Total Fusion Age	0.9216 ± 0.0244 ± 3.73%	396.2 ± 14.8 ± 3.73%		10	0.208 ± 0.003
Statistical F ratio	1.05	Convergence	0.000000372		Minimal External Error ± 21.4	Minimal External Error ± 21.4				
Error Magnification	1.0000	Number of Iterations	4		Analytical Error ± 14.8	Analytical Error ± 14.8				
Number of Data Points	4	Calculated Line	Weighted 70x.2							

Results	301 7906 ± 3.5888 ± 1.19%	0.6169 ± 0.0374 ± 0.608%	265.2 ± 16.1 ± 6.08%	0.49	Normal Isochron	0.6168 ± 0.0374 ± 6.08%	265.2 ± 6.08%	0.47	46.32 ± 4	
Statistical F ratio	1.05	Convergence	0.000000372		Minimal External Error ± 19.1	Minimal External Error ± 19.1		1.05	Statistical F ratio	
Error Magnification	1.0000	Number of Iterations	3		Analytical Error ± 16.1	Analytical Error ± 16.1		1.0000	Error Magnification	
Number of Data Points	4	Calculated Line	Weighted 70x.2							

Results	301 7906 ± 3.5888 ± 1.19%	0.6169 ± 0.0374 ± 6.08%	265.2 ± 16.1 ± 6.08%	0.49	Inverse Isochron	0.6169 ± 0.0374 ± 6.08%	265.2 ± 6.08%	0.49	46.32 ± 4	
Statistical F ratio	1.05	Convergence	0.000000372		Minimal External Error ± 19.1	Minimal External Error ± 19.1		1.05	Statistical F ratio	
Error Magnification	1.0000	Number of Iterations	3		Analytical Error ± 16.1	Analytical Error ± 16.1		1.0000	Error Magnification	
Number of Data Points	4	Calculated Line	Weighted 70x.2							

Fig. A5.2.3. Summarised statistics of sample Ar3-bot, including plateau age, normal isochron age and inverse isochron age statistics.

Sample Ar3-bot 11WG1_B2

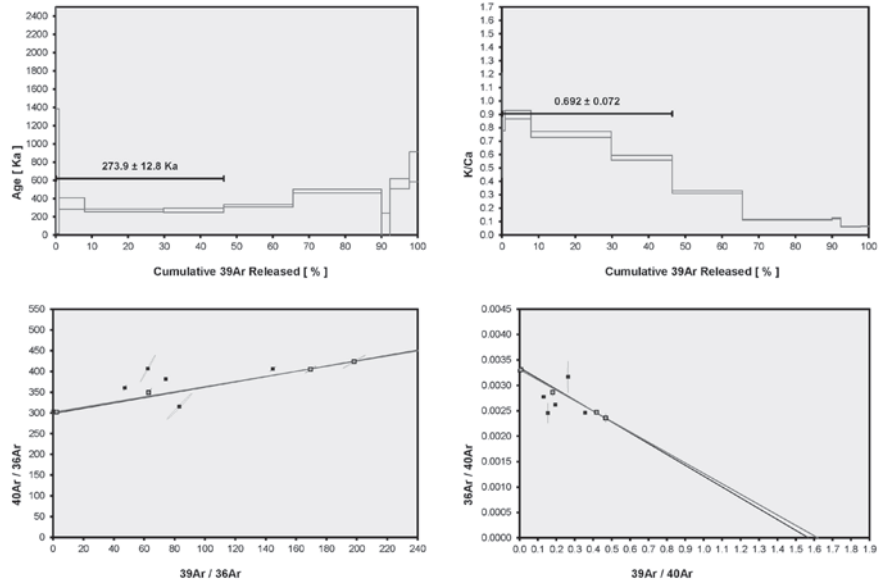


Fig. A5.2.4. Plots of sample Ar3-bot, including plateau age, K/Ca plateau, normal isochron and inverse isochron.

Sample Ar-4 11WG1_B1

Relative Abundances	36Ar	%1σ	37Ar	%1σ	38Ar	%1σ	39Ar	%1σ	40Ar	%1σ	Age ± 1σ (Ka)	40Ar(t) 39Ar(k) (%)	K/Ca ± 1σ	
11WG1_10W_B1 10.00W	1660.056	0.301	68.664	23.356	306.306	1.771	52.232	0.981	500330.292	0.062	21756.3 ± 7598.2	0.94	0.19	
11WG1_15W_B1 15.00W	245.757	1.116	542.030	6.174	64.093	5.620	963.725	0.531	76711.897	0.133	1499.9 ± 367.2	4.41	1.98	
11WG1_20W_B1 20.00W	4	128.970	1.401	1791.971	4.775	84.552	4.916	3906.917	0.153	41960.745	0.134	390.6 ± 90.0	7.85	8.01
11WG1_25W_B1 25.00W	4	234.249	0.852	3579.251	3.357	149.603	2.587	6872.393	0.196	73897.318	0.102	263.6 ± 37.7	5.73	14.09
11WG1_35W_B1 35.00W	4	184.349	1.043	14096.863	2.855	272.829	1.905	16477.862	0.114	66063.528	0.131	314.9 ± 15.2	18.36	33.79
11WG1_50W_B1 50.00W		224.169	0.760	32883.118	2.848	245.189	2.497	12015.519	0.133	77202.066	0.093	460.0 ± 18.7	16.71	24.60
11WG1_70W_B1 70.00W		163.166	1.465	3512.1815	2.894	157.012	2.791	5486.027	0.190	54745.549	0.090	692.8 ± 56.5	16.17	11.20
11WG1_95W_B1 95.00W		27.510	7.841	5696.374	3.082	27.942	10.211	879.036	0.552	8205.769	0.579	218.7 ± 315.6	5.45	1.80
11WG1_120W_B1 120.00W		74.479	1.801	10847.489	3.169	45.910	5.817	1303.369	0.434	23958.438	0.319	855.8 ± 120.7	10.83	2.66
11WG1_135W_B1 135.00W		28.948	6.227	7394.718	3.414	32.144	9.967	823.382	0.490	9124.671	0.830	562.1 ± 284.2	11.79	1.68
Σ	2972.654	0.263	111972.303	1.357	1387.580	0.978	48820.463	0.066	932207.284	0.041				

Results	40(e)/36(e) ± 1σ	40(t)/39(k) ± 1σ	Age ± 1σ (Ka)	MSTD	Results	40(t)/39(k) ± 1σ	Age ± 1σ (Ka)	MSTD	39Ar(k) (%n)	K/Ca ± 1σ
Normal Isochron	295.9517 ± 4.8532 ± 1.64%	0.7652 ± 0.0854 Minimal External Error ± 11.17% Analytical Error ± 26.5	327.2 ± 35.5 ± 11.17%	1.85	Age Plateau	0.7263 ± 0.0346 Minimal External Error ± 4.78% Analytical Error ± 19.2	310.5 ± 14.8 ± 4.78%	1.17	55.89 3	0.598 ± 0.113
Statistics	Statistical F ratio Error Magnification Number of Data Points	0.87 1.3599 3	Convergence Number of Iterations Calculated Line	0.00000229 9 Weighted York-2	Total Fusion Age	1.1003 ± 0.0499 Minimal External Error ± 4.54% Analytical Error ± 26.2	470.4 ± 21.4 ± 4.55%	1.21	Statistical T Ratio Error Magnification	
Results	40(e)/36(e) ± 1σ	40(t)/39(k) ± 1σ	Age ± 1σ (Ka)	MSTD	Normal Isochron	0.7652 ± 0.0854 Minimal External Error ± 11.16% Analytical Error ± 36.5	327.2 ± 36.5 ± 11.17%	1.85	55.89 3	0.187 ± 0.003
Inverse Isochron	296.0848 ± 4.9171 ± 1.68%	0.7637 ± 0.0857 Minimal External Error ± 11.22% Analytical Error ± 36.6	326.5 ± 36.6 ± 11.22%	1.89	Inverse Isochron	0.7637 ± 0.0857 Minimal External Error ± 11.22% Analytical Error ± 36.6	326.5 ± 36.6 ± 11.22%	1.89	55.89 3	
Statistics	Statistical F ratio Error Magnification Number of Data Points	0.87 1.3740 3	Convergence Number of Iterations Calculated Line	0.000075901 3 Weighted York-2					Statistical F ratio Error Magnification	

Fig. A5.2.5. Summarised statistics of sample Ar4, including plateau age and inverse isochron age and inverse isochron age statistics.

Sample Ar-4 11WG1_B1

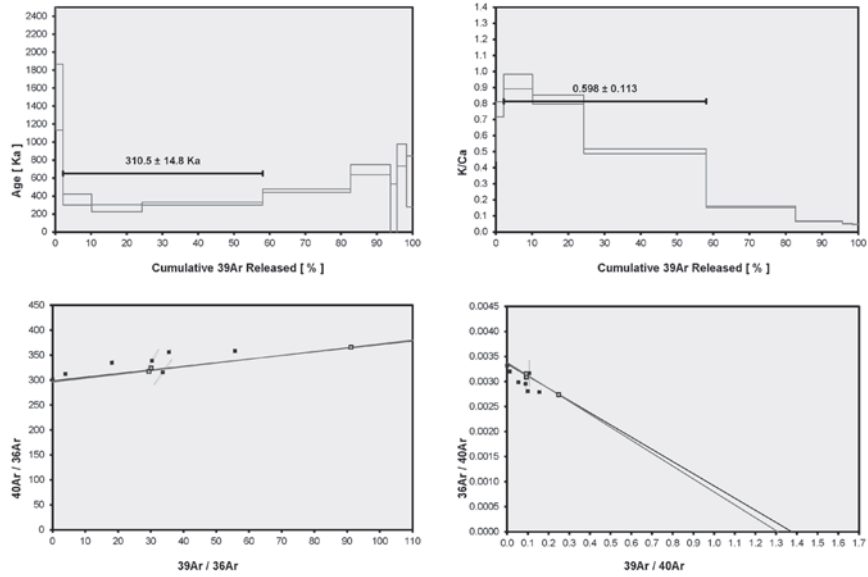


Fig. A5.2.6. Plots of sample Ar-4, including plateau age, K/Ca plateau, normal isochron and inverse isochron.

Appendix A5.3. Feldspar luminescence dating

Seven fluvial samples have been dated by feldspar luminescence dating. Two different measurement procedures were applied. For the first set of four Pleistocene samples (NCL-2209138, -2111096, -2111097, -2111102) we used conventional multiple-grain subsamples (aliquots with 2 mm in diameter) where bulk pIRIR feldspar signals are measured from approximately 50 to 100 grains per aliquot. The late Pleistocene sample NCL-2209138 was measured at a measurement temperature of 230°C (referred to pIRIR₂₃₀; Kars et al., 2012) whereas the three older samples (NCL-2111096, -2111097, -2111102) were measured at 290°C (referred to pIRIR₂₉₀; Buylaert et al., 2012).

For the second set of three Holocene samples (NCL-2111095, -100, -101) single-grain feldspar measurements were carried out (Reimann et al., 2012). To reduce the effect of thermal transfer and residual dose, which is especially important for young Holocene samples (Reimann et al., 2011), we measured the pIRIR signal at 150°C (referred to pIRIR₁₅₀; Reimann and Tsukamoto, 2012), thus at a lower temperature than the Pleistocene samples. Details of the pIRIR single-grain measurement procedure used in this study and performance tests on Geren and Gediz samples is provided in the supplement of Van Gorp et al. (2013).

The pIRIR₂₉₀ equivalent dose measurements for the three oldest samples (NCL-2111096, -2111097, -2111102) were repeated on 12 aliquots. Most of the aliquots of sample NCL-2111097 and NCL-211102 exceed the saturation threshold which was calculated based on the 2 times D₀ criterion (Wintle and Murray, 2006). For these two samples we could only calculate minimum age estimates based on this saturation criterion. The final pIRIR₂₉₀ D_e of sample NCL-2111096 was derived from an iterative average and the standard error of its pIRIR₂₉₀ D_e distribution. However, the pIRIR₂₉₀ age of this sample is estimated to be questionable as the pIRIR₂₉₀ dose recovery performance test was 10 to 20% overestimated.

The Multiple-grain pIRIR₂₃₀ equivalent dose measurement on sample NCL-2209138 was repeated on 92 aliquots to obtain a meaningful D_e distribution. The pIRIR₂₃₀ D_e distribution is significantly over-dispersed, indicating that the spread in the multiple-grain equivalent dose distribution cannot be explained from measurement uncertainties alone. The pIRIR single-grain D_e measurements were repeated on 200 to 400 individual feldspar grains. Approximately 30–40% of the grains fulfilled the quality criteria proposed by Reimann et al. (2012). The single-grain D_e distributions of all samples show very large over-dispersion values (85 to 120%). These values are greater than that of the small aliquot pIRIR₂₃₀ measurement, which is likely caused by averaging effects within multiple-grain aliquots (Cunningham et al., 2011).

The most likely reason for the large over-dispersion values in the pIRIR₂₃₀ multiple-grain distribution and the pIRIR₁₅₀ single-grain distributions is that the luminescence signal was not completely reset for all sand grains prior to burial. It is well known that the pIRIR signal resets significantly slower than the quartz OSL signal and the IRSL signal from feldspar (Buylaert et al., 2012, Kars et al., in press). To avoid age overestimation caused by incomplete resetting of the pIRIR signal in part of the grains, the burial dose from the pIRIR₂₃₀ and pIRIR₁₅₀ equivalent dose distribution were determined using the Minimum Age Model (MAM; Galbraith et al., 1999). The expected over-dispersion for well-bleached samples was estimated to be 20% and 27%, for pIRIR₂₃₀ single-aliquot and pIRIR₁₅₀ single-grain D_e distributions, respectively. For

the analysis of the pIRIR₁₅₀ single-grain D_e distributions the MAM was combined with a simplified bootstrapping approach to obtain meaningful uncertainty estimates (Cunningham and Wallinga, 2012). Details regarding age models, assigned uncertainties and the statistical procedure are provided in Van Gorp et al. (2013, supplement 2). Single-grain D_e distributions are shown in Fig. A5.3.1 to A5.3.3.

Laboratory fading measurements (see Wallinga et al., 2007 for details) on all single-aliquot samples (NCL-2209138, -2111096, -2111097, -2111102) using the pIRIR₂₃₀ and pIRIR₂₉₀ signal show that anomalous fading in these samples is negligible and a fading correction is not needed. In contrast, for the pIRIR₁₅₀ signal a laboratory fading rate of $2.1 \pm 0.4\%$ /decade was measured for the three single-grain samples (likely related to lower preheat and pIRIR measurement temperature); this rate was used to correct the single-grain pIRIR₁₅₀ burial ages for fading following the correction model of Huntley and Lamothe (2001).

Dose rates were determined for each sample separately. Samples were ground, mixed with molten wax and cast into a puck of fixed geometry. After a delay of at least 2 weeks to allow Radon build-up, the samples were measured for at least 24 hours in a Canberra broad-energy gamma spectrometer. Activity concentrations were subsequently converted into dose rate, which was attenuated for water content, organic content and grain size. Furthermore, a minor contribution of cosmic radiation (attenuated for depth) and internal alpha radiation was added. To obtain a dose rate for the K-feldspar extracts we accounted for internal dose rate within the K-feldspar samples as a result of K and Rb decay (Kars et al., 2012).

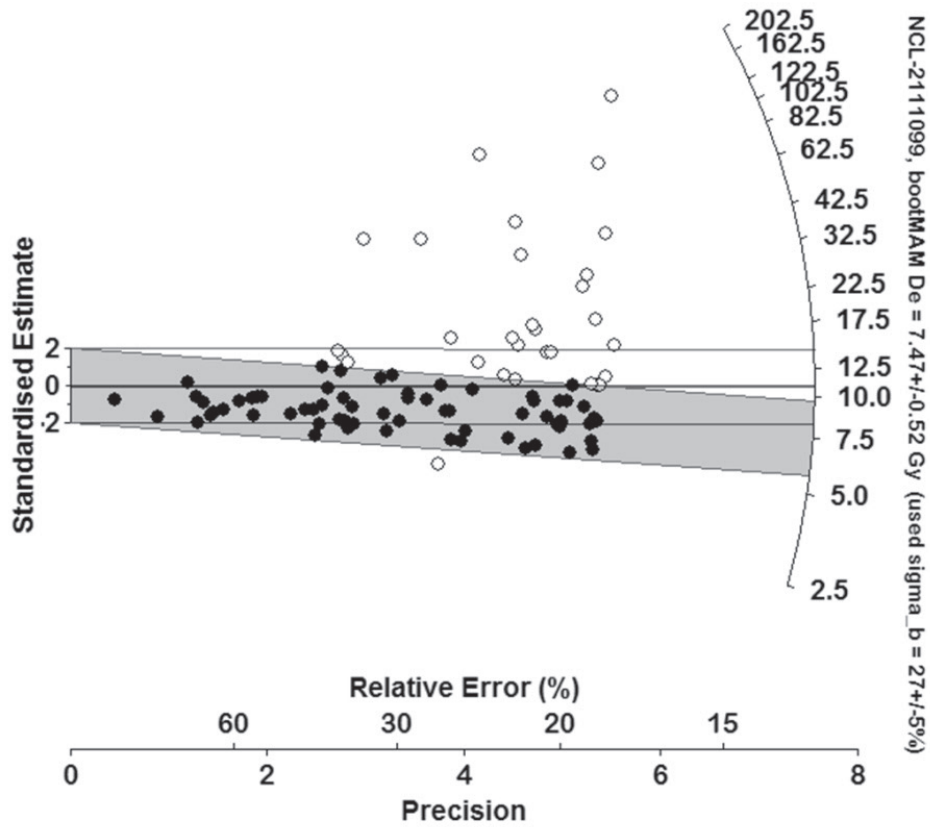


Fig. A5.3.1. Radial plot single-grain $pIRIR_{150} D_e$ distribution of sample NCL-2111095. The grey bar represents the bootMAM (Cunningham and Wallinga, 2012) and the open bar the CAM estimate (Galbraith et al., 1999).

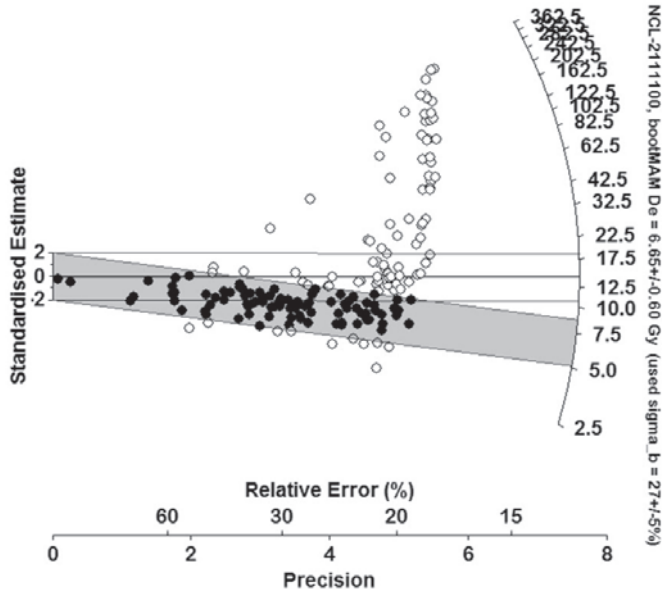


Fig. A5.3.2. Radial plot single-grain $pIRIR_{150} D_e$ distribution of sample NCL-2111100. The grey bar represents the bootMAM estimate (Cunningham and Wallinga, 2012) and the open bar the CAM estimate (Galbraith et al., 1999).

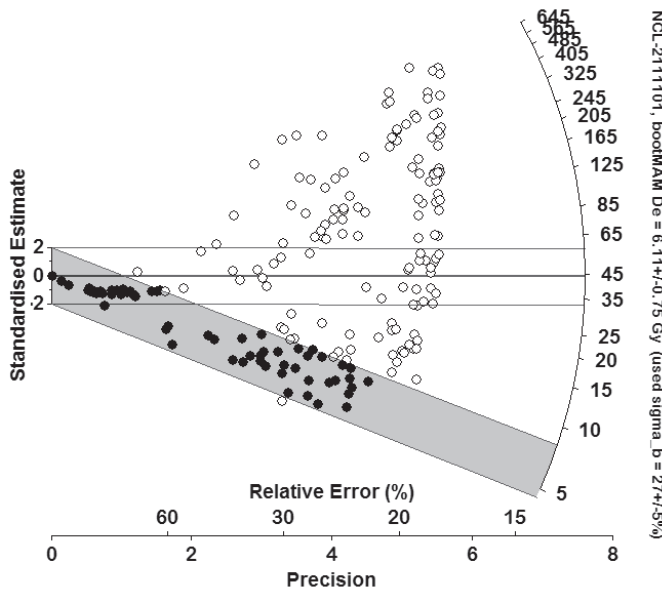


Fig. A5.3.3. Radial plot single-grain $pIRIR_{150} D_e$ distribution of sample NCL-2111101. The grey bar represents the bootMAM estimate (Cunningham and Wallinga, 2012) and the open bar the CAM estimate (Galbraith et al., 1999).

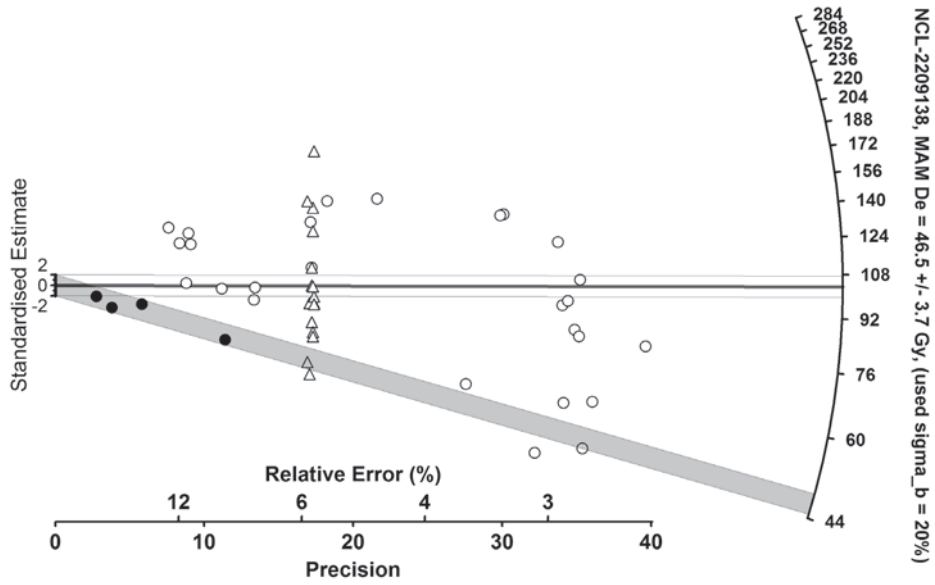


Fig. A5.3.4. Radial plot multiple-grain $pIRIR_{230}$ of sample NCL 2209138. The grey bar represents the iterative mean estimate.

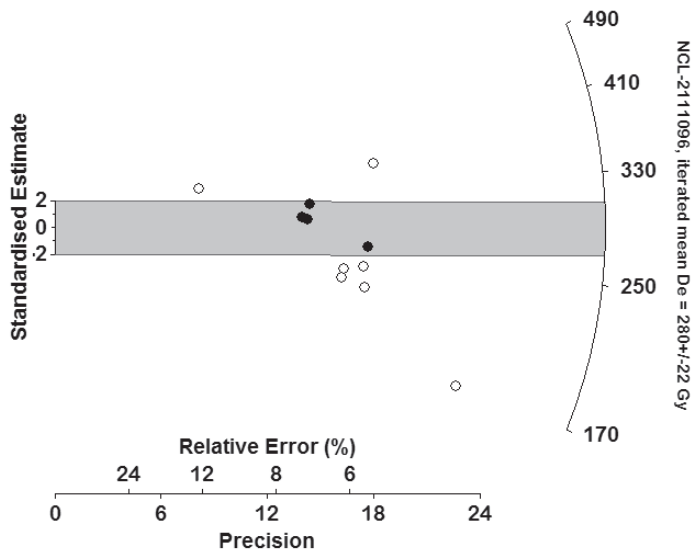


Fig. A5.3.5. Radial plot multiple-grain $pIRIR_{290}$ of sample NCL-2111096. The grey bar represents the iterative mean estimate.

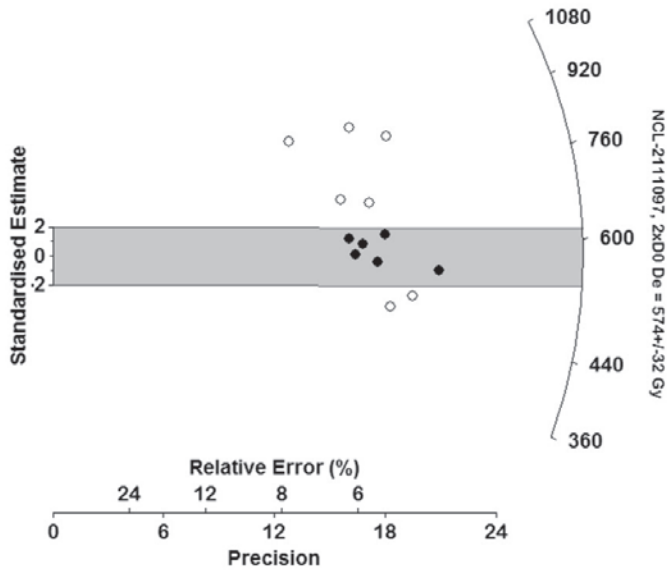


Fig. A5.3.6. Radial plot multiple-grain pIRIR₂₉₀ of sample NCL-2111097. The grey bar represents the lower saturation level calculated based on the 2 times D0 criteria. Note: it is a minimum estimate.

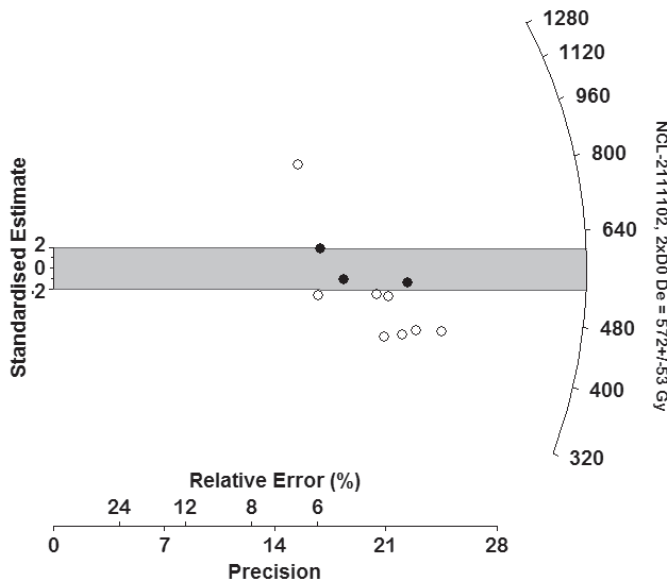
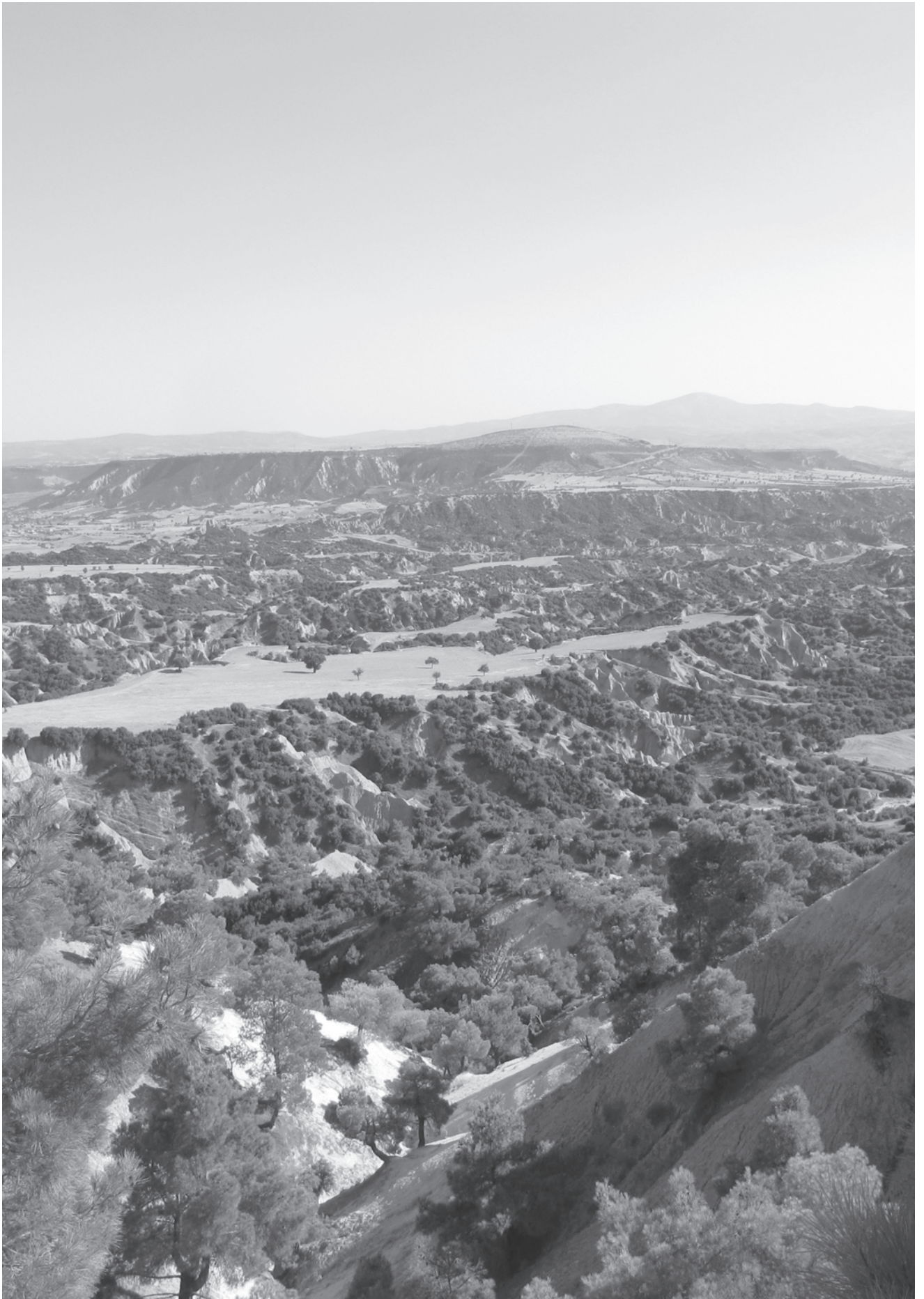


Fig. A5.3.7. Radial plot multiple-grain pIRIR₂₉₀ of sample NCL-2111102. The grey bar represents the lower saturation level calculated based on the 2 times D0 criteria. Note: it is a minimum estimate.



Chapter 6

Synthesis

The main focus of this thesis was to unravel the response of a small, upland catchment to damming events at its outlet. A range of methodologies have been used for this purpose, including field mapping, dating with Luminescence, $^{40}\text{Ar}/^{39}\text{Ar}$ and radiocarbon, Remote sensing (DEM extraction of stereo-imagery), GIS analysis and landscape evolution modelling. It has become clear that answering such a question requires all these different methodologies. In this Chapter, the most important conclusions and methods that led to these conclusions are summarized in an integrative way. The first part will discuss specific results from Chapter 2-4. Fieldwork (including dating) and model results are discussed separately. For both field and model results, tectonic influence, climatic influence and damming influence will be discussed. Finally an integrative reconstruction of catchment response is given. In the second part, limitations, remaining questions and implications of this thesis work for the wider research field are discussed.

6.1 Drivers of middle Pleistocene to Holocene evolution of the Geren Catchment

The reconstruction of middle-Pleistocene to Holocene landscape evolution of the Geren Catchment and the role that damming events played is described in Chapter 2 and 5, where Chapter 2 focussed on the late Holocene damming event and its local stream reach response. Chapter 5 focussed on mid-Pleistocene catchment response of the Geren Catchment, using a combined field-model approach. Below, an integrative fieldwork and modelling summary is given in a larger perspective than Geren evolution alone, focussing on main drivers of catchment evolution, tectonics, climate and damming events.

6.1.1 Response to external drivers: indications from field reconstruction

Long-term landscape evolution is driven by external drivers which become especially more important when a 300 ka timescale is investigated. Tectonics and damming events influence base level, while climate influences vegetation cover and erosivity. Below, indications for each driver are discussed.

Tectonics

The upper Gediz is located on the northern uplifting footwall of the Alaşehir graben and fluvial incision is partly driven by this uplift and by regional uplift (Westaway et al., 2004). Based on 140 m of incision in the last 1 Ma, a time-averaged incision of 0.14 mm a^{-1} (Maddy et al., 2012b) can be derived. However, as also noted in Maddy et al. (2012b), this average incision rate has often been disturbed by lava incursions. Projecting time-averaged incision from İbrahimğa terrace T2 - T1, with an altitude around 500 m at 1 Ma (Maddy et al., 2012b), to the 310.5 ka fluvial terrace at around 375 m below lava flow Ar-4 (Chapter 5), leads to a time-averaged incision rate of at least 0.18 mm a^{-1} (Fig. 6.1), which is slightly higher than the original time averaged incision rate. Time-averaged incision from terrace Ar-4 to

present river level (around 350 m) has been 0.08 mm a^{-1} , which is significantly lower, while time-averaged incision from the fluvial terrace on top of flow Ar-4 to present is 0.16 mm a^{-1} . Although fluvial terraces such as the ones presented here are often interpreted as quasi-equilibrium terraces in all examples, they have a specific context in relation to other driving factors, leading to a 300 ka time period of disturbed or hampered incision. Direct coupling of observed incision to uplift rates is therefore not advisable and better longitudinal control on terrace occurrence for the last 300 ka is needed.

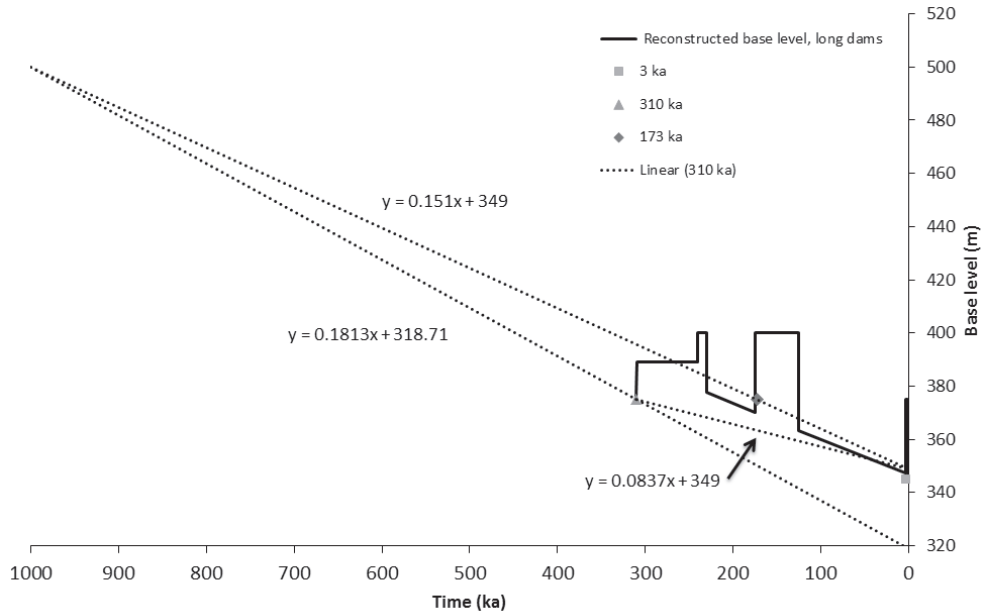


Fig. 6.1: Time-averaged incision rates between different terrace levels, the slope coefficient is in mm a^{-1} . The thick line is the reconstructed long dam duration base level used in this thesis. Thin dotted lines indicate other linear interpolations with average incision rates based on some fluvial terraces only.

Climate influence on Gediz and lower Geren evolution

The preserved early Pleistocene terrace staircase formation of the Gediz River is, with increasing confidence, linked to obliquity driven climate variation, under an uplifting regime (Maddy et al., 2005; Maddy et al., 2012b). Due to the mid-Pleistocene revolution, where insolation driven climate cycles became driven by the approximate 100 ka Milankovic cycles, terrace formation in uplifting areas is believed to have been driven by these cycles for larger systems in Europe (Gibbard and Lewin, 2009) and worldwide (Bridgland and Westaway, 2008), but also smaller Mediterranean river systems (Schoorl and Veldkamp, 2003). Preservation of mid Pleistocene terraces appears to be limited for the Upper Gediz River.

With the information on dated sediments and landscape reconstructions, the influence of climate on landscape evolution can be assessed. The pre-310 ka terrace below lava flow Ar-4 is not cemented and could be correlated with the more humid phase of MIS9, while the Calcium carbonate - cemented pre-173 ka terrace could be correlated to the start of the

colder and more arid MIS6. The cemented base of the pre-140 ka limestone sandy deposits in the Geren near IR-10 could have occurred MIS6 or 7. It is suggested that Mediterranean semi-arid intergranular terrace cementation in occurs in the wet-warm stages (Kelly et al., 2000; Candy and Black, 2009). Both our cemented terraces are overlain by uncemented aggradation sequences. These could be correlated with cold-stage aggradation, which is a suggested mechanism in the Mediterranean (Macklin et al., 2002), especially the extensive limestone fine sandy silty aggradations of IR-10 could be linked to the prolonged cold stage of MIS6. The non-cemented 3 m fill terrace of IR-9 dates to warmer and more humid MIS 5a. Travertines are also tentatively put in the humid stages of MIS 7 and MIS 5, although their formation is perhaps volcanically driven rather than climatically. The non-cemented late Pleistocene fluvial aggradation below IR-7 is older than 16.8 ka and tentatively dates to MIS2, while a final aggradation dates to the early to middle Holocene. Although some of these terrace correlations are indicative of potential climate driven terrace formation, they are not conclusive due to lack of preservation and low-resolution age constraints, a still prevailing issue recognized from areas throughout the Mediterranean (Macklin et al., 2002). Finally, linking aggradation and incision events in small uplifting catchments to climate is difficult due to the often transient conditions in these catchments (Tucker, 2009) and their complex internal feedbacks (Coulthard and Van De Wiel, 2007; Cowie et al., 2008; Schoorl et al., 2014).

Lavas and damming events

The damming history of the Gediz has been suggested to play an important role in the mid to Late Pleistocene evolution (Maddy et al., 2007), especially its influence on tributary catchments in the early Pleistocene is demonstrated (Maddy et al., 2012a). The reconstruction of Mid Pleistocene to Holocene damming events of the Geren Catchment presented in this thesis has delivered several significant results. First, the age of the youngest Holocene volcanic activity has been lowered to 3.0 – 2.6 ka (Chapter 3). This puts this event in historical times, which confirms the description of a very fresh lava by Strabo, who arrived there only 0.5 to 1 ka later (Falconer, 1903). This conclusion may advocate new archaeological investigation to the occurrence and consequences of this volcanic event.

Previously, four volcanic phases have been categorized in the Kula area, named from oldest to youngest β 1 to β 4 (Canet and Jaoul, 1946). These phases were later reduced to three phases β 2- β 4 (Richardson-Bunbury, 1996), based on relative topography and soil formation on top of these flows, and the increasing availability of reliably dated flows (Westaway et al., 2004). These phases are roughly put in the early Pleistocene, middle Pleistocene and Holocene. The length of the early Pleistocene period, based on the most recent dating results, stretches from 1.3 Ma until 1 Ma (Maddy et al., 2012b; Veldkamp et al., submitted; Maddy et al., submitted). No evidence of volcanic activity has been observed or dated in the period between 1 Ma and 300 ka. The age of the oldest middle-Pleistocene volcanic activity has now been raised to 310.5 ± 14.8 ka (Chapter 5). In combination with other mid to late Pleistocene and Holocene dates (Richardson-Bunbury, 1996; Westaway et al., 2004; Westaway et al., 2006) within the region, a period of volcanic activity emerges covering the last 300 ka and which is probably still ongoing. The duration of this period of activity is of the same order of magnitude as the active period in the early Pleistocene, suggesting that there have been two main volcanic activity periods. And thus the apparent division between mid-Pleistocene β 3 and Holocene β 4 groups can only be made based on its relative weathered surface and arable soil mantle and

not based on different phases of volcanic activity (Richardson-Bunbury, 1996). Furthermore, clearly not all $\beta 3$ lavas have been dated, making their exact period and timing still a matter of ongoing research.

The newly dated mid-Pleistocene basalts near the Gediz-Geren confluence and the already dated Palankaya dam suggest a phase from 310 ka until at least 175 ka in which incision by the Gediz River was seriously hampered by lava dams which entered the river from its southern left bank. Local base level was raised twice from around 370 – 375 m to around 390 – 400 m. The Gediz River was diverted around these flows, thereby shifting the Gediz valley and the Gediz – Geren confluence progressively eastward. At least one of the dams has been relatively long lived, evidenced by fluvial reestablishment on top of the lavaflow. In the period from the mid and late Pleistocene to the Holocene, the Gediz River incised and created a narrow gorge in the stretch downstream of the Gediz-Geren confluence towards Palankaya and further down. It is likely that some of the major landslides in the area occurred during this stage and that these landslides have possibly limited base level lowering in this period. Lava dams are not observed to have occurred again until in the Holocene, when a lava flow from the south again filled and dammed the Gediz and Geren valley between 3.0 ± 0.2 and 2.1 ± 0.5 ka. Two dam locations have been identified. Upstream, lake formation and infilling occurred, indicated by fluvial and alluvial deposits which together form a sediment wedge and bury former cemented gravel terraces. Downstream, a lake was formed which was only locally infilled due to the upstream sediment trap, and in which the Geren formed a delta. This dam again diverted the Gediz River eastward and shifted the Geren outlet reach inward. Both dam locations show evidence of sudden breaching. With basalt-rich debris deposits and, at the upstream breach, imbricated boulders. The lower Geren stream path was shortened and changed from meandering into a straight channel. The current Gediz channel is mainly incising into basement lithology next to its original channel floor, and its channel elevation is not yet as low as it was before the Holocene damming event. Duration and type of dam removal have thus differed between the Mid-Pleistocene and Holocene dams, where long-lived and perhaps gradual removal of the oldest mid Pleistocene lava dam occurred, while the youngest Holocene dam breached suddenly and created an outburst flood.

6.1.2 Response to external drivers: model results

Tectonics

Simulation of catchment evolution of scenarios with and without tectonically induced gradual base level lowering showed linear and non-linear effects on catchment evolution. Net erosion timeseries of scenarios without gradual base level lowering, both with and without damming events, showed a complex, but comparable sediment export when looking at average and standard deviation (Fig. 4.5). The net erosion timeseries of scenarios with gradual base level lowering showed, as expected, an increased average net erosion and an increased standard deviation. Thus, more sediment was exported, and there were more events with high export. Interestingly, the timeseries of net erosion shows clusters of higher variability of unequal length and unequally spaced in time. This variability is reflected in sediment storage buildup and removal. These clusters are interpreted as internally driven periods of higher activity, bearing the signature of the specific landscape (Schoorl et al., 2014). However, gradual base level lowering has activated these clusters and was therefore necessary to change the system

behaviour towards this alternation between active and less active net erosion periods.

Climate

Simulations in Chapter 4 did not incorporate any climate variability; rainfall was constant during its 300 ka simulation time. Nevertheless, an interesting conclusion can be drawn from its results considering the recognition of climate cycles in sediment stacks. If the total amount of sediment that is stored in the catchment since the start of the run (Fig 4.6) is compared with net erosion, the high variability clusters coincide with phases of decrease in sediment storage. Although these clusters are driven by internal dynamics, they do cause quasi-cyclic sediment export from the catchment. If this catchment would be draining in a lake or would be building up a fan in a subsiding basin, these quasi-cyclic patterns could be mistaken for climatically driven sediment cycles.

The simulations of Chapter 5 did incorporate climate-driven rainfall variability. Climate variation and more active sedimentation and erosion events show a weak correlation with glacial periods (The “No dams” scenario in Fig. 5.9), although timing and nature of these events differs between up and downstream reaches. Thus, a general correlation of gully evolution with climate appears to occur, while, when looking more in detail to exact timings, these correlations become less evident. A possible direct effect of rainfall intensity on MIS substage level is thus counteracted, or shredded, by the landscape complexity and consequently, phases of incision or aggradation are the result of their interactions. The addition of damming events obscures the large scale correlation, especially in the downstream gully reach.

Damming events

In Chapter 2, modelling response to natural long-lived dams in an experimental catchment setup revealed that cumulative sediment yield of dammed catchments is lower than non-dammed catchment until 15 ka after simulation. Furthermore, comparison of a high erodibility landscape with a low erodibility landscape showed that high erodibility landscapes generate higher and more variable sediment yields, less incision of the trunk stream due to higher sediment loads leading to transport-limited conditions. Their response to damming differs from low erodibility landscapes. In high erodibility landscapes, stream capture occurred due to a combination of sediment load driven avulsions on top of the filled lake and headward erosion into the lake fill by secondary channels with sufficient stream power and low sediment load. Furthermore, this high sediment load led to prolonged delayed incision of the trunk stream, whereas in the low erodibility landscape, longitudinal profiles are similar to the non-dam scenario within 5 ka. Differences in dam erodibilities demonstrated that, in transport-limited landscapes, lower erodibility dams created more prolonged knickpoints, while in detachment-limited landscapes, only the least erodible dam scenario generated a somewhat delayed incision of the trunk stream. A qualitative comparison of model results with actual studies on response to natural damming shows that both delayed incision and knickpoint persistence occurs, as well as rapid gorge formation. However if one wants to model an actual field situation, model adjustments and calibration should be performed for each separate field situation. Nevertheless, model results encouraged further model work on longer timescales and larger spatial scales.

In Chapter 4, modelling response to damming is extended to larger spatial and longer temporal scales. The objective was to unravel if and how damming events affected sediment yield, elevation changes and sediment dynamics. Since incision of the Gediz River is clearly occurring in the mid and late Pleistocene, the no-dam and dam scenario that endured gradual base level lowering were compared into more detail. The main conclusion is that a short-lived damming event such as the Holocene lava damming event described in Chapter 3 can have a long-term impact on catchment evolution. Net erosion timeseries revealed complex, but substantially different sediment output for both scenarios, where dam scenarios showed large sudden changes in sediment output variability. Sometimes these changes were directly related to damming events and sometimes they were lagging or unrelated to damming events. Although there clearly is a dam-related response of annual net erosion, this response is non-linear and it is superimposed on the non-linear response to gradual base level lowering. Again, this non linearity is driven by internal catchment dynamics (Wainwright, 2006; Coulthard and Van De Wiel, 2007). Monitoring spatial differences of elevations and sediment storage of dam and non-dam scenarios revealed that this difference migrates upstream into the catchment and is still on-going at least 250 ka after the first damming event. Enhanced gully erosion and dampened slope erosion occurring at the same time indicate legacy effects and decoupling of slope and gully response to damming events. The exact timing of these effects on elevation change and sediment storage and release events is, however, sensitive to parameter settings.

The addition of field reconstruction-derived damming events to the climate- and uplift-driven simulation in Chapter 5, as already stated, obscures any correlation between climate and gully activity (Fig 5.9). This dam legacy effect occurs both through dampening and enhancing of incision phases, which is in line with findings of Chapter 4 where no climate variability was applied.

6.1.3 Integrative summary of Geren catchment evolution

During the mid-Pleistocene, the Geren Catchment was already draining towards the Gediz at or near its current outlet position. Limestone gravels, sands and silts which originate from a northern limestone plateau, now cap ridges throughout the catchment, but notably in its centre part where elongated limestone ridges form 15 m thick aggradation sequences. Dating suggest that these deposits can be contemporaneous with the mid-Pleistocene damming events at the Geren outlet. However, modelled gully elevations over time (300 ka – present) suggest that gully incision and aggradation could also be correlated to climate variations, where increased rainfall leads to aggradation or less incision, although damming events dampen this correlation considerably. Subsequent incision of these mid-Pleistocene limestone ridges did not occur until after around 82 ka. Comparing simulated gully elevations with this dated location indicates that exact simulation of this location did not occur, which could either be due to model or dating uncertainty. However, modelling does suggest that such a prolonged period of hampered incision is best explained if the Geren base level was stable for a longer period, either suggesting a stable Palankaya dam for a prolonged period of several tens of thousands of years, or suggesting damming by subsequent landslides. From 82 ka onwards, the Geren Catchment endured a confined incision phase, a process induced from fieldwork and best reproduced by the simulation with long dam duration input. At the end of the Pleistocene, several incision – aggradation phases occurred in the lower reach of the Geren trunk stream, while a Holocene phase of aggradation occurred around 2.5 ka. This

aggradation is followed by the most recent incision, which in its downstream reach is driven by ongoing post-lava Gediz migration and incision. This exact timing and sequence of events is again not reproduced by model results, although again, the long dam duration scenario reproduces downstream aggradation in the late Pleistocene best. The subsequent Holocene incision and aggradation phases are poorly reproduced. A separate Holocene simulation study could perhaps increase model performance on this timescale.

The multiple lava damming events thus impacted the Geren and Gediz incision history and their impact is ongoing. Even the early Pleistocene lava plateaus influence current evolution, as ongoing river incision created a plateau morphology, in which a resistant basalt caprock overlies less resistant Miocene basinfills and deformed basement, resulting in oversteepened slopes. This may create boundary conditions for landsliding until today (*cf.* Ely et al., 2012).

6.1.4 Unresolved and newly emerged questions

Some questions on evolution of the Geren Catchment remain unresolved. The base level reconstruction suggests that the significance of either the Palankaya dam or major landsliding should be investigated further, looking in the Selendi catchment as well as in the gorge downstream of the Geren-Gediz confluence. Another topic to be investigated is the relative importance of human impact on the last 2 to 3 ka of catchment evolution, as fieldwork suggests catchment wide floodplain sedimentation around 2.5 ka in an inhabited and used landscape.

Another remaining question is why the average relief of the eastern part of the catchment is significantly lower than the rest of the catchment. Fieldwork has led to two hypotheses: 1) the substrate becomes finer and more easily erodible while going eastward, which has a direct impact on erosive capacity of each subcatchment, therefore denudation rate of the eastern part is simply higher and 2) the eastern subcatchment has been connected to the upstream part of the Hudut catchment, thereby having had an increased drainage area and increased stream power. Again, landscape evolution modelling could be a valuable tool to resolve these questions.

6.1.5 Considerations on dating results

Different dating techniques have been applied and integrated in landscape reconstruction. Tephrites/basanites and Phonotephrites (Chapter 5, appendix S2) have been dated using $^{40}\text{Ar}/^{39}\text{Ar}$ – dating. Mid-Pleistocene tephrites/basanites yielded meaningful $^{40}\text{Ar}/^{39}\text{Ar}$ – ages. By convention, age estimates are reported with a 1σ range (Renne et al., 2009), however, at 2σ level, sample Ar-3bot and Ar-4 can belong to the same lava flow (Table 5.2). The long dam model scenario already accounts for this due to its prolonged stable base level phase from 300 ka until 240 ka (0-60000 simulation years, Fig. 5.8). In our case the young phonotephrites did not yield a meaningful age due their low enrichment in radiogenic argon, although Holocene dating has successfully been done with $^{40}\text{Ar}/^{39}\text{Ar}$ elsewhere (Wijbrans et al., 2011).

Fortunately, this lava flow is both underlain and overlain by fluvial sands. These have been dated using post-Infrared-Infrared luminescence dating and constrained the age of the flow to the late Holocene. Other fluvial samples have been dated with mixed results. Luminescence dating was carried out in two phases, the results of which both are used in Chapter 3 and 5. The first phase was done using multiple-grain post-IRIR on Holocene and Late Pleistocene

samples and includes the dated fluvial sands below the Holocene Kula lava flow of 3 ka (Chapter 3). In the second phase, a newly developed low-temperature single-grain Post-IRIR technique was applied (Reimann et al., 2012; Reimann and Tsukamoto, 2012) on young Holocene samples which all turned out to be younger than the multiple-grain dates. This led to the age constraint of the Holocene flow between 3.0 and 2.6 ka, however, it is not unlikely that the 3 ka multiple-grain age will turn out younger if it is measured with the new single-grain technique, due to averaging effects.

The radiocarbon age of C-1 of 13.3 ka and the luminescence age of 16.8 ka of IR-7 suggest that the muds of C-1 are younger than the sands of 16.8. This is stratigraphically not impossible. However, the radiocarbon age is derived from a humic acid fraction, which could have been transported from elsewhere after deposition, making it a minimum age. The luminescence sample is measured with a multiple-grain technique and perhaps single grain measurements would result in a slightly younger age, making both samples perhaps contemporaneous.

It is therefore important to be confident about what the age estimate represents. Their uncertainties should be assessed and combined to lead to an overall uncertainty, which probably is always higher than normally reported uncertainties. Therefore, in landscape reconstruction studies, it is perhaps better to speak of “age estimates”, rather than “dates”. For instance, luminescence age uncertainty from a layer in the middle of a stacked sequence does not inform about the total period of deposition, which can either be smaller or larger than its age uncertainty. It is however often difficult to quantify such an uncertainty. Interestingly, perhaps model output of calibrated and well-tested models could aid in lowering age uncertainty. If a terrace is dated with a 20 ka uncertainty, occurrence of an aggradation phase in the model within this period can better constrain this.

6.2 LAPSUS, an ever evolving reduced complexity landscape evolution model

Landscape evolution model (LEM) LAPSUS has been used for the first time on a 300 ka timescale. Earlier studies demonstrated the potential of LAPSUS for long-term landscape evolution modelling (Temme and Veldkamp, 2009; Temme et al., 2011b; Baartman et al., 2012b) at millennial and late Pleistocene (10^4 ka) timescales. In this thesis, long-term landscape evolution modelling was done on a 10^5 ka timescale. Reduced-complexity model (Brasington and Richards, 2007) LAPSUS was judged suitable for such a study opposed to reductionist, more physically based models, because these models require more detailed data and more detailed parameter descriptions (Temme et al., 2011a; Van De Wiel et al., 2011; Murray, 2013). An example would be uncertainties of the incorporation of daily rainfall data from measured timeseries instead of annual, climate proxy derived rainfall. However, it is acknowledged that these simplifications, undervalue for instance the role of extreme rainfall events on catchment evolution (Baartman et al., 2013b).

6.2.1 Model choices and limitations

Beside these model-specific assumptions on boundary conditions, choices had to be made on model simplifications. A subset of the LAPSUS modelling framework has been used to model

landscape evolution of 300 ka. Due to the specific interest in response to base level change, some significant simplifications were accepted to be able to execute this model exercise. First, only water runoff and erosion was used as a landscape evolution process. Calibration was done by varying the erodibility factor K and sedimentation factor P only. The exponents of the hillslope runoff continuity model (Kirkby, 1971) were kept constant, although their values ideally should vary according to whether runoff occurs on a hillslope or in a river (Bartman et al., 2012a). Another still unresolved point of attention is lateral erosion, which occurs at stream banks and gully walls. Furthermore, multi-process interactions in an evolving landscape (Temme and Veldkamp, 2009; Temme et al., 2011a) are now not simulated. For instance, landsliding is a significant process in upland catchment evolution, both in the form of hampering incision and supplying sediment to the river system (Korup et al., 2010).

To incorporate the more transport-limited properties of already eroded and redeposited sediments, these sediments have been assigned a higher erodibility factor dynamically. Yet, weathering and soil formation (Temme and Veldkamp, 2009) are not simulated. It is thus assumed that erodible material is available at all locations at any time, the rationale for this is that the Geren Catchment has in general been eroding relatively unconsolidated Miocene silts, sands and gravels. Only the less erodible basalt and limestone plateaus have been assigned a lower erodibility. However, the unconsolidated substrate varies vertically and spatially, and incorporating spatial and vertical variation of substrate will increase subcatchment-scale erosion and fluvial pattern formation accuracy. In Chapter 4 and 5 a calibrated set of K and P is used where P is magnitudes higher than K . This calibration result was due to the observation that increasing P modulates long-term profile incision rates in LAPSUS. It is recommended to further explore the relative role of K and P on long-term profile development in order to create more realistic fluvial profiles.

Another aspect which could be further developed is the possibility of catchment border migration and subsequent stream capture. Stream capture such as described in Chapter 3 was driven by headward erosion of a small stream, but the actual rerouting was due to stream bifurcation and avulsion on top of the relatively flat lake fill. There are recent developments in model capabilities for headward erosion-driven stream capture (Goren et al., 2014). In LAPSUS, the addition of slope processes such as subsurface flow (Keesstra et al., 2013), shallow landsliding (Claessens et al., 2005) and collapse are probably necessary to make headward stream capture possible. Nonetheless, any additional process or property to incorporate in long-term landscape evolution modelling will increase data demands, model demands and parameter uncertainty and could lead to model equifinality.

Other initial and external driver conditions have been simplified as well. The used palaeodem in Chapter 4 and 5 is based on hydrologically correct interpolation of field and GIS derived palaeosurfaces. This is a relatively simple interpolation method. Similar simplified interpolation approaches have been used to interpolate palaeosurface and terraces to palaeodems (Alexander et al., 2008; Bartman et al., 2012b). However, more sophisticated interpolation techniques of Quaternary surfaces and their uncertainty assessment have recently been pursued (Geach et al., 2014). In Chapter 4 and 5, the representation of dams and their removal have been simplified, by an instantaneous uplift and lowering of the most downstream part of the outlet reach. Although in the theoretical simulations in Chapter 2, dams were dynamically removed by incision after lake infilling. Dam leakage (Crow et al., 2008) and gradual dam incision after

lake infilling (Ely et al., 2012) have not been explicitly simulated in Chapter 4 and 5. The reason is that dam removal is mostly driven by the Gediz River and not the Geren. Therefore such a simplified boundary condition was assessed appropriate. Finally, DEM-resolution has been kept constant (30m) in this explorative model study. We however acknowledge that model results can be sensitive to DEM-resolution (Schoorl et al., 2000; Claessens et al., 2005).

6.3 Research implications

Typically, Quaternary field reconstruction delivers detailed snapshots of a certain type of landscape on a certain point in time, such as illustrated in the fieldwork area by detailed reconstruction of a fluvial terrace staircase reconstructing incision and climatic history (Maddy et al., 2012b), while palaeosols inform on climatic and palaeolandscape activity and stability phases (Veldkamp et al., submitted).

In this thesis it was attempted to integrate field reconstruction and landscape evolution modelling in such a way, that their result is more than the sum of its parts. In other words some conclusions derived in this thesis could not have been derived from either fieldwork or modelling alone (Temme, 2008). The clearest example from this thesis work is that model results suggest that damming, or prolonged base level stability, has been necessary to explain the Geren incision-aggradation history derived from fieldwork, thereby enhancing our understanding of catchment evolution in a way which would not have been able from either fieldwork or modelling alone. Such a combination thus potentially clarifies catchment history and mechanisms, while perhaps generating questions or interests in field sites which would otherwise not have been noted. Nevertheless, in its current form the approach still has limitations such as limited spatial accuracy, lack of incorporation of all relevant processes and uncertainties of boundary conditions, stressing the ongoing and iterative nature of this approach in understanding long-term landscape dynamics (Temme, 2008).

6.3.1 Long-term landscape evolution: towards an interdisciplinary field-model approach

The last decennia have seen an explosion of LEMs, driven by increased computer power and availability of digital elevation models (Coulthard, 2001; Tucker and Hancock, 2010). The current state of science in LEMs is that they mainly need to be calibrated to the specific landscape which is modelled and break down when this calibrated set is used on other areas. This might be perceived as a drawback in using those models, and many pursue the road of increasing physical detail in models as the way to go. It is clear that, in the light of the still increasing computer calculation power (e.g. parallel computing), increasing this level of detail can deliver significant progress towards modelling more accurate process descriptions on a catchment scale. However, this will be at the cost of parameterisation at more detailed scales, for instance coefficients of friction for colliding grains (*cf.* Murray, 2013). Furthermore the amount of accurate data that will be needed as an input is currently not available (e.g. the exact 3D grain configuration of sand bars in a stream in a landscape). The amount of data that will be produced by such models will be vast and their analysis an enormous task. It is therefore advocated that calibration of LEMs to specific field areas is a standard procedure. This consequently implies that in any landscape reconstruction project where not only history but also driving mechanisms are studied, field reconstruction, dating and landscape evolution

modelling should co-evolve. This allows researchers to use modelling to test different hypotheses or generate new hypotheses that can be tested in the field.

In this thesis, typical traditional field reconstruction outcomes are presented in Chapter 3 and 5, in the form of schematic picture stories (Fig 3.11, Fig 5.6) and longitudinal profile reconstructions (Fig 3.12). These reconstructions are based on determining stratigraphy and, after dating, chronology, leading to a chronostratigraphy. These detailed snapshots are valuable, however, pathways between these snapshots are simplified and often linearly interpolated (see Fig. 6.1). On the other hand, LEMs are able to reconstruct these pathways in very detailed manner. However, they generally do not postdict the exact location of e.g. a certain aggradation or erosion event on Quaternary timescales, although various successful examples on shorter timescales, from decadal- to even millennial scale do exist (see Temme et al., 2013 for an overview of recent examples). Analysis of model performance on Quaternary timescales is not done on a cell-by-cell comparison. Rather, aggregated information is used, such as total net erosion (Chapter 3), stream profile evolution (Chapter 3). Additionally, qualitative evaluation of spatial patterns of net erosion and sediment redistribution can be used to complex spatial catchment response to imposed drivers (Chapter 4) but exact numbers of exact locations should be interpreted with caution. An example that might be useful and can be translated to field-derived landscape snapshots could be elevation change of a certain gully reach (Chapter 5). Although in this case an exact location or reach is monitored, this stream bed change is governed by upstream evolution and interactions, as well is its downstream base level and therefore represents aggregated catchment dynamics. Phases of incision, aggradation and stability can be compared with drivers such as climate and base level change. A key advantage is that their timing and magnitude can be compared with the field-derived snapshots of change. By changing drivers and boundary conditions, the most likely drivers responsible for the catchment's pathways of change can be assessed. In Chapter 5, this is done in a rather explorative and qualitative way and perhaps expansion with sensitivity or uncertainty analysis is advisable for similar future studies. Model results could in this way also inform on unresolved or unnoticed processes or feedbacks in a landscape.

Model benchmarking

For both the landscape evolution modelling community and the field reconstruction community it is not clear what the strengths and weaknesses of available models are. Model benchmarking basically means providing a standardized test for LEMs, and listing their strong and weak points using one or some catchments whose evolution is well constrained. Perhaps this automatically means that long-term landscape reconstruction studies should involve landscape evolution modelling specialists, field reconstruction specialists and dating specialists, as well as overall generalists, thus creating an interdisciplinary geomorphology team. Additionally, it can be helpful if the geomorphological community creates a “template” for combined field reconstruction and model studies, which every worker could use, and which states possibilities the community has to offer, together with guidelines on methodologies.

Another issue to be further explored is the analysis of model outputs. Several concepts already emerged which can help to understand system behaviour, such as self-organized criticality (Van De Wiel and Coulthard, 2010) and shredding of environmental signals (Jerolmack and Paola, 2010). These analyses are insightful to understand system behaviour, and perhaps

comparison of sediment yield with for instance lake deposits could be done for catchments which drain into lakes. However, otherwise their connection to field observations is limited. Another way to look at model outputs such as average total net erosion, or its variability through time, or changes from gully aggradation to erosion is in the light of system stability and change of states (Phillips, 2013b). Finally, spatial expression of the complexity can be assessed, such as sediment waves (Schoorl et al., 2014), which are upstream migrating erosion-sedimentation areas, produced by catchment complexity. This complexity is also observed in the 1000 ka averaged gully elevation signal of the Geren Catchment simulations (Fig. 5.8) and its spatial migration or stability through time can be assessed and compared with observed field records.

6.4 Final conclusions

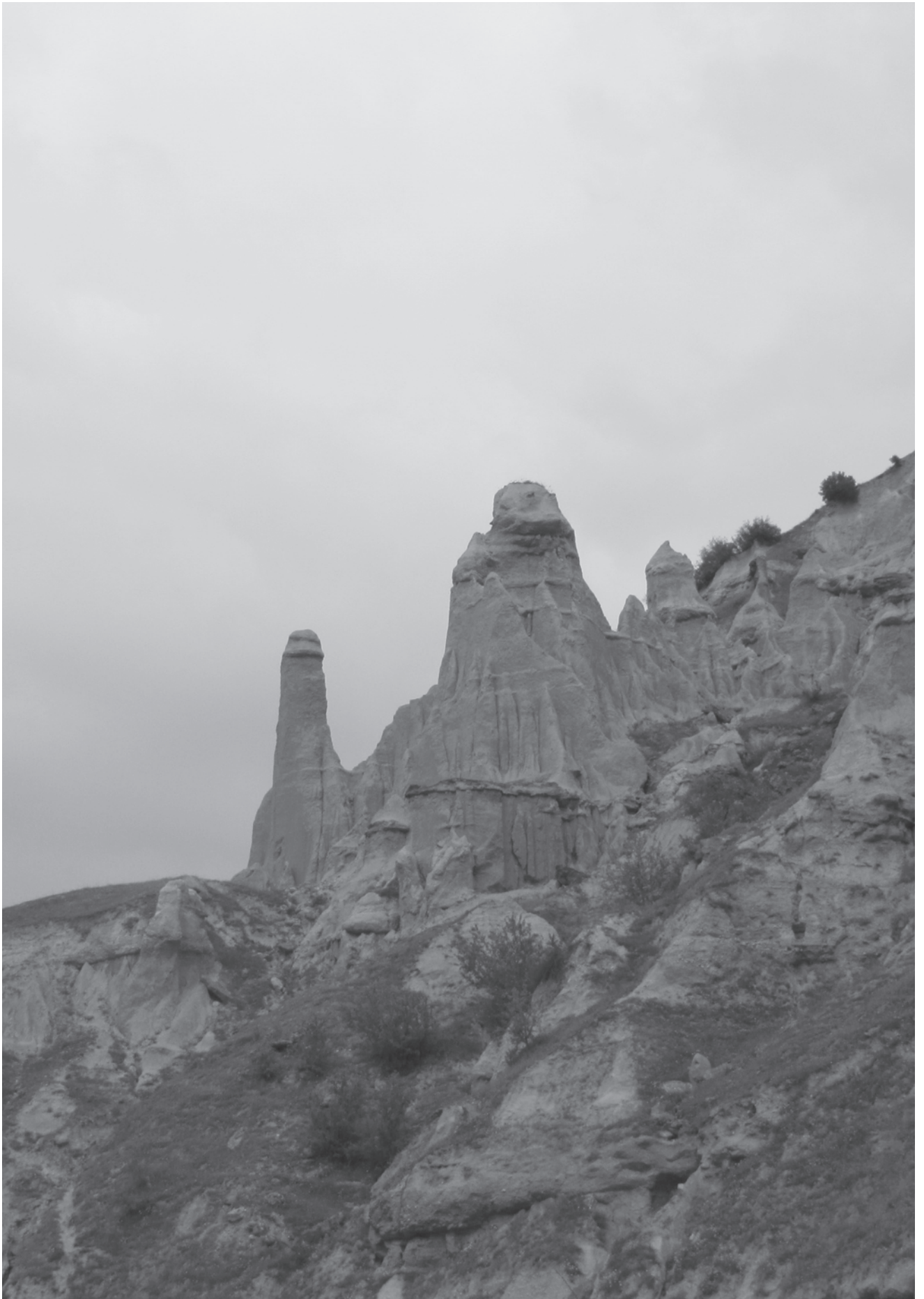
The final conclusions of this thesis are:

Thesis-specific

- Total net erosion of dammed catchments remains lower than non-dammed catchments after 15000 due to sediment storage behind the dam body.
- Dams in transport-limited landscapes have a longer term impact on longitudinal profile evolution than dams in detachment-limited landscapes.
- Holocene volcanic activity the Kula volcanic field, western Turkey is age constrained to 3.0 – 2.6 ka, making it potentially having had impact on human settlements around that time.
- Lava damming of the same river on two locations leads to distinct but interrelated responses, where sediment trapping by the upstream dam is not visible downstream. Breaching of one of the two dams can invoke breaching of the other dam
- The Gediz and Geren river reaches at and around Holocene lava flow are still responding to damming by this lava flow.
- Landscape evolution modelling shows that internal catchment dynamics can create cyclic patterns of sediment export, therefore, cyclic sediment records do not always indicate a cyclic external driver causing this pattern.
- Short-term lava dams can have long-term (10^5 a timescale) impact on catchment evolution, therefore current catchment dynamics can bear the legacy of these past short-term events
- Non-linear response to damming events can either cause long-term dampening or amplification of catchment incision.
- Combined field reconstruction and modelling suggest that uplift-driven incision of the Geren Catchment has been hampered by multiple mid Pleistocene long duration damming events.

General conclusions

- Long-term time-averaged incision rates based on fluvial terraces cannot directly be related to uplift rates if catchment-specific information is not incorporated, as timing of terrace formation is not only related to uplift and climate, but is also governed by specific landscape history.
- Combining field reconstruction and modelling enhances our understanding of long-term evolution of a specific landscape and increases knowledge on long-term impact on current catchment complexities.
- An aggregated landscape evolution model output such as long-term stream bed change can be useful for comparison with field-derived fluvial terrace sequences.
- The long-term effects that lava dams can have suggests that this can be equally true for landslide dams, which occur in most incising upland catchments in the world.
- Although both field and modelling case studies can be useful to understand specific problems of specific areas, the challenge in the field of long-term landscape reconstructions lies in large scale combined model-field-dating studies, in which global model benchmarking, and validation with well-studied field areas will enhance insight in when and where to use which model, resulting in increased understanding of long-term Quaternary landscape dynamics.



References

- Alexander, R.W., Calvo-Cases, A., Arnau-Rosalèn, E., Mather, A.E., Lázaro-Suau, R., 2008. Erosion and stabilisation sequences in relation to base level changes in the El Cautivo badlands, SE Spain. *Geomorphology* 100(1-2), 83-90.
- Alexanderson, H., Murray, A.S., 2012. Luminescence signals from modern sediments in a glaciated bay, NW Svalbard. *Quaternary Geochronology* 10, 250-256.
- Arnold, L.J., Roberts, R.G., Galbraith, R.F., DeLong, S.B., 2009. A revised burial dose estimation procedure for optical dating of young and modern-age sediments. *Quaternary Geochronology* 4(4), 306-325.
- Baartman, J.E.M., Veldkamp, A., Schoorl, J.M., Wallinga, J., Cammeraat, L.H., 2011. Unravelling Late Pleistocene and Holocene landscape dynamics: the upper Guadalentín basin, SE Spain. *Geomorphology* 125(1), 172-185.
- Baartman, J.E.M., Van Gorp, W., Temme, A.J.A.M., Schoorl, J.M., 2012a. Modelling sediment dynamics due to hillslope-river interactions: Incorporating fluvial behaviour in landscape evolution model LAPSUS. *Earth Surface Processes and Landforms* 37(9), 923-935.
- Baartman, J.E.M., Temme, A.J.A.M., Schoorl, J.M., Braakhekke, M.H., Veldkamp, T.A., 2012b. Did tillage erosion play a role in millennial scale landscape development? *Earth Surface Processes and Landforms* 37(15), 1615-1626.
- Baartman, J.E.M., Masselink, R., Keesstra, S.D., Temme, A.J.A.M., 2013a. Linking landscape morphological complexity and sediment connectivity. *Earth Surface Processes and Landforms*.
- Baartman, J.E.M., Temme, A.J.A.M., Veldkamp, T., Jetten, V.G., Schoorl, J.M., 2013b. Exploring the role of rainfall variability and extreme events in long-term landscape development. *Catena* 109, 25-38.
- Bøtter-Jensen, L., Andersen, C.E., Duller, G.A.T., Murray, A.S., 2003. Developments in radiation, stimulation and observation facilities in luminescence measurements. *Radiation Measurements* 37(4-5), 535-541.
- Brasington, J., Richards, K., 2007. Reduced-complexity, physically-based geomorphological modelling for catchment and river management. *Geomorphology* 90(3-4), 171-177.
- Bridgland, D., Westaway, R., 2008. Climatically controlled river terrace staircases: A worldwide Quaternary phenomenon. *Geomorphology* 98(3-4), 285-315.
- Buis, E., Veldkamp, A., 2008. Modelling dynamic water redistribution patterns in arid catchments in the Negev Desert of Israel. *Earth Surface Processes and Landforms* 33(1), 107-122.
- Bunbury, J.M., Hall, L., Anderson, G.J., Stannard, A., 2001. The determination of fault movement history from the interaction of local drainage with volcanic episodes. *Geological Magazine* 138(2), 185-192.
- Burchsted, D., Daniels, M., Wohl, E.E., 2014. Introduction to the special issue on discontinuity of fluvial systems. *Geomorphology* 205, 1-4.
- Buylaert, J.P., Jain, M., Murray, A.S., Thomsen, K.J., Thiel, C., Sohbat, R., 2012. A robust feldspar luminescence dating method for Middle and Late Pleistocene sediments. *Boreas* 41(3), 435-451.
- Candy, I., Black, S., 2009. The timing of Quaternary calcrete development in semi-arid southeast Spain: Investigating the role of climate on calcrete genesis. *Sedimentary Geology* 220(3-4), 6-15.
- Canet, J., Jaoul, P., 1946. Report on the geology of the Manisa-Aydin-Kula-Gordes area.
- Capra, L., 2007. Volcanic natural dams: identification, stability, and secondary effects. *Natural Hazards* 43(1), 45-61.
- Carrivick, J.L., Turner, A.G.D., Russell, A.J., Ingeman-Nielsen, T., Yde, J.C., 2013. Outburst flood evolution at Russell Glacier, western Greenland: effects of a bedrock channel cascade with intermediary lakes. *Quaternary Science Reviews* 67, 39-58.
- Cheng, H., Edwards, R.L., Hoff, J., Gallup, C.D., Richards, D.A., Asmerom, Y., 2000. The half-lives of uranium-234 and thorium-230. *Chemical Geology* 169(1-2), 17-33.
- Claessens, L., Heuvelink, G.B.M., Schoorl, J.M., Veldkamp, A., 2005. DEM resolution effects on shallow landslide hazard and soil redistribution modelling. *Earth Surface Processes and Landforms* 30(4), 461-477.
- Claessens, L., Schoorl, J.M., Veldkamp, A., 2007. Modelling the location of shallow landslides and their effects on landscape dynamics in large watersheds: An application for Northern New Zealand. *Geomorphology* 87(1-2), 16-27.
- Costa, J.E., Schuster, R.L., 1988. Formation and failure of natural dams. *Bulletin of the Geological Society of America* 100(7), 1054-1068.
- Coulthard, T.J., Kirkby, M.J., Macklin, M.G., 1998. Non-linearity and spatial resolution in a cellular automaton model of a small upland basin. *Hydrology and Earth System Sciences* 2(2-3), 257-264.
- Coulthard, T.J., 2001. Landscape evolution models: a software review. *Hydrological Processes* 15(1), 165-173.

References

- Coulthard, T.J., Lewin, J., Macklin, M.G., 2005. Modelling differential catchment response to environmental change. *Geomorphology* 69(1-4), 222-241.
- Coulthard, T.J., Lewin, J., Macklin, M.G., 2007. Non-stationarity of basin scale sediment delivery in response to climate change. In: Habersack, H., Piegay, H., Rinaldi, M. (Eds.), *Developments in Earth Surface Processes*, pp. 315-331.
- Coulthard, T.J., Van De Wiel, M.J., 2007. Quantifying fluvial non linearity and finding self organized criticality? Insights from simulations of river basin evolution. *Geomorphology* 91(3-4), 216-235.
- Cowie, P.A., Whittaker, A.C., Attal, M., Roberts, G., Tucker, G.E., Ganas, A., 2008. New constraints on sediment-flux-dependent river incision: Implications for extracting tectonic signals from river profiles. *Geology* 36(7), 535-538.
- Crow, R., Karlstrom, K.E., McIntosh, W., Peter, L., Dunbar, N., 2008. History of Quaternary volcanism and lava dams in western Grand Canyon based on lidar analysis, $^{40}\text{Ar}/^{39}\text{Ar}$ dating, and field studies: implications for flow stratigraphy, timing of volcanic events, and lava dams. *Geosphere* 4(1), 183-206.
- Cunningham, A.C., Wallinga, J., Minderhoud, P.S.J., 2011. Expectations of scatter in equivalent-dose distributions when using multi-grain aliquots for OSL dating. *Geochronometria* 38(4), 424-431.
- Cunningham, A.C., Wallinga, J., 2012. Realizing the potential of fluvial archives using robust OSL chronologies. *Quaternary Geochronology* 12, 98-106.
- Dalrymple, G.B., Hamblin, W.K., 1998. K-Ar ages of Pleistocene lava dams in the Grand Canyon in Arizona. *Proc. Natl. Acad. Sci. U. S. A.* 95(17), 9744-9749.
- Darvill, C.M., 2013. Section 4.2.10: Cosmogenic nuclide analysis. In: Clarke, L.E., Niell, J.M. (Eds.), *Geomorphological techniques*. British Society for Geomorphology, London.
- Davis, W.M., 1899. The geographical cycle. *The Geographical Journal* 14(5), 481-504.
- Del Carlo, P., Branca, S., De Beni, E., Castro, M.D.L., Wijbrans, J.R., 2012. The Mt. Moio eruption (Etna): stratigraphy, petrochemistry and $^{40}\text{Ar}/^{39}\text{Ar}$ age determination with inferences on the relationship between structural setting and magma intrusion. *Journal of Volcanology and Geothermal Research* 241-242, 49-60.
- Demir, T., Seyrek, A., Guillou, H., Scaillet, S., Westaway, R., Bridgland, D., 2009. Preservation by basalt of a staircase of latest Pliocene terraces of the River Murat in eastern Turkey: evidence for rapid uplift of the eastern Anatolian Plateau. *Global and Planetary Change* 68(4), 254-269.
- Demoulin, A., Beckers, A., Rixhon, G., Braucher, R., Bourles, D., Siame, L., 2012. Valley downcutting in the Ardennes (W Europe): Interplay between technically triggered regressive erosion and climatic cyclicity. *Geologie en Mijnbouw/Netherlands Journal of Geosciences* 91(1-2), 79-90.
- Dietrich, W.E., Bellugi, D.G., Sklar, L.S., Stock, J.D., Heimsath, A.M., Roering, J.J., 2003. Geomorphic Transport Laws for Predicting Landscape form and Dynamics, *Prediction in Geomorphology*. American Geophysical Union, pp. 103-132.
- Duffield, W., Riggs, N., Kaufman, D., Champion, D., Fenton, C., Forman, S., McIntosh, W., Hereford, R., Plescia, J., Ort, M., 2006. Multiple constraints on the age of a Pleistocene lava dam across the Little Colorado River at Grand Falls, Arizona. *Bulletin of the Geological Society of America* 118(3-4), 421-429.
- Duller, G.A.T., Bøtter-Jensen, L., Murray, A.S., 2003. Combining infrared- and green-laser stimulation sources in single-grain luminescence measurements of feldspar and quartz. *Radiation Measurements* 37(4-5), 543-550.
- Duller, G.A.T., 2007. Assessing the error on equivalent dose estimates derived from single aliquot regenerative dose measurements. *Ancient TL* 25, 15-24.
- Ely, L.L., Brossy, C.C., House, P.K., Safran, E.B., O'Connor, J.E., Champion, D.E., Fenton, C.R., Bondre, N.R., Orem, C.A., Grant, G.E., Henry, C.D., Turrin, B.D., 2012. Owyhee River intracanyon lava flows: does the river give a dam? *Bulletin of the Geological Society of America* 124(11-12), 1667-1687.
- Emiliani, C., Milliman, J.D., 1966. Deep-sea sediments and their geological record. *Earth Science Reviews* 1(2-3), 105-132.
- Ermini, L., Casagli, N., 2003. Prediction of the behaviour of landslide dams using a geomorphological dimensionless index. *Earth Surface Processes and Landforms* 28(1), 31-47.
- Ersoy, Y.E., Helvacı, C., Sözbilir, H., 2010. Tectono-stratigraphic evolution of the NE-SW-trending superimposed Selendi basin: implications for late Cenozoic crustal extension in western Anatolia, Turkey. *Tectonophysics* 488(1-4), 210-232.
- Falconer, W., 1903. *The geography of Strabo*, II. Bell & Sons, London.
- Fenton, C.R., Poreda, R.J., Nash, B.P., Webb, R.H., Cerling, T.E., 2004. Geochemical discrimination of five pleistocene Lava-Dam outburst-flood deposits, western Grand Canyon, Arizona. *Journal of Geology* 112(1), 91-110.

- Fenton, C.R., Webb, R.H., Cerling, T.E., 2006. Peak discharge of a Pleistocene lava-dam outburst flood in Grand Canyon, Arizona, USA. *Quaternary Research* 65(2), 324-335.
- Florsheim, J.L., Ustin, S.L., Tang, Y., Di, B., Huang, C., Qiao, X., Peng, H., Zhang, M., Cai, Y., 2013. Basin-scale and travertine dam-scale controls on fluvial travertine, Jiuzhaigou, southwestern China. *Geomorphology* 180-181(0), 267-280.
- Foster, G.R., Meyer, L.D., 1972. A closed-form soil erosion equation for upland areas. In: Shen, H.W. (Ed.), *Sedimentation: symposium to honour professor H.A Einstein*, Colorado State University, Fort Collins, CO., pp. 190-207.
- Foster, G.R., Meyer, L.D., 1975. Mathematical simulation of upland erosion by fundamental erosion mechanics. *Sediment-Yield Workshop, Present and Prospective Technol for Predict Sediment Yields and Sources*, Proc, USDA Sediment Lab, 190-207.
- Freeman, T.G., 1991. Calculating catchment area with divergent flow based on a regular grid. *Computers and Geosciences* 17(3), 413-422.
- Galbraith, R.F., 1990. Radial plots: graphical assessment of spread in ages. *Nuclear Tracks and Radiation Measurements* 17(3), 207-214.
- Galbraith, R.F., Roberts, R.G., Laslett, G.M., Yoshida, H., Olley, J.M., 1999. Optical dating of single and multiple grains of quartz from Jinmium rock shelter, northern Australia: Part I, experimental design and statistical models. *Archaeometry* 41(2), 339-364.
- García-García, F., Sánchez-Gómez, M., Navarro, V., Pla, S., 2011. Formation, infill, and dissection of a latest-Pleistocene landslide-dammed reservoir (Betic Cordillera, southern Spain): Upstream and downstream geomorphological and sedimentological evidence. *Quaternary International* 233(1), 61-71.
- Geach, M.R., Stokes, M., Telfer, M.W., Mather, A.E., Fyfe, R.M., Lewin, S., 2014. The application of geospatial interpolation methods in the reconstruction of Quaternary landform records. *Geomorphology* 216, 234-246.
- Gibbard, P.L., Lewin, J., 2009. River incision and terrace formation in the Late Cenozoic of Europe. *Tectonophysics* 474(1-2), 41-55.
- Gilbert, G.K., 1880. Report on the geology of the Henry Mountains, Washington.
- Goren, L., Willett, S.D., Herman, F., Braun, J., 2013. Coupled numerical-analytical approach to landscape evolution modeling. *Earth Surface Processes and Landforms*, n/a-n/a.
- Goren, L., Willett, S.D., Herman, F., Braun, J., 2014. Coupled numerical-analytical approach to landscape evolution modeling. *Earth Surface Processes and Landforms* 39(4), 522-545.
- Gosse, J.C., Phillips, F.M., 2001. Terrestrial in situ cosmogenic nuclides: Theory and application. *Quaternary Science Reviews* 20(14), 1475-1560.
- Gottdang, A., Mous, D.W., Van der Plicht, J., 1995. The HVEE (super 14) C system at Groningen. *Radiocarbon* 37(2), 649 - 656.
- Grant, G.E., O'Connor, J.E., Wolman, M.G., Editor-in-Chief: John, F.S., 2013. *9.2 A River Runs Through It: Conceptual Models in Fluvial Geomorphology*, Treatise on Geomorphology. Academic Press, San Diego, pp. 6-21.
- Hamblin, W.K., 1990. Late Cenozoic lava dams in the western Grand Canyon. In: Beus, S.S., Morales, M. (Eds.), *Grand Canyon Geology*. Oxford University Press/Museum of Northern Arizona Press, New York, pp. 385-433.
- Hancock, G.R., 2008. The impact of depression removal on catchment geomorphology, soil erosion and landscape evolution. *Earth Surface Processes and Landforms* 33(3), 459-474.
- Hancock, G.R., Lowry, J.B.C., Coulthard, T.J., Evans, K.G., Moliere, D.R., 2010. A catchment scale evaluation of the SIBERIA and CAESAR landscape evolution models. *Earth Surface Processes and Landforms* 35(8), 863-875.
- Hancock, G.R., Coulthard, T.J., 2012. Channel movement and erosion response to rainfall variability in southeast Australia. *Hydrological Processes* 26(5), 663-673.
- Hewitt, K., 1998. Catastrophic landslides and their effects on the Upper Indus streams, Karakoram Himalaya, northern Pakistan. *Geomorphology* 26(1-3), 47-80.
- Huntley, D.J., Lamothe, M., 2001. Ubiquity of anomalous fading in K-feldspars and the measurement and correction for it in optical dating. *Canadian Journal of Earth Sciences* 38(7), 1093-1106.
- International Water Management Institute (IWMI) and General Directorate of Rural Services (GDRS), T., 2000. *Irrigation in the basin context: the Gediz study*, IWMI, Colombo, Sri Lanka.
- Jerolmack, D.J., Paola, C., 2010. Shredding of environmental signals by sediment transport. *Geophysical Research Letters* 37(19).

References

- Kars, R.H., Busschers, F.S., Wallinga, J., 2012. Validating post IR-IRSL dating on K-feldspars through comparison with quartz OSL ages. *Quaternary Geochronology* 12, 74-86.
- Kaufman, D.S., O'Brien, G., Mead, J.I., Bright, J., Umhoefer, P., 2002. Late Quaternary spring-fed deposits of the Grand Canyon and their implication for deep lava-dammed lakes. *Quaternary Research* 58(3), 329-340.
- Keesstra, S.D., Temme, A.J.A.M., Schoorl, J.M., Visser, S.M., 2013. Evaluating the hydrological component of the new catchment-scale sediment delivery model LAPSUS-D. *Geomorphology*.
- Kelly, M., Black, S., Rowan, J.S., 2000. A calcrite-based U/Th chronology for landform evolution in the Sorbas basin, southeast Spain. *Quaternary Science Reviews* 19(10), 995-1010.
- Kirkby, M.J., 1971. Hillslope process-response models based on the continuity equation. In: Brunsden, D. (Ed.), *Slopes, forms and processes*. Transactions of the IBG. Special publication, pp. 15-30.
- Kirkby, M.J., 1987. Modelling some influences of soil erosion, landslides and valley gradient on drainage density and hollow development. *Catena Supplement* 10, 1-14.
- Knudsen, O., Marren, P.M., 2002. Sedimentation in a volcanically dammed valley, Brúarjökull, northeast Iceland. *Quaternary Science Reviews* 21(14-15), 1677-1692.
- Koppers, A.A.P., 2002. ArArCALC-software for $^{40}\text{Ar}/^{39}\text{Ar}$ age calculations. *Computers and Geosciences* 28(5), 605-619.
- Korup, O., 2002. Recent research on landslide dams - A literature review with special attention to New Zealand. *Progress in Physical Geography* 26(2), 206-235.
- Korup, O., Strom, A.L., Weidinger, J.T., 2006. Fluvial response to large rock-slope failures: Examples from the Himalayas, the Tien Shan, and the Southern Alps in New Zealand. *Geomorphology* 78(1-2), 3-21.
- Korup, O., Tweed, F., 2007. Ice, moraine, and landslide dams in mountainous terrain. *Quaternary Science Reviews* 26(25-28), 3406-3422.
- Korup, O., Densmore, A.L., Schlunegger, F., 2010. The role of landslides in mountain range evolution. *Geomorphology* 120(1-2), 77-90.
- Korup, O., 2013. 9.15 Landslides in the Fluvial System. In: Schroder, J.F. (Ed.), *Treatise on Geomorphology*. Academic Press, San Diego, pp. 244-259.
- Krbetschek, M.R., Götze, J., Dietrich, A., Trautmann, T., 1997. Spectral information from minerals relevant for luminescence dating. *Radiation Measurements* 27(5-6), 695-748.
- Kuiper, K.F., Deino, A., Hilgen, F.J., Krijgsman, W., Renne, P.R., Wijbrans, J.R., 2008. Synchronizing rock clocks of earth history. *SCIENCE* 320(5875), 500-504.
- Lague, D., 2014. The stream power river incision model: Evidence, theory and beyond. *Earth Surface Processes and Landforms* 39(1), 38-61.
- Lee, J.Y., Marti, K., Severinghaus, J.P., Kawamura, K., Yoo, H.S., Lee, J.B., Kim, J.S., 2006. A redetermination of the isotopic abundances of atmospheric Ar. *Geochimica et Cosmochimica Acta* 70(17), 4507-4512.
- Levine, R., Meyer, G.A., 2014. Beaver dams and channel sediment dynamics on Odell Creek, Centennial Valley, Montana, USA. *Geomorphology* 205, 51-64.
- Lisiecki, L.E., Raymo, M.E., 2005. A Pliocene-Pleistocene stack of 57 globally distributed benthic $\delta^{18}\text{O}$ records. *Paleoceanography* 20(1), 1-17.
- Lucchitta, I., Curtis, G.H., Davis, M.E., Davis, S.W., Turrin, B., 2000. Cyclic aggradation and downcutting, fluvial response to volcanic activity, and calibration of soil-carbonate stages in the western Grand Canyon, Arizona. *Quaternary Research* 53(1), 23-33.
- Macaire, J.J., Cocirca, C., De Luca, P., Gay, I., De Goer De Herve, A., 1992. Origins, ages and evolution of the tardi- and postglacial lacustrine systems in the "lac Chambon" basin, Puy-de-Dome, France. *Comptes Rendus - Academie des Sciences, Serie II* 315(9), 1119-1125.
- Mackin, J.H., 1948. Concept of the graded river. *Bulletin of the Geological Society of America* 59(5), 463-512.
- Macklin, M.G., Fuller, I.C., Lewin, J., Maas, G.S., Passmore, D.G., Rose, J., Woodward, J.C., Black, S., Hamlin, R.H.B., Rowan, J.S., 2002. Correlation of fluvial sequences in the Mediterranean basin over the last 200 ka and their relationship to climate change. *Quaternary Science Reviews* 21(14-15), 1633-1641.
- Macklin, M.G., Lewin, J., 2008. Alluvial responses to the changing earth system. *Earth Surface Processes and Landforms* 33(9), 1374-1395.
- Maddy, D., Demir, T., Bridgland, D.R., Veldkamp, A., Stemerink, C., van der Schriek, T., Westaway, R., 2005. An obliquity-controlled early Pleistocene river terrace record from western Turkey? *Quaternary Research* 63(3), 339-346.
- Maddy, D., Demir, T., Bridgland, D.R., Veldkamp, A., Stemerink, C., van der Schriek, T., Schreve, D., 2007. The Pliocene initiation and early Pleistocene volcanic disruption of the palaeo-Gediz fluvial system, western

- Turkey. *Quaternary Science Reviews* 26(22-24), 2864-2882.
- Maddy, D., Demir, T., Bridgland, D.R., Veldkamp, A., Stemerink, C., van der Schriek, T., Westaway, R., 2008. The early Pleistocene development of the Gediz River, Western Turkey: an uplift-driven, climate-controlled system? *Quaternary International* 189(1), 115-128.
- Maddy, D., Veldkamp, A., Jongmans, A.G., Candy, I., Demir, T., School, J.M., van der Schriek, T., Stemerink, C., Scaife, R.G., Van Gorp, W., 2012a. Volcanic disruption and drainage diversion of the palaeo-Hudut River, a tributary of the Early Pleistocene Gediz River, western Turkey. *Geomorphology* 165-166, 62-77.
- Maddy, D., Demir, T., Veldkamp, A., Bridgland, D.R., Stemerink, C., van der Schriek, T., Schreve, D., 2012b. The obliquity-controlled early Pleistocene terrace sequence of the Gediz river, western Turkey: a revised correlation and chronology. *Journal of the Geological Society* 169(1), 67-82.
- Maddy, D., Schreve, D., Demir, T., Veldkamp, A., Wijbrans, J., Van Gorp, W., Scaife, R.G., School, J.M., Stemerink, C., Van der Schriek, T., submitted. The Earliest securely-dated hominins in Anatolia. *Quaternary Science Reviews*.
- Manville, V., Hodgson, K.A., Nairn, I.A., 2007. A review of break-out floods from volcanogenic lakes in New Zealand. *New Zealand Journal of Geology and Geophysics* 50(2), 131-150.
- Mather, A.E., Stokes, M., Griffiths, J.S., 2002. Quaternary landscape evolution: A framework for understanding contemporary erosion, southeast Spain. *Land Degradation and Development* 13(2), 89-109.
- McDougall, I., Harrison, T.M., 1999. *Geochronology and Thermochronology by the ⁴⁰Ar/³⁹Ar method*. 2nd ed. Oxford University Press., New York.
- Min, K., Mundil, R., Renne, P.R., Ludwig, K.R., 2000. A test for systematic errors in ⁴⁰Ar/³⁹Ar geochronology through comparison with U/Pb analysis of a 1.1-Ga rhyolite. *Geochimica et Cosmochimica Acta* 64(1), 73-98.
- Murray, A.B., Paola, C., 1994. A cellular model of braided rivers. *Nature* 371(6492), 54-57.
- Murray, A.B., Paola, C., 2003. Modelling the effect of vegetation on channel pattern in bedload rivers. *Earth Surface Processes and Landforms* 28(2), 131-143.
- Murray, A.B., 2013. 2.5 Which Models Are Good (Enough), and When? In: Shroder, J.F. (Ed.), *Treatise on Geomorphology*. Academic Press, San Diego, pp. 50-58.
- Murray, A.S., Wintle, A.G., 2003. The single aliquot regenerative dose protocol: Potential for improvements in reliability. *Radiation Measurements* 37(4-5), 377-381.
- O'Connor, J.E., Beebe, R.A., 2009. Floods from natural rock-material dams. In: Burr, D.M., Carling, P.A., Baker, V.R. (Eds.), *Megaflooding on Earth and Mars*. Cambridge University Press, Cambridge, pp. 128-171.
- O'Connor, J.E., Clague, J.J., Walder, J.S., Manville, V., Beebe, R.A., Editor-in-Chief: John, F.S., 2013. 9.25 Outburst Floods, *Treatise on Geomorphology*. Academic Press, San Diego, pp. 475-510.
- O'Connor, J.M., Jokat, W., Le Roex, A.P., Class, C., Wijbrans, J.R., Keßling, S., Kuiper, K.F., Nebel, O., 2012. Hotspot trails in the South Atlantic controlled by plume and plate tectonic processes. *Nat. Geosci.* 5(10), 735-738.
- Olafsson, J., 1979. Physical characteristics of Lake Myvatn and River Laxa. *Oikos* 32(1-2), 38-66.
- Ordóñez, S., González Martín, J.A., García del Cura, M.A., Pedley, H.M., 2005. Temperate and semi-arid tufas in the Pleistocene to Recent fluvial barrage system in the Mediterranean area: The Ruidera Lakes Natural Park (Central Spain). *Geomorphology* 69(1-4), 332-350.
- Ouimet, W.B., Whipple, K.X., Crosby, B.T., Johnson, J.P., Schildgen, T.F., 2008. Epigenetic gorges in fluvial landscapes. *Earth Surface Processes and Landforms* 33(13), 1993-2009.
- Özkul, M., Gökğöz, A., Kele, S., Baykara, M.O., Shen, C.C., Chang, Y.W., Kaya, A., Hançer, M., Aratman, C., Akin, T., Örü, Z., 2014. Sedimentological and geochemical characteristics of a fluvial travertine: A case from the eastern mediterranean region. *Sedimentology* 61(1), 291-318.
- Pain, C.F., Oilier, C.D., 1995. Inversion of relief — a component of landscape evolution. *Geomorphology* 12(2), 151-165.
- Pedley, M., González Martín, J.A., Ordóñez Delgado, S., García Del Cura, M.Á., 2003. Sedimentology of quaternary perched springline and paludal tufas: Criteria for recognition, with examples from Guadalajara Province, Spain. *Sedimentology* 50(1), 23-44.
- Peeters, I., Van Oost, K., Govers, G., Verstraeten, G., Rommens, T., Poesen, J., 2008. The compatibility of erosion data at different temporal scales. *Earth and Planetary Science Letters* 265(1-2), 138-152.
- Phillips, J.D., 2006. Evolutionary geomorphology: Thresholds and nonlinearity in landform response to environmental change. *Hydrology and Earth System Sciences* 10(5), 731-742.
- Phillips, J.D., 2013a. Thresholds, mode switching, and emergent equilibrium in geomorphic systems. *Earth Surface Processes and Landforms*.

References

- Phillips, J.D., 2013b. State transitions in geomorphic responses to environmental change. *Geomorphology*.
- Planchon, O., Darboux, F., 2002. A fast, simple and versatile algorithm to fill the depressions of digital elevation models. *Catena* 46(2-3), 159-176.
- Purvis, M., Robertson, A., 2004. A pulsed extension model for the Neogene-Recent E-W-trending Alasehir Graben and the NE-SW-trending Selendi and Gordes basins, western Turkey. *Tectonophysics* 391(1-4), 171-201.
- Quinn, P., Beven, K., Chevallier, P., Planchon, O., 1991. The prediction of hillslope flow paths for distributed hydrological modelling using digital terrain models. *Hydrological Processes* 5(1), 59-79.
- Reimann, T., Tsukamoto, S., Naumann, M., Frechen, M., 2011. The potential of using K-rich feldspars for optical dating of young coastal sediments – a test case from Darss-Zingst Peninsula (southern Baltic Sea coast). *Quaternary Geochronology* 6(2), 207-222.
- Reimann, T., Thomsen, K.J., Jain, M., Murray, A.S., Frechen, M., 2012. Single-grain dating of young sediments using the pIRIR signal from feldspar. *Quaternary Geochronology* 11, 28-41.
- Reimann, T., Tsukamoto, S., 2012. Dating the recent past (<500 years) by post-IR IRSL feldspar - Examples from the North Sea and Baltic Sea coast. *Quaternary Geochronology* 10, 180-187.
- Reimer, P.J., Baillie, M.G.L., Bard, E., Bayliss, A., Warren Beck, J., Bertrand, C.J.H., Blackwell, P.G., Buck, C.E., Burr, G.S., Cutler, K.B., Damon, P.E., Lawrence Edwards, R., Fairbanks, R.G., Friedrich, M., Guilderson, T.P., Hogg, A.G., Hughen, K.A., Kromer, B., McCormac, G., Manning, S., Ramsey, C.B., Reimer, R.W., Remmele, S., Southon, J.R., Stuiver, M., Talamo, S., Taylor, F.W., van der Plicht, J., Weyhenmeyer, C.E., 2004. IntCal04 terrestrial radiocarbon age calibration, 0-26 cal kyr BP. *Radiocarbon* 46(3), 1029-1058.
- Reimer, P.J., Bard, E., Bayliss, A., Beck, J.W., Blackwell, P.G., Bronk Ramsey, C., Buck, C.E., Cheng, H., Edwards, R.L., Friedrich, M., Grootes, P.M., Guilderson, T.P., Hafliðason, H., Hajdas, I., Hatté, C., Heaton, T.J., Hoffmann, D.L., Hogg, A.G., Hughen, K.A., Kaiser, K.F., Kromer, B., Manning, S.W., Niu, M., Reimer, R.W., Richards, D.A., Scott, E.M., Southon, J.R., Staff, R.A., Turney, C.S.M., van der Plicht, J., 2013. IntCal13 and Marine13 radiocarbon age calibration curves 0-50,000 years cal BP. *Radiocarbon* 55(4), 1869-1887.
- Renne, P.R., Deino, A.L., Hames, W.E., Heizler, M.T., Hemming, S.R., Hodges, K.V., Koppers, A.A.P., Mark, D.F., Morgan, L.E., Phillips, D., Singer, B.S., Turrin, B.D., Villa, I.M., Villeneuve, M., Wijbrans, J.R., 2009. Data reporting norms for 40Ar/39Ar geochronology. *Quaternary Geochronology* 4(5), 346-352.
- Richardson-Bunbury, J.M., 1996. The Kula volcanic field, western Turkey: the development of a Holocene alkali basalt province and the adjacent normal-faulting graben. *Geological Magazine* 133(3), 275-283.
- Rixhon, G., Braucher, R., Bourlès, D., Siame, L., Bovy, B., Demoulin, A., 2011. Quaternary river incision in NE Ardennes (Belgium)-Insights from 10Be/26Al dating of river terraces. *Quaternary Geochronology* 6(2), 273-284.
- Roach, I.C., Hill, S.M., Lewis, A.C., 2008. Evolution of a small intraplate basaltic lava field: Jerrabattgulla creek, upper shoalhaven river catchment, southeast New South Wales. *Aust. J. Earth Sci.* 55(8), 1049-1061.
- Roberts, R.G., Galbraith, R.F., Yoshida, H., Laslett, G.M., Olley, J.M., 2000. Distinguishing dose populations in sediment mixtures: A test of single-grain optical dating procedures using mixtures of laboratory-dosed quartz. *Radiation Measurements* 32(5), 459-465.
- Safran, E.B., Bierman, P.R., Aalto, R., Dunne, T., Whipple, K.X., Caffee, M., 2005. Erosion rates driven by channel network incision in the Bolivian Andes. *Earth Surface Processes and Landforms* 30(8), 1007-1024.
- Sawaske, S.R., Freyberg, D.L., 2012. A comparison of past small dam removals in highly sediment-impacted systems in the U.S. *Geomorphology* 151-152(0), 50-58.
- Schneider, B., Kuiper, K., Postma, O., Wijbrans, J., 2009. 40Ar/39Ar geochronology using a quadrupole mass spectrometer. *Quaternary Geochronology* 4(6), 508-516.
- Schoorl, J.M., Sonneveld, M.P.W., Veldkamp, A., 2000. Three-dimensional landscape process modelling: The effect of DEM resolution. *Earth Surface Processes and Landforms* 25(9), 1025-1034.
- Schoorl, J.M., Veldkamp, A., 2001. Linking land use and landscape process modelling: a case study for the Alora region (south Spain). *Agriculture Ecosystems & Environment* 85(1-3), 281-292.
- Schoorl, J.M., Veldkamp, A., Bouma, J., 2002. Modeling water and soil redistribution in a dynamic landscape context. *Soil Science Society of America Journal* 66(5), 1610-1619.
- Schoorl, J.M., Veldkamp, A., 2003. Late Cenozoic landscape development and its tectonic implications for the Guadalhorce valley near Alora (Southern Spain). *Geomorphology* 50(1-3), 43-57.
- Schoorl, J.M., Boix Fayos, C., De Meijer, R.J., Van Der Graaf, E.R., Veldkamp, A., 2004. The 137Cs technique applied to steep Mediterranean slopes (Part II): Landscape evolution and model calibration. *Catena* 57(1), 35-54.
- Schoorl, J.M., Temme, A.J.A.M., Veldkamp, A., accepted. Modelling centennial sediment waves in an eroding

- landscape – catchment complexity. *Earth Surface Processes and Landforms*.
- Schoorl, J.M., Veldkamp, A., Claessens, L., Van Gorp, W., Wijbrans, J.R., 2014 submitted. Edifice growth and collapse of the Pliocene Mt. Kenya: evidence of large scale debris avalanches on a high altitude glaciated volcano. *Global and Planetary Change*.
- Schumm, S.A., 1973. Geomorphic thresholds and complex response of drainage systems. In: Morisawa, M. (Ed.), *Fluvial Geomorphology*. SUNY Binghamton Publication in Geomorphology, pp. 299-310.
- Schumm, S.A., 1979. Geomorphic thresholds: the concept and its applications. *Transactions Institute of British Geographers* 4(4), 485-515.
- Seyitoglu, G., 1997. Late Cenozoic tectono-sedimentary development of the Selendi and Usak-Güre basins: A contribution to the discussion on the development of east-west and north trending basins in western Turkey. *Geological Magazine* 134(2), 163-175.
- Snyder, N.P., Whipple, K.X., Tucker, G.E., Merritts, D.J., 2003. Channel response to tectonic forcing: Field analysis of stream morphology and hydrology in the Mendocino triple junction region, northern California. *Geomorphology* 53(1-2), 97-127.
- Stasiuk, M.V., Hickson, C.J., Mulder, T., 2003. The vulnerability of Canada to volcanic hazards. *Natural Hazards* 28(2-3), 563-589.
- Stemerink, C., Maddy, D., Bridgland, D.R., Veldkamp, A., 2010. The construction of a palaeodischarge time series for use in a study of fluvial system development of the Middle to Late Pleistocene Upper Thames. *Journal of Quaternary Science* 25(4), 447-460.
- Stokes, M., Mather, A.E., 2003. Tectonic origin and evolution of a transverse drainage: The Río Almanzora, Betic Cordillera, Southeast Spain. *Geomorphology* 50(1-3), 59-81.
- Takaku, J., Tadono, T., 2009. High resolution DSM generation from ALOS PRISM - Status updates on over three year operations, *International Geoscience and Remote Sensing Symposium (IGARSS)*, pp. III769-III772.
- Temme, A.J.A.M., Schoorl, J.M., Veldkamp, A., 2006. Algorithm for dealing with depressions in dynamic landscape evolution models. *Computers and Geosciences* 32(4), 452-461.
- Temme, A.J.A.M., 2008. *Understanding Landscape Dynamics over thousands of years: combining field and model work*. Phd, Wageningen University and Research, Wageningen.
- Temme, A.J.A.M., Baartman, J.E.M., Schoorl, J.M., 2009. Can uncertain landscape evolution models discriminate between landscape responses to stable and changing future climate? A millennial-scale test. *Global and Planetary Change* 69(1-2), 48-58.
- Temme, A.J.A.M., Veldkamp, A., 2009. Multi-process Late Quaternary landscape evolution modelling reveals lags in climate response over small spatial scales. *Earth Surface Processes and Landforms* 34(4), 573-589.
- Temme, A.J.A.M., Claessens, L., Veldkamp, A., Schoorl, J.M., 2011a. Evaluating choices in multi-process landscape evolution models. *Geomorphology* 125(2), 271-281.
- Temme, A.J.A.M., Peeters, I., Buis, E., Veldkamp, A., Govers, G., 2011b. Comparing landscape evolution models with quantitative field data at the millennial time scale in the Belgian loess belt. *Earth Surface Processes and Landforms* 36(10), 1300-1312.
- Temme, A.J.A.M., Schoorl, J.M., Claessens, L., Veldkamp, A., Editor-in-Chief: John, F.S., 2013. 2.13 Quantitative Modeling of Landscape Evolution, *Treatise on Geomorphology*. Academic Press, San Diego, pp. 180-200.
- Thomsen, K.J., Murray, A.S., Jain, M., Bøtter-Jensen, L., 2008. Laboratory fading rates of various luminescence signals from feldspar-rich sediment extracts. *Radiation Measurements* 43(9-10), 1474-1486.
- Tucker, G.E., Lancaster, S.T., Gasparini, N.M., Bras, R.L., Rybarczyk, S.M., 2001. An object-oriented framework for distributed hydrologic and geomorphic modeling using triangulated irregular networks. *Computers and Geosciences* 27(8), 959-973.
- Tucker, G.E., 2009. Natural experiments in landscape evolution. *Earth Surface Processes and Landforms* 34(10), 1450-1460.
- Tucker, G.E., Hancock, G.R., 2010. Modelling landscape evolution. *Earth Surface Processes and Landforms* 35(1), 28-50.
- Tzedakis, P.C., McManus, J.F., Hooghiemstra, H., Oppo, D.W., Wilmstra, T.A., 2003. Comparison of changes in vegetation in northeast Greece with records of climate variability on orbital and suborbital frequencies over the last 450 000 years. *Earth and Planetary Science Letters* 212(1-2), 197-212.
- Tzedakis, P.C., Hooghiemstra, H., Pälike, H., 2006. The last 1.35 million years at Tenaghi Philippon: revised chronostratigraphy and long-term vegetation trends. *Quaternary Science Reviews* 25(23-24), 3416-3430.
- Van De Wiel, M.J., Coulthard, T.J., 2010. Self-organized criticality in river basins: Challenging sedimentary records of environmental change. *Geology* 38(1), 87-90.

References

- Van De Wiel, M.J., Coulthard, T.J., Macklin, M.G., Lewin, J., 2011. Modelling the response of river systems to environmental change: Progress, problems and prospects for palaeo-environmental reconstructions. *Earth-Science Reviews* 104(1-3), 167-185.
- Van Gorp, W., Veldkamp, A., Temme, A.J.A.M., Maddy, D., Demir, T., Van der Schriek, T., Reimann, T., Wallinga, J., Wijbrans, J., Schoorl, J.M., 2013. Fluvial response to Holocene volcanic damming and breaching in the Gediz and Geren rivers, western Turkey. *Geomorphology* 201, 430-448.
- Van Gorp, W., Temme, A.J., Baartman, J.E., Schoorl, J.M., accepted. Landscape Evolution Modelling of naturally dammed rivers. *Earth Surface Processes and Landforms*.
- Van Gorp, W., Veldkamp, A., Temme, A.J., Schoorl, J.M., in revision. Modelling long-term (300 ka) upland catchment response to multiple lava dam events. *Earth Surface Processes & Landforms*.
- Veldkamp, A., Kroonenberg, S.B., 1993. Late Quaternary chronology of the Allier terrace sediments (Massif Central, France). *Geologie en Mijnbouw* 72(2), 179-192.
- Veldkamp, A., Tebbens, L.A., 2001. Registration of abrupt climate changes within fluvial systems: Insights from numerical modelling experiments. *Global and Planetary Change* 28(1-2), 129-144.
- Veldkamp, A., Buis, E., Wijbrans, J.R., Olago, D.O., Boshoven, E.H., Marée, M., van den Berg van Saparoea, R.M., 2007. Late Cenozoic fluvial dynamics of the River Tana, Kenya, an uplift dominated record. *Quaternary Science Reviews* 26(22-24), 2897-2912.
- Veldkamp, A., Schoorl, J.M., Wijbrans, J.R., Claessens, L., 2012. Mount Kenya volcanic activity and the Late Cenozoic landscape reorganisation in the upper Tana fluvial system. *Geomorphology* 145-146, 19-31.
- Veldkamp, A., Candy, I., Jongmans, A.G., Maddy, D., Demir, T., Schoorl, J.M., Schreve, D., Stemerink, C., van der Schriek, T., submitted. Reconstructing Early Pleistocene (1.3 Ma) terrestrial environmental change in western Anatolia: Did it drive fluvial terrace formation? *Geomorphology*.
- Viveen, W., Braucher, R., Bourlès, D., Schoorl, J.M., Veldkamp, A., van Balen, R.T., Wallinga, J., Fernandez-Mosquera, D., Vidal-Romani, J.R., Sanjurjo-Sanchez, J., 2012. A 0.65 Ma chronology and incision rate assessment of the NW Iberian Miño River terraces based on ¹⁰Be and luminescence dating. *Global and Planetary Change* 94-95(0), 82-100.
- Viveen, W., Schoorl, J.M., Veldkamp, A., van Balen, R.T., Desprat, S., Vidal-Romani, J.R., 2013a. Reconstructing the interacting effects of base level, climate, and tectonic uplift in the lower Miño River terrace record: A gradient modelling evaluation. *Geomorphology* 186, 96-118.
- Viveen, W., Schoorl, J.M., Veldkamp, A., van Balen, R.T., Vidal-Romani, J.R., 2013b. Fluvial terraces of the northwest Iberian lower Miño River. *Journal of Maps* 9(4), 513-522.
- Wainwright, J., 2006. Degrees of separation: Hillslope-channel coupling and the limits of palaeohydrological reconstruction. *Catena* 66(1-2), 93-106.
- Walder, J.S., O'Connor, J.E., 1997. Methods for predicting peak discharge of floods caused by failure of natural and constructed earthen dams. *Water Resources Research* 33(10), 2337-2348.
- Wallinga, J., 2002. Optically stimulated luminescence dating of fluvial deposits: a review. *Boreas* 31(4), 303-322.
- Wallinga, J., Bos, A.J.J., Dorenbos, P., Murray, A.S., Schokker, J., 2007. A test case for anomalous fading correction in IRSL dating. *Quaternary Geochronology* 2(1-4), 216-221.
- Werner, B.T., 1995. Eolian dunes: computer simulations and attractor interpretation. *Geology* 23(12), 1107-1110.
- Westaway, R., Pringle, M., Yurtmen, S., Demir, T., Bridgland, D., Rowbotham, G., Maddy, D., 2004. Pliocene and Quaternary regional uplift in western Turkey: The Gediz River terrace staircase and the volcanism at Kula. *Tectonophysics* 391(1-4 SPEC.ISS.), 121-169.
- Westaway, R., Guillou, H., Yurtmen, S., Beck, A., Bridgland, D., Demir, T., Scaillet, S., Rowbotham, G., 2006. Late Cenozoic uplift of western Turkey: Improved dating of the Kula Quaternary volcanic field and numerical modelling of the Gediz River terrace staircase. *Global and Planetary Change* 51(3-4), 131-171.
- Wijbrans, J., Schneider, B., Kuiper, K., Calvari, S., Branca, S., De Beni, E., Norini, G., Corsaro, R.A., Miraglia, L., 2011. ⁴⁰Ar/³⁹Ar geochronology of Holocene basalts; examples from Stromboli, Italy. *Quaternary Geochronology* 6(2), 223-232.
- Wijbrans, J.R., Pringle, M.S., Koppers, A.A.P., Scheveers, R., 1995. Argon geochronology of small samples using the Vulkaan argon laserprobe. *Proceedings of the Royal Netherlands Academy of Arts and Sciences* 98(2), 185-218.
- Wintle, A.G., Murray, A.S., 2006. A review of quartz optically stimulated luminescence characteristics and their relevance in single-aliquot regeneration dating protocols. *Radiation Measurements* 41(4), 369-391.
- Wohl, E., Beckman, N.D., 2014. Leaky rivers: Implications of the loss of longitudinal fluvial disconnectivity in headwater streams. *Geomorphology* 205, 27-35.

Summary

Combining field reconstruction and landscape evolution modelling can be useful to investigate the relative role of different drivers (tectonics, climate, local base level) on long term catchment evolution. In this thesis, field reconstruction and landscape evolution modelling are combined to unravel the long-term (300 ka) response to lava damming events of evolution of the Geren Catchment, a tributary of the upper Gediz river near Kula, Western Turkey. This catchment was considered suitable for such a study because its high preservation of remnant landscape surfaces and fluvial terraces which could be dated, while its base level evolution could be reconstructed by identifying and dating lava flows.

In Chapter 2, landscape evolution modelling of an idealized catchment revealed long-term (15 ka) catchment response to natural damming. Evolution of a high erodible and low erodible landscape was simulated using landscape evolution model (LEM) LAPSUS (Landscape process modelling at multi dimensions and Scales). The natural dam was given four different erodibilities, to mimic both the potentially more erodible landslide dams and resistant lava dams. In a low erodible landscape damming led to persistent preservation of the sediment wedge formed behind the dam, while in a high erodible landscape, damming additionally led to knickpoint persistence, hampered incision of the main river and stream rerouting. The highest erodible dam was almost removed after 15 ka, while its sediment wedge was still partly present. Comparison of results with natural dam events from literature showed that modelled response characteristics are observed in actual situations and that simulations on Quaternary timescales are useful.

In Chapter 3, field reconstruction resulted in a young lava flow being age constrained to the late Holocene (3.0 – 2.6 ka), by luminescence dating of fluvial sands below and on top of the flow. This lava flow dammed the Gediz river at two locations. the upstream lake was silted, while the downstream lake was not. Dams were breached catastrophically and possibly in a cascading event. The Gediz created an epigenetic gorge and its current river bed is still not at its pre-lava flow level. Results are summarized in a conceptual diagram.

Furthermore, field reconstruction and $^{40}\text{Ar}/^{39}\text{Ar}$ dating revealed multiple lava dam events which have infrequently raised and lowered the base level of the Geren Catchment in the middle to late Pleistocene (311 – 175 ka). Sediment-capped palaeosurfaces in the Geren suggest change from an active fluvial system to a more lacustrine environment in the middle Pleistocene, followed by fluvial reactivation and stepped incision in the late Pleistocene.

A second landscape evolution modelling study was conducted in Chapter 4, on a 300 ka timescale, with a larger catchment. Four scenarios have been applied on a reconstructed paleoderm of the Geren Catchment. In the first scenario, the palaeoderm was given constant rainfall for 300 ka. In the second scenario, three short (1 ka) damming events were added at its catchment outlet. In the third scenario, the palaeoderm endured gradual base level lowering at its outlet, based on the known incision rate of its base level, the Gediz river. In the fourth scenario, base level lowering and damming events were combined. Results were interpreted by evaluating 1 ka-averaged net erosion, catchment sediment storage, longitudinal profile development and spatial differences in net erosion and sediment storage. Results showed that the net erosion signal of the catchment is complex in all cases. However, average net erosion

and its variability increased due to constant base level lowering. Additionally, alternating phases of high and low variability occurred in net erosion, where high variability coincided with a strong decrease in total catchment sediment storage. Adding damming events to the gradual base level lowering scenario generated similar average net erosion as the base level lowering scenario, however its temporal pattern showed significantly different alternation of high and low variability periods. Furthermore, dampened upstream erosion was observed. Over time, this dampening migrates upstream indicating a long-term legacy of short term dam events.

Field reconstruction and landscape evolution modelling were combined in Chapter 5, to be able to reconstruct and understand actual Geren catchment response to identified base level evolution over a 300 ka period. In all simulations, rainfall and vegetation are varied over time based on arboreal pollen. Because exact significance and duration of dam events were not known, three scenarios of landscape evolution in the Geren Catchment were investigated: i) uplift driven gradual base level lowering, ii) gradual base level lowering and short damming events and iii) gradual base level lowering and long damming events. Output was evaluated for erosion-aggradation evolution in trunk gullies at two different distances from the catchment outlet. Climate influences erosion – aggradation activity in the upstream reach, although internal feedbacks influence timing and magnitude. Scenario i shows the most correlation with the climate signal, although its correlation is weak. Lava damming events leave an aggradation signal in the downstream reach, while complex and lagged response to these dams obscure correlations with climate and leave a legacy of the past in current landscape evolution. Catchment response of the long dam scenario correspond best with field reconstruction and dating. The combination of climate and base level explains a significant part of the landscape evolution history of the Geren Catchment.

In Chapter 6, a reflection and synthesis of Chapters 2-5 is presented. Indications for response to tectonics, climate and damming events are discussed separately for both field and modelling results. It is concluded that (lava) damming events of Pleistocene age can hamper, but also enhance incision on a 300 ka timescale. Furthermore, they can still have effect on current and future catchment evolution. However, catchment response to this evolution is complex and catchment specific and model results do not exactly reproduce its catchment history. An aggregated landscape evolution model output such as stream bed elevation change can be useful for comparison with fluvial terrace sequences. Combining field reconstruction and modelling suggests that the 300 ka incision history of the Geren is best explained if the catchment endured prolonged dam events. The combination of field reconstruction, dating and landscape evolution modelling therefore can enhance our understanding of long-term evolution of a specific landscape and increases knowledge on long term impact of past events on current catchment complexities and it is suggested to embed this research approach more structurally in long-term landscape reconstructions.

Samenvatting

De combinatie van veldreconstructie en landschapsevolutiemodellering kan een bruikbare manier zijn om de relatieve rol van verschillende externe factoren (tektoniek, klimaat, erosiebasis) op stroomgebiedsevolutie te onderzoeken. In dit proefschrift zijn veldreconstructie en landschapsevolutiemodellering gecombineerd om de lange termijn (300 ka) respons van het Geren stroomgebied op afdammingen door lavastromen te onderzoeken. Het Geren stroomgebied, een zijrivier van de bovenloop van de Gediz Rivier bij Kula, West Turkije, is geschikt voor een dergelijke studie vanwege de preservatie van oude landschapsoppervlakken en dateerbare rivierterrassen. Bovendien kan de evolutie van de erosiebasis van dit stroomgebied worden gereconstrueerd door middel van het identificeren en dateren van lavastromen.

In hoofdstuk 2 staat het onderzoek beschreven waarbij landschapsevolutie is gesimuleerd op een geïdealiseerd stroomgebied met landschapsevolutiemodel LAPSUS (LandscApe ProcesS modelling at mUlti dimensions and Scales). Het landschapsevolutiemodel laat een lange termijn (15 ka) respons op afdammingen zien. Voor de simulatie zijn vier verschillende erodibiliteiten gebruikt voor de dam om zowel de minder stabiele dammen veroorzaakt door aardverschuivingen, alsmede de meer stabiele dammen veroorzaakt door lavastromen te kunnen nabootsen. In een landschap met een lage erodibiliteit veroorzaakt afdamming preservatie van de sedimentwig die is opgebouwd achter de dam. In een landschap met hoge erodibiliteit veroorzaakt dit daarnaast ook een blijvend knikpunt in de riviergradiënt en wordt rivierinsnijding langdurig belemmerd. De dam met de hoogste erodibiliteit is na 15 ka vrijwel geheel verdwenen, terwijl de door de dam veroorzaakte sedimentwig nog deels gepreserveerd is. Een vergelijking van modelresultaten met bekende voorbeelden van natuurlijke afdammingen laat zien dat gemodelleerde karakteristieken daadwerkelijk voorkomen. Dit resultaat laat zien dat simulaties op Kwartaire tijdschalen waardevol zijn.

Hoofdstuk 3 beschrijft onderzoek waarbij zowel dateringen als veldreconstructies zijn toegepast om een landschapreconstructie te kunnen maken. Luminescentiedatering is toegepast op fluviatiele zanden onder en bovenop een jonge lavastroom. De ouderdom van de stroom werd gedateerd als laat Holocene (3.0 – 2.6 ka). Veldreconstructie wees uit dat deze lavastroom de Gediz Rivier op twee locaties had afgedamd. De bovenstroomse afdamming resulteerde in een met sediment opgevuld meer, terwijl het benedenstroomse meer niet was opgevuld. Damdoorbraken vonden catastrofaal plaats, waarbij de benedenstroomse doorbraak mogelijk de aanleiding tot de bovenstroomse doorbraak was. De Gediz Rivier creëerde hierdoor een nieuwe kloof naast en evenwijdig aan zijn voormalige loop en zijn huidige rivierniveau is nog steeds niet op het niveau van voor de lavastroom van 3.0-2.6 ka. Ook het Geren stroomgebied is beïnvloed door de benedenstroomse afdamming. Hier zijn deltaïsche afzettingen uit de tijd van de afdamming waargenomen. Tevens heeft een verandering van een meanderende naar een rechte stroomgeul sinds de damdoorbraak tot het heden plaatsgevonden. Veldreconstructie en $^{40}\text{Ar}/^{39}\text{Ar}$ datering wezen uit dat gedurende het midden tot laat Pleistoceen meerdere van zulke afdammingen door lavastromen hebben plaatsgevonden (311 - 175 ka). Deze hebben de erosiebasis van het Geren stroomgebied diverse malen verhoogd en verlaagd. Paleo oppervlakken in het Geren stroomgebied die bedekt zijn met sedimenten wijzen op de verandering van een fluviatiel systeem naar een

meer lacustriene omgeving in het midden Pleistoceen.

Een tweede landschapsevolutiemodellering wordt beschreven in hoofdstuk 4. De simulatie is nu uitgevoerd op een tijdschaal van 300 ka, met een groter stroomgebied dan in hoofdstuk 2. Hiervoor zijn vier scenario's gebruikt en toegepast op een gereconstrueerd paleo-hoogtemodel van het Geren stroomgebied. In het eerste scenario is alleen respons op constante regenval gesimuleerd. In het tweede scenario zijn drie korte afdam perioden (1 ka) toegevoegd. In het derde scenario is de respons op geleidelijke verlaging van de erosiebasis onderzocht, gebaseerd op de bekende gemiddelde insnijdingsnelheid van de Gediz Rivier. In het vierde scenario is geleidelijke verlaging van de erosiebasis gecombineerd met drie korte afdammingen. Millenia-gemiddelden van netto erosie, sedimentopslag in het stroomgebied, lengteprofielen en ruimtelijke verschillen in netto erosie en sedimentopslag zijn geïnterpreteerd. In alle gevallen is er een complex netto erosie signaal te zien, echter in de scenario's met geleidelijke erosiebasisverlaging is het gemiddelde en de variabiliteit van de netto erosie hoger. In deze scenario's wisselen fases met hoge en lage variabiliteit elkaar af, waarbij hoge variabiliteit overeenkomt met fases van grote afname in sedimentopslag. Het toevoegen van afdammingen aan het scenario met geleidelijke erosiebasisverlaging resulteert in vergelijkbare gemiddelde netto erosie, echter het temporele patroon van fases met hoge en lage netto erosie is significant verschillend. Bovendien is bovenstroomse erosie in deze scenario's minder hoog. Deze lagere erosie migreert naar bovenstroomse gebieden, wat duidt op een lange termijn nalatenschap van afdammingen in het bovenstroomse landschap.

In hoofdstuk 5 wordt beschreven hoe veldreconstructie en landschapsevolutiemodellering gecombineerd zijn om de respons van het Geren stroomgebied op erosiebasisveranderingen te reconstrueren en begrijpen over een 300 ka periode. In alle modelsimulaties zijn regenval en vegetatie gevarieerd aan de hand van een beschikbare pollenreeks. Omdat de exacte significantie en duur van lavadammen niet bekend is, zijn drie scenario's gebruikt: i) geleidelijke erosiebasisverlaging, ii) geleidelijke erosiebasisverlaging en kortdurende afdammingen en iii) geleidelijke erosiebasisverlaging en langdurende afdammingen. De evolutie van erosie-aggradatie op twee verschillende afstanden langs de hoofd stroomgeul in het Geren stroomgebied is geëvalueerd. Klimaat beïnvloedt erosie-aggradatie in het bovenstroomse deel, hoewel interne dynamiek de timing en magnitude beïnvloeden. Zelfs scenario i heeft slechts een zwakke correlatie met het klimaatsignaal. Lava-afdammingen veroorzaken aggradatie in het benedenstroomse deel. Complexe en vertraagde respons op deze afdammingen verhullen correlaties met klimaat en vormen zo een nalatenschap van het verleden in de huidige landschapsevolutie. De respons van het stroomgebied op het scenario met langdurige afdammingen correspondeert het best met veldreconstructie en dateringsresultaten. De combinatie van klimaat en erosiebasisverlaging verklaart een significant deel van de landschapsevolutie geschiedenis van het Geren stroomgebied.

In hoofdstuk 6 wordt een reflectie en synthese van hoofdstuk 2 t/m 5 gepresenteerd. Respons op tektoniek, klimaat en afdammingen worden afzonderlijk besproken voor veld- en modelresultaten. Een van de conclusies is dat Pleistocene afdammingen door lavastromen insnijding kunnen verhinderen maar ook versterken op een 300 ka tijdschaal. Bovendien kunnen deze Pleistocene gebeurtenissen effect hebben op de huidige en toekomstige stroomgebiedsevolutie. Echter, deze evolutie is complex en specifiek voor het stroomgebied en modelresultaten reproduceren niet exact de stroomgebiedsgeschiedenis. Een geaggregeerde

output van een landschapsevolutiemodel, zoals hoogteverandering van een locatie in een belangrijke geul, kan bruikbaar zijn voor een vergelijking met rivierterrassequenties. De combinatie van veldreconstructie, dateringen en landschapsevolutiemodellering kan daarom ons begrip vergroten van lange termijn evolutie van een landschap. Het biedt bovendien meer inzicht in de lange termijn invloed van gebeurtenissen uit het verleden (zoals een afdamming) op complexiteiten in huidige stroomgebieden. Aanbevolen wordt om deze aanpak structureler in te bedden in lange termijn landschapsreconstructies.

Özet

Uzun dönemli havza evrimlerinin araştırılmasında farklı etken ve süreçlerin (tektonik, iklim, yerel taban seviyesi) karşılıklı etkilerinin ortaya konmasında arazi rekonstrüksiyonu ile yer şekillerinin gelişim modellerinin birleştirilmesi oldukça önemli faydalar sağlayabilir. Bu çalışmada, batı Anadolu'da Gediz Nehri'nin bir kolu olan Geren Çayı havzasında uzun süre varlığını muhafaza eden volkanik lav setlerinin havzanın gelişimine olan etkilerini ortaya koymak amacı ile arazi rekonstrüksiyonu ile yer şekillerinin gelişim modelleri birlikte ele alınmıştır. Gerek sahada paleo yer şekillerinin parçalar halinde olsalar dahi önemli ölçüde muhafaza edilmiş olması, tarihlendirilebilir nehir taraçalarının mevcudiyeti ve gerekse de mevcut lav akıntılarının belirlenmesi ve tarihlenmesi yolu ile taban seviyesi değişmelerinin belirlenmesi gibi etkenlerin birlikte mevcudiyeti bu havzanın çalışma sahası olarak belirlenmesinde önemli faydaları olmuştur.

Bölüm 2 de idealize edilmiş bir havzada yer şekilleri gelişim modellemesi oluşturulmuş ve 15 bin yıllık sürede nehri bloke eden doğal setlere bağlı olarak havzada hangi türde yer şekilleri oluştuğu araştırılmıştır. Kolayca aşınabilir ve zor aşınabilir yer şekillerinin gelişimini ortaya koymak amacı ile az dirençli heyelan setleri ve daha dirençli lav setleri taklit edilmiş ve bunun için dört farklı dirence sahip doğal setler kullanılmıştır. Düşük erozyon potansiyeline sahip bir havzayı drene eden akarsuyunun doğal bir setle bloke edilmesi sonucunda setin gerisinde sürekli olarak kama şeklinde sediman birikimlerinin oluştuğu, buna karşılık yüksek erozyon potansiyeline sahip bir havzada ise nehrin bloke edilmesi setin gerisinde sediman birikimine ilave olarak sürekli bir eğim kırıklığı oluşumuna sebep olduğu ve bununla nehrin yatağını derine kazmasını yavaşlatarak yön değiştirmesine sebep olduğunu ortaya koymuştur. En hızlı erozyona uğrayan doğal set 15 bin yıllık zaman periyodu sonunda hemen hemen ortadan kaldırılmasına rağmen, onun gerisinde biriken sediman kalıntıları varlıklarını kısmen muhafaza etmişlerdir. Bu çalışmada elde edilen sonuçlar tabiatta doğal olarak oluşmuş ve literatüre yansıyan bulgular ile karşılaştırıldığında, sonuçlar itibari ile aralarında dikkate değer uyumluluk olduğunu ortaya koymuştur. Bundan dolayı bu çalışmada kullanılan yer şekilleri gelişim modellemesi süre itibari ile bütün Kuvaternere uygulanabilir özelliktedir.

Bölüm 3 Arazide yer şekillerinin rekonstrüksiyonu, Gediz'i bloke eden bir lavın yaşlarının tayini ile mümkün olmuştur. Lavın yaş tayini ise onun altında ve üstünde yer alan flüviyal kumların yaşlarının luminescence metodu ile belirlenmesi ile mümkün olmuştur. Böylece lavın yaşının Geç Holosen (3.0 – 2.6) olduğu sonucuna varılmıştır. Bu lav akıntısı Gediz'i iki farklı lokasyonda bloke ederek iki göl oluşturmuştur. Yukarı kesimdeki gölde siltasyon tespit edilirken, aşağı kesimde bulunan gölde bu durum tespit edilmemiştir. Nehri bloke eden bu lav setleri muhtemelen kademeli bir şekilde ve ani olarak yıkılmışlardır. Bunun sonucunda Gediz epigenetik bir kanyon (boğaz) oluşturdu ve güncel nehir yatağı halen daha nehir bloke edilmeden evvelki yatak seviyesine erişememiştir. Sonuçlar kavramsal bir diyagram şeklinde verilmiştir. Arazi bulgularına $^{40}\text{Ar}/^{39}\text{Ar}$ tarihllemeler Orta ve Geç Pleistosen arasındaki dönemde (311 – 175 bin yıl) nehrin birçok kez lav akışları ile bloke edildiğini ve bu durumun Geren havzasında sık sık taban seviyesinde yükselme ve alçalmalara sebep olduğunu ortaya koymuştur. Geren Havzasında sedimanla kaplı paleo yüzeylerde yapılan tespitler, Orta Pleistosen'de flüviyal sistemden gölsel bir ortama geçildiğini ve Geç Pleistosen'de ise yeniden flüviyal sürece geçildiğini ve nehrin derine kazmasının hızlandığını ortaya koymuştur.

Bölüm 4 te daha büyük bir havzada 300 bin yıllık bir dönemde daha büyük ölçekte ikinci bir yerşekilleri gelişim modellemesi yapılmıştır. Birinci senaryoda Paleo-DEM i oluşturulan Geren Havzasına 300 bin yıllık bir periyotta aynı miktarda yağış verilmiştir. İkinci senaryo olarak nehrin bilinen derine kazma oranı dikkate alınarak taban seviyesi kademeli olarak alçaltıldı. Üçüncü senaryo olarak havzanın ağız kesiminde biner yıllık kısa periyodlarla nehir 3 defa bloke edildi. Sonuçlar nehrin bin yıllık ortalama net derine kazma oran ve miktarı, havzadaki sediman depolanması, akarsuyun boyuna profilinin gelişimi, havzada net erozyon miktarının mekânsal olarak değişimi ve sediman depolanma oranları dikkate alınarak yorumlanmıştır. Sonuçlar bütün durumlarda havzanın net erozyon durumunun kompleks bir durum gösterdiğini ortaya koymuştur. Bununla birlikte ortalama net erozyon miktarı ve onun değişimi taban seviyesinin sabit olarak alçaltılmasına bağlı olarak artma eğilimi gösterdiği tespit edilmiştir. Bütün bunlara ilave olarak net erozyon miktarında periyodik olarak azalma ve artmalar tespit edilmiştir. Net erozyon miktarındaki yüksek değişim havzanın toplam sediman miktarının hızla azaldığı zamanlara denk gelmiştir. Kademeli taban seviyesi alçaltılması olayına nehrin bloke edilmesi faktörünün ilave edilmesi de tıpkı taban seviyesi alçaltılması senaryosunda olduğu gibi benzer ortalama net erozyon miktarı üretmiştir. Bununla birlikte erozyonun oran ve miktarlarında zaman içerisinde önemli ölçüde salınımlar tespit edilmiştir.

Güncel Geren havzasının belirlenen taban seviyesi gelişimine olan uyumunu yeniden kurma ve anlamak için arazi rekonstrüksiyonu ve yer şekilleri gelişim modellemesi Bölüm 5 te birlikte ele alınmıştır. Nehrin bloke edilmesi olaylarının tam olarak önemi ve süresi bilinmediğinden Geren Havzasında üç farklı yer şekilleri gelişim senaryosu araştırılmıştır: I) tektonik yükselme ile iklim (arboreal polen ile ilişkili olarak yağış ve bitki örtüsü), II) tektonik yükselme, iklim ve kısa süreli nehrin bloke edilmesi durumları ve III) tektonik yükselme, iklim ve nehrin uzun süreli bloke edilmesi durumları. Çıktılar, havza çıkışına iki farklı mesafede bulunan ana gulliler üzerindeki erozyon-birikim gelişimine bağlı olarak değerlendirilmiştir. Hernekadar dahili birtakım faktörler zaman ve büyüklüğünü etkilese de, havzanın yukarı kesiminde erozyon ve birikim süreçleri iklimin kontrolü altındadır. Hernekadar korelasyonu zayıf ise de birinci senaryo iklim sinyalleri ile en büyük ilişkiyi gösterdi. Hernekadar iklimin etkisini maskeleyip ve daha komplike birtakım yer şekillerinin oluşmasına sebebiyet verse de, nehrin lav akıntıları ile bloke edilmesi sonucunda genellikle oluşan setin aşağı kesiminde bir agradasyon (birikme) oluşumu gerçekleşir. Hernekadar oldukça yakın döneme ait havza gelişimi zayıf bir şekilde taklit edilse de, havzanın uzun süreli nehir blokajlarına olan tepkisi en iyi şekilde arazi rekonstrüksiyonu ve tarihllemeler sonucunda ortaya konulabilmektedir. Bununla birlikte Geren Havzasında mevcut yer şekillerinin gelişim tarihinin önemli bir kısmı en iyi şekilde ancak iklim ve taban seviyesi değişimlerinin kombinasyonu ile ilgili olarak açıklanabilir.

Bölüm 6 da 2-5 bölümlerinin bir sentezi yapılmaktadır. Tektonik, iklim ve nehrin bloke edilmesi olaylarını işaret eden belirtiler ve deliller hem arazi tespitleri ve hem de modelleme sonuçlarına bağlı olarak ayrı ayrı tartışılmıştır. Bulgular, Pleyistosen yaştaki lav setlerinin 300 er bin yıllık zaman süresince nehrin yatağını derine kazmasını yavaşlatıp veya zorlaştırdığı gibi derine kazmayı artırabileceğini de ortaya koymuştur. Ayrıca, bu lav setleri hem günümüz ve hem de gelecekteki havza evolüsyonunu etkileyebilecektir. Bununla birlikte, havzanın bu gelişime olan tepkisi karmaşıktır ve havza spesifiği ile model sonuçları tam olarak bütünü ile havza gelişim tarihini yeniden ortaya koymaktan uzaktırlar. Birikimin öncelikli olduğu

bir yer şekilleri gelişim modellemesinden elde edilen sonuçların, örneğin akarsu yatak değişimi, arazide tespit edilen flüviyal taraçalar ile karşılaştırılması fayda sağlayabilir. Arazi rekonstrüksiyonu ile modellemelerden elde edilen sonuçların birleştirilmesi gösteriyor ki Geren nehrinin 300 bin yıllık derine kazma tarihini en iyi şekilde açıklamanın yolu nehri bloke eden doğal setlerin uzun süre varlıklarını muhafaza etmeleri ile mümkün olabilir. Yer şekillerinin arazideki rekonstrüksiyonu ile model çalışmalarının birleştirilmesi bu bakımdan bizim herhangi bir spesifik yer şeklinin uzun zaman süresi içerisinde nasıl bir evrim geçirdiğini anlamamıza önemli ölçüde katkı sağlayacağı gibi, halihazırdaki havzanın da uzun dönemler sonucunda nasıl bir evrim geçireceği hususunda geniş bilgi sahibi olmamızı sağlar. Bu sebeplerden dolayı bu çalışma yapı itibarı ile daha ziyade uzun dönemli yer şekilleri gelişiminin rekonstrüksiyonunu amaçlamaktadır.

Dankwoord

Het uitoefenen van een PhD doe je nooit alleen. Ik heb dan ook veel mensen te bedanken voor hun steun op zowel het inhoudelijke als het persoonlijke vlak. Een aantal mensen wil ik hierbij speciaal noemen, maar ook diegenen die ik onverhoopt vergeet dank ik hartelijk!

Als eerste wil ik mijn promotor Tom Veldkamp bedanken. Tom, als geestelijk vader van dit project bood je mij in 2008 de kans om mijn ambitie als onderzoeker na te jagen. Jij wist mij op momenten dat ik vast zat weer de juiste richting in te duwen. Daarnaast is veldwerk met jou (vooral in combinatie met Darrel) een boeiende en leerzame ervaring geweest. Het constant opstellen en proberen te falsificeren van hypothesen en de boeiende discussies en oplossingen die daaruit voortkomen zijn voor mij ontzettend leerzaam geweest. Daarnaast heb je het talent om net even een hoek verder te lopen dan de rest en vervolgens een sleutelwaarneming te doen, frustrerend maar vooral bewonderenswaardig! Jeroen Schoorl was vanaf het begin mijn co-promotor. Jeroen, jij bent ontzettend belangrijk geweest voor zowel het modelwerk als in het veld. Als bouwer van LAPSUS liet je mij vrij in hoe ik met het model wilde werken maar fungeerde wel regelmatig als klankbord en geweten. Het rijden door het Turkse landschap met jouw favoriete jaren '90 dance aan was memorabel, alsmede de recordtijd bandenwissel samen met Tom! Mijn tweede co-promotor is Arnaud Temme. Arnaud, jij bent vanaf het begin nauw betrokken geweest bij mijn project. Je deur stond altijd open en het was een logische stap om jou toe te voegen aan het officiële begeleidingsteam. Dank voor al je hulp en support!

Ik wil ook de collega's van de leerstoelgroepen Landdynamiek (LAD) en later Bodemgeografie en Landschap (SGL) hartelijk bedanken voor hun steun en gezelschap. Jetse, Kasper, Gert, Gerard, Lieven, Bart, Martha, Peter, Christina, en alle anderen, bedankt. Hartelijk dank ook Mieke en Henny voor het orde scheppen in alle administratieve zaken waar ik mee te maken kreeg. Het plotselinge tragische verlies van Marthijn heeft ons allen geraakt. Zijn kennis, kunde, enthousiasme en vriendelijke persoonlijkheid zullen mij altijd bijblijven.

Toen ik begon bij de leerstoelgroep LAD-SGL bestond deze uit een grote groep PhD-studenten. Ik bedank deze dan ook als groep: dank jullie allen voor jullie hulp, inspiratie, alle LAD/SGL activiteiten of gewoon praten over wetenschap, maatschappij of niks onder het genot van een kop koffie, lunch of biertje! Een aantal personen wil ik met name noemen: Luciana, thanks for your warm welcome and all your help in the unforgettable place called "corner office"! Jantiene bedankt voor je hulp, je bereidheid altijd even mee te willen denken en het LAPSUS-prutsen! Paranimf Monique, het was geweldig om jou als maatje en vaste kamergenoot te hebben tijdens vrijwel het gehele PhD-traject. Je natuurlijke opgewektheid werkt inspirerend en dank voor je gastvrijheid wanneer deze Amsterdammer weer eens in Wageningen was gestrand. Phuong, thanks for your company in the final stage of my project. I will never pronounce "pho" wrong again! Dank aan Alice Versendaal en Tony Reimann voor het met een glimlach meten en analyseren van mijn niet altijd eenvoudige luminescentie monsters. Ik wil Jakob Wallinga bedanken voor in eerste instantie zijn hulp en advies bij de luminescentiedateringen in Delft. Ik ben verheugd dat je vervolgens naar Wageningen bent verhuisd. Dank ook voor de frisse blik van studenten Kate Heerema, die als BSc-student is meegeweest naar Turkije, en Maricke van Leeuwen, wier MSc-thesis ik mede heb begeleid.

Voor het dateren van de basalten ben ik gedurende mijn PhD regelmatig op de VU geweest. Ik wil Roel van Elsas en Brett Davidheiser bedanken voor hun hulp bij monsterpreparatie en meting. Jan Wijbrans, dank voor alle hulp en open discussies over het analyseren en interpreteren van de resultaten.

Organising and attending the Kenya course has been a great experience and I therefore would like to thank all staff and participants and especially co-organisers Monique, Jantiene, Derek, Lieven and Claudius. Thanks to the organisers and participants of the inspirational SSOG-workshop at Heimbüchenthal, Germany.

Darrel Maddy has been of key importance for the origin and the development of my project. Darrel, I have learned a lot from your knowledge and skill, but also your enthusiasm and passion for research. Thanks also for your help and hospitality during the two pleasant periods I had in Newcastle. I hope our roads will cross again.

I would like to thank those that accompanied me on the different fieldworks to Turkey. Tuncer Demir, thank you very much with all your careful help at any level during all the fieldworks I did in Turkey and for providing the Turkish summary! The fieldwork I had with Darrel's student Adam was definitely the most memorable one! Adam, being escorted through the Turkish landscape by Turkish officials and drinking disproportionately large amounts of tea at offices was not how we envisaged the fieldwork! Nevertheless thanks for your company and courage! I would furthermore like to thank Rob Scaife. Rob, thanks for your sensible advice and discussions during several fieldworks and for assisting me with taking dGPS-points in a burning hot Geren Catchment. I would also like to thank Tim van der Schriek, Chris Stemerding and David Bridgland for their pleasant company during several fieldworks.

Natuurlijk zijn er ook veel mensen die al jarenlang een rol spelen in mijn leven en daardoor indirect ook belangrijk zijn geweest. Frans, Boris, Arjan K., Jethro, paranimf Assil, Laurien, Petra, Loes, Marijke, Toon, Arjan G., Nina, de FG-ers, de Bacchus crew, de Heumerds en de Plaggestampers, dank voor de momenten van afleiding en gezelligheid. Of het nou op Lowlands, diverse feesten, huwelijken, vakanties, in een café of gewoon thuis is geweest. Ik prijs mij gelukkig met jullie als vrienden.

Ik wil Femke hartelijk bedanken voor de kunde en tijd die ze heeft gestoken in het opmaken van de drukversie mijn proefschrift. Dank ook aan Mart en Jopie, niet in het minst voor het regelmatig inspringen het afgelopen half jaar zodat ik mijn focus kon leggen op het afronden van dit proefschrift. Mijn lieve zus Sylvia, Bas, nichtje Julia en neefje Nathan, Fons, Ineke, Theo, de De Goedes, jullie hebben altijd hart en interesse getoond in mijn wel en wee.

Ik draag dit proefschrift op aan mijn ouders. De randvoorwaarden die zij al van jongs af aan hebben geschapen zorgden ervoor dat ik de keuzes heb kunnen maken die ik heb gemaakt. Het lijkt misschien een vanzelfsprekendheid maar dat is het niet. Pap en Mam, ik ben jullie ontzettend dankbaar voor alles!

Tenslotte is er een persoon waarop mijn besluit om te gaan promoveren misschien wel net zoveel impact heeft gehad als op mezelf. Lieve Janneke, bedankt voor je geduld, steun, hulp, luisterend oor en afleiding gedurende de afgelopen jaren. De komst van onze dochter Sanne gedurende het laatste halfjaar van mijn proefschrift zette alles weer in perspectief. Ik verheug me ontzettend op onze toekomst samen!

List of Publications

- Van Gorp, W., Veldkamp, A., Temme, A.J., Schoorl, J.M. Modelling long-term (300 ka) upland catchment response to multiple lava damming events. Under revision for *Earth Surface Processes & Landforms*.
- Van Gorp, W., Temme, A.J., Baartman, J.E., Schoorl, J.M., 2014. Landscape Evolution Modelling of naturally dammed rivers. *Earth Surface Processes and Landforms*.
- Van Gorp, W., Veldkamp, A., Temme, A.J.A.M., Maddy, D., Demir, T., Van der Schriek, T., Reimann, T., Wallinga, J., Wijbrans, J., Schoorl, J.M., 2013. Fluvial response to Holocene volcanic damming and breaching in the Gediz and Geren rivers, western Turkey. *Geomorphology* 201, 430-448.
- Baartman, J.E.M., Van Gorp, W., Temme, A.J.A.M., Schoorl, J.M., 2012. Modelling sediment dynamics due to hillslope-river interactions: Incorporating fluvial behaviour in landscape evolution model LAPSUS. *Earth Surface Processes and Landforms* 37(9), 923-935.
- Maddy, D., Veldkamp, A., Jongmans, A.G., Candy, I., Demir, T., Schoorl, J.M., van der Schriek, T., Stemerink, C., Scaife, R.G., Van Gorp, W., 2012. Volcanic disruption and drainage diversion of the palaeo-Hudut River, a tributary of the Early Pleistocene Gediz River, Western Turkey. *Geomorphology* 165-166, 62-77.

Curriculum vitae

Wouter van Gorp was born on the 9th of September 1980 in Amsterdam, the Netherlands. He followed secondary school (VWO) at the St. Nicolaaslyceum in Amsterdam and graduated in 1998. He started studying “Operations Research and Management” at the University of Amsterdam, where he obtained a quantitative basis which is useful until the current day. However, he realised that his heart lies at investigating natural and geographical problems. He decided to switch to Physical Geography in 2000, in which he enrolled after an enjoyable summer deficiency course in physics at the James Boswell Institute in Utrecht. During his study Physical Geography at the University of Amsterdam, he investigated the influence of nocturnal cloud cover on soil temperature for his BSc. degree. For his MSc. he specialised in earth surface processes. He was involved in fieldwork, GIS and modelling studies. For his MSc. thesis research, he made a Neogene landscape reconstruction of the Carcavo basin in southeast Spain and he obtained his MSc. degree in 2006.

In the years 2007-2008, Wouter worked as a GIS-specialist at Geodan, a geo-information company. Here, he worked with many GIS software packages and databases for different clients from the public sector, for example the water boards Delfland and Rijnland and the Amsterdam police. Although he enjoyed working here, he had an ambition to perform scientific research. He successfully applied for a PhD position at Wageningen University in 2008, from which this thesis is the result.

Wouter has continued interest in research at the intersection of GIS, fieldwork and modelling in the field of earth sciences. He lives together with his girlfriend Janneke and their daughter Sanne.



PE&RC Training and Education Statement

With the training and education activities listed below the PhD candidate has complied with the requirements set by the C.T. de Wit Graduate School for Production Ecology and Resource Conservation (PE&RC) which comprises of a minimum total of 32 ECTS (= 22 weeks of activities)



Review of literature (4.5 ECTS)

- Late-Quaternary landscape evolution in the Kula basin, Turkey: unravelling the role of local base level change: introduction

Writing of project proposal (4.5 ECTS)

- Late-Quaternary landscape evolution, unravelling the role of local base level change in the Kula basin, Turkey

Post-graduate courses (7.5 ECTS)

- Land dynamics: getting to the bottom of Mount Kenya; PE&RC/LAD (2009)
- 1st mid-European summer school on geomorphology: complex response of earth surface process to environmental change (2010)
- Workshop: modelling concepts of biogeomorphology; WUR (2011)
- Argon geochronology and aspects of absolutely calibrating the geological timescale; GTSnext, NSG, Free University Amsterdam (2012)
- Workshop: improving understanding of fluvial landscape development; ITC, Twente University (2013)
- Analysing sediment connectivity; WIMEK (2013)

Laboratory training and working visits (4.5 ECTS)

- Luminescence dating of fluvial sediments, sample preparation; Netherlands Centre of Luminescence, Delft (2010, 2011)
- Ar-Ar dating of basalt samples, preparation, analysis and interpretation; VU University, Amsterdam

Invited review of (unpublished) journal manuscript (2 ECTS)

- Environment, Development and Sustainability: soil loss mapping (2012)
- Environment, Development and Sustainability: soil conservation (2013)
- Palaeolimnology: landslide damming (2014)

Deficiency, refresh, brush-up courses (2.4 ECTS)

- Analytical methods (2009)
- Geology and landscapes of the world (2012)

Competence strengthening / skills courses (4.5 ECTS)

- PhD Competence assessment; WGS (2009)
- Writing and presenting a scientific paper; WIMEK (2010)
- Research methodology; MGS/WIMEK/PE&RC (2010)

PE&RC Annual meetings, seminars and the PE&RC weekend (2.2 ECTS)

- PE&RC Day: expect the unexpected (2008)
- PE&RC Mini-symposium: the role of long-term landscape reconstruction for understanding current-day rates of landscape change (2008)
- PE&RC Introduction weekend (2009)
- The last leg of the PhD and projection to the future (2013)

Discussion groups / local seminars / other scientific meetings (6.7 ECTS)

- Spatial Methods (SPAM) (2009-2011)
- MSN (2012)

International symposia, workshops and conferences (9 ECTS)

- FLAG Fluvial Archives Group; poster and oral presentation; Portugal (2010)
- EGU; poster and oral presentation; Vienna (2013)
- IAG; oral presentation; Paris (2013)
- NAC 12; 2 poster presentations; Veldhoven (2014)

Lecturing / Supervision of practical's / tutorials (3 ECTS)

- Soil and water I (2008-2013)
- Soil and water II (2009)
- Geology and landscapes of the world (2012)

Supervision of a MSc student (3 ECTS)

- Landscape evolution modelling



Printed by: Gildeprint Drukkerijen - Enschede

